An investigation of the effect of cuprizone-induced demyelination using histological, behavioural, proteomics and immunological approaches

Monokesh Kumer Sen

A thesis submitted in fulfilment of the requirements for the award of
Doctor of Philosophy (PhD)
School of Medicine, Western Sydney University, Penrith, NSW, Australia
June, 2019

Supervisory panel

A/Prof. David A. Mahns, Western Sydney University, Australia
Dr. Simon J. Myers, Western Sydney University, Australia
A/Prof. Peter J. Shortland, Western Sydney University, Australia
Prof. Jens R. Coorssen, Brock University, Canada

Statement of authentication

The work presented in this thesis is, to the best of my knowledge and belief, original except as acknowledged in the text. I hereby declare that I have not submitted this material, either in full or in part, for a degree at this or any other institution.

Monokesh Kumer Sen

21.06.2019

Acknowledgements

I would like to thank First and foremost to the Almighty.

My PhD completion would not be possible without the advice and help from my supervisory panel A/Prof. David A. Mahns, Dr. Simon J. Myers, A/Prof. Peter J. Shortland and Prof. Jens R. Coorssen. Particular thank you to my panel members for sharing their abundant knowledge, asking so many 'whys' and provoking to think 'critically', write 'clearly' and understand the science throughout my PhD journey. I am especially grateful to Prof. Jens R. Coorssen, for providing me the opportunity to peruse my PhD when I wrote him four years ago expressing my interest.

I would like to extend my gratitude to Dr. Chandra S. Malladi for his technical support on two dimensional gel electrophoresis, western blotting and day-to-day discussions. I would also extend my gratitude to Dr. Erika Gyengesi, Dr. Sindy Kueh and Dr. Andy Liang for their technical support in histology and to use microscope. The large amount of animal studies in my PhD would not be possible without the constant help of the stuffs from the Animal House including Ashleigh Deschamps, Nikola Mills and Nicole Jones. I also thank Dr. David Harman and Meena Mikhael for helping me in Mass spectrometry analysis of my protein samples. My thanks to Michael Withers for providing technical assistance in IT related problems.

My stressful journey would not be as joyful without the presence and support from the excellent faces of Melissa A Partridge and Dr. Arlene D'Silva, you are amazing. I would like to extend my thanks to Mohammed Saad Mohammed Almusleshi for his collaboration that has been presented in the thesis. Very special thanks to Dr. Carol Gano, Dr. Seaky Lim, Dr. Melissa Mangla, Ahilya Singh, Rustam Asgarov, Dr. Faheem Jan, Madhuri Venigalla, Szeifoul Afadlal, Dr. Orsolya Kekesi, Sajal Roy and Dr. Elias Mollah for their encouragement and support.

Coming to Australia would not have been a smooth transition without the help of my dearest teachers Prof. Anawarul Haque and Dr. Shamima Nashrin back in Bangladesh. My gratitude also extends to Dr. Nirupam Biswas, Dr. Shabah Shadli and my eldest brother Bonkim Sen for their encouragement and contribution towards higher studies.

I am grateful to my family members, especially my dearest parents (Bidyut Chandra Sen and Sarashati Sen) for believing in me, raising me like any other normal child and trusting in my capabilities. My gratitude extends beyond words to them. A big thanks to my beautiful wife Rinkey Rani Shome for her belief and constant in me.

My gratitude also extend to WSU-International Postgraduate Research Scholarship for providing my tuition fees and living expenses. A great thank to the Rotary Club of Narellan for supporting WSU-Multiple Sclerosis research.

To others whom I may have forgotten, I am sorry, but thank you for your contributions.

Lastly, thanks to beautiful Australia and School of Medicine of Western Sydney University for giving me the opportunity to pursue PhD.

Monokesh Kumer Sen

Dedication

Dedicated to my parents whom I love the most

TABLE OF CONTENTS

Thesis structure

This thesis is composed of six themed chapters. **Chapter-1** (**Introduction**) lays out the theoretical dimensions of the research, focusing on the three key themes of cuprizone (CPZ), oligodendrocytosis and gliosis (astrocytes and microglial activation). **Chapter-2** provides the detailed **Materials and Methods** used for this thesis. **Chapter-3**, presents the investigation of whether disruption of blood brain barrier following short (5-week) and long (12-week) term CPZ-feeding results in associated with infiltrates T-cells into the brain (**Paper I**). **Chapter-4** is a systematic review of literature on the behavioural phenotypes associated with CPZ (**Paper II**). In **Chapter-5**, tests whether CPZ induces sensorimotor deficits and histological changes (oligodendrocytosis, gliosis and neuronal loss) in pathways associated with sensorimotor function (**Paper III**). **Chapter-6** is an overall discussion, recommendation for further research and conclusion.

These papers are published in the following peer-reviewed journals

Paper I: **Sen MK**, Almuslehi MSM, Gyengesi E, Myers SJ, Shortland PJ, Mahns DA and Coorssen JR (2019). Suppression of the peripheral immune system limits the central immune response following cuprizone-feeding: Relevance to modelling multiple sclerosis. Cells, 8(11), 1314; https://doi.org/10.3390/cells8111314.

Paper II: **Sen MK**, Mahns DA, Coorssen JR and Shortland PJ (2019).
Behavioural phenotypes in the cuprizone model of central nervous system demyelination. Neuroscience and Biobehavioral Reviews, 107:23-46. doi: 10.1016/j.neubiorev.2019.08.008.

Paper III: **Sen MK**, Almuslehi MSM, Coorssen JR, Mahns DA, and Shortland PJ (2020).
Behavioural and histological changes in cuprizone-fed mice. Brain, Behavior, and Immunity, https://doi.org/10.1016/j.bbi.2020.01.021.

Abstract

Feeding cuprizone (CPZ) to animals has been long known to lead to regional degeneration of oligodendrocytes (OLG) and has been used to model the demyelinating aspect of human conditions like multiple sclerosis (MS). The MS aetiology is unknown and no single animal model faithfully replicates the myriad of symptoms. Currently, there are two competing hypotheses regarding the pathophysiology underlying the initiation of MS: 'outside-in' and 'inside-out'. In this thesis, the broad objective was to develop an animal model of progressive demyelination reminiscent to MS. CPZ was used to induce OLG degeneration (termed oligodendrocytosis) and pertussis toxin (PT) was used to breach blood brain barrier (BBB) in order to test whether demyelination within the brain when combined with a breach of the BBB could trigger an adaptive immune response in the brain and thereby provide new evidence for an 'inside-out' hypothesis. The second broad aim was to investigate sensorimotor behavioural deficits and associated regulating pathways to find a link between CPZ-induced behavioural deficits and MS clinical symptoms. The results of the present thesis are presented in the following published manuscripts.

In paper I, I investigated whether oligodendrocytosis can trigger an adaptive immune response while the BBB was compromised. In this study, I combined the standard (0.2%) or half dose (0.1%) of CPZ-feeding for 5 weeks (or 12 weeks) with disruption of the BBB using PT. I found a concurrent marked loss of OLG (and consequent demyelination) and an increased innate immune response involving microglia and astrocytes at both time points. 5 weeks of 0.1% and 0.2% CPZ-feeding produced comparable oligodendrocytosis but a dose-dependent demyelination and gliosis, suggesting a slower onset and/or clearance of myelin debris following 0.1% CPZ. Even when the BBB was disrupted during CPZ-feeding, a detectable CD4/8 signal was not found in the brain. However, dose-dependent reductions in the splenic CD4/8 signals were observed following CPZ-feeding suggesting that peripheral immune function was compromised by CPZ-feeding. Having observed that a low dose of CPZ produced comparable oligodendrocytosis but had smaller effects on the peripheral immune system, the duration of low dose CPZ-feeding was extended to 12 weeks, with and without PT injection, to test whether a slower, progressive demyelination (i.e. more reminiscent of MS) could trigger an adaptive immune response in the CNS. Prolonged 0.1% CPZ-feeding produced comparable oligodendrocytosis, demyelination and suppression of splenic CD4/8 signal, but, once again, detectable CD4/8 signal was not found in the brain

suggesting that the peripheral action of CPZ is a major impediment to studying the role of the peripheral immune system following demyelination and disruption of the BBB. CPZ-feeding evoked changes in the whole brain proteome that mainly related to immune function, metabolism, cellular structure and synaptic function were observed. Notably, many of the CPZ-induced changes involved mitochondrial and endoplasmic reticulum functions indicating that internal biochemical/metabolic dysregulation is a potential key step in CPZ-mediated oligodendrocytosis.

In paper II, I reviewed the behavioural phenotypes observed in CPZ model and compared these to the clinical prevalence in MS patients. In this review, I identified a potential miss-match between the behavioural investigation using the CPZ model and the clinical prevalence of MS. Current behavioural tests in the CPZ model are focused mainly on motor, anxiety and cognition, but did not include all of the common MS clinical symptoms (e.g. pain and fatigue). Only a few studies have investigated other key symptoms such as pain, visual disturbances, fatigue and depression and none have examined symptoms such as sleep disturbances. I also found inappropriate use of behavioural instruments measuring deficits and suggested the appropriate application of instruments. In addition, I found that most of the histological correlations associated with behavioural deficits have focused on corpus callosum demyelination, which is inappropriate, rather than the functional relevant regions of the central nervous system (CNS). I suggest regionally relevant histological and biochemical analysis in order to validate the appropriate interpretation of behavioural deficits.

In paper III, whether CPZ changes in sensorimotor function are associated with changes (oligodendrocytosis, demyelination and gliosis) in functionally relevant structures of the sensorimotor pathways in the CNS were investigated. Within 2-3 weeks of CPZ-feeding, mice showed hyperactivity using the grooming and rearing tests and crossed the ladder more quickly compared to control mice. On both the ladder and beam tests, CPZ mice exhibited more foot slips compared to controls. In contrast, no changes in nociceptive thresholds to thermal or mechanical stimuli were seen between groups. Histological analysis showed a significant concurrent oligodendrocytosis, demyelination and gliosis in the cerebrum, cerebellum and brain stem. No loss of specific subpopulations of neurons or motoneurons staining was found but a significant increase in astrocyte staining was seen throughout the white matter tracts of all levels of the spinal cord. Importantly, components of the descending motor pathways in and around the cerebellar nuclei involved in motor function displayed

marked demyelination and gliosis, whereas these changes did not exist (except gliosis) in the regions associated with sensory pathways, such as the spinothalamic tract. The results suggest that CPZ induces subtle motor changes such as ataxia and that this is associated with deficits in CNS regions associated with motor and balance functions such as the cerebellum and brainstem.

In summary, the results of this thesis provide evidence for the ***first*** time that:

- Peripheral immune system suppression limits the migration of T-cells into the CNS in CPZ-fed mice even when the BBB is compromised.
- CPZ-induced mitochondrial stress is associated with the oligodendrocytes degeneration.
- Increasing the complexity of the locomotor tasks can detect early subtle motor behavioural deficits consistent with ataxia.
- Profound demyelination and gliosis in the deep cerebellar nuclei and brain stem regions were associated with motor and balance functions.
- Gliosis (but not demyelination) was observed in spinal cord white and grey matter regions but no changes were observed in nociceptive response using thermal and mechanical paw withdraw tests.

Invited talks and conference proceedings

This work has been disseminated at the following meetings (based on the most recent year of presentation):

1. *Shortland PJ, **Sen MK**, Almuslehi MSM, Coorssen JR and Mahns DA **(2019)*** Behavioural and histological changes in cuprizone-fed mice (**Poster**).
   Society for Neuroscience, Chicago, USA.
2. ***Sen MK**, Almuslehi MSM, Mahns DA, Coorssen JR and Shortland PJ **(2018).***
   Detection of early behavioral deficits in cuprizone-fed mice (**Poster**).
   Australasian Neuroscience Society, Queensland, Australia.
3. ***Sen MK (2018).***
   Use of 2D proteomics approach in cuprizone animal model (**Oral**).
   School of Medicine seminar, Western Sydney University, Australia.
4. ***Sen MK**, Almuslehi MSM, Myers SJ, Mahns DA, Coorssen JR and Shortland PJ **(2018).***
   Variability of oligodendrocytes loss and demyelination in the cuprizone-fed mice (**Poster**).
   HDR Showcase, Western Sydney University, Australia.
5. ***Sen MK**, Almuslehi MSM, Mahns DA, Coorssen JR and Shortland PJ **(2018).***
   Detection of early behavioural deficits in cuprizone treated mice (**Poster**).
   Health beyond research and innovation showcase, Warwick Farm, NSW, Australia.
6. ***Sen MK**, Shortland PJ, Myers SJ, Coorssen JR and Mahns DA **(2017).***
   Treatment with pertussis toxin does not induce a multiple sclerosis like phenotype in cuprizone-treated mice (**Poster**).
   Society for Neuroscience, Washington DC, USA.
7. ***Sen MK**, Almuslehi MSM, Shortland PJ, Myers SJ, Coorssen JR and Mahns DA **(2017).***
   Identification of differently expressed proteins in pertussis toxin injected cuprizone treated mice (**Poster**).
   HDR Showcase, Western Sydney University, Australia.
8. ***Sen MK**, Almuslehi MSM, Myers SJ, Shortland PJ, Coorssen JR and Mahns DA **(2017).***
   Identification of novel proteoforms in pertussis toxin-injected cuprizone-ingested mice (**Poster**).
   Inter-University Neuroscience and Mental Health, Western Sydney University, Australia.
9. ***Sen MK**, Shortland PJ, Myers SJ, Coorssen JR and Mahns DA **(2017).***
   Treatment with pertussis toxin does not reveal a multiple sclerosis-like phenotype in cuprizone treated mice (**Oral and Poster**).
   UNSW Brain Science Symposium, University of New South Wales, Australia.
10. ***Sen MK (2016).***
    Improve understanding the early stages of multiple sclerosis pathogenesis (**Oral**).
    Campbelltown hospital, NSW, Australia.

Chapter-1
INTRODUCTION

Abbreviations

APC	Adenomatous polyposis coli	LPL	Lipoprotein lipase
APO	Apolipoprotein	LRP	Lipoprotein receptor-related protein
ATP	Adenosine triphosphate	LYZ	Lysozyme
AMSC	Adipose mesenchymal stem cell	MAG	Myelin associated glycoprotein
PDGFR-α	Anti-platelet-derived growth factor alpha	MHC	Major histocompatibility complex
B6	C57BL/6	MMP	Matrix metalloproteinase
BBB	Blood brain barrier	MS	Multiple sclerosis
BDNF	Brain derived neurotrophic factor	MBP	Myelin basic protein
Calr	Calreticulin	MOG	Myelin oligodendrocyte glycoprotein
CD	Cluster of differentiation	NeuN	Neuronal nuclei
CNS	Central nervous system	NG-2	Chondroitin sulfate proteoglycan
CNPase	2′,3′-cyclic nucleotide-3′-phosphodiesterase	NGF	Nerve growth factor
CPZ	Cuprizone	NOGO A	Neurite outgrowth inhibitor A
DNA	Deoxyribonucleic acid	NOR	Node of Ranvier
EAE	Experimental autoimmune encephalomyelitis	NF-κB	Nuclear factor-kappa B
GFAP	Glial fibrillary acidic protein	OLG	Oligodendrocyte
GSTP 1	Glutathione S-transferase pi isoform	OPC	Oligodendrocyte progenitor cell
HMGCS	Hydroxymethylglutaryl-CoA synthase	Oligo	Oligodendrocyte transcription factor
IBA 1	Ionized calcium binding adaptor molecule 1	PLP	Proteolipid protein
IHC	Immunohistochemistry	PDGF	Platelet-derived growth factor
IgG	Immunoglobulin G	RCA-1	Ricinus communis agglutinin-1
IFN-γ	Interferon gamma	ROS	Reactive oxygen species
IGF	Insulin-like growth factor	RNS	Reactive nitrogen species
IL	Interleukin	TGF-β	Transforming growth factor beta
IP-10	Interferon gamma-induced protein 10	TLR	Toll-like receptor
ITG-β	Integrin beta	TNF-α	Tumour necrosis factor alpha
LGALS	Galactose-specific lectin	TSPO	Translocator protein
LIF	Leukaemia inhibitory factor	VEGF	Vascular endothelial growth factor

1.1 Cuprizone (CPZ) model

1.1.1 Chemical constituent and a brief history of CPZ animal model

Cuprizone (CPZ) is a chemical compound derived from a biochemical reaction of cyclohexanone and oxaldihydrazone [1, 2]. Its empirical formula and molecular weight are $C_{14}H_{22}N_4O_2$ and 278.36 respectively [3].

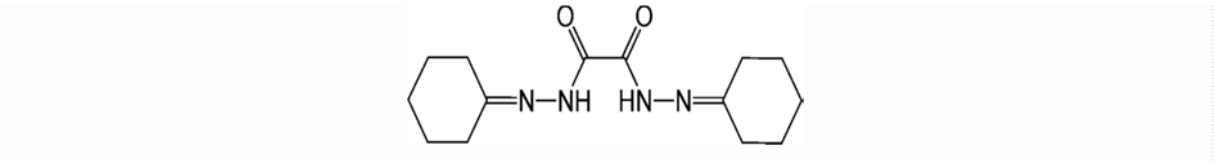

Chemical structure of CPZ (adopted from [1])

The first observations of the demyelinating properties of CPZ were reported in the early 1960s by W. Carlton in a series of studies [2, 4, 5]. In these studies it was found that CPZ-feeding caused growth retardation and demyelination in the cerebrum and cerebellum [2, 4, 5]. Later, it was identified that preferential loss of oligodendrocytes (OLG) resulted in demyelination and glial activation [6]. Three decades later, a detailed study from Hiremath et al. [7] showed the effective/optimum dose, duration and strain-dependent effects of CPZ on demyelination and glial activation [7]. Follow up investigations revealed that CPZ was preferentially toxic to mature OLG with regeneration of new OLG as the result of the proliferation of oligodendrocyte progenitor cells (OPC) when CPZ-feeding was stopped [8]. The gender equality of demyelination and glial reactivity in C57BL/6 (B6) mice strain was shown by Taylor and co-workers [9]. Despite the marked OLG degeneration, demyelination and innate immune involvement, only the inactive adaptive immune cells in the brain was observed [10]. Furthermore, CPZ appears to produce an atrophy of the peripheral immune organs [e.g. spleen and thymus, 11, 12, 13]. The milestones in the progression of the CPZ model are listed in **Table 1**.

Table 1: Milestones in the progression of CPZ model

Chronology	Milestone	Reference
1	Mice showed growth retardation, weakness and myelin loss in the cerebrum and cerebellum.	[4]
2	Astrocytes activation in the brain and cerebellum.	[2]
3	CPZ-feeding involved in the formation of mega/giant mitochondria in liver.	[14]
4	CPZ-induced OLG death resulting in secondary demyelination.	[6]
5	Astrocytes and microglia involved in the removal of vacuolated myelin.	[6]
6	CPZ-feeding depleted (e.g. monoamine oxidase and cytochrome oxidase) or elevated (e.g. succinate dehydrogenase) liver and brain mitochondrial enzymes.	[15]
7	Initiation of remyelination after removal of CPZ from chow.	[16]
8	0.2% CPZ-feeding for 4-5 weeks in B6 mice showed reproducible demyelination and glial activation.	[7]
9	Degeneration of mature OLG and regeneration of OPC in the corpus callosum once CPZ-feeding stopped.	[8]
10	CPZ-feeding was associated with the changes of lipid profile in brain (e.g. 30% reduction of brain cerebroside).	[17]
11	Microglia promoted OPC proliferation through the secretion of insulin-like growth factor (IGF-1/2).	[8, 18]
12	First quantitative assessment of behavioural (e.g. motor) changes using modern instrument (e.g. complex wheel).	[19]
13	Presence of inactive T-cell and absence of B-cell.	[10]
14	Chemically synthesized agent (e.g. IGF-1) increased OPC in the corpus callosum in CPZ-fed mice.	[20]
15	Marked loss of mature OLG, demyelination and glial activation in hippocampus.	[21]
16	Regional variability of glial response in the cerebrum.	[22]
17	'Bottom-up' proteomics approach showed majority of the altered proteins were involved in mitochondrial function.	[23]
18	Similar OLG degeneration, demyelination and glial response in both male and female B6 mouse strain.	[9]
19	A detail report on loss of mature OLG, demyelination and glial activation in cerebellum.	[24]
20	Lack of mature OLG loss, demyelination and glial activation in spinal cord.	[25]
21	No formation of glial scar in the acute and chronic phases of astrogliosis.	[26]
22	Astrocytes regulate microglial recruitment and lack of astrocytes (/knock-out) impairs phagocytic process.	[27]
23	Preferential toxicity to mature OLG whereas OPC, microglial and astroglial cells were protected *in vitro*.	[28]
24	Peripheral immune organs (e.g. spleen and thymus) atrophy.	[11-13]
25	'Top-down' proteomics approach showed changes in protein profiles in cortex, peripheral blood mononuclear cell and spleen.	[29]
26	Suppression of T-cell function implicated by reduction in protein disulphide isomerase (that participates in the assembly of major histocompatibility complex, MHC-I molecule).	[29]
27	Blood brain barrier (BBB) disruption using stereotactic application of lysolecithin or ethidium bromide did not infiltrate B or T-lymphocytes in the demyelinating areas (e.g. corpus callosum) after 5 week of CPZ-feeding.	[30]
28	Recruitment of peripheral immune cells (e.g. cluster of differentiation, CD3 T-cells) in the corpus callosum and secondary disease progressions (e.g. demyelination and inflammation) in 2 weeks CPZ-feeding once BBB was disrupted using pertussis toxin and immune system was boosted using complete Freund's adjuvant.	[31]
29	CPZ-induced changes in lipid distribution in corpus callosum did not recover entirely after remyelination suggesting progressive degeneration.	[32]

1.2 Oligodendrocytes degeneration in CPZ model

1.2.1 Oligodendrocytes (OLG)

Oligodendrocytes (OLG) represent ~70% of all glial cells in the central nervous system [CNS, 33]. OLG form a lipid-rich myelin sheath around axons with periodic gaps called nodes of Ranvier [NOR, 34, 35, 36]. The insulated axon allows rapid, saltatory conduction of electrical impulses between the NOR [34, 37-39]. The loss of OLG results in the demyelination of axons which compromises the speed of saltatory conduction. Moreover, the loss of myelin impedes the transfer of essential substrates (e.g. lactate) from OLG to axons (via monocarboxylate transporters) resulting in energy deprivation and axonal/neuronal degeneration [40-42].

OLG are mainly categorized into two types based on their proliferation, regeneration and myelinating properties (**Figure 1**). The first category is oligodendrocyte progenitor cells (OPC) that represent ~5-8% of the total numbers of cells in the CNS [43]. They originate during the embryonic development from neuro-epithelial cells in the sub-ventricular zone of the cerebrum [44, 45] and the dorsal portion of the spinal cord [34, 46, 47]. OPC are mitotic (similar to stem cells), highly proliferative leading to the generation of mature OLG [48]. Consequently OPC are the largest dividing cell population among glial cells [49, 50]. They are found throughout the CNS with numbers in the white matter that are 1.5 times higher than those found in the grey matter [49]. During demyelination OLG are lost/degenerate and OPC rapidly migrate to the injury sites and proliferate. These events are regulated by the expression of several transcription factors such as OLG transcription factors 1-2, myelin transcription factor 1 and SRY-box containing gene 10 [48]. The second category of OLG is the mature OLG, which is non-mitotic. They mature from OPC in a stepwise process [51, 52] that is regulated by many factors including, growth factors, neurotransmitters and transcription factors [50].

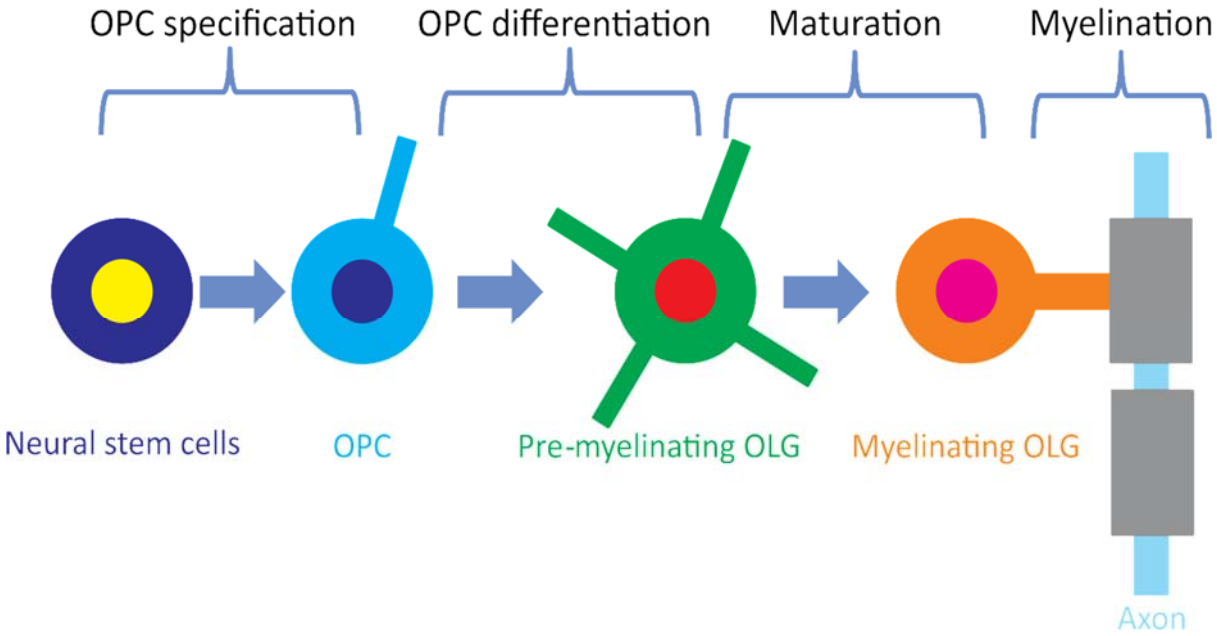

Figure 1: Stepwise process of development of OPC into myelinating OLG

Mature OLG are sub-categorized into four types (I-IV) based on their size, number of processes and function as summarized in **Table 2**. Both types I and II have small somata with type I generating 15-30 myelin segments in multiple adjacent axons and are found throughout the CNS [38, 53, 54]. Type II produces thin myelin and support medium diameter (60-70 µm) axons located mainly in the cerebrum and cerebellum [36, 53, 54]. Type III OLG have larger cell bodies, and ensheath a small number of larger diameter axons mainly in the cerebellum and spinal cord. Type IV OLG are mainly found in the brain stem and spinal cord, and are similar to Schwann cells of the peripheral nervous system in that they myelinate a single axon despite being of different embryonic developmental paths [36, 38, 53, 54]

Table 2: C**ategories of mature OLG**

Type	General characteristics	Schematic images	Main abundance	Reference
I	Small round cell body Large number of thin cellular process Produce thin myelin and support 15-30 short diameter axon		Throughout the CNS mainly in forebrain, cerebellum and spinal cord	[36, 53, 54]
II	Small cuboidal cell bodies and few thin cellular process Produce thin myelin and support medium (60-70 µm) axon		Mainly in white matters of cerebrum and cerebellum	[36, 53, 54]
Similarities between I and II	Support myelin volumes of approximately 500 μm^3 Intermodal length typically 50-150 µm		- -	[53]
III	Larger cell bodies than I and II One or two long cellular process Support medium axons thin myelin with longer intermodal length generally 200-500 µm	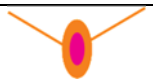	Mainly restricted in cerebellum and spinal cord	[36, 53, 54]
IV	Elongated cell bodies and longer process Generate thick myelin to support 1-3 large axon with very long intermodal length up to 1000 µm	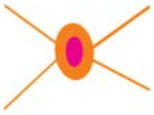	White matter of brain stem and spinal cord	[36, 53, 54]
Similarities between III and IV	Support myelin volumes of approximately 30,000 μm^3		-	[53]

1.2.2 Mechanisms of CPZ-induced OLG injury and cell death (oligodendrocytosis)

The mechanism of CPZ-induced OLG apoptosis remains ill-defined. A few lines of evidence have shown that CPZ is preferentially toxic to OLG both *in vitro* and *in vivo* [28, 55, 56]. As summarized in **Table 3**, CPZ ingestion causes an imbalance of essential ions such as copper, iron, zinc, sodium and manganese in the different parts of the body including brain and liver [3, 15, 57-59]. Ions imbalance leads to the perturbation of mitochondrial [12, 23, 28, 29, 60-62] and endoplasmic reticulum [29, 63-69] function. As a result, mega-mitochondria formation occurs in the liver, thymus, cerebrum and cerebellum [12, 61, 62, 70]. In addition, the function of mitochondrial enzymes such as superoxide dismutase, carbonic anhydrase II, monoamine oxidase and cytochrome C oxidase are suppressed [57, 71, 72]. These cumulative events decrease mitochondrial functions including adenosine triphosphate (ATP) synthesis and increase production of reactive oxygen (ROS) and nitrogen species (RNS) production [73]. Elevated concentrations of ROS and RNS enhance further the disruption of mitochondria and endoplasmic reticulum functions [63, 64]. Dysregulation of endoplasmic reticulum functions leads to a misfolded protein response and subsequently OLG stress [63, 74, 75]. Consequently, OLG apoptosis occurs due to decreased energy supply and lower levels of anti-oxidant enzymes to neutralize toxic products [e.g. ROS/RNS, 76, 77, 78]. Loss of myelin (i.e. demyelination) and the activation of microglia and astrocytes (i.e. gliosis) are the main consequences of loss or degeneration of OLG is termed as oligodendrocytosis [29, 79], which is also called oligodendrocytopathy [80, 81]. Activated innate immune cells (e.g. microglia) remove the myelin debris (termed phagocytosis) from the area of demyelination and, in the process, produce toxic substances such as ROS and RNS. Inappropriate (/failure) clearance of myelin debris from the sites of demyelination by microglia or the lack of microglial recruitment by the astrocytes further increase the production of ROS and RNS resulting in exacerbation of OLG degeneration [27, 82].

Table 3: Ion imbalance in CPZ-fed animal

Ion	Tissue	Condition	Reference
Iron	Serum:↓, liver:↑and corpus callosum:x	B6, oral feeding, 0.2%, 4 weeks	[59]
Copper	Blood:↓, liver:↓, kidney:x, cerebellum:x, hippocampus:x, cortex:x, thalamus:x and striaturm:x	B6, oral feeding, 0.2%, 6 weeks	[58]
Manganese	Blood:x, liver:↓, cerebellum:↓, striatum:↓, kidney:↓, cortex:x, hippocampus:x and thalamus:x		
Iron	Blood:x, liver:↑, kidney:x, cerebellum:x, hippocampus:x, cortex:x, thalamus:x and striaturm:x		
Zinc	Blood:x, liver:x, kidney:↓, cerebellum:x, hippocampus:x, cortex:x thalamus:x and striaturm:x		
Copper	Liver:x, kidney:↑, heart:↑, stomach:x, spleen:↑, large intestine:x, small intestine:↑, prosencephalon-mesencephalon:x, cerebellum:↑ and pons-medulla:↑	*CD mice, drinking water, 0.2%, 9 months	[3]
Zinc	Liver:↑, kidney:↑, heart:x, stomach:x, spleen:x, large intestine:↑, small intestine:↑, prosencephalon-mesencephalon:↑, cerebellum:↑ and pons-medulla:↑		
Sodium	Brain:↑	Swiss mice, 0.5%, oral feeding, 4 weeks	[15]
Potassium	Brain:↓		
Copper	Brain:↓		

Key: ↑, increase; ↓, decrease; and x, no change. *Only 3 months data was considered as CPZ studies mainly varies between 1-3 months.

1.2.3 Why are OLG vulnerable to CPZ?

Oligodendrocytes (OLG) are considered to be the most CPZ-sensitive glial cells in the CNS [8, 28, 76, 82] due to the following reasons. Firstly, mature OLG increase their surface area and increase gene expression during remyelination, and support axons up to 100 times that of their own weight [39, 76, 77, 83] by producing around 5000-50,000 μm^2 of myelin membrane with a volume up to 3×10^4 μm^3 [53, 84]. To execute this job, OLG use large amounts of ATP and oxygen. For example, to synthesize one gram of myelin it needs ~3.24×10^{23} ATP molecules [85]. An uninterrupted supply of energy from essential metabolites, such as glucose and lactate [86, 87], and a constant supply of oxygen is needed to avoid hypoglycaemia- or hypoxia-related damage to OLG [88]. Unfortunately, in both conditions, increased ROS and RNS are produced which increase the exposure of OLG to oxidative injury [76, 89]. Secondly, insufficient production of de-toxicant substances increases the vulnerability to oxidative injury. For example, glutathione has protective effects against oxidative stress [90, 91]. Compared with astrocytes or macrophages, OLG have three times less glutathione, thereby increasing their susceptibility to oxidative injury [89, 92] whereas astrocytes or macrophages remain viable [89, 93]. Moreover, OLG have low levels of metallothionein [94] and lower abundance of manganese superoxide dismutase [95] which also contribute to their vulnerability to oxidative stress. Thirdly, increased iron content in OLG increases iron-induced susceptibility to oxidative injury [96, 97]. OLG have 20 times more iron compared with astrocytes [92]. Moreover, OLG carry a large amount of iron storage protein ferritin [97]. Iron is essential for glycolysis, oxidative phosphorylation and the ATP production that is required to support myelin synthesis [97-99]. Increased intracellular iron concentrations in OLG lead to free radical production by the conversion of hydrogen peroxide to free-radical ions (via Fenton's reaction) and consequent damage to cellular membranes, proteins, DNA and lipid peroxidation [74, 100-103]. Finally, during myelination the normal process of protein assembly/folding in the endoplasmic reticulum is impaired [74] due to the increased iron and free-radical production that trigger an unfolded protein response [63, 104, 105]. Together, these events trigger the reduction of OLG function and exacerbation of apoptosis [106, 107].

1.2.4 CPZ is preferentially toxic to mature OLG over OPC and neurons

Both *in vitro* and *in vivo* studies have argued that mature OLG are more susceptible than OPC and neurons to CPZ-induced injury [28, 108-111]. CPZ concentrations from 20-500 μM did not have any effect on viability of neuronal cell lines (e.g. SH-SY5Y and GN11) and primary mixed glial cells (microglia and astrocytes) *in vitro* [28, 111]. In addition, primary cultures of cortical neurons from newborn Wistar rats were unaffected when bathed in buffer containing 200 μM of CPZ [111]. These results indicate that CPZ has no effect at these concentrations on neuronal cells *in vitro*. Likewise, *in vivo* studies showed that following 0.2% CPZ-feeding for 5-10 weeks, no loss of neuron was found in cortex, optic nerve and hippocampus [108-110] suggesting that neurons are resistant to CPZ-induced toxicity. One study, using fluoro-jade (a fluorescent marker of neuronal degeneration) found that following prolonged CPZ-feeding (0.2% for 12 weeks) leads to an ongoing neural degeneration when animals were examined at 17 weeks (5 weeks after the cessation of CPZ-feeding) in the hilus neurons of the hippocampus suggesting that neurons were primarily unaffected at early stages, whereas prolonged CPZ-feeding triggered a state of progressive neuronal degeneration [112]. ***Whether CPZ affects other neurons such as Purkinje neurons in the cerebellum and motor neurons in the spinal cord remains untested.*** In contrast, when mature OLG were incubated with as little as 50 μM CPZ, loss of OLG was evident and increased in a dose dependent manner whereas OPC were unaffected in the same CPZ dosing [28]; this sensitivity profile persisted when OLG/OPC were co-cultured with glial cells [55]. This relative toxicity of CPZ on OLG, vis-a-vis the relative insensitivity of OPC/neurones/glia was confirmed using mitochondrial staining. In mitochondria of mature OLG showed the reduction of mitochondrial transmembrane potential which is an indication of loss of mitochondrial function whereas intact mitochondria were present in OPC [28, 55]. Likewise, *in vivo* studies showed dose- and time-dependent CPZ-induced degeneration (and subsequent regeneration) of OLG [8, 82, 113]. In the 'acute' phase, following 0.2% CPZ-feeding for 5-6 weeks in B6 mice, loss of mature OLG starts in the first week of feeding with an increased number of OPC becoming evident, indicating that the latter are either unaffected by CPZ-feeding or that oligodendrocytosis is a strong stimulus for OPC proliferation and migration to the site of demyelination [8]. The reason for OPC insensitivity to CPZ is not clear, but may be related to the proliferative ability of OPC (similar to stem cell) compared to the post-mitotic and non-migratory status of mature OLG [51, 114]. In addition, "unknown internal protecting machinery" has been proposed for OPC to limit CPZ-induced mitochondrial injury [28, 60]. What happens in the longer feeding paradigm? In the 'chronic' phase when mice are fed with

0.2% CPZ for 12-14 weeks, an increased loss of mature OLG but OPC depletion was reported possibly due to toxicity induced by secretion of the inflammatory mediators (cytokines and chemokines) including tumor necrosis factor, interleukin-1β, interferon- γ, and nitric oxide resulting in longer lasting demyelination and irreversible remyelination [82].

In CPZ model, the detection and quantification of different stages of OLG development (e.g. mature or immature) are mainly accomplished immunohistochemically (IHC; **Table 4)** and with conventional myelin staining procedures such as Luxol Fast Blue (a copper phthalocyanine dye that binds to the lipoprotein components of the myelin sheath). For IHC, molecular marker/antibody based detection is used as each marker is expressed only in a particular stage of OLG development [74]. For example, the proliferating OPC can be recognised by the expression of anti-platelet-derived growth factor alpha (PDGFR-α) or the chondroitin sulphate proteoglycan (NG-2) markers [115] whereas differentiating OPC and mature OLG can be detected by the expression of transcription factor Olig-2 [115-117]. However, commonly used antibodies for mature OLG are adenomatous polyposis coli (APC), glutathione S-transferase pi isoform (GSTP1), 2′,3′-cyclic nucleotide-3′-phosphodiesterase (CNPase) or neurite outgrowth inhibitor A [NOGO A, 118, 119, 120]. Fully developed (i.e. differentiated) OLG are detected based on the expression of myelin proteins such as myelin basic [MBP, 27, 121], myelin oligodendrocyte glycoprotein [MOG, 122], myelin associated protein [MAG, 121] or proteolipid protein [PLP, 21] using their corresponding antibodies. In addition, conventional histology staining such as Luxol Fast Blue [23, 123, 124], Sudan Black [29] or Black Gold II [125, 126] are commonly used to measure myelin status (e.g. loss or subsequent regeneration) in the CNS. However, it has been shown that the Gallyas silver staining method is the preferred method used for myelin staining due to a higher signal-to-noise ratio of this technique compared to other staining methods. In this method, colloidal silver ions bind to the negatively charged side chains of the proteins such as myelin protein [127, 128]. What happens in the peripheral nervous system in CPZ-fed mice? Schwann cell (also called as neurilemma cell) plays similar role to wrap up the peripheral axon like OLG in the CNS. Whether CPZ degenerate schwann cell in the periphery is not investigated.

Table 4: Frequently used OLG markers in CPZ studies

Protein marker	Stage	Status in CPZ		Reference
		Acute	**Chronic**	
PDGFR-α	Proliferating/resting OPC	↑	↓	[115, 123]
NG-2	Proliferating/resting OPC	↑	↓	[22, 115]
Olig-2	Differentiating OPC and mature OLG	↓	↓	[115, 116]
APC	Mature OLG	↓	↓	[115, 123]
NOGO A	Mature OLG	↓	↓	[24, 129]
GSTP1	Mature OLG	↓	↓	[119]
CNPase	Mature OLG	↓	↓	[120]
MBP, PLP, MOG and MAG	Developed OLG	↓	↓	[27, 121, 122]

Key: ↑, increase and ↓, decrease

1.2.5 Variability of OLG degeneration in CPZ

Whether or not CPZ causes homogenous OLG loss throughout the CNS has not been systematically investigated. The existing literature suggests that a higher level of OLG degeneration is seen in the cerebrum and cerebellum. In cerebrum, the magnitude of CPZ-induced oligodendrocytosis is duration, dose of CPZ, and region-dependent. For example, there is significant loss of mature OLG in the corpus callosum by 2 weeks of CPZ-feeding [8] whereas, in the hippocampus it takes 3-4 weeks [21] suggesting regional variability. Following OLG loss, near complete demyelination (histologically detectable and statistically significantly different) in the hippocampus was seen after 5-6 weeks [21, 130] compared to 4.5 weeks in the corpus callosum [22]. Likewise, OPC recruitment to the demyelinating areas is greater by 4 weeks in the corpus callosum whereas in cerebral cortex it takes 4.5 weeks [22]. Interestingly, within the corpus callosum itself, there is a regional variation in OLG loss and demyelination. For example, 0.2% CPZ-feeding for 5 weeks shows limited changes in the rostral region whereas the caudal area of the corpus callosum was highly demyelinated [131]. In the cerebellum, loss of mature OLG is observed in CPZ-fed animals in both white and grey matter areas [24, 132, 133]. During the remyelination, the rostral regions such as the lingual cerebelli, and lobulus simplex recover faster than caudal regions such as the comissura cerebelli lobulus and lobulus paramedianus, reflecting regional variabilities in CPZ-induced pathological change [24]. In brain stem, reports have so far been inconsistent and unclear. For example, a decreased number of carbonic anhydrase II positive OLG [57], decreased myelin lipid content [17], reduced oligodendroglia [134], and vacuolation of the OLG cytoplasm [6] have been reported in the brain stem but no clear description of the status of mature or immature OLG in different areas of brain stem have been reported. In the spinal cord, the only two studies conducted reported no OLG loss [25, 60] ***suggesting that more detailed investigation is needed both in white and grey matter regions of the CNS to determine the regional distribution of CPZ-induced OLG loss***.

The age of an animal has a great impact on CPZ-induced OLG degeneration. In juvenile (3-4 weeks old) B6 mice, CPZ-feeding resulted in a reduction of mature OLG and an increased number of proliferating OPC in the corpus callosum after one week of feeding and reached a peak within 2 weeks of CPZ-feeding. In contrast, late initiation of OPC proliferation is observed in young adult mice [i.e. 6-7 weeks old, 129]. In older mice (i.e. 8 months old) no changes of mature OLG are observed [135] after 6 weeks of 0.2% CPZ-feeding. In another study, reduced regeneration of mature OLG from proliferating OPC was found when animals

were 12-16 months old [136]. The causes of age-related vulnerability of OLG de- and regeneration in the CPZ model are unknown. However, it can be inferred that the reduction of age-dependent immune regulation [137], decreased length of internodes [138] and decreased epigenetic modulation in older animals [139, 140] may regulate OLG loss and regeneration. The degree of OLG loss also differs between different strains of animal in different parts of the CNS regions. In cerebrum, greater OLG loss is found in the lateral corpus callosum than the midline corpus callosum in SJL mice [141]. Likewise, the cerebral cortex of CPZ-fed BALB/cJ mice showed less change compared to B6 mice whereas similar pathological changes are observed in the corpus callosum [142]. Moreover, both CD1 and B6 mice showed depletion of mature OLG upon CPZ-feeding but the severity was greater in B6 than CD1 in different CNS structures [e.g. corpus callosum and dorsal fornix, 121]. However, when higher CPZ concentrations such as 0.6% [124, 143], 1% [144, 145] and 2% [68] were used in larger species like rats a comparable levels of OLG and myelin loss were observed to that seen in mice. However, no single study using CPZ has systematically compared the oligodendrocytosis between strains (mice vs rat) and their underlying genetic make-up.

The variability apparent in the studies highlighted above could occur for several reasons. The distinct anatomical structure and variation in the density of OLG in different parts of the CNS structures may play a vital role in regional variability. For example, the number of NOGO A positive mature OLG [22] and NG-2 positive OPC are greater in the white (1.5 times) than the grey matter [49]. Similarly, the density of NOGO A positive OLG is lower in the cerebral cortex than in the white matter lobes of the cerebellum [24]. Secondly, the regional sensitivity may be due the operation of regionally specific, subcellular signalling pathways [38, 146]. For example, loss of the non-receptor tyrosine kinase Fyn (a signalling molecule of the Src kinase family) causes more hypo-myelination [147] in the brain than the spinal cord [148]. Likewise, mice haplo-insufficient for type III neuregulin-1 (a growth factor that promotes oligodendrocyte and Schwann cell development) showed less myelination in the corpus callosum but no effect on the optic nerve and spinal cord, further indicating regional differences in the regulation of OLG function and their susceptibility injury [149]. Whether the expression of Fyn or neuregulin-1 contributes to the regional heterogeneity of oligodendrocytosis in CPZ-fed animals remains untested. Another possibility for these effects could be that different regions of the CNS have different subtypes of OLGs based on biochemical profile and axon myelination. Most recently, RNAscope analysis showed 12 different subtypes of mature OLGs distribute not only differentially in the brain and spinal

cord but also respond differentially in response to injury [150]. The distribution of different OLG subtypes in the CNS may also contribute to the regional variability of OLG loss. In one study, increased degeneration of type I OLG was detected in the cortex [6]. ***However, the effect on other subtypes, especially type III and IV OLG, which are mainly present in the brain stem and spinal cord, remains untested.*** Fourthly, regional variabilities of mitochondrial function may play a role in susceptibility to OLG injury [60, 151]. For example, following 4 weeks of 0.2% CPZ-feeding there was a loss of mature OLG in the cerebrum whereas spinal cord OLG were intact despite the presence of similar changes in mitochondria complex IV and superoxide dismutase in both regions of interest [60] suggesting additional factors play a role in the degeneration of OLG. Moreover, it could also possible that differential absorption or entrance of CPZ into the different parts of the CNS evokes differential response to the OLG remains untested.

1.3 Immune response in the CPZ model

1.3.1 Innate immune response

Components of the innate immune system, such as microglia and astrocytes, rapidly respond to injury or infection [152, 153] with the response of these cells being used as markers of the effects of CPZ [82].

1.3.1.1 Astrocytes

Astrocytes, the 'glue' of the CNS, are characterized by the non-overlapping star shaped extensions from the cell body and comprise ~30% of the glial cells in the CNS [154-156]. They actively participate in numerous critical aspects of CNS development by regulating neurogenesis, synapse formation, propagation of action potential, BBB formation, neurotransmission, phagocytosis and developing brain circuits [155, 157, 158]. Based on cell morphology and anatomical locations, astrocytes are subdivided into two types: fibrous and protoplasmic. Fibrous astrocytes have small cell bodies, fewer processes and are mainly found in white matter. Grey matter dominant protoplasmic astrocytes have relatively more processes and larger cell bodies. In addition regional variations in morphology have been observed such as velate in the cerebellum and radial astrocytes in the spinal cord [159]. Reactive astrocytes may play either 'bad-A1' or 'good-A2' roles in the CNS as summarized in **Figure 2**. Upon activation, A1 astrocytes upregulate neurotoxic factors such as complement cascades. A1 astrocytes are abundant in various human neurological diseases including Alzheimer's, Huntington's, Parkinson's, amyotrophic lateral sclerosis and multiple

sclerosis [160]. A1 astrocytes secrete soluble, highly neurotoxic substances such as TNF-α and IL-1β/6 that degrade neurons and OLG through a caspase 2/3 dependent mechanism [155, 160]. In contrast, neurotrophic factors such as nerve growth factor (NGF), brain derived neurotrophic factor (BDNF), and leukaemia inhibitory factor (LIF) secretion by A2 astrocytes promote neuron growth and synapse repair [160]. A1 astrocytes can be detected by the expression of complement component C3 whereas A2 astrocytes can be detected by the expression of S100 calcium-binding protein A10 (S100A10) as shown before [160].

1.3.1.2 Astrocytes and CPZ

As a result of CPZ-feeding astrocytes become hypertrophic with enlarged somata and processes indicative of activation **(Figure 2)**. In CPZ model, strong astrocytic activation occurs both in cerebrum and cerebellum [21, 22, 24, 161]. In relation with the degree of OLG loss, the highest number of astrocytes response is observed by 4.5-5 weeks of CPZ-feeding [22]. During the remyelination, when new mature OLG are generated (via migration and maturation of OPC), astrocyte activation decreases [82]. However, how astrocytes become reactive and the roles of A1 and A2 phenotypes have not been defined in the CPZ model. When astrocytes secrete growth factors including IGF-1/2 and PDGF-α which promote OPC proliferation [82, 162] and recruit microglia is considered an A2 function [27] whereas the upregulation of the inflammatory mediators (e.g. cytokine IL-6 [163] and neuronal nitric oxide synthase [164]) are indications of A1 function. Measuring the expression of intermediate filament proteins such as glial fibrillary acidic protein (GFAP), vimentin and nestin, astrocytes are detected immunohistochemically [165, 166]. In the CPZ model, the activation of astrocytes is mainly detected using GFAP as a marker [26, 27], which is expressed predominantly on the processes of the astrocytes but with increasing astrocyte activation GFAP is readily detected in the soma [155, 165]. However, other intermediate filament protein markers, such as vimentin and nestin, also increase their expression in reactive astrocytes during CPZ-induced oligodendrocytosis [27, 167]. Detail information on these markers/antibodies is shown in **Table 5**

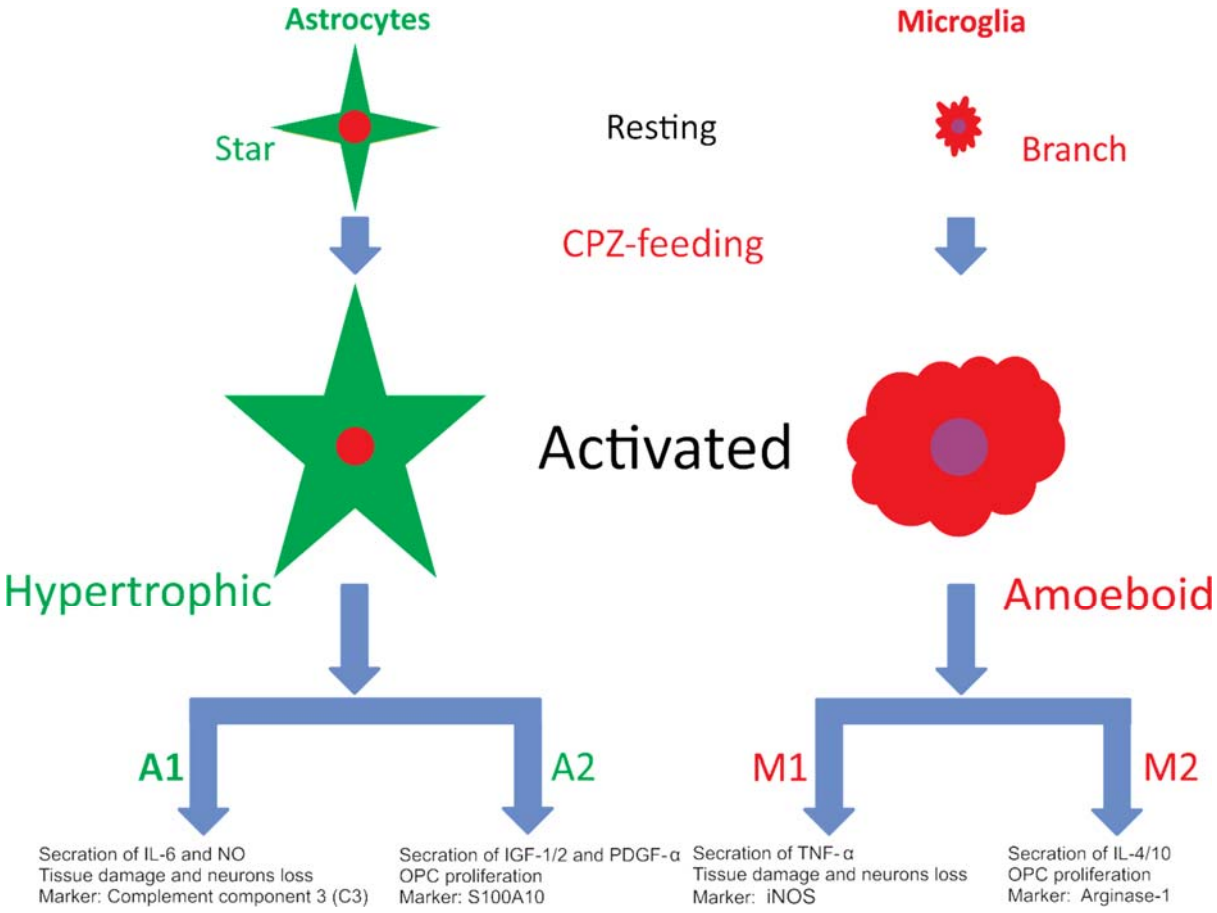

Figure 2: Different faces of astrocytes and microglia in CPZ model.
Quiescent astrocytes are normally star shaped. Upon CPZ-feeding, astrocytes become hypertrophied. Hypertrophied astrocytes secrete mediators which can be either beneficial (i.e. neuroprotective) or detrimental (i.e. cytotoxic). Astrocytes termed A2 produce protective effects whereas A1 astrocytes evoke cytotoxic effects. A2 astrocytes facilitate OPC proliferation by the secretion of IGF-1/2 or PDGF-α whereas NO and IL-6 are released from the A1 astrocytes to damage tissues and neurons. These different phenotypes can be detected using the differential expression of protein markers such as C3 for A1 astrocytes or S100A10 for A2 astrocytes. Likewise, in response to CPZ-feeding, microglia turn from a normal branch shape (resting stage) to amoeboid shape (activated stage). Activated microglia secrete both beneficial and detrimental cytokines. Like astrocytes, microglia are divided into 2 phenotypes. M2 microglia have anti-inflammatory actions by the production of IL4, IL10 and IL13. They help OPCs to proliferate and facilitate remyelination. M2 microglia can be detected using expression of the specific protein marker arginase-1. In contrast, M1 microglia

damages the tissue and neurons by the release of pro-inflammatory cytokines such as TNF-α, IL1β, IL6 and IFNγ; they can be detected using iNOS.

1.3.1.3 Microglia

Microglia are a resident population of cells in the CNS that are derived from the same mesodermal origin that gave rise to the peripheral immune system, including macrophages and monocytes [168-170]. Consequently, the presence of macrophages in the close vicinity of CNS lesions make it difficult to distinguish macrophages from activated microglia as both share a similar amoeboid shape and antigenic markers [65, 171]. Human microglia are, on average, 4.2 years old, and turnover at a median rate of ~28% per year with most (i.e. >96%) thus being renewed throughout the life span [172] by clonal expansion [173] and migration [174, 175]. In CNS, microglia constitute about 5-20% of the total glial cell population and total numbers range from 100-200 billion depending on health status [176-178]. As part of their homeostatic functions, microglial cell bodies remain immobile while the processes continuously scan the surroundings and communicate with other cells such as neurons and astrocytes [179]. In infection, degeneration or tissue injury, microglia can respond within one minute [180] and undergo morphological changes from normal 'branched' to active 'amoeboid' shapes [179, 181]. There has been considerable debate whether the innate immune response is detrimental or beneficial. In unfavourable conditions (e.g. tissue injury) microglia become activated (e.g. increased expression or proliferation) and polarized, playing both neuro-destructive M1 or neuroprotective M2 roles. As shown in **Figure 2** the 'classical M1' response is involved in pro-inflammatory effects to eliminate harmful intracellular substances such as microorganisms while the 'alternative M2' microglial response is to extracellular stimuli such as the clearance of myelin debris through phagocytosis [65, 182, 183].

1.3.1.4 Microglia and CPZ

Dose and time-dependent activation of microglia [7] occurs within the first week of CPZ-feeding, well before the histological detection of demyelination (at 3-4 weeks) in the corpus callosum, cerebral cortex, thalamus, basal ganglia, hippocampus and cerebellum [22, 161]. The microglial activation can be both 'M1' and 'M2' in the CPZ model and can be detected using the expression of specific markers such as interferon gamma-induced protein 10 (IFNγ-10) or iNOS for M1 and arginase-1 for M2 [65, 184-186]. M1 activation occurs mainly through triggering factors such as interferon (IFN)-γ, interleukin (IL)-12/23, tumour necrosis factor (TNF)-α, granulocyte and colony-stimulating factors, whereas the major stimulating factors in M2 pathways are IL-4/10, IgG and glucocorticoids [186-188]. Upregulation of toll-like receptor-4 (TLR-4), lysozyme (LYZ)-1/2, TNF-α and matrix metalloproteinase (MMP)-

12 are also considered as M1 responses. In addition, activated microglia in CPZ-fed mice secrete high amount of amino acid metabolites and reactive oxygen/nitrogen species [18, 189]. These substances exacerbate the OLG and tissue damage [65, 190]. Moreover, the increased expression of phagocytosis regulating genes such as lipoprotein receptor-related protein (LRP)-1, calreticulin (Calr), CD14 and integrin beta (ITGB)-2 and galactose-specific lectin (LGALS)-3 by microglia facilitate phagocytosis and the removal of myelin debris [190]. Moreover, increased expression of chemokine ligands (CXCL)-10/13, IGF-1/2, IL-1ß, transforming growth factor beta (TGFB)-1, vascular endothelial growth factor (VEGF)-a/b and platelet-derived growth factor (PDGF)-α/β from microglia facilitate OPC recruitment and differentiation [18, 184, 190]. The source of increased microglia numbers in CPZ-fed animals is unclear. It has been proposed that increased number of microglia in CPZ-fed animal arise due to local proliferation, recruited from the other sites of the CNS, or infiltrate from the peripheral blood circulation [10, 191]. Immunohistochemical staining of ionized calcium-binding adapter molecule 1 [IBA 1, a general microglial marker; 168], has been used widely to detect microglia in CPZ studies [116]. IBA 1 is a calcium-binding actin-cross-linking protein specifically expressed in microglia/macrophages, however, it does not differentiate between active and resting microglia [168, 192, 193]. To detect activated microglia, ricinus communis agglutinin-1 (RCA-1) 1 can be used [194]. Select antibodies can be used to detect peripheral macrophage CD68 [195] and CD45 [10] as shown in **Table 5**.

Table 5: Commonly used astrocytes and microglia markers in CPZ study

Cell type	Protein marker	Developmental stage	State in CPZ		Reference
			Acute	**Chronic**	
Astrocytes	GFAP	Reactive astrocytes	↑	↑	[26]
	Vimentin	Proliferating astrocytes	↑	↑	
Microglia	IBA 1	General microglia/macrophage	↑	↑	[116]
	RCA-1	Activated microglia	↑	↑	[194]
	Mac-3	Phagocytic microglia/ macrophage	↑	↑	[142]
		Proliferating microglia/macrophage	↑		[184]
	Ki67	Proliferating microglia/macrophage			
	CD45	Macrophage			[10]
	CD11b	Microglia/macrophage	↑	↑	[196]
	CD68/ED1	Mainly macrophage	↑	↑	[195]
Astrocytes/ microglia	Toll like receptor 2 (TLR2)	Astrocytes/microglia	↑	↑	[197]
	Nestin	Astrocytes/microglia	↑	↑	[22]
	Translocator protein (TSPO)	Astrocytes/microglia	↑	↑	[198]

Key: ↑, increase and ↓, decrease

1.3.1.5 Regional heterogeneity of glial activation

Whether the magnitude of gliosis is equally distributed throughout the CNS in the CPZ model has not been clearly defined. To date, it has been revealed that the pattern of astrocytes activation depends upon OLG degeneration, duration of CPZ-feeding and the specific location of the analysis within the CNS. In cerebrum, highest amount of microglial and astrocytes activation is found in the corpus callosum compared to cerebral cortex [22]. - ***Whether the magnitude of gliosis is equally distributed throughout the cortex (e.g. auditory, motor and somatosensory) has yet to be investigated.*** Likewise, in the cerebellum, highest activation of microglia are found at 4-6 weeks of CPZ-feeding whereas it takes ~8 weeks to become the highest activation of astrocytes in the cerebral cortex [24, 132]. ***In the spinal cord, no gliosis has been found in cervical and thoracic regions [25] but the lumbar region remains to be investigated***. Unfortunately, no description of the glial activation in the brain stem was found despite a thorough search of the literature. Known effects are summarised in **Figure 3**. The literature thus clearly indicates a regional variability in CPZ-induced gliosis which may arise from several factors. From the existing data, it has been found that the glial activation depends upon OLG loss. For example, the highest number of OLG loss occurs in cerebrum and cerebellum resulting in increased glial activation suggesting first OLG loss then glial activation. In contrast, in spinal cord, no loss of OLG is found and no glial activation noted. ***Based on the limited studies in spinal cord and brain stem, it is not possible to draw a clear conclusion about the regional sensitivity of OLG and glia to CPZ, suggesting additional investigation is needed whether or not CPZ induced toxicity is regionally distributed or not***.

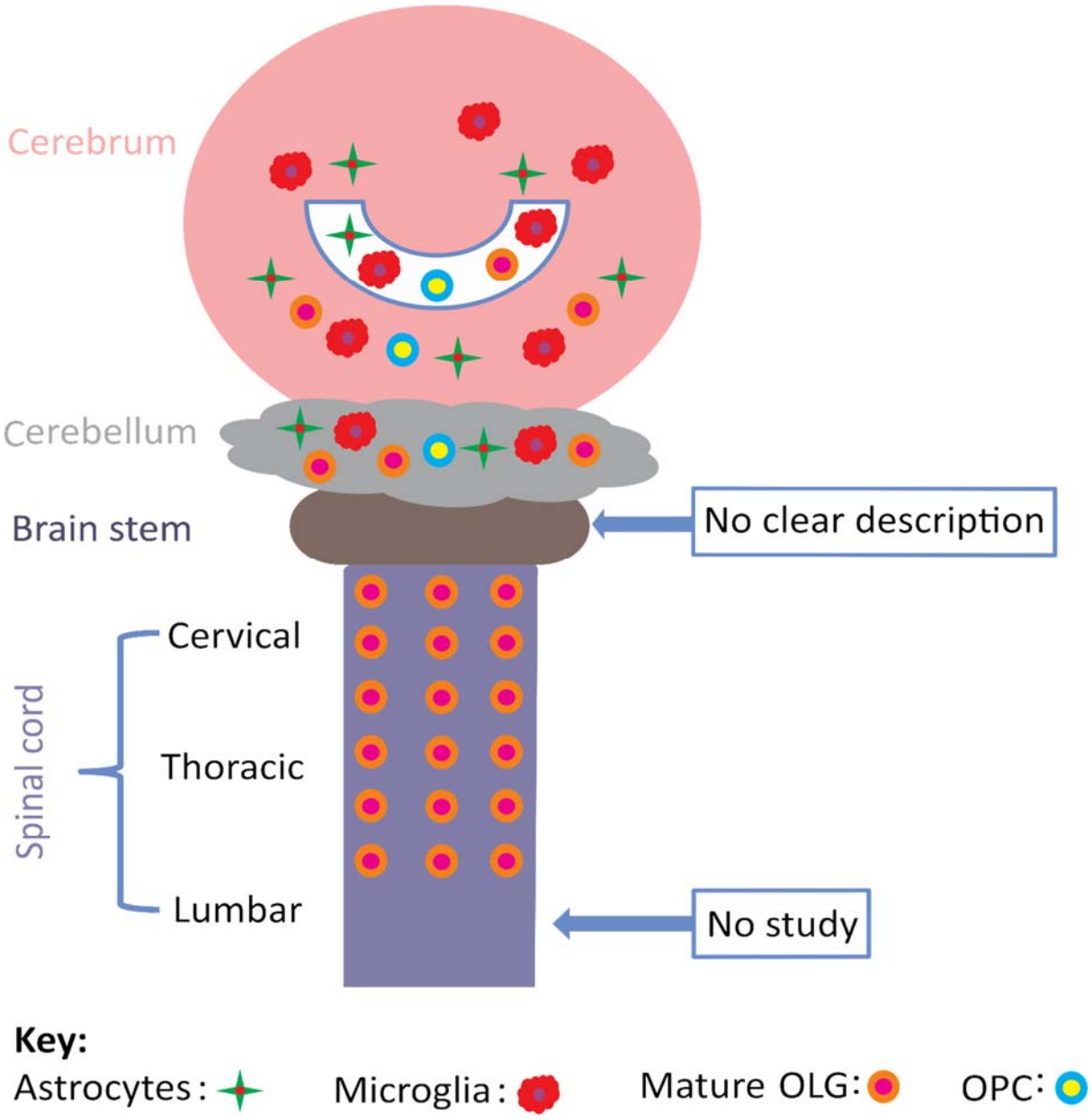

Figure 3: Regional variability of CPZ outcome.

CPZ causes concurrent loss of mature OLG and the activation of microglia and astrocytes in the cerebrum and cerebellum. Migration of OPCs to the demyelinating site leads to local increases in OPC number and regeneration of mature OLG. Regeneration of new OLGs facilities wrapping the unmyelinated axons resulting remyelination. Many publications have investigated changes in the conducted in cerebrum and cerebellum in the CPZ model. However, only a few studies were concentrated in the brain stem. Unfortunately from these studies no investigation has shown clearly the effect of CPZ-feeding on demyelination, OLGs de- and regeneration, or gliosis. Likewise, a very limited number of studies were conducted in the spinal cord. These studies showed no loss of OLG and glial activation in cervical and thoracic regions [25, 60]. However, lumbar spinal cord remains to be investigated. This differential outcome of OLGs de- and regeneration and glial activation followed by CPZ-feeding suggests a regional heterogeneity in the CNS.

1.3.2 Adaptive immune response

Despite oligodendrocytosis, demyelination and glial activation, there is no apparent involvement of peripheral adaptive immune cells during 4-5 weeks of CPZ-feeding; notably, the BBB remains intact [10, 30]. Flow cytometry analysis showed the presence of inactive T-cells, but no B-cells in the corpus callosum during CPZ-feeding and recovery phases [10]. In addition, IHC staining for the pan T-cell marker (termed CD3) showed few T-cells in the corpus callosum in CPZ-fed animal [190]. An absence of B- and T-cells at demyelinating sites, such as the corpus callosum and cerebral cortex, persisted even when the BBB was breached using stereotaxic injection of ethidium bromide or lysolecithin in mice fed with CPZ for 5 weeks [30]. However, combining transient CPZ-feeding (2 weeks) with breach of the BBB and a peripheral '*immune booster'* (complete Fraud's adjuvant) led to CD3 infiltration of the brain and a secondary demyelination and inflammation process mediated by T-cells [31]. The immunogenicity of the myelin fragments appears to be enhanced by post-translation modification of the parent molecules (where arginine is converted to citrulline) through the processes of citrullination as demonstrated in animal [199] and human studies [200]. ***Whether the failure to initiate an immune response with prolonged feeding (≥5 weeks) is due to a suppressive toxic effect of CPZ on the peripheral immune system is unclear***.

1.4 Multiple sclerosis (MS)

The BBB separates the CNS from the peripheral immune system. In most MS patients, the BBB is compromised and free access of adaptive cells into the CNS is observed [201, 202]. Immune cells inside the CNS become reactive and create neuro-inflammation that leads to demyelination and axonal damage [203, 204]. Approximately 2-5 million people worldwide suffer from this disease [205, 206]. Unfortunately, till now, the underlying causes of MS are not clearly known. Environmental factors (e.g. deficiency of vitamin D, smoking and viral infection) and genetic susceptibility (e.g. major histocompatibility complex, MHC I-II) are suggested as possible initial triggers [203, 204, 207, 208]. The clinical features of MS are the presence of two or more episodes of demyelinating lesions (~95% patients) in the brain and/or spinal cord and the presence of oligoclonal immunoglobulin G (IgG, ~90% patients) in cerebrospinal fluid [203, 207]. The pattern of demyelination and inflammation is largely heterogeneous in MS [209-212]. All active lesions show profound reduction of myelin proteins such as MBP, MOG, PLP and MAG. In addition, infiltration of T-lymphocytes and macrophages into the demyelinating sites are found. These lesions are categorised into four

patterns (I, II, III and IV) depending upon the presence of immunoglobulin, activation of the complement cascade, OLG degeneration pattern, distribution of myelin protein loss and extent of demyelination (**Table 6**). Type I and II lesions are defined by the involvement of immunoglobulin G/complement complexes, with limited OLG dystrophy, whereas type III and IV lesions are defined by the marked apoptosis and depletion of mature OLG and an intact BBB [209-211].

Table 6: Heterogeneity of MS

Patterns I and II:

Similarities:

- Disruption of BBB which is confirmed by the presence of IgG
- Plaques are centred on small veins and showed sharply demarcated edges with peri-venous extensions
- Presence of remyelination shadow plaques (complete remyelinated lesions)
- Presence of T-lymphocytes and macrophages
- Less OLG damage
- Similar pattern of loss of myelin proteins (MBP, PLP, MOG and MAG)

Dissimilarities:

- Pattern I is found mainly in acute MS (patients who die or are subjected to biopsy within the first year after disease onset) whereas pattern II occurs mostly in acute, relapsing remitting MS, secondary progressive MS and primary progressive MS
- Deposition of complement complex (part of immune system promoting phagocytosis and inflammation) is only found in pattern II lesions

Patterns III and IV:

Similarities:

- Absence of remyelination shadow plaque
- Presence of T-lymphocytes and macrophages
- Large numbers of OLG damaged
- Demyelinating lesions are around inflamed vessels
- Absence of IgG and complement complex

Dissimilarities:

- Preferential loss of MAG in pattern III
- Pattern III lesions are mostly found in patients with acute MS whereas pattern IV are found in primary progressive MS with prominent cognitive, cerebellar and brainstem involvement.

A long-standing unresolved question, however, is what initiates demyelination [213, 214]? Two alternative theories have been proposed: the first is termed 'outside-in' because of infiltration of autoreactive peripheral immune cells into the CNS is thought to be the causative factor; the second is termed 'inside-out' as demyelination resulting from internal metabolic disturbances is thought to initiate the disease cascade, leading to inflammation that then recruits autoimmune cells into the CNS [31, 213-215]. These alternate models of MS initiation are summarized in **Figure 4**. 'Outside-in' theorists propose that the dysregulated peripheral immune system leads to an autoimmune response against components of myelin in the CNS [216, 217]. This theory has been developed and tested using the experimental autoimmune encephalomyelitis (EAE) animal model [216, 217]. In EAE, animals (i.e. mainly mice) are immunised with exogenous antigens (e.g. either MBP, PLP or MOG) and also peripherally injected with complete Freund's adjuvant (CFA) to activate peripheral immune cells, including T- and B-cells. When these procedures are combined with a breach of the BBB (e.g. by pertussis toxin (PT) injection), autoreactive adaptive immune cells from the periphery migrate into the CNS resulting in degeneration of OLG, demyelination and gliosis [216, 217]. It is argued that a similar process results in autoimmune cell migration into the CNS in MS [218-220]. However, there are several key differences between the EAE model and clinical MS. First, the autoimmune response in humans occurs spontaneously, whereas in EAE the immune response is initiated in the periphery by the administration of exogenous antigens (MBP/PLP/MOG) and immune activators [221, 222]. Second, $CD8^+$ T-cells are the predominant immune cells in MS whereas in EAE, $CD4^+$ T-cells predominate [223, 224] [225, 226]. Moreover, the spinal cord is the main demyelinating site in EAE [217, 227, 228] whereas MS is a disease of the human cerebral and cerebellar cortex. Although therapies developed in EAE improve outcomes in animals, these therapies generally have more limited success in clinical MS in terms of stopping disease initiation and progression [221, 229].

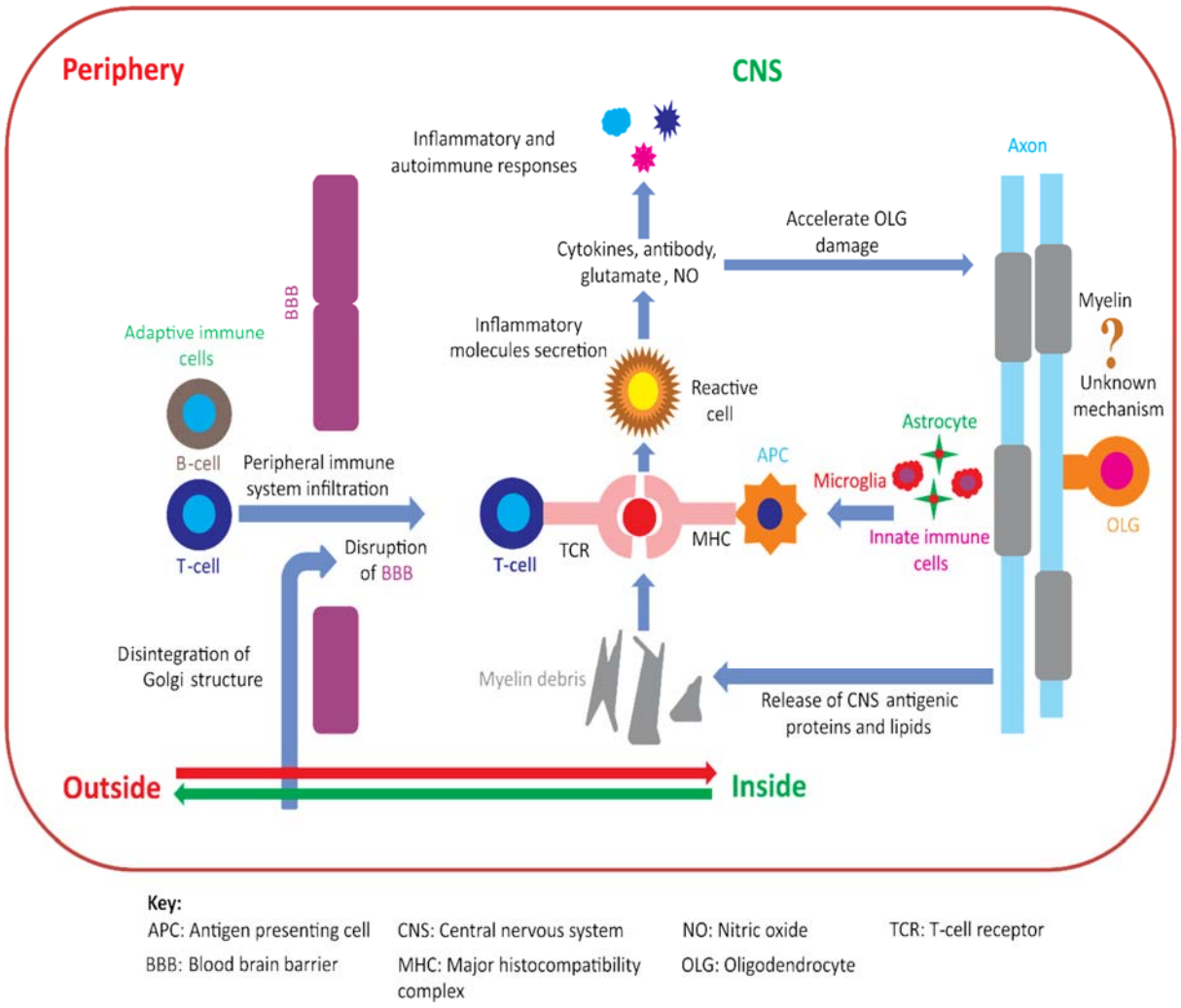

Figure 4: Initiation of oligodendrocytosis and autoimmunity in MS.
Two competing theories exist. In the 'Outside-In' theory, an unknown trigger leads to peripheral adaptive T- and/or B-cells entering into the CNS following a disruption of the BBB. T-cells inside the CNS cause OLG apoptosis resulting in destruction of the myelin sheath and production of damaged myelin. Innate astrocytes and microglia present myelin debris as an antigen to T-cells and exacerbate the process of OLG damage. In contrast, in the 'Inside-Out' theory, damage to OLG inside the CNS leads to oligodendrocytosis with the ensuing glial response (and consequent cytokines and chemokines released) leading to compromised BBB that allows peripheral immune cells access to the CNS. Once within the central CNS, T-cells (CD4 and CD8) cells interact with APC, via the MHC, and become reactive.

Due to the inability of the EAE model to address questions about the initial events in the generation of auto-reactivity and the progression of MS, recent work has focused on the 'inside-out' theory and the need to develop a new animal model. In support of the 'inside-out' theory, it has been shown that extensive OLG loss occurs without disruption of the BBB in MS patients with type III and IV lesions [209, 210]. Notably, only a few inflammatory parenchymal T- and B-cells were found in the active demyelinating sites in the brain [230, 231]. Moreover, abnormal white matter exhibits reduced myelin density, extensive axonal loss and chronic fibrillary gliosis without focal inflammation [232]. Furthermore, ablation of MS patient's immune system followed by replacement with autologous haematopoietic stem cell transplantation (e.g. T cell depleted and CD34 selected autologous peripheral blood stem cell transplantation) while halting the autoimmune response did not stop demyelination, markers of axonal damage (amyloid precursor protein) and disease progression [233]. In contrast to these observations that are typically seen during late stages of disease, in the initial stage of MS, myelin degeneration or abnormality begins at the inner sheath and may occur at sites where there is no evident inflammation, suggesting the operation of processes that are not inevitably linked to inflammation and immune autoreactivity [234]. Additionally, therapies that target suppression of immune function - e.g. Priliximab (cMT 412), Glatiramer acetate, Natalizumab (Tysabri®) and Alemtuzumab (Lemtrada®) - while effectively suppressing the autoimmune reactions (e.g. decreasing the number of relapses in the relapsing remitting MS), have little or no effect during the progressive phase suggesting that alternative mechanisms underpin disease initiation and progression in MS [229, 235]. Recent studies in animal models have shown that the degeneration of OLG can trigger a secondary immune response suggesting that the earliest events in MS may occur without autoimmune involvement [31, 215].

Hypothesis and Objectives

The broad objective of this thesis was to develop an animal model to explore the very early stages of demyelination that may be associated with conditions such as multiple sclerosis (MS). Cuprizone (CPZ) was used to induce degeneration of OLG to model the processes of demyelination in the absence of adaptive immune cell infiltration. Whether breaching the blood brain barrier (BBB) results in infiltration of adaptive immune cells into the CNS is not clearly defined in the CPZ model. Therefore, to further test the 'inside-out' theory of MS, it was hypothesized that disruption of the BBB would lead to infiltration of adaptive immune cells into the CNS in response to CPZ-induced oligodendrocytosis.

Objectives:

- Quantification of OLG and myelin in the brain
- Quantification of microglia and astrocytes in the brain
- Quantification of CD4 and CD8 T-cell signal intensity in brain and spleen
- Quantification of whole brain proteome changes

The behavioural deficits associated with CPZ-induced demyelination and relevant CNS structures are not clearly defined. I hypothesized that demyelination in the sensorimotor network is associated with behavioural deficits and that increasing the complexity of the motor assessment tasks will detect subtle locomotor deficits during the early phases of CPZ-feeding. Therefore, the second broad aim of this thesis was to measure behavioural deficits and identify regulating pathways associated with those deficits.

Objectives:

- Investigation of motor behavioural deficits using different locomotor tasks of varying complexity
- Investigation of nociceptive behaviour using flexion withdrawal reflex threshold tests
- Quantification of OLG and myelin in CNS white and grey matter regions
- Quantification of microglia and astrocytes in CNS white and grey matter regions
- Quantification of neurons in the cerebellum and spinal cord

Chapter-2

MATERIALS AND METHODS

Abbreviations

2DE	Two-dimensional gel electrophoresis	LST	Lateral striatum
Ab	Antibody	LVN	Lateral vestibular nucleus
AFD	Automated frozen disruption	M1	Primary motor cortex
AC	Anterior commissure	M2	Secondary motor cortex
ANOVA	Analysis of variance	MBP	Myelin basic protein
APC	Adenomatous polyposis coli	MCC	Midline corpus callosum
AU	Auditory cortex	MCP	Middle Cerebellar peduncle
B6	C57Bl/6	MP	Membrane protein
BBB	Blood brain barrier	MST	Middle striatum
BSA	Bovine serum albumin	MVN	Medial vestibular nucleus
Calb	Calbindin	MW	Molecular weight
CCBB	Colloidal coomassie brilliant blue	NeuN	Neuronal nuclei
CCX	Cerebellum cortex	NOGO A	Neurite outgrowth inhibitor A
CD	Cluster of differentiation	OCT	Optical cutting temperature
Ctrl	Control	OLG	Oligodendrocyte
CY	Cylinder	OPT	Optic tract
CHAPS	3-((3-cholamidopropyl) dimethylammonio)-1-propanesulfonate	PANTH ER	Protein analysis through evolutionary relationships
ChAT	Choline acetyltransferase	PBS	Phosphate buffered saline
CPZ	Cuprizone	PFA	Paraformaldehyde
CNS	Central nervous system	*pI*	Isoelectric point
CV	Cerebellar vermis	PN	Prepositor nucleus
CVN	Cerebellar vestibular nucleus	PT	Pertussis toxin
DAPI	4′,6-diamidino-2-phenylindole	PYT	Pyramidal tract
DAVID	Database for annotation, visualization and integrated discovery	PVDF	Polyvinylidene difluoride
DF	Dorsal funiculus	RN	Red nucleus
DFX	Dorsal fornix	RR	Rotarod
DH	Dorsal horn	ROI	Region of interest
DLF	Dorsal lateral funiculus	RPM	Revolutions per min
DN	Dentate nucleus	RSD	Relative standard deviation
DPA	Dynamic plantar aesthesiometer	S1FL	Primary somatosensory front limb
DTT	Dithiothreitol	S1HL	Primary somatosensory hind limb
EAE	Experimental autoimmune encephalomyelitis	S2	Secondary somatosensory
EC	External capsule	SCP	Superior cerebellar peduncle
GFAP	Glial fibrillary acidic protein	SDS	Sodium dodecyl sulphate
GO	Gene ontology	SEM	Standard error of the mean
HEPES	4-(2-hydroxyethyl)-1-piperazineethanesulfonic acid)	SN	Substantia nigra
HP	Hippocampus	SP	Soluble protein
HR	Hargreaves	SPVN	Spinal vestibular nucleus
HTH	Hypothalamus	STRING	Search tool for retrieval of interacting genes/proteins
IBA 1	Ionized calcium-binding adapter molecule 1	SUVN	Superior vestibular nucleus
IC	Internal capsule	TBST	Tris buffered saline-tween 20
ICN	Inferior colliculus nucleus	TH	Thalamus
ICP	Inferior cerebellar peduncle	TBP	Tri-butyl phosphine
IEF	Isoelectric focussing	VF	Ventral funiculus
IPN	Interposed nucleus	VH	Ventral horn
IP	Intraperitoneal	VI	Visual cortex
IPG	Immobilised pH gradient	VLF	Ventral lateral funiculus
IS	Inverted screen	VP	Ventral pallidum
KEGG	Kyoto encyclopaedia of genes and genomes	WB	Western blot
LCC	Lateral corpus callosum		
LC/MS/MS	Liquid chromatography mass spectrometry		

2.1 **Suppliers and materials**

Suppliers	**Materials**
Amresco, USA	Urea, Thiourea, HEPES, CHAPS, CBB, Triton X100, Sodium azide, Ammonium sulphate, Mineral oil, Tween 20, Tris, Tris-glycine-SDS electrode buffer, Glycerol and BSA
Sigma-Aldrich, USA	Polyvinylpyrrolidone, Formalin, Goat serum, PFA, CPZ, PT, PBS, EDTA, EGTA, Ammonium bicarbonate, Protease and Phosphatase inhibitors
Bio-Rad, USA	Protean IEF Cell, Electrophoretic tank, IPG strip, Ampholytes, PVDF, Acrylamide, TBP, Bromophenol blue, Agarose, Focussing tray and 2DE standard
Merck, Germany	Acetic acid, Acetic anhydride, SDS, Acetonitrile and Mounting medium
Abcam, UK	Goat anti-rabbit IgG H&L (HRP), Goat anti-rabbit IgG H&L (HRP), Rabbit anti-CD4, Rabbit anti-β-actin, Rabbit anti-CD4, Alexa Fluor 488 conjugated rabbit anti-ChAT and Mouse anti-MBP
Invitrogen, USA	Rat anti-CD8, Alexa Fluor 594 conjugated goat anti-rabbit IgG and Alexa Fluor 488 conjugated goat anti-rat IgG
Waters, USA	Formic acid, Mass spec glass vial, NanoAcquity ultra performance liquid chromatography, Xevo QToF mass spectrometer, C18 Symmetry trapping column and C18 BEH analytical column
Merck-Millipore, USA	Alexa Fluor 488 conjugated mouse anti-GFAP, Rabbit anti-NOGO A, 3 Kd cut-off filter column, Luminata Crescendo Western HRP Substrate, Rabbit anti-APC and Mouse anti-NeuN
Santa-Cruz Biotechnology, USA	Mouse anti-CD8 and Mouse anti-mouse IgGκ BP-HRP
Chem-Supply, Australia	Silver nitrate, Gelatine, Ammonium nitrate, Sodium carbonate and Chromium potassium sulphate dodecahydrate
Astrol Scientific, Australia	Ethanol, Methanol and DTT
VWR, USA	Xylene, Pyridine and Vortex
Sino Biological, USA	Mouse CD4 and CD8 recombinant protein (His Tag)
Promega Corporation, USA	Trypsin
Vector Laboratories, USA	Vectasheild plus 4′,6-diamidino-2-phenylindole
Tory laboratories, Australia	Sodium pentabarbitone
Cenvet, Australia	Isoflurane
Camlab, UK	Whatman paper
Bio-chemicals, Australia	Sodium chloride
Wako, Japan	Rabbit anti-IBA 1
Life Technologies, USA	EZQ™ Protein Quantitation Kit
BDH chemicals, UK	Potassium ferricyanide
Knittel Glass, Germany	Slide and Cover slip
Sakura, USA	6-well plate, OCT and Cryomold
Coles, Australia	Skimmed milk and Sucrose
Animal Resources Centre, Australia	C57Bl/6 mice

Gordon's specialty stockfeeds, Australia	Mice chow
Tecniplast, Italy	Animal home case (GM500)
Corning Incorporated, USA	Falcon tube and Microtips
GE Healthcare, USA	FLA-9000 and LAS-4000
Bioseb, France	Dynamic plantar aesthesiometer and Hargreaves apparatus
Peri-Star, China	Perfusion pump
Sartorius, Germany	Mikro dismembrator
Zeiss, Germany	Olympus microscope
Leica, Germany	Cryostat
UGO Basile, Italy	Rotarod
Beckman Coulter, USA	Ultracentrifuge
John Morris Scientific, Australia	Speed Vac
Logitech, China	C525 HD Webcam
Thermo Scientific, Australia	-80°C freezer
Electrical balance	Adam, Australia
NIH, USA	ImageJ
DECODON, Germany	Delta 2D
GraphPad prism, USA	GraphPad Prism
CorelDRAW, Canada	CorelDRAW
FUJIFILM Corporation, Japan	MultiGauge
Adobe, USA	Adobe Photoshop

2.2 **Methods**

2.2.1 Animals and housekeeping

Male C57BL/6 (B6) mice were purchased from Animal Resources Centre, Australia (www.arc.wa.gov.au). As B6 mouse produces reproducible demyelination and gender indifference [7, 29, 82, 141], this strain was used throughout (studies I-III). Mice were acclimatised for one week to adapt to their new environment prior to the start of a study. Basic enrichments including nesting material (crinkle nest) and a pipe tube (polyvinyl chloride) were provided. Animals were maintained on a 12 hours light/dark cycle (8am-8pm light; 8pm-8am dark, 50-60% humidity and 21-23°C room temperature, RT) throughout the entire period. Mice were housed in pairs in individual GM500 ventilated cages (Tecniplast, Italy) that measured 40.5x20.5x18.5 cm. Research and animal care procedures were approved by the Western Sydney University animal ethics committee (A10394/A11938) in accordance with the Australian Code of Practice for the Care and Use of Animals for Scientific Purposes as laid out by the National Health and Medical Research Council of Australia. Three independent studies were carried out and the total number of animals used is summarized in **Table 1**.

Table 1: Number of animals and key focus of studies

Study	Number of animals	Age	Intervention (feeding)	Main focus of analysis
I	60	6 week	5 weeks	Behaviour, histology, western blot and proteomics
II	48	6 week	12 weeks	Behaviour, histology, western blot and proteomics
III	20	4 week	5 weeks	Behaviour and histology

2.2.2 Cuprizone (CPZ)-feeding (used in studies I-III)

Oral CPZ-feeding ([Bis(cyclohexanone)oxaldihydrazone], Sigma-Aldrich, USA) was used to induce oligodendrocyte (OLG) degeneration and demyelination as previously described [8, 29, 82, 113]. Standard rodent powder chow (Gordon's Specialty Stockfeeds, Australia) with and without CPZ was prepared freshly each day and provided (along with water) *ad libitum.* Naïve, control (Ctrl) mice received normal food without CPZ for the entire period. Age and weight matched animals were used for CPZ and Ctrl groups. The dose and duration of feeding are summarized in **Table 2**.

Table 2: CPZ-feeding in different studies

Study	Intervention	Feeding dose (w/w)
I	5 weeks feeding	0.1 and 0.2% CPZ
II	12 weeks feeding	0.1% CPZ
III	5 weeks feeding	0.2% CPZ

2.2.3 Pertussis toxin (PT) injection (used in studies I-II)

Three doses of 400 ng of PT (Sigma-Aldrich) dissolved in 200 µl of 0.01 M phosphate buffered saline (PBS, Sigma-Aldrich) were injected intraperitoneally (IP) to breach the blood brain barrier [BBB, 236, 237-239]. This is the same dose used to breach the BBB in the experimental autoimmune encephalomyelitis model [EAE, 236, 237, 238]. All PT+CPZ groups (PT+0.1% and PT+0.2% CPZ) received CPZ and three injections of PT on day 14th, 16th, and 23rd of CPZ-feeding. Age matched PT controls (with no CPZ) received three injections of PT on day 14th, 16th, and 23rd. PT injections were timed to coincided with the onset of CPZ-mediated oligodendrocytosis and gliosis [7, 8, 82]. The evidence of BBB breach using PT was assessed using horseradish peroxidase-substrate staining in the follow up study from our lab [240].

2.2.4 General monitoring of animal health (studies I-III)

Mice were weighed using an electrical balance (Adam, www.adamequipment.com, Australia) at the beginning of all studies, throughout the feeding period (at 3-7 days interval) and prior to culling to assess the impact of CPZ-feeding and PT injections on weight gain. Throughout the studies, all mouse activities daily monitoring for signs of abnormal posture, gait and body condition were conducted.

2.2.5 Spontaneous activities test (study III)

The number of rears (vertical activity) and grooming events (fur licking and limb scratching) were measured quantitatively using cylinder (CY) test by the same trained observer. In this test, mice were placed in a transparent plastic CY (14 cm high and 10.5 cm diameter) 14 cm above the bench surface for 2 minutes. Each trial (n=3/time point, with 1 hour, h rest between trials) was recorded (Logitech C525 HD Webcam, China) and individual events counted manually.

2.2.6 Behavioural assessments (studies I-III)

Behavioural assessments of different mice groups were carried out in a blinded manner by same trained observed. The code linking individual animals to experimental groups was not released until all groups had completed their feeding and behavioural analysis had been completed. All tests were conducted in the first 1-5 hours of the light phase (i.e. 9am-1pm) to ensure constant timing of tests and to minimize sleep cycle and tiredness. All tests were conducted at RT in normal lighting condition of the laboratory. All conditions for the training (2-3 times) and test sessions were identical. After a 30 minutes habituation in the behaviour lab, mice were trained and tested with the accelerating rotarod (RR), inverted screen (IS), walking beam (WB), walking ladder (WL), dynamic plantar aesthesiometer (DPA) and Hargreaves (HR) apparatus. All instruments were cleaned after each trial with 70% ethanol (Astrol Scientific, Australia, prepared in distilled water). The number of behavioural tests were conducted in different studies are shown in **Table 3**.

Table 3: Type of behaviour tests were performed in various studies

Study	Type of behavioural test	Number of animals/group	Number of groups/study
I	Rotarod	10	6
II	Rotarod and inverted screen	12	4
III	Rotarod, walking ladder, walking beam, dynamic plantar aesthesiometer and Hargreaves	10	2

2.2.6.1 Rotarod (RR)

Locomotor activity and balance of mice were measured using the accelerating RR apparatus (UGO Basile, Italy), which is equipped with a motor driven rotating rod [215, 241]. Each animal was placed on the accelerating (initial speed was 4 revolutions per minute (rpm) that accelerated up to 40 rpm) rod for 5 minutes (n=3 trails/mouse/time point, 1 hour rest between trials). In study I and III, RR test was carried out in week 1, 2, 3, 4 and 5 whereas in the study II, the RR test was alternated (i.e. every second week, 1, 3, 5, 7, 9 and 11) with inverted screen test (see *below*). Latency to fall (i.e. mice fall from the rod), first flipping time (i.e. mice start to flip along with the rod) and number of flips were measured.

2.2.6.2 Inverted screen (IS)

Muscle/grip strength was measured using the IS apparatus as described before [242]. Briefly, a customised (1 mm diameter wire, 12 mm^2 mesh with total area of 42 cm^2) IS apparatus was used. Each mouse was placed at the centre of the IS, which was inverted for 60 seconds above (35 cm) a soft surface and the latency to fall was recorded (n=3 trials/mouse/time point, 30 minute rest between trials). This test was conducted on weeks 2, 4, 6, 8, 10 and 12.

2.2.6.3 Walking ladder

The ladder test was also used to assess motor coordination [243-246]. A customized 60 cm long ladder was made of transparent plastic (3 mm width and 15 cm high) with 3 mm diameter metal rungs placed at 12 mm intervals (47 rungs in total). The ladder was placed 13 cm above the bench surface. A desk lamp (25 W) was placed behind the starting side and the home cage at the distal end of the ladder to encourage the animal to move toward the safety of the darker home cage. The home cage containing nesting material was located at the end of the ladder in order to attract the mouse to walk towards their home confidently. On each test day, three trials were performed (30 minute rest between each trial) and all trials were recorded (Logitech C525 HD Webcam, China) for further analysis. Each video was analysed offline. The time to cross the ladder and the total number of ‘complete’ (no contact/extension beneath target rung) and ‘partial’ (contact with and extension beneath target rung) foot slips in both hind- and fore- limbs per mouse was quantified. The number of exploration events where the mouse ceased waking to rear/head dipping was counted.

2.2.6.4 Walking beam

The beam was used to assess motor coordination of mice as previously described [247, 248]. A customized 70 cm long wooden beam was placed horizontally 50 cm above the soft bench surface. The beam started at a width 11 mm at one end that progressively narrowed to 8 mm at the other. Mice were placed at the wide end and allowed to cross the beam towards the narrow end positioned in the mouse's home case. A desk lamp (25 W) was placed behind the starting side of the beam to encourage mice to walk towards the home cage. The cut-off time of total walking was 1 minute. Each trial (n=3 trials in total and 30 minute rest between each trial) was recorded (Logitech C525 HD Webcam, China) and analysed offline. The number of foot hind limb slips (right, left and combined) as well as the time to cross the beam was quantified at each time point during the study. In addition, the measurement of the number of exploration was carried out.

2.2.6.5 Paw withdrawal thresholds

Hind paw withdrawal thresholds to mechanical (gram force) and thermal (seccond) stimuli were determined using dynamic plantar aesthesiometer (DPA) and Hargreaves (HR) apparatuses (Bioseb, France) respectively [249, 250]. Mice were placed inside a chamber (6.7 cm long, 2.3 cm wide and 3 cm high with 5 mm^2 ventilation) on a wire mesh and glass screen platforms for mechanical and thermal tests respectively. Mice were acclimatized for 45 minutes (30 minute in the behaviour lab and 15 minute in the chamber) prior to the start of the test. The mechanical stimulus was given using DPA apparatus to either the right or left hind paw to measure the tactile threshold. From the point of initial contact, the force was 2 gram forces/second and increased by time until the animals withdraw its paw or the 20 grams maximal force was achieved. Thermal stimuli were derived using the HR apparatus, an infrared heat source (power flux: 0.64 mW/cm^2) was randomly delivered to the right or left hind paw and the paw withdrawal latency (15 second cut-off) was recorded. On each trial day, 5 consecutive paw withdrawal latencies were measured and the mean value for each trial was calculated and used for further analysis.

2.2.7 Histology

2.2.7.1 Tissue preparation

Mice were terminally anesthetized with Letobarb^{TM} (250 mg/kg sodium pentabarbitone, Tory laboratories, Australia, studies I and II) injection or isoflurane (Cenvet, Australia, study III) exposure. Mouse limbs were fixed onto a polystyrene block using pins and the heart was exposed by lifting the superior part of the abdomen. A perfusion needle was inserted into the left ventricle of heart to infuse 30 ml of 0.9% saline for 5 minutes using perfusion pump (Peri-Star, China) and fluid exsanguinated via a small cut to the right atrium for 5 minutes. The saline was replaced using cold 50 ml 4% paraformaldehyde (PFA, prepared in phosphate buffer, Sigma-Aldrich) for ~5 minutes. Curling/stiffness of the tail and pallor of liver were taken as indications of an effective perfusion. Central nervous system (CNS) and spleen samples were collected and post fixed with 4% PFA at 4°C for one week and stored in 0.01 M PBS solution containing 0.02% sodium azide (Amresco, USA) to prevent bacterial growth at 4°C ≤1 month or until sectioned.

2.2.7.2 Sectioning

Samples (CNS and spleen) were placed in a falcon tube containing 10 ml of 30% sucrose (Coles, Australia) solution for 48 hours at RT to cryo-protect the tissue. Complete submersion of sample was taken as an indication of effective cryo-protection. Samples were then embedded in 4% gelatine (Chem-Supply, Australia) in a cryomold (Sakura, USA) and set at -20°C for 20 minutes. Gelatine embedded sections were fixed to the tissue chuck holder using tissue-tek optimal cutting temperature (OCT, Sakura) compound. Tissue was then mounted in the cryostat (Leica, Germany) and 20-50 µm thick coronal sections were cut as mentioned in **Table 4**. Sections were transferred to either 6-well plates containing cold (5-6°C) 0.01 M PBS (free floating) or mounted onto 0.5% gelatine-coated slides (Knittel Glass, Germany). Tissue slices were either immediately used for staining or kept in anti-freezing solution (glycerol, ethylene glycol and 0.01 M PBS at 1:1:2 v/v) at -20°C for ≤ 3 months or until use.

Table 4: Tissue section thickness

Study	Tissue	Section thickness
I	Brain	50 µm
	Spleen	20 µm
II	Brain	40 µm
III	Whole CNS	40 µm

2.2.7.3 Slide coating

CD4 and CD8 staining in spleen and silver staining were carried out on gelatine-coated slides. Gelatine (0.5%) was heated at 45°C for 10 minutes followed by addition of 0.05% positively charged chromium potassium sulphate dodecahydrate (Chem-Supply, Australia) to attach negatively charged tissue sections. The solution was cooled to RT for 30 minutes and then filtered using Whatman filter paper (pore size: 11 µm, UK) to remove any undissolved particles. Clean glass slides (Knittel Glass, Germany) were coated by dipping 5 times (at 5 second interval) before air drying for 48 hour prior to use.

2.2.7.4 Silver staining (studies I-III)

All tissue sections (40-50 µm) from study I-III were mounted onto gelatine-coated slides and air dried for 48 hours before immersion in 10% natural formalin (Sigma-Aldrich) for 2 weeks at RT to increase the contrast of staining. All sections in a study were stained in parallel to maintain consistency. Slides were washed with distilled water and incubated in pyridine (VWR, USA): acetic anhydride (Merck, Germany) solution (ratio 2:1) for 30 minutes at RT. Sections were then rehydrated with serial dilutions of ethanol 80, 60, 40 and 20% for 20 seconds in each step followed by two washes with distilled water. Washed slides were immersed in ammonical silver nitrate (Chem-Supply, Australia) containing developing solution for 45 minutes at RT. The developing solution contained an equal amount of stocks A and B (50-50 ml). A: 5 g sodium carbonate in 100 ml distilled water, B: mixture of 0.2 g ammonium nitrate and 0.2 g silver nitrate in 100 ml distilled water. Sections were then washed for 30 seconds with bleaching agent potassium ferricyanide (BDH chemicals, UK) to de-stain over developed (i.e. dark staining) sections followed by dehydration sequentially using 20, 40, 60 and 80% of ethanol for 20 seconds in each step. Sections were cleaned by immersing the slides in 200 ml xylene (VWR, USA) for 5 minutes to clean the sections by removing gelatine and ethanol at RT. Finally, slides were covered with glass cover slips (Knittel Glass, Germany) with mounting medium (Merck, USA) and air dried for 72 hours [128, 251].

2.2.7.5 Immunofluorescence staining (studies I-III)

Free floating coronal CNS tissue sections (40-50 µm) were bathed with warm (40-50°C) 0.01 M PBS for 3x5 minutes to remove residual gelatine. Minimizing the non-specific binding of antibodies was carried out by immersing tissue sections into 5-10% normal goat serum (prepared in 0.01 M PBS) at RT for 2 hours on an orbital shaker (50 rpm). Sections were then transferred into primary antibodies dissolved in 0.1% Triton X-100 (TX-100, Amresco) in 0.01 M PBS. Primary antibodies, such as neurite outgrowth inhibitor A (NOGO A), adenomatous polyposis coli (APC), glial fibrillary acidic protein (GFAP), ionized calcium-binding adapter molecule 1 (IBA 1), calbindin (Calb), myelin basic protein (MBP), neuronal nuclei (NeuN) and choline acetyltransferase (ChAT) were used. For the detection of CD4 and CD8 cells, anti-cluster of differentiation (CD)4 and anti-CD8 antibodies were used (**Tables 5** and **6)**. For spleen immunofluorescence staining (spleen was used as a positive control of CD4 and CD8) with CD4 and CD8, mounted sections (20 µm) were used. All primary antibodies were incubated for 12 hours at RT while shaking in an orbital shaker (50 rpm). Sections were washed thrice in 0.01 M PBS and then incubated in secondary Alexa Fluor conjugated (either 488 or 555) antibodies for 2 hours at RT with agitation on a shaker. Following three more washes in 0.01 M PBS, sections were mounted on uncoated slides and cover-slipped (Knittel Glass, Germany) using 1.5 µg/ml vectasheild plus 4′,6-diamidino-2-phenylindole (DAPI, Vector Laboratories) to counterstain nuclei. Tissue sections were dried for 30 minutes in RT in the dark and stored at 4°C in the dark until imaged (≤15 days). The tissues were imaged using Fluorescence Microscope, Germany.

Table 5. Antibodies used for immunofluorescence staining

		Primary				Secondary		
Study	**Target protein/ antigen**	Antibody	**Species**	**Dilution**	**Company/Catalogue**	**Antibody**	**Dilution**	**Company/Catalogue**
I-III	Astrocytes	GFAP	Alexa Fluor 488 conjugated mouse	1:1000	Merck-Millipore, USA /MAB3402X	-	-	-
	Microglia	IBA 1	Rabbit	1:1000	Wako, Japan /019-19741	Goat Alexa Fluor 488 conjugated anti-rabbit IgG	1:500	Invitrogen, USA /A-21428
I-II	Mature OLG	NOGO A	Rabbit	1:500	Merck-Millipore /AB5664P			
	CD4	CD4	Rabbit	1:200	Abcam, UK /AB183685			
	CD8	CD8	Rat	1:100	Invitrogen /MA1-70041	Goat Alexa Fluor 594 conjugated anti-rat IgG	1:500	Invitrogen /A-11007
III	Mature OLG	APC	Rabbit	1:500	Merck-Millipore /AB5664P	Goat Alexa Fluor 488 conjugated anti-rabbit IgG	1:500	Invitrogen /A-21428
	Lower motor neurons	NeuN	Mouse	1:500	Merck-Millipore /MAB377	Goat Alexa Fluor 488 conjugated anti-mouse IgG	1:500	Invitrogen /R37120
	Alpha motor neurons	ChAT	Alexa Fluor 488 conjugated rabbit	1:50	Abcam /ab192465	-	-	-
	Purkinje neurons	Calb	Rabbit	1:1000	Merck-Millipore /AB1778	Goat Alexa Fluor 488 conjugated anti-rabbit IgG	1:500	Invitrogen /A-21428
	Myelin protein	MBP	Mouse	1:500	Abcam /ab62631			Invitrogen /R37120

2.2.7.6 Antibody optimization

The specificity of primary and secondary antibodies was optimized using a primary control (without primary antibody), secondary control (without secondary antibody), combination of primary and secondary antibodies, and blank (no primary or secondary antibody) as discussed previously [252, 253]. The specificity of the antibodies was confirmed by the signal obtained from the combination of primary and secondary antibodies whereas no signal was observed when primary antibody and secondary antibody were used alone. Dilutions of antibodies were started from low to high (for both primary and secondary antibodies) for short to long duration of incubation. For example, for IBA 1 primary antibody, dilutions were ranged from 1:500, 1:1000 and 1:2000 (dilution in 0.01 M PBS and 0.1% Triton X-100) with incubation times of 8-20 hours at RT. Similarly, for secondary antibody dilutions ranged from 1:250 to 1:500 with incubation times of 2-5 hours. The most intense signal (e.g. fluorescence intensity) was detected when 1:1000 dilution of primary antibody was incubated for 10-12 hours with 1:250 secondary antibody dilutions for 2 hours. The same strategy was applied to other antibodies. Due to the direct conjugation of Alexa Fluor to GFAP and ChAT primary antibodies, no secondary antibody was used. Fluorescent signals were confirmed by comparing with previously published literature [26] and sections without using antibody. Non-specific binding was minimised using goat serum (study I: 5% and studies II-III: 10%) for 2-5 hours at RT. The optimum blocking of non-specific binding was found when 2 hours incubation using 5-10% serum was used.

2.2.7.7 Quantification

2.2.7.7.1 Silver myelin intensity

All images were captured using Carl Zeiss Brightfield microscope using the same parameter settings for exposure time (e.g. 1 ms at 20x magnification) and illumination intensity. Images were opened in ImageJ (www.imagej.nih.gov) software and the region of interest (ROI) was contoured and the mean optical density quantified (measured as mean grey value: sum of all the pixels in the ROI divided by the number of pixels; range black (0) to white (256)). In order to quantify the extent of myelin present (which stains black), data were analysed as the reciprocal of the light intensity (i.e. the smaller the value, the lower the myelin content) and normalised to the Ctrl group in studies I and II. In study III, optical intensity inversely corresponds to myelin (more intensity less myelin) and data was presented as fold change relative to the Ctrl group. The number of sections and animals quantified are stated in **Table 6**.

2.2.7.7.2 Immunofluorescence intensity measurement

Images were captured using fluorescent microscope set-up using same exposure (e.g. 100 msec at 20x magnification) and magnification. Images were opened in ImageJ and fluorescence intensity was measured from each ROI as discussed before (see *silver staining quantification*) and data was presented according to their intensity (bigger the number, more the fluorescence intensity) in studies I and III. In study III, data were presented as fold change relative to Ctrl. The number of sections and animals quantified are stated in **Table 6**.

2.2.7.7.3 Unbiased stereological counting

To quantify the number of positively stained NOGO A, APC, GFAP, IBA 1 or NeuN cells, Unbiased Sterioinvestigator Workflow (www.mbfbioscience.com/stereology) was used. The use of this software allowed visualizing three dimensional structure of the cell and estimating total population of cells in a region of interest. At low magnification (e.g. 10x or 20x objective), the ROI was contoured and nucleated cells (DAPI positive) were counted at high magnification (63x). To obtain the cell density, total cell number was divided by total measured volume and the data is expressed as 10^4 cells/mm^3. In study III, cell density was presented as fold change relative to Ctrl. For study I every 6^{th} section (300 µm), for study II every 7^{th} section (280 µm) and for study III every 9^{th} section (360 µm) were quantified. The number of sections and animals quantified are stated in **Table 6**. Due to the small number of cells such as in NOGO A or APC positive OLG cells in CPZ-fed animal in areas such as corpus callosum, the minimum requirement of number of 3-5 cells/marker per counting frame as previously described [254, 255] was not achieved, thus the coefficient error (CE) increased above 10% whereas Ctrl group containing large number of cells and showed lower CE (>10) value. The detail parameters of the counting are given in the corresponding manuscripts.

2.2.7.7.4 Manual counting

Due to the small area or low number of cells, ChAT positive neurons in spinal cord, Calb-positive Purkinje neurons in the cerebellum were counted manually and expressed as fold change relative to Ctrl. The number of sections and animals quantified are stated in **Table 6**.

2.2.7.8 Anatomical structures

The different CNS regions were identified according to the mouse brain atlas and spinal cord landmarks as outlined before [251, 256-258].

Table 6: The number of sections and animals quantified

Study		CNS regions	Staining (tissue sections/number of animals)								
			Silver	APC	NOGO A	MBP	GFAP	IBA 1	NeuN	ChAT	Calb
I	Cerebrum	Corpus callosum (CC, midline and lateral)	5/5	-	7/5	-	7/3	7/3	-	-	-
II		MCC and LCC	9/5	-	9/5	-	9/5	9/5	-	-	-
III	Cerebrum	Cortex (AU, VI, M1, M2, S1FL, S1HL and S2)	3/5	-	-	-	3/5	3/5	-	-	-
		Cingulum (CG)	3/5	-	-	-	3/5	3/5	-	-	-
		CC	8/5	5/5	-	-	8/5	8/5	-	-	-
		Anterior commissure (AC)									
		Dorsal fornix (DFX)	4/5	-	-	-	4/5	4/5	-	-	-
		Hippocampus (HP)	5/5	3/4	-	-	3/5	3/5	-	-	-
		Striatum (lateral, LST and middle, MST)	3/5	-	-	-	3/5	3/5	-	-	-
		Ventral palladium (VP)									
		Optic tract (OPT)	3/5	-	-	-	3/5	3/5	-	-	-
		Thalamus (TH)	3/5	-	-	-	3/5	3/5	-	-	-
		Hypothalamus (HTH)	3/5	-	-	-	3/5	3/5	-	-	-
		Capsule (internal, IC and external, EC)	3/5	-	-	-	3/5	3/5	-	-	-
	Cerebellum	Cerebellar peduncle (superior, SCP; middle, MCP and inferior, ICP)	3/5	3/5 (SCP only)	-	-	3/5	3/5	-	-	-
		Cerebellar vestibular nucleus (CVN)	3/5	3/5	-	-	3/5	3/5	-	-	-
		Interposed nucleus (IPN)	3/5	3/5	-	-	3/5	3/5	-	-	-
		Dentate nucleus (DN)	3/5	3/5	-	-	3/5	3/5	-	-	-
		Cerebellum cortex (CCX)	2/5	3/5	-	-	3/5	3/5	-	-	-
		6,9 and 10 cerebellar vermis (CV)	-	-	-	-	-	-	-	-	3/5
	Brain stem	Substantia nigra (SN)	3/5	-	-	-	3/5	3/5	-	-	-
		Red nucleus (RN)	3/5	-	-	-	3/5	3/5	-	-	-
		Inferior colliculus nucleus (ICN)	3/5	3/5	-	-	3/5	3/5	-	-	-
		Vestibular nucleus (superior, SUVN; spinal, SPVN	3/5	3/5	-	-	3/5	3/5	-	-	-

	and lateral, LVN									
	Medial vestibular nucleus (MVN)	3/5	3/5	-	-	3/5	3/5	-	-	-
	Prepositor nucleus (PN)	3/5	3/5	-	-	3/5	3/5	-	-	-
	Pyramidal tract (PYT)	3/5	3/5	-	-	3/5	3/5	-	-	-
Spinal cord	Cervical (DF, DLF, VLF and VF)	5/5	3/5	-	5/5	5/5	5/5	-	-	-
	Thoracic (DF, DLF, VLF and VF)	5/5	3/5	-	5/5	5/5	5/5	-	-	-
	Lumbar (DF, DLF, VLF and VF) (DF)	5/5	3/5	-	5/5	5/5	5/5	-	-	-
	Cervical (DH)	5/5	-	-	5/5	5/5	5/5	-	-	-
	Cervical (VH)	5/5	-	-	5/5	5/5	5/5	5/5	5/5	-
	Thoracic (DH)	5/5	-	-	5/5	5/5	5/5	5/5	-	-
	Thoracic (VH)	5/5	-	-	5/5	5/5	5/5	-	5/5	-
	Lumbar (DH)	5/5	-	-	5/5	5/5	5/5	-	-	-
	Lumbar (VH)	5/5	-	-	5/5	5/5	5/5	5/5	5/5	-

Key: AU, auditory cortex; DF, dorsal funiculus; DH, dorsal horn; DLF, dorsal lateral funiculus; LCC, lateral corpus callosum; MCC, midline corpus callosum; M1, primary motor cortex; S1FL, primary somatosensory front limb cortex, S1HL; primary somatosensory hind limb cortex; S2, secondary motor cortex; S2, secondary somatosensory; VF, ventral funiculus; VF, ventral horn; VLF, ventral lateral funiculus; VI, visual cortex and not performed: -

2.2.8 Two dimensional gel electrophoresis (2DE) and identification of proteins (studies I-II)

2.2.8.1 Sample collection

Mice were euthanized by overdose of isoflurane (Cenvet, Australia) exposure. Whole brains were collected following decapitation and immediately rinsed with ice cold 0.01 M PBS containing protease and phosphatase inhibitors to remove any trace amount of blood. Immediately brains were snap frozen in liquid nitrogen and stored at -80°C (Thermo Scientific, Australia) until homogenisation.

2.2.8.2 Homogenisation

Tissue homogenization was accomplished using an automated frozen disruption (AFD) procedure using Mikro-Dismembrator (Sartorius, Germany). Polytetrafluoroethylene (Teflon) tissue chambers (approximately 3 ml capacity) along with a grinding ball made of chromium steel were assembled and pre-cooled by immersing in liquid nitrogen bath for 5 minutes. Frozen tissues were transferred to above pre-cooled Teflon chambers and homogenized using Mikro-Dismembrator (a frequency of 40 Hz for 1 minute). The resulting pulverised frozen tissue was collected in to a fresh microfuge tubes and left in liquid nitrogen to prevent further thawing and transferred to -80°C until use as discussed previously [259-261].

2.2.8.3 Proteome fractionation

One gram of above pulverised tissue samples were transferred into fresh 15 ml falcon tubes (Corning Incorporated, USA) and added 1 ml of cold 20 mM HEPES (Amresco, USA) lysis buffer (0.104 g of HEPES salt was dissolved in 20 ml of distilled water supplemented with protease 1µl/ml protease and phosphatase inhibitors, Sigma-Aldrich). The sample was vortexed (VWR, USA) for 90 seconds followed by resuspension in HEPES buffer, the isotonicity was restored by the addition of an equivalent volume of ice cold two times concentrated 0.02 M PBS and incubated for further 5 minutes on ice. The samples were ultracentrifuged (Beckman Coulter, USA) at 125,000 x *g* using a SW 55 Ti rotor at 4°C for 2 hours. The resulting supernatant (SP1) was collected as total cytosolic soluble protein (SP). The membrane pellet was washed with ice cold 0.01 M PBS to extract cytosolic proteins (SP2) again and ultracentrifuged for 8 hours at 125,000 x *g*. After the centrifugation, the supernatant (SP2), was collected and pooled with SP1 fraction. The combined soluble protein fraction (SP1 plus SP2) was concentrated using an Amicon Ultra-4 centrifugal 3 Kd cut-off filter column (Centrifugal filter column Millipore, USA). In order to prevent PBS and HEPES salts interference during 1st dimension isoelectric focussing step, the resulting SP

samples were washed three times using cold 4 M urea (Amresco) buffer containing protease and phosphatase inhibitors. The final volume of the SP fraction was maintained below 500 µl. The above washed membrane pellet (MP) was resuspended with 500 µl of cold solubilisation buffer (9.616 g (8 M) urea, 3.045 g (2 M) thiourea and 0.8 g (4%) CHAPS were dissolved in distilled water to make a final volume to 20 ml, aliquoted 1 ml/tube and stored at -20°C) containing protease and phosphatase inhibitors. Both SP and MP fractions were aliquoted in small volumes (50 µl/tube) and stored at -80°C prior to protein estimation [259, 261].

2.2.8.4 Protein estimation

Protein concentrations for SP and MP fractions were quantified using EZQ™ Protein Quantitation Kit (Life Technologies, USA) using bovine serum albumin (BSA, Amresco) as standard protein. Standard protein BSA stock solution was prepared (12 mg/ml) in 2% sodium dodecyl sulphate (SDS, Merck, Germany) solution. From this stock BSA solution, different working concentrations ranging from 0.5 µg to 0.025 µg were prepared to generate a standard protein curve. Two microliters of each working standards with triplicate were spotted on Whatman filter paper (10x7 cm) along with SP and MP samples. After spotting, filter paper was air dried for 5 minutes on the bench surface and transferred to a plastic container. Carefully 50 ml of 100% methanol (Astral Scientific, Australia) was added and incubated for 5 minutes on an orbital shaker at 50 rpm. After incubation methanol solution was removed and air dried the filter paper for 5 minutes followed by 30 minute incubation with fresh fluorescent EZQ dye solution under dark. Immediately after the incubation, the filter paper was quickly rinsed with a buffer containing 10% methanol and 7% acetic acid for 20 seconds for 3 times and scanned on FUJI LAS-4000 biomolecular imager (GE Healthcare, USA) for 2 seconds. Using Multi Gause software (Fujifilm, Japan) intensity of protein spots was measured. Protein concentrations from unknown samples (SP and MP) were measured against standard curve [262].

2.2.8.5 Sample reduction and alkylation

Reduction and alkylation steps were carried out to maintain all proteins in a denaturation state before subjecting to isoelectric focussing. One hundred micrograms of proteins from both soluble and membrane fractions were (n=3) taken into a clean low protein binding microcentrifuge tubes and were mixed with 58.8 µl of 2DE solubilisation buffer. Then equal volume of rehydration buffer (2% broad range pH 3-10 carrier ampholytes, Bio-Rad) was

added to the protein solution. The above protein solution was mixed with two mild reduction buffers containing 2.3 µl of tri-butyl phosphine (TBP, Bio-Rad) and dithiothreitol (DTT, Astral Scientific). Reduction buffer was prepared using 0.3702 g (2 M) DTT salt mixed with 600 µl of TBP (0.2 M) and the final volume was made to 1.2 ml with distilled water. The combination of two agents at lower concentrations increases the capacity to cleave disulphide bond crosslinks to linearize proteins after alkalization. This reducing buffer was aliquoted in 25 µl/tube and stored at -20°C. The tube was vortexed and incubated for 1 hour at 25°C on a heating block. After incubation, 5.1 µl of 5.6 M acrylamide solution was added to all tubes vortexed and incubated for further 1 hour at 25°C. After the incubation, the SP and MP were protein samples ready for first dimension run on immobilised pH gradient (IPG strips, Bio-Rad) strip rehydration.

2.2.8.6 IPG strip rehydration

Non-linear pH 3-10 range 7 cm IPG strips were hydrated by loading 100 µg proteins (125 µl sample volume). At first, 125 µl of protein samples were dispensed into rehydration/equilibration tray. Peeled the plastic cover sheet from the IPG strip (7 cm, pH 3-10 non-linear) using forceps and gently placed the strip following gel side down and emergence of air bubbles beneath the IPG strip were avoided. After loading all IPG strips, tray was covered with plastic lid and left for 16 hours on a level bench to rehydrate the strips and load the protein sample.

2.2.8.7 Isoelectric focussing (IEF) on IPG strip

Next day, isoelectric focusing (IEF) was carried out using above rehydrated IPG strip to separate proteins based on the charge of protein. Rehydrated IPG strips were placed in the Protean IEF focussing tray using forceps. Paper wicks (2.5 cm long and 4 mm width Whatman filter) at each positive and negative end of the electrode were placed connecting IPG strips with the platinum electrodes. All the IPG strips were overlayed with 2-3 ml of mineral oil (Amresco) to prevent evaporation during the focusing period. Focussing tray was transferred into the Protean IEF cell. Initially 250 V was applied for 15 minutes and increased linearly to 4000 V at 50 µA/gel for 2 hours, with multiple electrode wick changes during voltage ramping to facilitate desalting. The following parameters were used during the focusing: focus temperature: 17°C, desalting: 15 minute, linear gradient: 2 hour, Vh: 37500 and holding voltage: 500 V. When focusing completed IPG strips were either stored at -20°C or immediately used for second dimension [259, 263-265].

2.2.8.8 Second dimension on 12.5% SDS-PAGE

Second dimension was carried out using 1 mm thick 8.4x7 cm SDS-polyacrylamide gel (PAGE) gels with 12.5% acrylamide (Bio-Rad) concentration. Gels were casted the day before the actual run using Mini-protean Bio-Rad casting apparatus and stored at 4°C overnight for homogenous polymerization. Before subjecting to 2^{nd} dimension focused IPG strips were incubated for 10 minutes each with 130 mM DTT in equilibration buffer followed by 10 minute alkylation with in equilibration buffer containing 350 mM acrylamide. This additional equilibration ensures that the cysteines were reduced and alkylated. Moreover, it helps to minimize vertical streaking and maximize separation of proteins in the second dimension gels. SDS-PAGE gel was placed to the casting stand. Using a paster pipet overlay warm agarose solution (0.5% low melting agarose, Bio-Rad) containing 2% bromophenol blue (Bio-Rad). Immediately, using a forceps carefully placed the IPG strips into the stacking gel while taking care not to trap any air bubbles beneath the IPF strip. The agarose was allowed to solidify for 2 minutes before mounting the gel into electrophoretic tank (Mini protein cell, Bio-Rad) containing tris-glycine-SDS electrode buffer (Amresco). Electrophoresis was carried out at 4°C/cold room by applying 150 v for 5 minutes followed by 90 v for 3 hours. When the tracking bromophenol dye reached to the bottom of the glass plate, electrophoresis was stopped and gels were removed from tank and immediately fixed [259, 260, 263, 265].

2.2.8.9 Protein fixation and staining

Proteins were fixed in 10% (v/v) methanol and 7% (v/v) acetic acid solution for 1 hour at RT under constant shaking (50 rpm). Gels were rinsed with distilled water for 3x20 minutes to remove methanol and acetic acid followed by staining with high sensitive 50 ml colloidal Coomassie Brilliant Blue (CBB, G-250, Amresco). For 100 ml of cCBB was prepared by mixing 5 ml (2%) cCBB, 5 ml (30%) phosphoric acid, 25 ml (20%) ammonium sulphate and 20 ml (100%) methanol. The final volume 100 ml was prepared by adding distilled water and used fresh in the day of preparation. Gels were incubated along with the dye solution for 20 hours at RT on an orbital shaker (50 rpm). After 20 hour, carefully gel solution was discarded and stained gels were washed using 0.5 M sodium chloride (Bio-chemicals, Australia) solution for 3x15 minutes interval to remove excess dye and imaged immediately using Typhoon^{TM} FLA-9000 gel imager (GE Healthcare, USA). Gels were preserved in 20% ammonium sulphate (50 ml/gel) and stored at 4°C until further use [260, 266-269].

2.2.8.10 Gel imaging and protein spot analysis

Quantitative analysis of gels was carried out using Delta 2D image analysis software (www.decodon.com/delta2d version 4.0.8, DECODON, Germany) as described previously [260, 266, 270-272]. Total spot numbers were calculated from the raw images using the Delta 2D automated spot detection system while gel edges and the protein ladder were excluded [260, 271]. Gel images were warped and fused to generate a master image ensuring consistent spot matching. The fluorescent volumes of individual spots (i.e. protein abundance) as a function of all spot volumes detected were measured using Delta 2D to assess changes across the different experimental groups. Four spot inclusion criteria were applied: 1) any changes in spot volumes were detectable in all biological replicates (n=5 animals/group) and their associated technical replicate gels (n=3 gels/fraction/animal; i.e. 15 gels/experimental group); 2) the relative standard deviation (RSD) for technical replicates did not exceed 30% within individual animals; 3) values had to differ significantly ($p<0.05$, t-test) between the naïve Ctrl group and at least one test group; and 4) have a fold change of ≥1.5 (increased/decreased fluorescence), were considered genuine changes, and thus candidates for analysis by LC/MS/MS. These criteria allowed for reliable and reproducible identification of CPZ, CPZ+PT or PT associated proteoform changes. The fold change ($p<0.05$, one-way ANOVA) of differentially abundant protein spots was calculated by dividing the average grey value (i.e. fluorescence intensity of the protein spot of each experimental group compared to the naïve Ctrl group) and presented in $\log_2$ scale as fold change relative to Ctrl

2.2.8.11 Experimental molecular weight (MW) and isoelectric point (*pI*) calculation

Precision Plus Protein Kaleidoscope MW and 2DE *pI* standard (Bio-Rad, USA) calibration gels (n=3) were used to calculate the experimental *pI* and MW of resolved proteoforms. IEF, second dimension and imaging of using standard proteins gels were carried out using 7 cm (pH 3-10, non-linear) IPG strips as discussed above. Experimental MW and *pI* of biological samples were then measured comparing the average migration of the protein standards and expressed as 'experimental MW and *pI*' [29, 260, 266]. The coefficient of variation (standard deviation/mean) for the MW and *pI* migration was 2.6% and 1.4% for 2DE standards respectively (n=3) and 4% for MW ladders for experimental gels (n=20). To quantify the gel shifting or likely post-translational modification (PTM) of proteins, experimental MW and *pI* values were plotted relative to theoretical values; significant changes were indicated when the

experimental measure fell above or below the 95% confidence intervals of the MW and *pI* calibration curves. The results are plotted as the average for both 5 and 12 weeks combined.

2.2.8.12 In-gel protein spot digestion

Protein spots of interest were cut using micro tip (Corning Incorporated) and stored at -20°C or subjected to trypsin digestion immediately. Excised protein gel pieces were transferred in 0.5 ml DNase and RNase free microfuge tubes (Corning Incorporated) and de-stained with 200 µl of 50 mM ammonium bicarbonate (Sigma-Aldrich) solution containing 50% acetonitrile (Merck, Germany) twice at 15 minute interval. After complete distaining, gel pieces were dehydrated using 100% acetonitrile. In-gel digestion was carried out by adding 20 µl of freshly prepared trypsin (Promega Corporation, USA) solution (final concentration 12.5 ng/µl) in 50 mM ammonium bicarbonate for 8 hours at 4°C. Digested peptides were removed from the gel following ultrasonic agitation in a sonicator (Soniclean, Australia) for 30 minutes. The solution was then acidified by the addition of 2 µl (2%) formic acid (Waters, USA). The resulting peptide solution was concentrated to 10 µl using a Speed Vac™ vacuum concentrator machine (1400 rpm for 10-15 minutes, John Morris Scientific, Australia) and then transferred into recovery glass vials (Waters, USA). These were either stored at -80°C for future use or immediately subjected to mass spectrometry [260].

2.2.8.13 Liquid chromatography mass spectrometry (LC/MS/MS)

The concentrated peptide solutions were analysed by LC/MS/MS using a nanoAcquity ultra performance liquid chromatography system (UPLC) linked to a Xevo QToF mass spectrometer as previously described [29, 260, 266, 273, 274]. Peptide sample solutions (3 µl) were loaded onto a C18 Symmetry trapping column (20 mm x 180 µm), and desalted for 3 minutes at 5 µl/minute flow rate using 1% solvent B (LC/MS grade 1% acetonitrile and 0.1% formic acid) in solvent A (Milli-Q water+0.1% formic acid). The peptides were washed off the trapping column at 400 nl/minute onto a C18 BEH analytical column (75 µm x 100 mm), packed with 1.7 µm particles of pore size 130 Å using a 60 minute ramped LC protocol. The initial solvent composition was held at 1% B for 1 minute followed by linear ramping to 50% B over 30 minute. A further linear ramp to 85% B commenced at 31 minute and held until 37 minute before the solvent composition was returned to 1% B. Separated peptides were analysed using tandem mass spectrometry with a constant cone voltage of 25 V and source temperature of 100°C implementing an emitter tip that tapered to 10 µm at 2.3

KV. A data directed acquisition (DDA) approach was performed which continuously scanned across the *m/z* range 350-1500 for peptides of charge state 2^+-4^+ with an intensity of more than 50 counts/second, with a maximum of three ions in any given 3 second scan. Selected peptides were de-isotoped, fragmented and the masses measured. The ramped collision energy profile was set to 15-35 V at low mass and 30-40 V at high mass. The mass of the precursor peptide was then excluded for 30 seconds. The DDA data were acquired using Masslynx software (version 4.1, Micromass, UK). The raw data from Masslynx were converted to a peak list (PKL) file format using ProteinLynx Global Server (Waters, USA) and analysed using Mascot Daemon (www.matrixscience.com) and queried against the SwissProt and MSPnr100 databases (*see* www.wehi.edu.au) using delimited and species-specific searches to identity the protein species using the following parameter settings: the enzyme trypsin and taxonomy *Mus musculus* (mouse) were fixed. No fixed modification was selected whereas variable modifications were carbamidomethyl, deamidated, oxidation and propipnamide. Only two missed cleavages of lysine or arginine residues were allowed; mass tolerance was set to 0.5 Da and peptide charge state was 2^+-4^+. When multiple proteins were detected from the same spot, the following criteria were applied to identify the most abundant and thus the most likely to have contributed to the originally detected change in spot volume: 1) a MASCOT score >100 and sequence coverage ≥5%; 2) the highest MASCOT score of the proteins identified; and 3) ≥4 unique matched peptides.

2.2.9 Literature mining and bioinformatics (studies I-II)

2.2.9.1 Literature mining

A PubMed (www.ncbi.nlm.nih.gov/pubmed/) literature search was carried out for papers published in the English language using the identified canonical protein name with either CPZ, experimental autoimmune encephalomyelitis (EAE) or multiple sclerosis (MS) to find literature relevant to molecular/cellular functions.

2.2.9.2 Genes and UniProt accession identification

Gene name, UniProt accession identification (UniProt ID) and subcellular location of the identified proteins were derived from the UniProt (www.uniprot.org) database [275]. The protein name obtained from LC/MS/MS was searched in UniProt against mouse (*Mus masculus*) database to obtain the information related to unique accession and gene IDs.

2.2.9.3 PANTHER

Proteins were classified and molecular functions were revealed using protein analysis through evolutionary relationships (PANTHER, www.pantherdb.org) database. A mapping of genes according to their classification and molecular functions was derived [276] using gene IDs of a protein.

2.2.9.4 DAVID

Cellular components, biological processes and physiological pathways of identified proteins were categorised using database for annotation, visualization and integrated discovery (DAVID, version 6.8, david.ncifcrf.gov) database. Uniprot accessions IDs were used in DAVID database and categorized proteins according to their (GO, gene ontology, www.geneontology.org) GO cellular components and biological processes. DAVID was also characterized protein's physiological pathways according to Kyoto encyclopaedia of genes and genomes (KEGG, www.genome.jp/kegg) category [277].

2.2.9.6 STRING

Protein species were further characterised and grouped using the search tool for retrieval of interacting genes/proteins (STRING; version 10.5, string-db.org/) to identify the protein-protein interaction [278]. In STRING database, protein IDs was used against *Mus masculus*. Protein-protein interaction map was generated based on their experimental evidence where each node represents a protein and connecting line represents the evidences of association such as text mining, co-expression, co-occurrence, databases, experiments, neighbourhood and gene fusion [279, 280].

2.2.10 Western blot (studies I-II)

2.2.10.1 Procedure

Proteins (brain, spinal cord, spleen and recombinant proteins) were separated on 10% SDS-PAGE gel (100 V for 2 hours at 4°C) and transferred (100 V for 2 hours at 4°C) onto a polyvinylidene difluoride (pore size: 0.22 µm, PVDF, Bio-Rad) membrane. The blotted membranes were incubated in blocking buffer containing skim milk (5% w/v, Coles, Australia) and polyvinylpyrrolidone (1% w/v, Sigma-Aldrich), in 0.05% tris buffered saline-tween 20 (TBST) for 1 hour at RT on shaker (50 rpm). **Table 7** shows the detail chemical constituents of buffer used in WB. Primary antibodies for CD4 and CD8 were incubated for 1 hour at RT. All antibodies and final optimised dilutions are listed in **Table 8**. Blots were then washed thrice with 0.05% TBST at 10 minute intervals and incubated for a further 2 hours at RT using horseradish peroxidase-conjugated (HRP) compatible secondary antibody. Blots were washed thrice using TBST and incubated in the dark using 2 ml of chemiluminescence detection reagent (500 µl/cm^2 membrane, Luminata Crescendo Western HRP Substrate, Merck-Millipore) for 2 minutes. Blots were scanned for 2 seconds on FUJI LAS-4000 biomolecular imager.

Table 7: Buffers related to WB

Buffers	**Chemicals**	**Quantity** (for 4 litre, make final volume using distilled water)
Transfer	25 mM Tris	12.12 g
	192 mM Glycine	57.6 g
	20% Methanol	800 ml
	pH	8.3
Tris buffered saline with Tween-20 (TBST)	10 mM Tris	4.85 g
	150 mM Sodium chloride	36 g
	0.1% Tween 20	4 ml

Table 8. Antibodies used for WB

Primary					**Secondary**		
Target protein/antigen	**Antibody**	**Species**	**Dilution**	**Company/ Catalogue**	**Antibody**	**Dilution**	**Company/ Catalogue**
CD4	Anti-CD4	Rabbit	1:500	Abcam/ AB183685	Goat anti-rabbit IgG H&L-HRP	1:2000	Abcam/ AB6721
CD8	Anti-CD8	Mouse	1:75	Santa-Cruz, USA/SC-1177	Mouse anti-mouse IgGκ BP-HRP	1:500	Santa-Cruz/ SC-516102

2.2.10.2 Sample preparation

Mice were euthanized using isoflurane exposure and samples (brain, spinal cord and spleen) were collected and washed to remove blood using 0.01 M PBS containing protease inhibitors, snap frozen in liquid nitrogen and stored in -80°C until protein extraction. Samples were powdered using AFD procedure (see *homogenisation section*). Equal ratios (~1 µl/1 µg tissue) of sample and pre-chilled solubilisation buffer was used to solubilize proteins, gently vortexed to mix properly and ultracentrifuged using 125,000 x *g* at 4°C for 1 hour. Resulting supernatant was collected as a total protein extract. Protein quantification was carried out as previously described using EZQ protein quantitation kit (see *protein estimation section*).

2.2.10.3 Positive control

To measure the CD4 and CD8 antibody specificity, biological (B6 mice) spleen samples and commercial CD4 and CD8 recombinant proteins (Sino Biological, USA) were used as positive control. Spinal cord homogenates of EAE from parallel experiment were also used as a positive control for CD4 signal detection in WB analysis in studies I and II. EAE was induced using an established method [281].

2.2.10.4 Optimization of antibodies

For optimization of CD4 and CD8 antibodies, different concentrations of primary and secondary antibodies, incubation and blocking time were used. CD4 primary antibody was used from 1:100-1:1000 dilutions (e.g. 1 µl antibody in 100 µl TBST). Dilutions of rabbit anti-CD4 antibody over 1:500 showed faint (or undetectable) signal/protein band whereas no bands were observed when 1:1000 and 2000 dilutions were used when 30 µg of spleen homogenate was used as a positive control. On the other hand, dilutions of secondary antibody goat anti-rabbit were 1:500, 1:1000 and 1:2000. Use of 1:2000 dilution showed sharp signal when primary antibody dilution 1:500 was used. In contrast, using goat anti-rabbit secondary antibody at 1:500 or 1:1000 dilutions resulted in an increased background (dark staining, high noise to signal) when 1:500 rabbit anti-CD4 primary antibody was used. Likewise, incubation time was also optimised. The highest signal to noise was observed when 1 h rabbit anti-CD4 primary antibody incubation at RT was used whereas in shorter incubation signal was indictable. Extended period of incubation (8-10 hour at RT or 4°C) generated background in the blot. Nonspecific binding of antibodies was minimised using a solution of 5% w/v skimmed milk (Coles, Australia) and 1% w/v polyvinylpyrrolidone (Sigma-Aldrich) in 0.05% TBST for 1 hour at RT. Increasing the duration of blocking time

up to overnight (8-10 hours) in RT or at 4°C increased the background. Taken together, 1 hour incubation with 1:500 rabbit anti-CD4 primary antibody followed by another 1 hour incubation with 1:2000 goat anti-rabbit secondary antibody when 1 hour blocking was used, optimal signal was detected. CD8 antibody was optimized the same way as discussed in CD4. For CD8, 1:75 dilution of mouse primary antibody and 1:500 dilution of mouse anti-mouse secondary antibody for 1 hour incubation each while1 hour blocking was used; a sharp signal was obtained.

2.2.10.5 Band quantification

The WB image was opened in the ImageJ. A band of interest in WB was contoured using a rectangular box and intensity was measured (bigger the band higher the number). This band intensity was expressed as a raw value (n=3 bands/animal, n=3 animals/group).

2.2.10.6 T-cell detection limits in peripheral and CNS tissues

To measure the detection limit of CD4 and CD8 antibody signals in WBs, spleen samples from naïve mice and commercial CD4/8 recombinant proteins were used. Initially, 20, 10 and 5 µg of homogenized spleen protein per lane were assessed by WB. For CD4, the lowest detectable signal was with 5 µg spleen protein, whereas 10 µg spleen proteins was needed to detect CD8; the minimal detectable concentrations of the commercial standards were 5 ng and 5 µg for CD4 and CD8, respectively. These lowest detected concentrations of both groups (spleen & commercial samples) were used as positive (spike) controls to confirm the expected minimal detection of CD4 and CD8 in WBs of total brain protein from the different experimental groups. Briefly, the lowest detectable amount of either CD4 or CD8 protein (spleen or the commercial standards) were resolved in parallel lanes of the same 1D gel along with 60 µg of brain protein and 60 µg of brain protein spiked with the lowest detectable amount of either CD4 or CD8 protein. Proteins were resolved, transferred, stained and imaged as before (see *WB procedure*).

2.2.10.7 Transfer efficiency

SDS-PAGE 1D gel prior to, and after, transfer onto PVDF membranes were fixed and stained with cCBB for 20 hours (see *protein fixation and staining section*) to determine the transfer efficiency of proteins. Imaging was carried out using a FLA-9000 gel imager. The density of the bands (n=3 bands/gel) with the molecular weights corresponding to the known molecular

weights of CD4/8 (37 & 50 KD, respectively) were quantified using Multigauge software (FUJIFILM Corporation, Japan).

2.2.11 Statistical analysis

Data were analysed using unpaired two-tailed t-test, one or two way analysis of variance (ANOVA) and are described in the each figure legend. For all studies appropriate Newman-Keuls or Tukey post hoc analyses were followed to determine specific differences between groups. Data were presented as Mean ± Standard Error of the Mean (SEM), unless indicated in the text. Statistically significant was considered when $p<0.05$. Statistical analyses were performed using GraphPad Prism 7.03 (GraphPad Software, USA) software.

2.2.12 Graphing

GraphPad Prism was used to generate graphs. Figures were constructed using CorelDRAW (version-2018, www.coreldraw.com, Canada) and Photoshop CS6 (64 Bit, Adobe, USA) software. Images were adjusted *en masse* for colour composition if necessary and are described in each manuscript.

Chapter-3 (Paper I)

This chapter has been published in Cells, 8(11), 1314; https://doi.org/10.3390/cells8111314.

cells

MDPI

Article

Suppression of the Peripheral Immune System Limits the Central Immune Response Following Cuprizone-Feeding: Relevance to Modelling Multiple Sclerosis

Monokesh K. Sen [1], Mohammed S. M. Almuslehi [1,2], Erika Gyengesi [1], Simon J. Myers [3], Peter J. Shortland [3], David A. Mahns [1,*] and Jens R. Coorssen [4,*]

1 School of Medicine, Western Sydney University, Locked Bag 1797, Penrith, NSW 2751, Australia; monokesh.sen@westernsydney.edu.au (M.K.S.); m.almuslehi@westernsydney.edu.au (M.S.M.A.); e.gyengesi@westernsydney.edu.au (E.G.)
2 Department of Physiology, College of Veterinary Medicine, Diyala University, Diyala, Iraq
3 School of Science and Health, Western Sydney University, Locked Bag 1797, Penrith, NSW 2751, Australia; s.myers@westernsydney.edu.au (S.J.M.); p.shortland@westernsydney.edu.au (P.J.S.)
4 Department of Health Sciences, Faculty of Applied Health Sciences, and Department of Biological Sciences, Faculty of Mathematics and Science, Brock University, St. Catharines, Ontario, ON L2S 3A1, Canada
* Correspondence: d.mahns@westernsydney.edu.au (D.A.M.); jcoorssen@brocku.ca (J.R.C.); Tel.: +02-4620-3784 (D.A.M.); +905-688-5550 (J.R.C.)

Received: 6 September 2019; Accepted: 18 October 2019; Published: 24 October 2019

Abstract: Cuprizone (CPZ) preferentially affects oligodendrocytes (OLG), resulting in demyelination. To investigate whether central oligodendrocytosis and gliosis triggered an adaptive immune response, the impact of combining a standard (0.2%) or low (0.1%) dose of ingested CPZ with disruption of the blood brain barrier (BBB), using pertussis toxin (PT), was assessed in mice. 0.2% CPZ(±PT) for 5 weeks produced oligodendrocytosis, demyelination and gliosis *plus* marked splenic atrophy (37%) and reduced levels of CD4 (44%) and CD8 (61%). Conversely, 0.1% CPZ(±PT) produced a similar oligodendrocytosis, demyelination and gliosis but a smaller reduction in splenic CD4 (11%) and CD8 (14%) levels and *no* splenic atrophy. Long-term feeding of 0.1% CPZ(±PT) for 12 weeks produced similar reductions in CD4 (27%) and CD8 (43%), as well as splenic atrophy (33%), as seen with 0.2% CPZ(±PT) for 5 weeks. Collectively, these results suggest that 0.1% CPZ for 5 weeks may be a more promising model to study the 'inside-out' theory of Multiple Sclerosis (MS). However, neither CD4 nor CD8 were detected in the brain in CPZ±PT groups, indicating that CPZ-mediated suppression of peripheral immune organs is a major impediment to studying the 'inside-out' role of the adaptive immune system in this model over long time periods. Notably, CPZ(±PT)-feeding induced changes in the brain proteome related to the suppression of immune function, cellular metabolism, synaptic function and cellular structure/organization, indicating that demyelinating conditions, such as MS, can be initiated in the absence of adaptive immune system involvement.

Keywords: inside-out; outside-in; oligodendrocytosis; demyelination; gliosis; histology; top-down proteomics; bioinformatics; mitochondria

1. Introduction

Currently, there are two competing theories regarding the pathophysiology underlying the initiation of Multiple Sclerosis (MS): 'outside-in' and 'inside-out' [1–4]. The former proposes that a dysregulated peripheral immune system leads to an autoimmune response against myelin components of the central nervous system (CNS). The central concept of this theory has been built mainly on the basis of studies

using the experimental autoimmune encephalomyelitis (EAE) animal model [5–7] and correlation of the end stage of treatment (e.g., paralysis and demyelination) with clinical tests and post-mortem samples from MS patients. In EAE, animals are injected with exogenous antigens such as myelin basic protein (MBP), proteolipid protein (PLP) or myelin oligodendrocyte glycoprotein (MOG) and complete Freund's adjuvant (CFA), activating peripheral immune cells, including T- and B-cells. When this immune response is combined with breach of the blood brain barrier (BBB) by injection of pertussis toxin (PT), autoreactive adaptive immune cells from the periphery migrate into the CNS leading to degeneration of oligodendrocytes (OLG), demyelination and gliosis [5,6,8–11]. It is argued that a similar process results in autoimmune cell migration into the CNS of MS patients [7,12–15]. The EAE animal model is thus the favourite choice of many researchers investigating the autoimmune aspects of MS [16].

There are, however, key differences between the EAE model and clinical MS. First, EAE relies on the use of exogenous antigens (MBP/PLP/MOG), whereas the autoimmune response in humans occurs spontaneously and is only detected following repeated episodes of clinical symptoms [17,18]. Second, the immune reaction in EAE is driven mainly by $CD4^+$ T-cells [19,20], whereas in MS, $CD8^+$ T-cells predominate [21–23]. Moreover, MS is a disease of the human cerebral and cerebellar cortices, whereas the effects of EAE are generally localized to the spinal cord [6,10,24–27], with largely non-overlapping changes in the brain proteomes being reported in EAE and MS patients [28,29]. Although therapies developed in EAE improve outcomes in animals, these therapies generally have more limited success in clinical MS in terms of halting disease initiation and progression [17,30]. In contrast to this 'outside-in' theory, the 'inside-out' hypothesis suggests that MS is initiated by an underlying degeneration of OLG and consequent demyelination that leads to the production of endogenous myelin antigens (e.g., peptidyl arginine deiminase, MBP, MOG and PLP) that then trigger an immune response in the CNS [3,4,31]. Histological evidence indicates that the loss of OLG and glial activation can occur in the absence of, or with only a limited number of, peripheral immune cells [32–35] and myelin injury [36]. The possibility of OLG triggering a secondary adaptive immune response has been reported following long-term diphtheria toxin exposure [37] or following a peripheral immune challenge after short-term CPZ-feeding (termed 'cuprizone autoimmune encephalitis' [31]). Cuprizone (CPZ) is synthesised by combining cyclohexanone and oxaldihydrazone [38]. While the mechanism of its toxic actions remain ill-defined, copper chelation [39] and dis-homeostasis of iron, zinc, sodium and manganese have been reported [40–44]. Such ion imbalance leads to endoplasmic reticulum stress, reduced mitochondrial ATP synthesis, and increased production of reactive oxygen and nitrogen species (reviewed in [2]). OLG appear to be preferentially susceptible to CPZ toxicity and likely degenerate due to their high energy demands and lower levels of anti-oxidant enzymes [45–47].

Intriguingly, longer-term CPZ-feeding did not evoke a peripheral immune response in the CNS [31,37,48]. Whether the failure of numerous CPZ studies [31,37,48] to observe an immune response associated with long duration feeding (>5 weeks) is due to a toxic effect of CPZ on the peripheral immune system remains unclear [31,37], but CPZ has been shown to have deleterious effects on immune organs like the spleen [49] and thymus [50].

To address this issue, this study compared whether a low (0.1%) or standard (0.2%) dose of CPZ when combined with disruption of the BBB by PT recruited peripheral immune cells into the CNS in mice. At first, a low and a standard dose of CPZ were used for 5 weeks and the amount of oligodendrocytosis (i.e., degeneration or loss of OLG), gliosis and demyelination was quantified; the low dose produced significant demyelination of the corpus callosum (CC), with limited suppression of splenic CD4/8 and no change in overall splenic mass. Having observed that 0.1% CPZ produced comparable oligodendrocytosis, but had less severe effects on the peripheral immune system, in the second study, 0.1% CPZ-feeding was extended to 12 weeks (±PT) to test whether a slower, progressive demyelination (i.e., more reminiscent of MS) and less severe effects on the peripheral immune organs could trigger an adaptive immune response in the CNS. Histological analyses were used to assess oligodendrocytosis, demyelination and gliosis in the CNS, as well as the levels of adaptive immune cells (CD4 and CD8) in brain and spleen.

In a subset of the mice in both experiments, the whole brain proteome was assessed using a well-established 'top-down' approach (i.e., two-dimensional gel electrophoresis coupled with liquid chromatography and tandem mass spectrometry) to identify changes in protein abundance correlated with key changes in molecular pathways [49,51–53]. To best understand the underlying molecular/cellular processes, a 'top-down' proteomic analysis was critical to identifying key protein species or *proteoforms*, the biologically active entities [54–56]. Thus, while much is assumed in the literature regarding the actions of CPZ at the molecular level by extrapolation of effects in vitro or at the cellular level, only such quantitative analyses can help to directly understand the underlying effects of CPZ(±PT).

2. Materials and Methods

2.1. Animals, Feeding, Injection and Monitoring

Seven-week-old male C57Bl/6 mice (n = 108) were purchased from the Animal Resources Centre, Murdoch, WA, Australia (www.arc.wa.gov.au) and co-housed (2 mice) in individual ventilated GM500 cages (Tecniplast, Buguggiate, VA, Italy) in the local animal care facility (School of Medicine, Western Sydney University). Animals were allowed to acclimatise for one week to the new environment prior to initiation of CPZ-feeding. Mice were maintained in a controlled environment (12-hour (h) light/dark cycle: 8am–8pm light, 8pm–8am dark, 50–60% humidity and at 21–23 °C, room temperature (RT)) throughout the entire period. Standard rodent powder chow (Gordon's specialty stockfeeds, Yanderra, NSW, Australia) and water were available *ad libitum*. Oral feeding of CPZ ([Bis(cyclohexanone)oxaldihydrazone, Sigma-Aldrich, St. Louis, MO, USA], 0.1–0.2% *w/w* freshly mixed with rodent chow) was used to induce oligodendrocytosis as previously described [2,57–59]. To breach the BBB, the same methods as previously established for EAE were used i.e., 2–3 intraperitoneal (IP) injections of PT [8,60–63]—but adapted so that the breach of the BBB was timed (i.e., 400 ng on days 14, 16, and 23) to coincide with the reported onset of CPZ-induced oligodendrocytosis, demyelination and gliosis [2,57–59]. The efficacy of BBB breach has been shown using immunoglobulin G staining in the CPZ-fed mice [64]. CPZ groups (0.1% and 0.2%) were fed freshly prepared (daily) CPZ in rodent chow for either 5 (n = 10/group) or 12 (n = 12/group) weeks. Age-matched, naïve control (Ctrl, 5-week study n = 10 and 12-week study n = 12) and PT only (5-week study n = 10 and 12-week study n = 12) groups were used. Mice were weighed at the beginning of the studies, weekly throughout, and prior to culling, and the data from both groups (5 and 12 weeks) were combined (Figure 1). Research and animal care procedures were approved by the Western Sydney University Animal Ethics Committee (ethics code: A10394) in accordance with the Australian Code of Practice for the Care and Use of Animals for Scientific Purposes as laid out by the National Health and Medical Research Council of Australia.

2.2. Histology and Immunohistochemistry

2.2.1. Tissue Preparation

At the end of each feeding period (5 or 12 weeks), all mice were terminally overdosed with sodium pentabarbitone (250 mg/kg, Lethobarb^{TM}, Tory laboratories, Glendenning, NSW, Australia) and perfused with 30 mL of 0.9% saline followed by 50 mL of cold 4% paraformaldehyde (PFA, Sigma-Aldrich) for ~5 minutes (min). Brain and spleen samples were collected and post fixed with 4% PFA at 4 °C for one week and stored in 0.01 M phosphate buffered saline (PBS, Sigma-Aldrich) solution containing 0.02% sodium azide (Amresco, Solon, OH, USA) at 4 °C for ≤1 month or until sectioned. Spleen weights were measured (n = 3 and 5 from 5- and 12-week studies, respectively) and expressed as a function of body weight (Supplementary Figure S5c). Prior to sectioning, whole brain and spleen were immersed in 30% sucrose for 48 h at RT for cryo-protection followed by embedding in 4% gelatine (Chem-Supply, Gillman, SA, Australia) at −20 °C. Brains (5 weeks: 50 µm and 12 weeks: 40 µm) and spleen (20 µm) were sectioned coronally on a Leica cryostat (Leica, Wetzlar, HE, Germany). Sections were transferred to either 6-well plate (Sakura, Torrance, CA, USA) containing cold (5–6 °C)

0.01 M PBS (free floating) or mounted onto 0.5% gelatine-coated slides (Knittel Glass, Braunschweig, NI, Germany) as described previously [65].

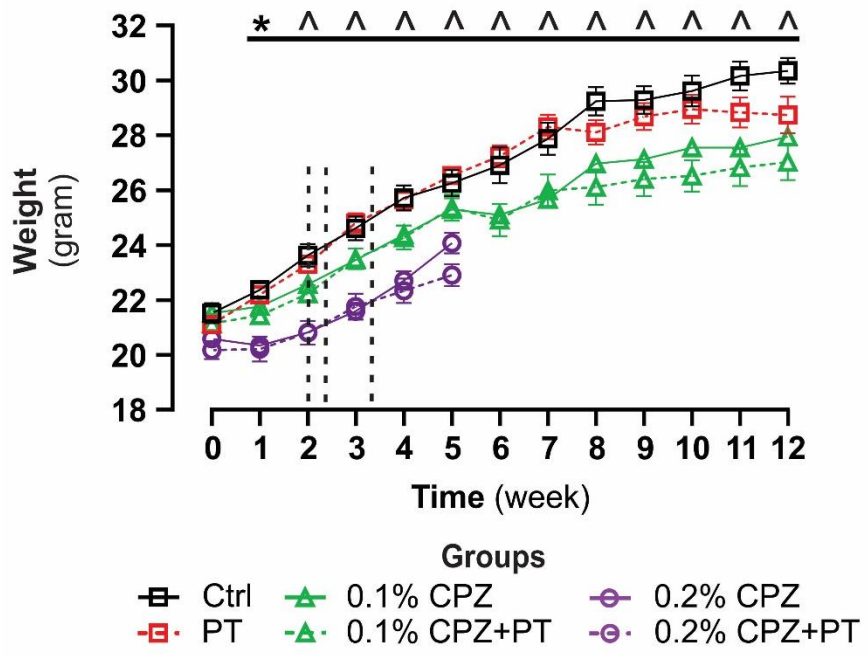

Figure 1. Body weight changes induced by CPZ-feeding. All mice gained weight over time. Groups fed the highest dose of CPZ(±PT) in each experiment gained weight significantly more slowly compared to other groups. Vertical dash lines indicate the timing of individual PT injections (i.e., days 14, 16, and 23). Data are expressed as mean ± SEM. Two-way ANOVA and Tukey post hoc analysis were used to determine differences among groups (* $p < 0.05$, ^ $p < 0.0001$, 5-week study $n = 22$ animals/group of which $n = 12$ animals/group continued feeding for 12 weeks).

2.2.2. Silver Myelin Staining and Analysis

Silver staining of myelin was performed at RT as previously described [66,67]. Briefly, tissue sections were mounted onto 0.5% gelatine-coated slides and air dried for 48 h before immersion in 10% formalin (Sigma-Aldrich) for 2 weeks to increase the contrast of the staining. Sections were stained in a large glass container in parallel to maintain the consistency of staining. Slides were washed with distilled water and pre-treated with lipid-solvent pyridine and acetic anhydride solution (ratio 2:1) for 30 min. Sections were then rehydrated with serial dilutions of ethanol 80, 60, 40 and 20% for 20 seconds (sec) in each step followed by two washes with distilled water. Slides were then immersed in ammonical silver nitrate (Chem-Supply) containing developing solution (0.2% ammonium nitrate, 0.2% silver nitrate and 5% sodium carbonate) for 45 min. Sections were then dehydrated by rinsing sequentially using 20, 40, 60, 80, and 100% ethanol for 20 sec in each step. Sections were cleared by immersing the slides in xylene for 5 min and then sealed using cover slips (Knittel Glass) and ~1 mL mounting medium (Merck, Darmstadt, HE, Germany), and air dried for 72 h. The sections were viewed with an Olympus Carl Zeiss Bright Field Microscope (Zeiss, Jena, TH, Germany) and all images were captured at the same microscope settings (i.e., a fixed exposure time, magnification and illumination intensity). In ImageJ (https://imagej.nih.gov/) software, the region of interest (ROI) was contoured, and the mean optical density quantified (sum of each pixel intensity [range black (0) to white (256)] divided by the number of pixels in the ROI). To quantify the amount of myelin present (which stains black), data were expressed as the reciprocal of the light intensity (i.e., the smaller the value, the lower the myelin content) and normalised to the Ctrl groups (n = 3–5 animals/group and 5–9 sections/animal). The effectiveness of CPZ-feeding is frequently determined by loss of myelin from the midline corpus callosum (MCC),

in this study the effectiveness of CPZ-induced demyelination was confirmed in the MCC and lateral corpus callosum (LCC). Anatomical landmarks were identified as described previously [68,69].

2.2.3. Immunofluorescence Staining and Analysis

All staining was performed at RT. Free floating brain (40–50 µm) and slide-mounted spleen (20 µm) coronal tissue sections were washed thrice with warm (40–50 °C) 0.01 M PBS to remove the gelatine and then immersed in 5–10% goat serum (Sigma-Aldrich) for 2 h with agitation at 50 rpm on a shaker table to block non-specific antibody (Ab) binding sites. Sections were then incubated (12 h) with primary monoclonal Ab to either neurite outgrowth inhibitor A (rabbit anti-Nogo A, 1:500, Merck-Millipore, Burlington, MA, USA), glial fibrillary acidic protein (mouse anti-Gfap-Alexa 488, 1:1000, Merck-Millipore), ionized calcium-binding adapter molecule 1 (rabbit anti-Iba 1, 1:1000, Wako, Chuo-Ku, OSA, Japan), anti-cluster of differentiation (rabbit anti-CD4, 1:200, Abcam, Cambridge, UK), or anti-CD8 (mouse anti-CD8, 1:100, Santa-Cruz Biotechnology, Dallas, TX, USA) diluted in 0.01 M PBS containing 0.1% Triton X100 (Tx100). Sections were then washed thrice with 0.01 M PBS and incubated with corresponding Alexa Fluor (either 488 or 555, dilution: 1:500) secondary Ab (diluted in 0.01 M PBS/0.1% Tx100 solution for 2 h while shaking at 50 rpm). Sections were then rinsed thrice with 0.01 M PBS and 1.5 µg/mL Vectasheild™ plus 4',6-diamidino-2-phenylindole (DAPI, Vector Laboratories, Burlingame, CA, USA) to counterstain nuclei. Slides were sealed with cover slips and stored in the dark at 4 °C until analysis. Images were captured as before (using an Olympus Carl Zeiss Fluorescence Microscope) using the same fixed parameters (exposure and magnification). Quantification was performed using ImageJ, measuring the fluorescence intensity of Gfap, Iba 1, CD4 and CD8 from each ROI as described in silver myelin staining and analysis (n = 3–5 animals/group and 5–10 sections/animal). Cells positively stained for Gfap, Iba 1 and Nogo A (and co-stained with DAPI) were counted using the unbiased stereo investigator optical fractionator workflow software [65,70]. To obtain the cell density, total cell number was divided by total measured volume and the data expressed as 10^4 cells/mm^3 (n = 3–5 animals/group and 5–9 sections/animal).

2.3. Two-Dimensional Gel Electrophoresis (2DE) and Analysis

2.3.1. Sample Collection, Homogenisation and Protein Estimation

At the end of each experiment (i.e., 5 or 12 weeks) period, mice (n = 5 animals/group) were euthanized by overdose of isoflurane (Cenvet, Blacktown, NSW, Australia) exposure. Whole brains were collected following decapitation and immediately rinsed with ice cold 0.01 M PBS containing a cocktail of protease, kinase, and phosphatase inhibitors (Sigma-Aldrich, [51,52]) to remove any traces of blood. Tissue homogenisation was accomplished by automated frozen disruption using a Mikro-Dismembrator (40 Hz for 1 min, Sartorius, Göttingen, NI, Germany) to facilitate optimal protein extraction [52,71]. Powdered tissue samples were mixed with cold 20 mM HEPES hypotonic lysis buffer (Amresco) containing the cocktail of protease, kinase, and phosphatase inhibitors and vortexed for 90 sec followed by the restoration of isotonicity using the addition of an equivalent volume of ice cold 0.02 M PBS and incubated for 5 min on ice. The samples were then centrifuged (Beckman Coulter, Indianapolis, IN, USA) at 125,000× g (using a SW 55 Ti rotor) at 4 °C for 2 h. The resulting first supernatant (SP1) was collected as total cytosolic soluble protein (SP). The pellet was washed with ice cold 0.01 M PBS to extract any remaining cytosolic proteins (SP2) and centrifuged 8 h at 125,000× g. The resulting supernatant (SP2) was pooled with the SP1 fraction, and this combined soluble protein fraction was concentrated using an Amicon Ultra-4 centrifugal 3 KD cut-off filter column (Merck-Millipore). To prevent salt interference during the 1st dimension isoelectric focussing step, the resulting SP samples were washed three times using cold 4 M urea (Amresco) buffer supplemented with the inhibitor cocktail. The pellet containing membrane proteins (MP) was resuspended with cold 2DE solubilisation buffer (8 M urea, 2 M thiourea and 4% CHAPS) containing the inhibitor cocktail [71,72]. Total protein concentrations in SP and MP fractions were measured using the EZQ™

Protein Quantitation Kit (Life Technologies, Eugene, OR, USA) according to the manufacturer's instructions, using bovine serum albumin (Amresco) as the standard.

2.3.2. Protein Separation

At first, proteins were separated based on their isoelectric point (1st dimension) as follows: 100 µg of proteins were loaded onto an immobilised pH gradient (IPG, 7 cm, non-linear, Bio-Rad, Hercules, CA, USA) strips and passively rehydrated for 16 h at RT. Rehydrated IPG strips were placed in the Protean isoelectric focusing (IEF) tray (Bio-Rad) and IEF was carried out in a PROTEAN IEF system (Bio-Rad) for high-throughput protein resolution, initially at 250 V for 15 min which then increased linearly to 4000 V at 50 µA/gel for 2 h, with multiple electrode wick changes during voltage ramping to facilitate desalting. The following parameters were used during IEF: focus temperature: 17 °C, desalting: 15 min, linear gradient: 2 h, holding voltage: 500 V. Following IEF, IPG strips were either stored at −20 °C or immediately resolved in the second dimension using sodium dodecyl sulphate-polyacrylamide gel electrophoresis (SDS-PAGE). Second dimension (2D) was carried out using 1 × 84 × 70 mm 12.5% acrylamide SDS-PAGE gels. Prior to 2D, IPG strips were incubated for 10 min with 130 mM DTT in equilibration buffer (6 M urea, 20% glycerol, 2% SDS and 375 mM tris) followed by 10 min alkylation in equilibration buffer containing 350 mM acrylamide. IPG strips were then inserted on top of the SDS-PAGE gels and covered with warm (40–50 °C) ~300 µL agarose solution (0.5% low melting agarose, Bio-Rad) containing 2% bromophenol blue (Bio-Rad). Electrophoresis was carried out at 4 °C by applying 150 V for 5 min followed by 90 V for 3 h or until the bromophenol dye reached the bottom of the gels as described previously [51,52,71,73].

2.3.3. Protein Fixation and Staining

Upon completion of electrophoresis, gels (5-week study n = 180 gels and 12-week study n = 120 gels) were fixed in 10% methanol and 7% acetic acid solution for 1 h at RT (on a shaker at 50 rpm). Gels were rinsed with distilled water for 3 × 20 min to remove residual methanol and acetic acid followed by staining with 50 mL of high sensitive colloidal Coomassie Brilliant Blue (G-250, Amresco) and continuous shaking, as previously described [52,74–78]. After 20 h, the solution was discarded and stained gels were washed using 50 mL of 0.5 M sodium chloride solution for 3 × 15 min to remove excess Coomassie dye. Scanning of gels was carried out at 100 µm resolution using a Typhoon™ FLA-9000 gel imager (GE Healthcare, Chicago, IL, USA). Excitation/emission wave lengths were 685/>750 nm and the photomultiplier tube was set to 600 V. Gels were preserved in 20% ammonium sulphate (50 mL/gel) and stored at 4 °C until spot excision [52].

2.3.4. Protein Resolution, Detection and Image Analysis

Quantitative analysis of gels was carried out using Delta 2D image analysis software (www.decodon.com/delta2d-version4.0.8, DECODON, Greifswald, MV, Germany) as described previously [49,52,53,74,78]. Briefly, total spot numbers were calculated from the raw images using the Delta 2D automated spot detection system, while gel edges and the protein ladder were excluded [52,79]. Gel images were warped and fused to generate a master image ensuring consistent spot matching. The fluorescent volumes of individual spots (i.e., protein abundance) were expressed as a function of all spot volumes detected and were measured using Delta 2D to assess changes across the different experimental groups. Four spot inclusion criteria were applied: 1) any changes in spot volumes were detectable in all biological replicates (n = 5 animals/group) and their associated technical replicate gels (n = 3 gels/fraction/animal, i.e., 15 gels/experimental group); 2) the relative standard deviation for technical replicates did not exceed 30% within individual animals; 3) values had to differ significantly ($p < 0.05$, t-test) between the naïve Ctrl group and at least one test group; and 4) have a fold change of ≥1.5 (increased/decreased fluorescence), to be considered genuine changes, and thus candidates for analysis by LC/MS/MS. These criteria allowed for reliable and reproducible identification of CPZ, CPZ+PT or PT associated proteoform changes. The fold change ($p < 0.05$,

one-way ANOVA) of differentially abundant protein spots was calculated by dividing the average grey value (i.e., fluorescence intensity of the protein spot of each experimental group compared to the naïve Ctrl group) and presented in $\log_2$ scale as fold change relative to Ctrl. Precision Plus Protein Kaleidoscope molecular weight (MW) and 2DE isoelectric point *(pI)* standard (Bio-Rad) calibration gels (n = 3) were used to calculate the experimental *pI* and MW of resolved proteoforms. The coefficient of variation (standard deviation/mean) for the MW and *pI* migration was 2.6% and 1.4% for 2DE standards, respectively (n = 3), and 4% for MW ladders for experimental gels (n = 20). To quantify the gel shift indicative of protein post-translational modification (PTM), experimental MW and *pI* values were plotted relative to theoretical values; significant changes were indicated when the experimental measure fell above or below the 95% confidence intervals of the MW and *pI* calibration curves. The results are plotted as the average for both 5 and 12 weeks combined.

2.3.5. In-Gel Protein Spot Digestion

Protein spots of interest were excised manually and de-stained for 2 × 15 min with 50 mM ammonium bicarbonate (Sigma-Aldrich) solution containing 50% acetonitrile (Sigma-Aldrich). After complete removal of Coomassie dye, gel pieces were dehydrated using 100% acetonitrile. In-gel digestion was carried out by adding 20 µL of freshly prepared trypsin (12.5 ng/µL, Promega Corporation, Madison, WI, USA) to a solution of 50 mM ammonium bicarbonate for 8 h at 4 °C. Digested peptides were removed from the gel by 30 min sonication. The solution was then acidified by the addition of 2 µL of 2% formic acid (Merck-Millipore). The resulting peptide solution was concentrated to 10 µL using a Speed Vac™ vacuum concentrator (1400 rpm for 10–15 min, John Morris Scientific, Chatswood, NSW, Australia) and stored at -80 °C for future use or immediately subjected to LC/MS/MS [52].

2.3.6. Liquid Chromatography Tandem Mass Spectrometry (LC/MS/MS)

The concentrated peptide solutions were analysed by LC/MS/MS using a nanoAcquity ultra performance liquid chromatography system linked to a Xevo QToF mass spectrometer as previously described [49,52,80,81]. In brief, peptide sample solutions (3 µL) were loaded onto a C18 symmetry trapping column (20 mm × 180 µm), and desalted for 3 min at 5 µL/min flow rate using 1% solvent B (LC/MS grade 1% acetonitrile and 0.1% formic acid) in solvent A (Mili-Q water + 0.1% formic acid). The peptides were washed off the trapping column at 400 nL/min onto a C18 BEH analytical column (75 µm × 100 mm), packed with 1.7 µm particles of pore size 130 Å using a 60 min ramped LC protocol. The initial solvent composition was held at 1% B for 1 min followed by linear ramping to 50% B over 30 min. A further linear ramp to 85% B commenced at 31 min and held until 37 min before the solvent composition was returned to 1% B. Separated peptides were analysed using tandem mass spectrometry with a constant cone voltage of 25 V and source temperature of 100 °C, implementing an emitter tip that tapered to 10 µm at 2.3 kV. A data-directed acquisition (DDA) approach was performed, which continuously scanned across the *m/z* range 350–1500 for peptides of charge state 2^+–4^+ with an intensity of more than 50 counts/sec, with a maximum of three ions in any given 3 sec scan. Selected peptides were de-isotoped, fragmented and the masses measured. The ramped collision energy profile was set to 15–35 V at low mass and 30–40 V at high mass. The mass of the precursor peptide was then excluded for 30 sec. The DDA was via Masslynx software (version 4.1, Micromass, Manchester, UK) and converted to a peak list file (PKL) format using the ProteinLynx Global Server (Waters, Milford, CT, USA). Data were analysed using MASCOT Daemon (www.matrixscience.com) and queried against the SwissProt and MSPnr100 databases (see www.wehi.edu.au) using delimited and species-specific searches to identify the protein species using the following MASCOT parameter settings: the enzyme trypsin and taxonomy *Mus musculus* (mouse) were fixed. Moreover, no fixed modification was selected whereas variable modifications were carbamidomethyl (C), deamidated (NQ), oxidation (M) and propionamide (C). Only two missed cleavages of lysine or arginine residues were allowed; mass tolerance of parent and MS/MS ions was set to ±0.05 Da and peptide charge state was 2^+–4^+. The results of the search were filtered by excluding peptide hits with a p-value greater

than 0.05. While the SwissProt and MSPnr100 databases were both used to best ensure confirmation of a protein identity, the higher of the two scores was documented in Table 1. When multiple proteins were detected from the same spot, the following criteria were applied to identify the most abundant and thus the most likely to have contributed to the originally detected change in spot volume: 1) The highest MASCOT score (>100) with a sequence coverage ≥5%; and 2) ≥4 unique matched peptides.

2.3.7. Literature Mining and Bioinformatics

A PubMed (www.ncbi.nlm.nih.gov/pubmed/) literature search was carried out for papers published in the English language using the identified canonical protein name with either CPZ, EAE or MS to find literature relevant to molecular/cellular functions. The UniProt (www.uniprot.org) database was used to obtain the gene and UniProt accession number (ID) of the identified protein species and analysis of subcellular localization [82]. A mapping of genes according to their classification and molecular functions was derived from protein analysis through evolutionary relationships (PANTHER, www.pantherdb.org) database using gene IDs of each identified protein [53]. Cellular components, biological processes and physiological pathways of the identified protein species were categorised using the database for annotation, visualization and integrated discovery (DAVID, version 6.8, david.ncifcrf.gov) database. UniProt accession IDs were used in the DAVID database to categorise proteins according to their GO (gene ontology, www.geneontology.org) cellular components, and biological processes. DAVID also characterised the physiological pathways associated with the identified protein species according to the Kyoto encyclopaedia of genes and genomes (KEGG, www.genome.jp/kegg) category [83]. Protein species were further characterised and grouped using the search tool for retrieval of interacting genes/proteins (STRING; version 10, string-db.org) to identify potential protein–protein interactions (PPI, [84]). Using the STRING database, a PPI map was generated in which each node represents a protein and connecting lines represent evidence of association (with line thickness indicating the strength of the potential interaction). Such associations are based on text mining, co-expression, co-occurrence, databases, experiments, neighbourhood and gene fusion of the identified proteins [85,86].

Table 1. 2DE LC/MS/MS analyses identified 33 proteins from 5- and 12-week studies.

Spot ID/Tissue Fraction	UniProt ID	Protein Name	Gene ID	Score/ Coverage %	Unique Peptides	MW/*pI*		Highest Fold Change		Data Base	Reference		
						Theoretical	Experimental	5 W	12 W		CPZ	EAE	MS
A4/MP	G3UVV4	Hexokinase 1	Hk1	270/10	10	101.8/6.2	220/6.4	0.66(0.2)↓	0.48(0.1PT)↓	M	-	-	[87]
5N3/SP	P05063	Fructose-bisphosphate aldolase C	Aldoc	510/33	12	39.3/6.6	73.4/5.9	0.32(PT)↓	×	S	-	[88]	[89]
D2/MP	Q99KI0	Aconitate hydratase	Aco2	407/25	18	85.4/8.1	182.9/8.2	2.37(0.2PT)↑	0.23(PT)↓	M	-	-	[90]
A10/MP	Q8K2B3	Succinate dehydrogenase flavoprotein subunit	Sdha	230/12	8	72.5/7	96/6	0.57(0.1PT)↓	0.61(0.1PT)↓	M	[91]	-	-
F2/MP	P08249	Malate dehydrogenase	Mdh2	983/57	25	36/8.9	70.2/6.9	2.30(0.1PT)↑	×	S	-	[88]	[92]
5O5R/MP	Q91WD5	NADH dehydrogenase iron-sulfur protein 2	Ndufs2	173/10	5	52.5/6.5	52.2/5.5	0.59(PT)↓	1.77(0.1PT)↑	M	[91]	-	-
5R5/SP	Q03265	ATP synthase subunit-α	Atp5a1	177/26	15	59.7/9.2	117.4/8.2	2.76(PT)↑	0.37(0.1)↓	S	[91]	-	[89]
A37/MP	Q60930	Voltage-dependent anion-selective channel protein	Vdac2	155/14	5	31.6/7.4	18.7/6.6	0.42(0.2PT)↓	0.5(0.1PT)↓	M	-	-	[90]
A34/MP	P05201	Aspartate aminotransferase	Got1	350/26	12	46.2/6.6	29.5/7.4	0.69(0.2PT)↓	0.38(0.1PT)↓	M	-	-	[89]
A1/MP	B2RXT3	Ogdhl protein	Ogdhl	291/10	10	114.5/6.4	243.3/5.9	0.69(0.2)↓	0.65(0.1PT)↓	M	-	-	-
B23/MP	Q8VDQ8	NAD-dependent protein deacetylase sirtuin-2	Sirt2	529/36	13	39.4/6.35	27.8/7	0.69(0.1PT)↓	0.33(0.1PT)↓	M	-	[93]	[93]
5C1/SP	Q9JHI5	Isovaleryl-CoA dehydrogenase	Ivd	650/39	17	46.3/8.5	79.4/6.2	0.42(0.2PT)↓	1.80(PT)↑	S	[49]	-	-
5G5/SP	Q91WQ3	Tyrosine-tRNA ligase	Yars	333/28	17	59/6.57	124.9/6.4	0.32(0.2PT)↓	1.97(PT)↑	S	-	-	-
A22/MP	P26443	Glutamate dehydrogenase 1	Glud1	324/12	7	61.3/8	106.8/6.8	2.24(0.2PT)↑	×	M	-	[94]	[95]
A16/MP	Q99MN9	Propionyl co-enzyme A carboxylase-β	Pccb	277/16	6	50.4/5.7	60.5/6.3	×	0.43(0.1PT)↓	M	-	-	-
B20/MP	P30275	Creatine kinase U-type	Ckmt1	137/22	11	46.9/8.4	83.2/7.5	0.44(0.2PT)↓	0.35(0.1)↓	S	-	-	-
A14/MP	P50396	Rab GDP dissociation inhibitor-α	Gdi1	227/20	8	50.5/4.9	77/5.9	0.6(0.2)↓	0.56(0.1PT)↓	M	-	-	[96]
5O4/MP	Q61598	Rab GDP dissociation inhibitor-β	Gdi2	148/10	5	50.5/5.9	55.6/5.7	0.38(PT)↓	×	M	-	-	[96]
5L6/MP	P46460	Vesicle-fusing ATPase	Nsf	466/36	33	82.6/6.5	116/6.3	0.52(0.2PT)↓	0.71(0.1PT)↓	S	-	-	-
B17/MP	P11798	Calcium/calmodulin-dependent protein kinase type II subunit-α	Camk2a	225/16	7	54/6.6	53.2/7	×	0.42(PT)↓	M	[97]	[98]	-
A11/MP	O08599	Syntaxin-binding protein 1	Stxbp1	244/12	5	68.7/6.3	90.6/6.3	0.71(0.2)↓	1.61(PT)↑	M	-	[94]	-
A5/MP	A0A0J9YUE9	Dynamin 1	Dnm1	172/9	8	93.9/6.2	200/6.2	1.61(0.2PT)↑	0.46(0.1PT)↓	M	[49]	-	-
E14/MP	Q9D8B3	Charged multivesicular body protein	Chmp4b	176/15	4	24.9/4.6	23.7/5	×	1.65(0.1PT)↑	M	-	-	-
5H2R/MP	P03995	Glial fibrillary acidic protein	Gfap	1802/72	45	49.8/5.2	83.7/5.0	1.86(0.2PT)↑	1.58(PT)↑	S	[99]	[100]	[101]
E2/MP	P08551	Neurofilament light polypeptide	Nefl	1594/57	92	61.4/4.6	53/4.9	0.71(0.2)↓	2.08(0.1PT)↑	S	-	[102]	[103]
5G3/SP	Q9D898	Actin-related protein 2/3 complex subunit 5	Arpc5l	152/26	4	16.9/6.3	26/5.9	0.62(0.2PT)↓	×	M	-	-	-
5I1/SP	P42208	Septin-2	Sept2	180/21	7	41.5/6.1	81/5.7	0.30(PT)↓	1.53(PT)↑	S	-	[93]	[104]
5I2/SP	Q9Z2Q6	Septin-5	Sept5	159/22	9	42.7/6.2	80.4/5.9	0.36(0.2PT)↓	0.46(0.1PT)↓	S	-	[100]	-
4L1/MP	P18872	Guanine nucleotide-binding protein G(o) subunit-α	Gnao1	186/15	5	40.6/5.3	68.5/4.7	7.35(0.2)↑	1.48(0.1PT)↑	S	-	[105]	-
4O3/MP	Q9D7N9	Adipocyte plasma membrane-associated protein	Apmap	148/8	5	46.4/5.9	85/5.6	4.09(0.1)↑	1.46(0.1PT)↑	M	-	-	-
5R1/MP	P14211	Calreticulin	Calr	187/13	7	47.9/4.3	155/4.4	2.50(0.2PT)↑	1.83(0.1PT)↑	S	-	[105]	[106]
5G2/SP	P62259	14-3-3 protein epsilon	Ywhae	110/23	6	29.1/4.6	49.9/4.5	0.66(0.2PT)↓	×	S	-	[100]	[107]
5E1/SP	Q9D154	Leukocyte elastase inhibitor A	Serpinb1a	191/36	18	42.5/5.8	76.7/5.5	0.28(0.2PT)↓	×	S	[49]	-	-

Key: MP, membrane protein; SP, soluble protein; MW, molecular weight; *pI*, isoelectric point; S, Swiss-Prot; M, MSPnr100; PT, pertussis toxin; 0.1, 0.1% CPZ; 0.1PT, 0.1% CPZ+PT; 0.2, 0.2% CPZ; 0.2PT, 0.2% CPZ+PT; W, week; ×, unchanged; ↑, increase; ↓, decrease; -, not found or investigated (details are shown in Figure 5). Some of the spots contained more than one clearly identifiable protein; presented here are the hits with the highest score, coverage and peptide count. UniProt and gene IDs were derived from the UniProt database. MASCOT score, sequence coverage, theoretical (MW/*pI*), and unique peptides number were acquired from the MASCOT database search. Experimental (MW/*pI*) was derived from 2D gels of identified protein spot. References are from the published literature in PubMed on CPZ, EAE and MS and used to compare currently identified proteins with the existing literature.

2.4. Western Blot (WB)

2.4.1. Sample Preparation

Stored brain, spinal cord and spleen samples (n = 3/group) were homogenised in the deep-frozen state as described earlier. Equal ratios (~1 µL/1 µg tissue) of sample and pre-chilled lysis buffer (25 mM Tris, 1 mM EDTA and 1 mM EGTA) containing the inhibitor cocktail were used to solubilize the powdered samples and protein was recovered using centrifugation (at 125,000× g, 4 °C, for 1 h). Protein quantification was then carried out as previously described using the EZQ protein quantitation kit (see above).

2.4.2. Procedure

Total protein extract (brain, spinal cord and spleen) and CD4/8 recombinant proteins were resolved by 10% SDS-PAGE (100 V for 2 h at 4 °C) and transferred (100 V for 2 h at 4 °C) onto 0.22 µm pore size polyvinylidene difluoride (PVDF, Merck-Millipore) membrane using transfer buffer containing 25 mM tris, 192 mM glycine and 20% methanol. The membranes were incubated in blocking buffer containing non-fat dry skimmed milk (5% *w/v*, Coles, Hawthorn East, VIC, Australia) and polyvinylpyrrolidone (1% *w/v*, Sigma-Aldrich), in 0.05% Tris buffered saline-Tween 20 (TBST) for 1 h at RT on an orbital shaker (at 50 rpm). Primary Abs for CD4 (rabbit anti-CD4, 1:500, Abcam) and CD8 (mouse anti-CD8, 1:75, Santa-Cruz Biotechnology) were incubated for 1 h at RT. Blots were then washed thrice with 0.05% TBST at 10 min intervals and horseradish peroxidase-conjugated (HRP) secondary Ab (goat anti-rabbit- or goat anti-mouse-HRP: CD8 1:500, Santa-Cruz Biotechnology and CD4 1:2000, Abcam) was added and incubated for 1 h at RT. Chemiluminescent visualization of the transferred proteins was carried out using an enhanced chemiluminescence detection reagent (500 µL/cm^2 membrane, Merck-Millipore). Blots were scanned for 2 sec on the ImageQuant^{TM} FUJI LAS-4000 biomolecular imager (GE Healthcare). ImageJ software was used to quantify the density of a band of interest on a blot by using a rectangular box to define the band. This band intensity was expressed as a raw value (n = 3 bands/animal, n = 3 animals/group) and presented relative to Ctrl.

2.4.3. Transfer Efficiency

Replicate 1D SDS-PAGE gels were resolved in parallel and one stained with Coomassie Brilliant Blue prior to, and the other after, transfer onto PVDF membrane to determine the transfer efficiency of proteins. Imaging was carried out using a Typhoon^{TM} FLA-9000 gel imager. The density of the bands (n = 3 bands/gel) with the molecular weights corresponding to the known molecular weights of CD4/8 (37 and 50 KD, respectively) were quantified using Multigauge image analysis software-version 3.0 (Fujifilm, Minato-Ku, TYO, Japan).

2.4.4. T-Cell Detection Limits in Peripheral and CNS Tissues

To measure the detection limit of CD4 and CD8 antibody signals in WBs, spleen samples from naïve mice and commercial CD4/8 recombinant proteins (Sino Biological, Wayne, PA, USA) were used. For CD4, the lowest detectable signal was achieved using 5 µg of spleen protein, whereas 10 µg of total spleen protein was needed to detect a CD8 band. The minimal detectable concentrations of the commercial recombinant protein standards were 5 ng and 5 µg for CD4 and CD8, respectively (Figure 3a). These lowest detectable concentrations for both groups (spleen and commercial samples) were used as positive (spike) controls to establish the expected minimal detection of CD4 and CD8 in WBs of total brain protein from the different experimental groups.

2.5. Statistical Analysis and Graphing

Statistical analyses were performed using GraphPad Prism-version 7.03 (www.graphpad.com, San Diego, CA, USA) software. Data were analysed using either one or two-way analysis of variance

(ANOVA) or an unpaired two-tailed t-test and, where appropriate, Newman-Keuls or Tukey post hoc analyses to determine specific differences among groups. Data are presented as means ± standard error of the mean (SEM), otherwise indicated in the text. Statistical significance was accepted when $p < 0.05$. Figures were assembled using CorelDRAW-version 2018 (www.coreldraw.com, Ottawa, ON, Canada) and Photoshop CS6 (Adobe, San Jose, CA, USA) image processing software. All Nogo A images were adjusted only for colour contrast (Supplementary Figures S1 and S2).

3. Results

3.1. Body Weight

Mice in all groups gained weight over the duration of feeding, but this was significantly slower in CPZ(±PT)-fed animals ($p < 0.05$, Figure 1). Significant reductions in weight gain started at week 1 after 0.2% CPZ±PT and week 2 after 0.1% CPZ±PT-feeding and continued until week 11. At week 12, 0.1% CPZ±PT groups were significantly ($p < 0.05$) different compared to the Ctrl group but not to the PT group. No direct or combined effect ($p > 0.05$) of PT was found in any group at any time point.

3.2. Marked Demyelination, Oligodendrocytosis and Gliosis

In both the 5- and 12-week studies, the Ctrl and PT groups exhibited intense silver staining of myelin in the midline corpus callosum (MCC) and lateral corpus callosum (LCC), whereas the 0.1% and 0.2% CPZ-fed(±PT) groups displayed a marked, concentration-dependent loss of silver staining ($p < 0.05$, Figure 2a; Supplementary Figures S1a, S2a, S3a). No differences in the extent of demyelination were found between the MCC and LCC regions in any of the groups with either duration of CPZ-feeding [($p > 0.05$, Figure 2a, (MCC); Supplementary Figure S3a, (LCC)]. Importantly, prolonged 0.1% CPZ (±PT)-feeding for 12 weeks produced a similar amount of demyelination to that seen at 5 weeks with 0.2% CPZ ($p < 0.05$, Figure 2a; Supplementary Figures S1a, S2a, and S3a). Consistent with the significant reduction in silver staining, 5 or 12 weeks of CPZ-feeding produced a significant loss (>90%) of mature, Nogo A positive OLG in the MCC and LCC; feeding with 0.1% was as effective as 0.2% CPZ at inducing OLG loss ($p < 0.05$, Figure 2b; Supplementary Figures S1b, S2b, S3b). Importantly, there were no differences in OLG loss when using 0.1% or 0.2% CPZ for 5 weeks, and 0.1% CPZ-feeding for 12 weeks produced a comparable loss of OLG to that seen at 5 weeks ($p > 0.05$, Figure 2b; Supplementary Figures S1b, S2b, S3b). Similarly, there were marked dose-dependent increases ($p < 0.05$) in the number and intensity of Gfap and Iba 1 staining (Figure 2c,d; Supplementary Figures S1c,d, S2c,d, S3c,d) in the CPZ-fed(±PT) groups compared to Ctrl or PT only animals (which were not different from each other, $p > 0.05$). Taken together, these results indicate that low dose CPZ-feeding for 5 weeks produced an almost complete loss of OLG but a more limited (i.e., slower) demyelination and gliosis response. When this feeding regime was prolonged for 12 weeks, it produced comparable changes to those seen at 5 weeks using 0.2% CPZ. PT had no direct or synergistic effects on any of the histological parameters studied at either time point.

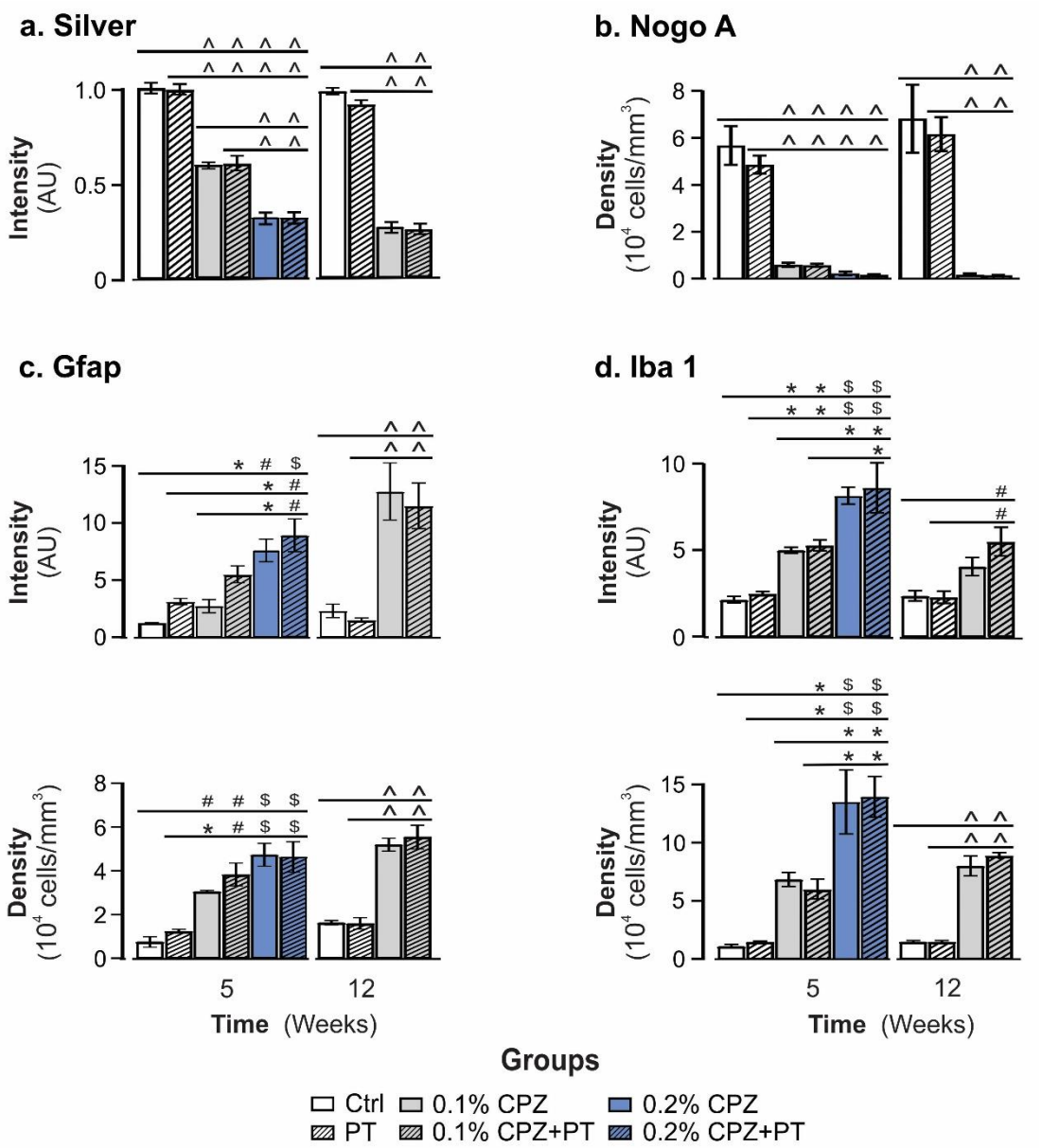

Figure 2. Quantification of demyelination, cell death and gliosis in the midline corpus callosum. (**a**) Silver staining. CPZ-feeding(±PT) led to significant demyelination and reduced silver staining intensity at 5 and 12 weeks. PT alone had no effect. Feeding 0.1% CPZ for longer (12 weeks) produced a comparable demyelination to that seen with 0.2% for 5 weeks. (**b**) Nogo A. CPZ-feeding(±PT) led to significant oligodendrocytosis with 0.1% CPZ was as effective as 0.2% CPZ at either time point. PT alone had no effect. (**c**) Gfap. Staining intensity increased in a dose dependent manner, in the CPZ(±PT) treated groups and this was associated with an increase the number of Gfap positive astrocytes at both time points. PT only did not evoke a Gfap response. (**d**) Iba 1. Increased Iba 1 fluorescence intensity and number of Iba 1 positive microglia were seen in both 5- and 12-week groups. PT alone produced no microglial response. Data are presented as mean ± SEM. One-way ANOVA and Tukey post hoc analysis was used to determine differences among groups (* $p < 0.05$, # $p < 0.01$, \$ $p < 0.001$ and ^ $p < 0.0001$). Quantitation based on analysis of 5–9 sections/animal, 3–5 animals/group.

3.3. Detection and Localisation of CD4 and CD8 T Cells

Immunofluorescence staining of brain sections failed to detect $CD4^+$ and $CD8^+$ positive cells in the CC in CPZ(±PT) groups (Supplementary Figure S4a, even when using high antibody titres and long incubation times). This was not due to the lack of antibody sensitivity, as immunofluorescent CD4 and CD8 positive cells were seen in histological sections of spleen (Supplementary Figure S6a). Likewise, CD4/8 signals in whole brain protein samples were undetectable by western blot (WB) analysis (Figure 3c), even at high protein loads (up to 120 µg). This was not due to the lack of protein transfer from SDS-PAGE gel to PVDF membrane, as transfer efficacy at the molecular weights corresponding to CD4/8 (37 and 50 KD, respectively) were 93 ± 1.6% and 98 ± 0.7%, respectively (Supplementary Figure S4b). Furthermore, CD4/8 signals were also detected by WB analysis when spleen (Figure 3a,c) and EAE spinal cord were used as positive controls (Supplementary Figure S4c; EAE was induced using an established method [8]). The capacity and sensitivity of WB to detect CD4/8 signal was also confirmed by other control experiments in which brain homogenates were spiked with spleen homogenate or commercially available CD4/8 recombinant proteins (Figure 3b). Notably, measurement of splenic weight showed a significant ($p < 0.05$) decrease in splenic mass (37 ± 0.1%) in 0.2% CPZ-fed(±PT) groups whereas no change was observed in 0.1% CPZ(±PT) groups at 5 weeks (Supplementary Figure S5a,c). In contrast, a significant ($p < 0.05$) reduction of splenic mass was observed in 0.1% CPZ(±PT) groups at 12 weeks (Supplementary Figure S5b,c). Moreover, 5 weeks of CPZ-feeding also resulted in a significant dose-dependent reduction in CD4/8 in spleen compared to Ctrl (Figure 3d, 0.2% > 0.1%, $p < 0.05$). Following 5 weeks of 0.1% CPZ-feeding(±PT), the reduction of CD4 (11 ± 0.03%) and CD8 (14 ± 0.03%) signal intensity was less marked than that seen with 0.2% CPZ(±PT) groups (CD4 44 ± 0.03% and CD8 61 ± 0.04%). Following 12 weeks of 0.1% CPZ(±PT), further reductions in spleen CD4 (27 ± 0.01%) and CD8 (43 ± 0.02%) signal intensity and splenic atrophy (33 ± 0.1%) were observed. In addition, immunofluorescence staining of spleen sections (n = 10 sections/animal and n = 3 animals/group) indicated a significant ($p < 0.05$) reduction of CD4 and CD8 in the 0.2% CPZ-fed group (Supplementary Figure S6a,b).

3.4. Brain Proteome Changes

All samples yielded well-resolved proteomes encompassing the full MW/*pI* range of the gels. Representative images of soluble (SP) and membrane (MP) proteomes from Ctrl and 0.2% CPZ-fed mice are shown in Figure 4a. A total of ~1650 consensus spots (i.e., protein spots that resolved consistently and were analysed across all gels) were detected from the combined analyses of whole brain soluble and membrane proteomes (Figure 4a; Supplementary Table S1). The spot quantification from the different groups from both time points is summarized in Supplementary Table S1. The different groups yielded comparable numbers of resolved protein spots at 5 weeks ($p > 0.05$), and this was also true for the 12-week samples ($p > 0.05$, Supplementary Table S1). In total, 845 ± 8 and 793 ± 11 spots were resolved from the soluble and membrane fractions, respectively, in the 5-week study, whereas 824 ± 11 and 717 ± 3 spots were resolved from the soluble and membrane fractions, respectively, in the 12-week study. Database hits of high-quality and confidence were returned following LC/MS/MS analysis and identified 33 different proteoforms from these spots including 73% in the membrane proteome and 27% in the soluble proteome (Table 1).

Table 1 summarizes the best identified proteoforms within each spot that displayed a 100% reproducible change across technical (n = 3 gels/fraction) and biological (n = 5 animals/group) replicates. All identified proteins had a MASCOT score exceeding 100, with 46% between 100–200; 21% between 201–300; 9% between 301–400; 6% between 401–500; and 18% exceeding 500. Moreover, each identification was based on at least 4 unique peptides: 61% based on 4–10 peptides; 27% based on 11–20 peptides; and 9% based on over 30 peptides. Similarly, sequence coverage was always ≥5% with 5–10% for 6 proteins; 11–20% for 11 proteins; 21–30% for 8 proteins; 31–40% for 5 proteins; and >50% for 3 proteins (Table 1). The combination of high MASCOT scores and the presence of ≥4 unique peptides with high coverage highlight the high confidence of the protein identifications.

As also shown in Table 1 and Figure 4b, several of the identified proteoforms displayed a mismatch between their theoretical and experimental MW and *pI*, indicative of post-translational modifications (e.g., phosphorylation and glycosylation). Only, 1 proteoform showed an increase whereas 19 (58%) showed a decrease and 13 (39%) showed the same experimental *pI* relative to the theoretical *pI*. In contrast, twenty-five (75%) proteoforms increased, 4 (12%) decreased, while another 4 remained unchanged in their experimental MW relative to theoretical MW. Interestingly, a subset of proteoforms was found showing an approximate doubling of the experimental MW relative to theoretical—hexokinase 1, aconitate hydratase, ATP synthase subunit-α, ogdhl protein, tyrosine-tRNA ligase and dynamin 1—potentially indicative of dimerization, whereas an approximate tripling of MW may indicate calreticulin trimers (Table 1) suggesting a possible increase in oligomerization/self-association of proteoforms due to CPZ-feeding(±PT).

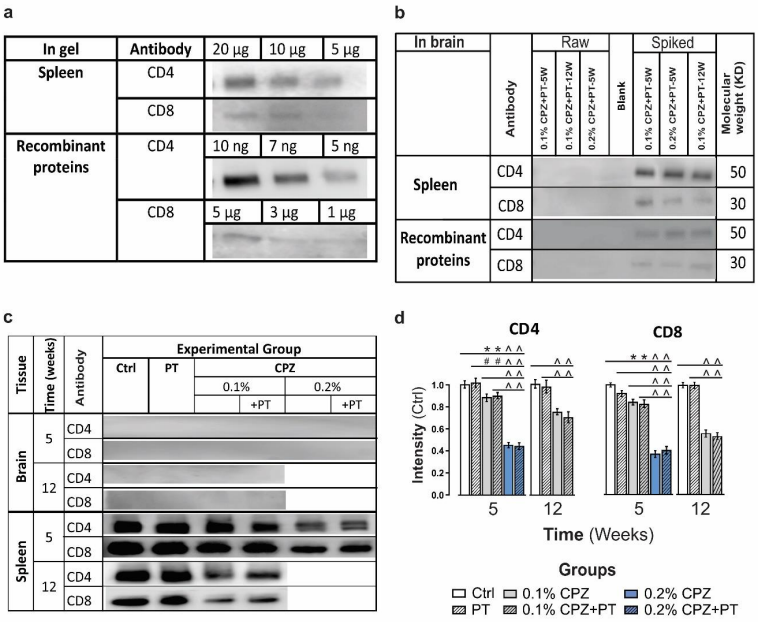

Figure 3. Western blot analysis. (**a**) Measurement of the detection limit of CD4/8 signal using naïve Ctrl spleen homogenates and CD4/8 recombinant proteins in gels. (**b**) Confirmation of CD4/8 signal detection using brain tissue samples (60 µg) spiked with either 5 µg or 10 µg of spleen homogenate or 5 ng and 5 µg commercial CD4 and CD8 recombinant proteins. (**c**) No CD4/8 signal was detected in CPZ(±PT) brain samples whereas a reduced CD4/8 signal intensity was found in spleen. (**d**) Quantification of splenic CD4/8 blots showed a significant reduction of CD4 and CD8 signal intensity in spleens of specific groups. Cropped CD4/8 western blots are presented unaltered and shown in their entirety in Supplementary Figure S7. Data are presented as mean (±SEM) relative to the Ctrl mice. One-way ANOVA and Newman-Keuls Multiple Comparison post hoc analysis were used to determine differences among groups (* $p < 0.05$, # $p < 0.01$ and ^ $p < 0.0001$).

Statistical comparisons of the spot intensities between all groups revealed significant and reproducible changes ($p < 0.05$) in 33 spots across Ctrls and experimental groups in the 5- and 12-week studies (Figure 5). Among the identified proteoforms, not all changes were sustained, or shared, between the 5- and 12-week studies (Supplementary Figure S8). In total, 23 shared proteoform changes were found in both the 5- and 12- week studies (i.e., ≥1.5-fold change in both studies), whereas 7 proteoforms that changed in the 5-week study (≥1.5-fold) did not in the 12-week study (<1.5 fold) and 3 other proteoforms were changed by 12 weeks (≥1.5-fold) but not at 5 weeks (<1.5 fold). The presence of changes at 5 weeks that were not evident at 12 weeks indicates that, relative to their age matched controls, such changes are time-dependent and resolved by 12 weeks.

Whether this return to control levels during prolonged feeding with 0.1% CPZ is due to compensatory mechanisms, aging or other processes remains unknown.

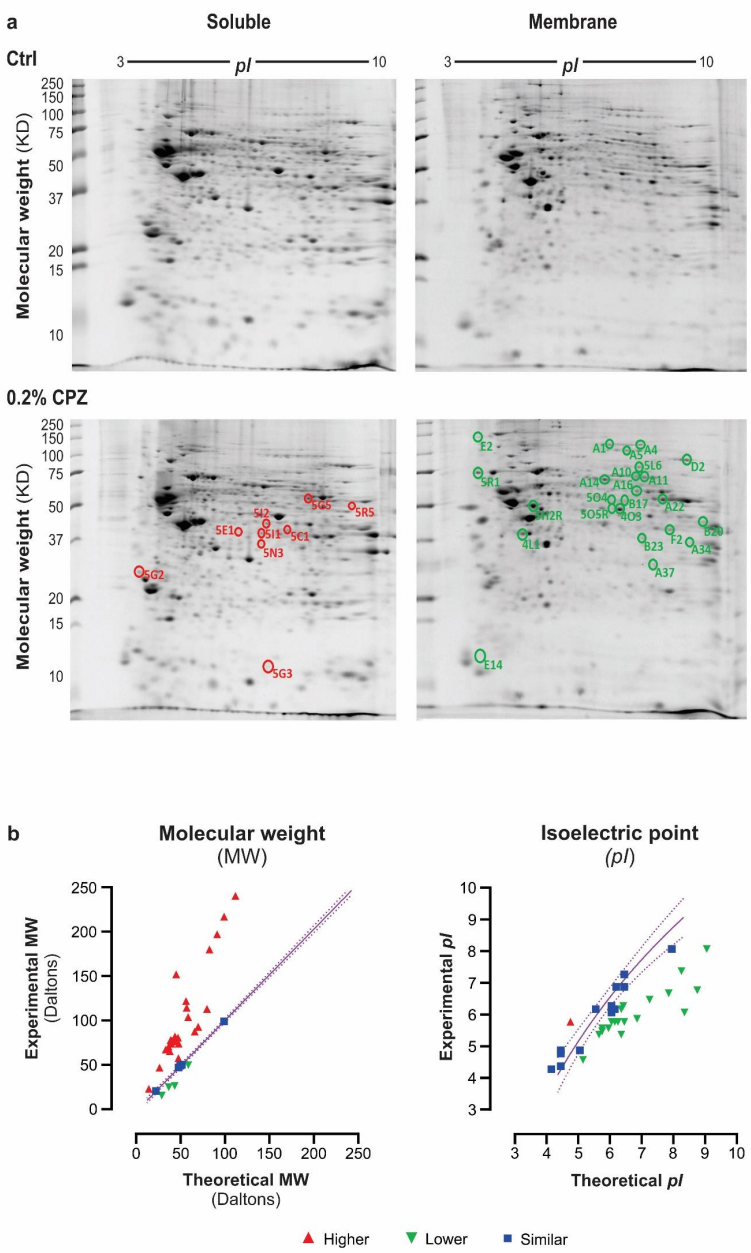

Figure 4. Top-down proteomic analysis. (**a**) Representative two-dimensional gel images of soluble (SP) and membrane (MP) brain proteomes from naïve Ctrl and 0.2% CPZ-fed groups used to detect proteoform changes. Proteoforms were resolved on the basis of their isoelectric point (*pI*) and molecular weight (MW). The total number of spots across different groups at both 5 and 12 weeks is given in Supplementary Table S1. Delta 2D software analysis revealed 33 unique spots for which the spot volume changed by at least 1.5-fold in at least one experimental group; soluble proteoforms are indicated by red circles and membrane proteoforms by green circles. The identities of the protein species are shown in Table 1 (n = 15 gels/fraction, n = 5 animals/fraction, 5-week study n = 180 gels and 12-week study n = 120 gels). (**b**) Comparison between theoretical and experimental MW (left) and *pI* (right) of identified proteoforms. Red represents increase, green decrease and blue indicates no statistically significant difference between the experimental and theoretical values. Purple dashed lines indicate 95% confidence intervals and the solid line represents full agreement between experimental and theoretical values.

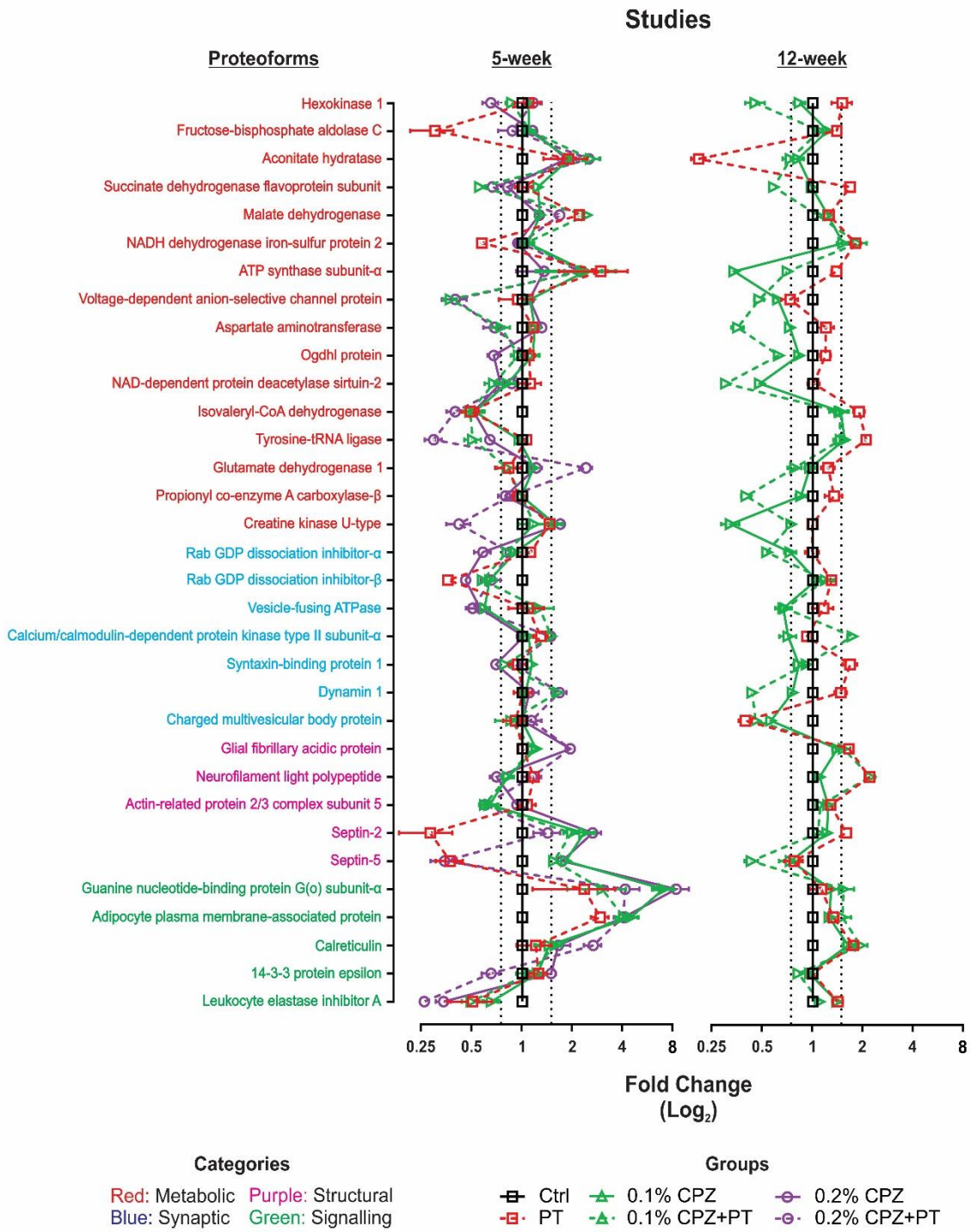

Figure 5. Log_2 fold changes in abundance for 33 proteoforms relative to Ctrl. Each point is the average change in spot volume ratio from all treated groups (PT, 0.1% CPZ, 0.1% CPZ+PT, 0.2% CPZ and 0.2% CPZ+PT) relative to Ctrls from the triplicate gels resolved for each of the 5- and 12-week samples. Only significant changes in abundance ($p < 0.05$) that exceeded the established 1.5-fold criteria (dash lines) in at least 1 experimental group were selected for excision, processing, and protein identification. Solid and dashed lines connect the protein changes within each experimental group with and without PT injection, respectively. Proteoforms (top left) indicate the different functional categories including metabolic (red), synaptic (blue), structural (purple) and signalling (green). Analysis was based on n = 180 gels (5-week study) and, n = 120 gels (12-week study); n = 5 animals/group.

Key: MP, membrane protein; SP, soluble protein; MW, molecular weight; *pI*, isoelectric point; S, Swiss-Prot; M, MSPnr100; PT, pertussis toxin; 0.1, 0.1% CPZ; 0.1PT, 0.1% CPZ+PT; 0.2, 0.2% CPZ; 0.2PT, 0.2% CPZ+PT; W, week; ×, unchanged; ↑, increase; ↓, decrease; -, not found or investigated (details are shown in Figure 5). Some of the spots contained more than one clearly identifiable protein; presented here are the hits with the highest score, coverage and peptide count. UniProt and gene IDs were derived from the UniProt database. MASCOT score, sequence coverage, theoretical (MW/*pI*), and unique peptides number were acquired from the MASCOT database search. Experimental (MW/*pI*) was derived from 2D gels of identified protein spot. References are from the published literature in PubMed on CPZ, EAE and MS and used to compare currently identified proteins with the existing literature.

3.5. Literature Mining

Literature mining via PubMed was used to assess the likely function(s) of identified proteoforms. This confirmed 8 proteoforms (creatine kinase U-type, glutamate dehydrogenase 1, vesicle-fusing ATPase, propionyl co-enzyme A carboxylase-β, tyrosine-tRNA ligase, actin-related protein 2/3 complex subunit 5, charged multi-vesicular body protein and adipocyte plasma membrane-associated protein) not previously related to CPZ, EAE or MS, and 25 proteins (but not specific proteoforms) previously associated with CPZ (8), EAE (13) and MS (16) studies (Table 1).

3.6. Biological Processes and Pathways

The 33 differentially expressed proteoforms were subjected to bioinformatic analysis using PANTHER, DAVID, UniProt and STRING for association with protein classes, molecular functions, physiological pathways, biological processes, cellular components, subcellular localizations and protein–protein interactions. Analysis using PANTHER indicated that the main protein classes were enzyme modulator (15%), nucleic acid binding (10%), oxidoreductase (10%) with 19% unclassified (Supplementary Figure S9a). Molecular function analysis using PANTHER indicated catalytic activity (40%) and binding (26%) roles with 18% unclassified (Figure 6a). However, the potential functions of all the proteoforms were inferred by literature mining for information on the canonical proteins (see *Discussion*). Physiological pathway analysis associated 26% of the proteins with KEGG metabolic pathways categories using DAVID (Figure 6b). GO biological process analysis showed the main categories were oxidation-reduction (13%) and transportation (13%), with 15% unclassified (Supplementary Figure S9b). Moreover, GO cellular component analysis (Figure 6c) indicated that most of the proteins were either cytoplasmic (25%), extracellular exosome (21%), mitochondrial (20%) or related to the myelin sheath (20%). Furthermore, subcellular localization analysis using UniProt revealed the main categories to be mitochondrial (31%) and cytoplasmic (26%; Supplementary Figure S9c). The identified proteoforms were also analysed using STRING software, providing PPI maps; this indicated that 15 of the 33 proteoforms (hexokinase 1, fructose-bisphosphate aldolase C, aconitate hydratase, succinate dehydrogenase flavoprotein subunit, malate dehydrogenase, NADH dehydrogenase iron-sulfur protein 2, ATP synthase subunit-α, voltage-dependent anion-selective channel protein, aspartate aminotransferase, ogdhl protein, isovaleryl-CoA dehydrogenase, tyrosine-tRNA ligase, glutamate dehydrogenase 1, propionyl co-enzyme A carboxylase-β and creatine kinase U-type) were potentially involved in major 'functional interactions' particularly with regard to the metabolic proteins (Figure 6d). Strong one-to-one connections were also indicated between synaptic (rab GDP dissociation inhibitor-α, rab GDP dissociation inhibitor-β, vesicle-fusing ATPase, calcium/calmodulin-dependent protein kinase type II subunit-α and dynamin 1) and structural (glial fibrillary acidic protein and neurofilament light polypeptide) proteoforms. This therefore, also revealed a second cluster of structural and signalling proteoforms. Among the connected proteoforms, 38% showed the highest connecting value (0.9), and 29% and 33% were high (0.7) and medium (0.4), respectively; no low value (0.15) connections were found.

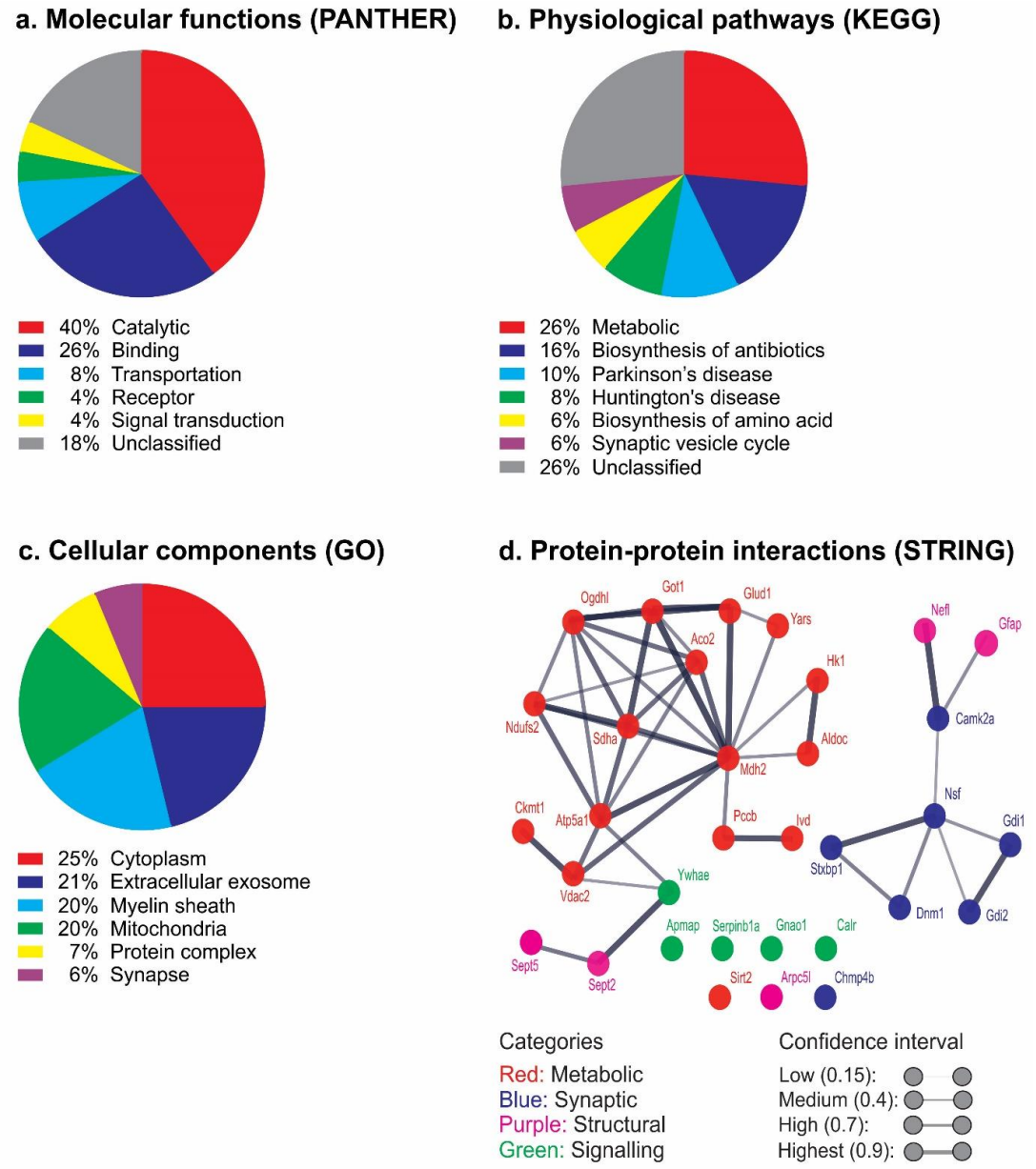

Figure 6. Functional clustering and protein–protein interactions. Pie charts show the distribution of proteins according to (**a**) Molecular functions (characterized using PANTHER), (**b**) Physiological pathways (categorised using KEGG), (**c**) GO cellular components. (**d**) Protein–protein interaction association network maps. The strength of connections is based on co-expression, gene fusion, co-occurrence, neighbourhood, databases, experiments, and text-mining collated in the STRING database. The strength of interactions is indicated by the thickness of the lines. STRING analysis revealed 4 protein clusters involved in metabolic (red), synaptic (blue), structural (purple) and signalling (green). Collectively, these proteins and their associations suggest that CPZ induced metabolic dysregulations and mitochondrial dysfunction.

Although the addition of PT injections during CPZ-feeding did not enhance the extent of OLG degeneration, demyelination and gliosis, it did produce several proteoform changes (Figures 5 and 7; Supplementary Figure S10a–c, Table S2). This is the first study to assess changes in the mouse brain proteome profile when the BBB is compromised by PT. Following 5 weeks of CPZ-feeding, PT injection more than doubled the number of significant CPZ-associated changes (18–46%), with PT alone contributing 15% of all proteoform changes, including fructose-bisphosphate

aldolase C, NADH dehydrogenase iron-sulfur protein 2, ATP synthase subunit-α, rab GDP dissociation inhibitor-β, septin-2 and 5, guanine nucleotide-binding protein G(o) subunit-α, adipocyte plasma membrane-associated protein and leukocyte elastase inhibitor A. Likewise, in the 12-week study, the small number of proteins identified following CPZ-feeding (6%) increased following the addition of PT (52%), with PT alone contributing 21% including aconitate hydratase, succinate dehydrogenase flavoprotein subunit, NADH dehydrogenase iron-sulphur protein 2, isovaleryl-CoA dehydrogenase, tyrosine-tRNA ligase, syntaxin-binding protein 1, glial fibrillary acidic protein, neurofilament light polypeptide, septin-2 and calreticulin. Statistical comparisons of the CPZ(+PT) groups with the PT only group (Supplementary Table S2) revealed that at least 50% of the PT-mediated proteoform changes were either increased (or decreased) when combined with CPZ-feeding; in the 5-week study, 25% increased (27% decreased) whereas, in the 12-week study 52% increased (6% decreased).

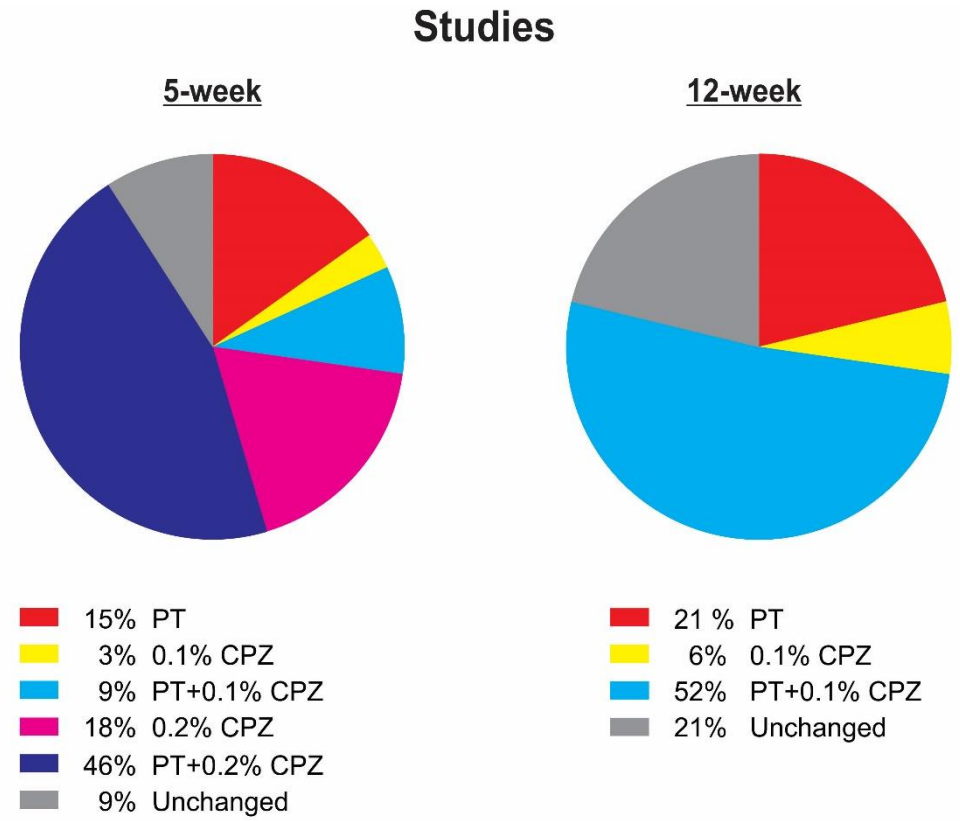

Figure 7. Highest fold change. Pie charts showing the highest increase or decrease fold change in abundance of the 33 proteoforms relative to Ctrls in the 5- and 12-week studies. PT alone or when PT was combined with CPZ showed greater change than CPZ alone. Quantification is based on ≥1.5-fold changes.

4. Discussion

The present study was designed to test whether CPZ-induced oligodendrocytosis, when combined with PT-induced BBB disruption, could induce an 'inside-out' activation of the immune system causing infiltration and detection of CD4/8 immune cells into the brain parenchyma. The effectiveness of CPZ-feeding was confirmed by the reduced weight gain in these groups, the almost complete demyelination of the corpus callosum using the standard feeding paradigm of 0.2% CPZ for 5 weeks, and changes to the brain proteome [58,59,108,109]. The results also demonstrated that 0.2% or 0.1% CPZ(±PT) produced comparable oligodendrocytosis but dose- and time-dependent demyelination and gliosis within the corpus callosum, indicating that 0.1% CPZ is as effective as higher doses when fed for a longer period of time. The presence of comparable oligodendrocytosis, but less marked

demyelination and gliosis following 5 weeks of 0.1% CPZ-feeding, suggested a slower transition between oligodendrocytosis and demyelination and/or better clearance of myelin debris. In this transition state, limited gliosis may impede subsequent remyelination [110] and induce a slow, progressive demyelination reminiscent of MS. CPZ-induced a dose dependent (0.2% > 0.1%) atrophy of the spleen and extending the CPZ-feeding resulted in time dependent atrophy in 0.1% CPZ(±PT)-fed groups as well. Likewise, CPZ produced a dose-dependent (0.2% > 0.1%) suppression of CD4/8 in the spleen. Prolonged low-dose feeding of CPZ for 12 weeks did not cause a further decrease in CD4 compared to 5 weeks; however, with prolonged feeding, the reduction of CD8 deteriorated to levels seen at 5 weeks using the standard CPZ-feeding. Our results are thus consistent with a previous study where apoptosis of CD4 and CD8 positive cells and atrophy of thymus were observed following 0.2% CPZ-feeding [50]. In contrast, 5 weeks of 0.1% CPZ-feeding produced less CD4 and CD8 suppression and no splenic atrophy, suggesting this lower dose may be a better model to examine the aetiology of MS.

Following CPZ-feeding(±PT) in either experiment, there were no detectable CD4 or CD8 signals in brain tissue. There are several possible reasons for this: firstly, insensitivity of the immunohistological or biochemical assays. This is unlikely, as WB sensitivity was confirmed by spiking whole brain homogenates with biological (spleen) and commercially available CD4/8 recombinant proteins, and both high protein loads (60–120 µg) and high antibody titres were used [111]. Additionally, these results are consistent with previous studies using immunofluorescence and flow cytometry [48,112] as well as BBB disruption using ethidium bromide or lysolecithin [48]. Secondly, the BBB was breached during weeks 1–2 of CPZ-feeding, and this is a transient event [113]. However, whether infiltration occurred at this early time point, but resolved before the 5- or 12-week endpoints remains unknown. Was the lack of a detectable adaptive immune response the result of failure to generate an antigen? This seems unlikely, as marked gliosis, demyelination and oligodendrocytosis occurred. Alternatively, was there a direct effect of CPZ on peripheral immune function? This would be consistent with the observed suppression of CD4/8 signal in the spleens of CPZ-fed animals. It was recently reported that combining two weeks of 0.2% CPZ-feeding with an 'immune booster' (CFA) produced a secondary $CD3^+$ (pan T-cell marker) response, a response that was not observed with 0.2% CPZ-feeding alone or when CPZ-feeding was continued [31]. Consequently, it can be expected that prolonged CPZ-feeding is unlikely to facilitate infiltration of immune cells into the CNS as continued feeding would result in sustained immune suppression (and reduction of mitochondrial ATP production) which is known to lead to declining health and death of mice. Likewise, extending observations beyond the cessation of CPZ-feeding is unlikely to reveal immune cell infiltration since cessation of CPZ-feeding results in spontaneous remyelination, reduction in myelin debris (a potential antigen), and cessation of glial activation (i.e., the antigen presenting cells) (reviewed in [2,39,57,58,114]).

Notably, the prolonged CPZ-feeding preferentially suppressed CD8 signal intensity in the spleen, and these are the cells that predominate in human MS CNS pathology [22]. These observations are further supported by the large number of changes in spleen (n = 22) and peripheral blood mononuclear cell-derived (n = 5) proteoforms in the CPZ-fed animals [49]. In the spleen, the vast majority (87%) of these changes included membrane associated structural and metabolic proteins suggesting perturbation of adaptive immune function [49]. The spleen and thymus are responsible for the maturation, selection and proliferation of T-cells [115,116], key functions that are impeded by the ion dishomeostasis induced by CPZ [41–44]. Such effects on the peripheral immune system may explain why the severity of disease and extent of peripheral immune involvement in EAE and Theiler's murine encephalomyelitis were suppressed by CPZ [117–119]. Although, there is no evidence as to whether T-cells become functionally inactivated ('T-cell anergy'; [120,121]) due to the suppression of adaptive immune organs (e.g., thymus) following CPZ-feeding, there is some evidence indicating that CPZ may otherwise affect T-cell functions. Copper plays both direct and indirect roles (via interleukin-2) in the maturation and production of functional T-cells [122]. Consequently, it can be argued that CPZ, like other copper chelators (e.g., 2,3,2-tetraamine), can reduce T-cell function [123,124]. Moreover, it has been shown that when lymph node cells harvested from CPZ-fed mice are exposed to neuroantigens (e.g., concanavalin

A and MBP) in vitro, there is reduced cellular proliferation. Likewise, reduced T-helper cell 1 cytokines (e.g., interferon-γ and tumor necrosis factor-α) and CD4 T-cell response to interleukin-17 are observed in EAE mice fed with CPZ [119]. Together, these findings indicate that CPZ can modify the functional capacity of T-cells, and this may potentially affect migration into the CNS.

The suppression of CD4/8 in the spleen indicated that CPZ has direct effects on the peripheral immune system that may limit the maturation and migration of adaptive immune cells to the CNS. Moreover, calcium/calmodulin-dependent protein kinase type II subunit-α, a protein known to play a role in CD8 T-cell proliferation and the transition to a cytotoxic phenotype [125,126] decreased in abundance following CPZ-feeding. Likewise, leukocyte elastase inhibitor A, a protein that supresses proteases including those released by T-cells [127], also decreased in abundance. These findings extend earlier proteomic analyses [49] that found CPZ reduced the abundance of protein disulphide isomerase (subunits A2, A3 and A6) in spleen, a protein involved with folding and assembly of functional major histocompatibility complex class I molecules [128]. In addition, the CPZ-induced dysregulation of mitochondria identified in the present study presumably extends to the immune system as several studies have shown that mitochondrial dysfunction leads to the suppression of T-cell function and a compromised immune system [129,130]. Collectively, these findings indicate that CPZ has suppressive effects on the capacity of the peripheral immune system to launch a response, making it more difficult to address the 'inside-out hypothesis'. Therefore, strategies to overcome peripheral immune organ suppression should be the next stage of investigation in evaluating the 'inside-out' hypothesis of MS using the CPZ model.

While there is growing evidence that MS may initiate as a slow, low-grade primary oligodendrocytosis, a substantial gap still exists in our understanding of the molecular mechanisms underlying the fundamental susceptibility to and initiation of oligodendrocytosis [1–4]. Therefore, a quantitative 'top-down' proteomic approach was carried out to resolve protein species from whole brains of the CPZ-fed(±PT) mice. To date, proteome analyses of MS have mainly assessed tissue from late-stage post mortem brain samples and cerebrospinal fluid [89,96] or EAE animals [88,93,100,105]; these analyses provide useful insight into the 'final readout' of the disease or its autoimmune aspects [131–133] but not necessarily insight into the processes involved in disease aetiology and progression, including the role of oligodendrocytosis [1,49].

Here, CPZ-mediated oligodendrocytosis and glial activation were confirmed using histology, and the changes in protein abundance were quantified using a high sensitivity 'top-down' analysis rather than the more common 'bottom-up' (i.e., 'shotgun') analyses; this is critical, as the 'top-down' approach has the highest inherent capacity to resolve intact proteoforms (i.e., isoforms, splice variants, and post-translationally modified species) as well as provide better sequence coverage, and assessment of lower molecular weight species, with a high degree of consistency across technical and biological replicates [54,55,134]. This approach thus detected changes in 33 proteoforms (16 metabolic, 7 synaptic, 5 structural and 5 signalling), of which 8 have not been previously associated with CPZ, EAE or MS. Furthermore, it also provided high quality confirmation of changes in the abundance of 25 proteoforms of proteins previously related to MS or animal models of the disorder. In contrast to earlier work [49,91,97,99,135], this study used three technical replicates for each of the 5 biological replicates per experimental group, ensuring that only the most reproducible changes in proteoform abundance were assessed. Consequently, in contrast to the detection of ~700–1200 spots in previous studies [49,88,100,105], ~1650 protein spots per condition were resolved in this study.

The most striking observation to emerge from the proteomic analysis was the large number of changes in metabolic proteoforms involved in glycolysis, Krebs cycle and oxidative phosphorylation pathways and the regulation of mitochondrial function. Bioinformatics platforms (DAVID, PANTHER, UniProt and STRING) further revealed the likely association between metabolic dysregulation and CPZ-feeding. Understanding the molecular pathways and potential PPI is important to understanding how dysregulation of biological processes may lead to a disease [132,136]. It is thus notable that over 80% of proteins do not function alone but in complexes [136]. The data here suggested that 79% of the

identified proteoforms may be clustered in two complexes, with 58% being metabolic in origin, which is consistent with previous observations [136,137]. The strong PPI highlight the likely cross-talk and shared biochemical reactions among the metabolic proteoforms [136]. Interestingly, protein-to-protein connection analysis revealed that malate dehydrogenase may have 11 connections with other identified proteoforms, which was the highest seen, and that the ATP synthase subunit-α had the second highest with 7 connections (Figure 6d). The central placement and increased inter-connectedness of malate dehydrogenase or ATP synthase subunit-α with other proteoforms implies that these proteoforms may be pivotal for CPZ-induced metabolic dysregulation. This explanation is further supported by the increased abundance of ATP synthase subunit-α and malate dehydrogenase (in contrast to the decreased abundance of most of the other identified metabolic proteoforms), perhaps as a compensatory response to the CPZ-induced metabolic perturbations. The increased abundance of ATP synthase subunit-α after CPZ-feeding leads to the accumulation of protons in the inter-membrane space of mitochondria and increased generation of reactive oxygen species [91]. Likewise, an increase in the abundance of aconitate hydratase (6 PPI connections, Figure 6d), an iron-sulphur protein containing 4Fe-4S clusters, is likely to regulate iron-induced oxidative stress in the CPZ model. Disruption of iron metabolism is linked to increased oxidative stress and lipid peroxidation [138]; CPZ-feeding is associated with the dysregulation of iron [43] and thus increased oxidative stress results in accentuation of mitochondrial perturbations [139]. Moreover, we observed a synergy between CPZ-feeding(±PT) with regard to synaptic protein dynamin 1 (increased at 5 weeks but decreased at 12 weeks) suggesting that CPZ-feeding interferes with the fission and fusion dynamics of mitochondria. The initial increase in dynamin 1 is consistent with mitochondrial response to metabolic stress, wherein the mitochondria divide, generating new functional mitochondria, and target damaged mitochondria for autophagy [140]. Perturbations to the fission and fusion dynamics of mitochondria are consistent with the formation of mega-mitochondria reported in the CNS, in particular in OLG [141,142]. The current data are consistent with previous investigations [49,50,91,99] corroborating the hypothesised link between mitochondrial dysregulation with CPZ-feeding and the emergence of structural and functional abnormalities that may predispose OLG to degeneration and death [1].

This susceptibility of OLG may be explained, in part, by the intense energy requirements associated with the production and maintenance of the expansive myelin sheath [143,144]. The high metabolic rate of OLG means that the increased production of reactive oxygen (and nitrogen) species, coupled with their low levels of anti-oxidants (e.g., glutathione [145], metallothionein [146] and manganese superoxide dismutase [147]) predisposes them to oxidative injury [45,148]. In addition, increased abundance (in 5- and 12-week studies) of the endoplasmic reticulum (ER) stress-related chaperone protein calreticulin may be associated with unfolded protein responses that enhance oligodendrocytosis [144,149]. This finding extends previously observed changes in ER proteins such as ribosome-binding protein 1, endoplasmin [49] and heat shock protein [99] reinforcing the role of ER stress in the CPZ-fed mice. The presence of heat shock protein and activating transcription factor 4 in MS [89,150,151] and EAE [105,150] indicate the association of protein misfolding and ER stress with OLG degeneration and demyelination.

The apparent oligomerization of some proteoforms in response to CPZ-feeding(±PT) may be indicative of toxic protein aggregation [152,153], effects that have also been observed in an EAE study [154] and MS patients [155]. The oligomerization of proteoforms has been documented in other studies, as with calreticulin and dynamin, assessed using SDS-PAGE or crystallographic analysis [156–158]. Likewise, the divergence of molecular weight was also observed in other proteomic studies of CPZ-fed mice (protein phosphatase 1G, 59.38 vs. 104.7 KD) and MS cerebrospinal fluid (albumin, 67 vs. 180 KD and alpha 1 antitrypsin, 47 vs. 100 KD) [49,159]. Indeed, changes in theoretical vs. experimentally observed isoelectric point have also been reported in previous studies on CPZ (ornithine carbamoyltransferase, 8.81 vs. 6.9 and ribosome-binding protein 1, 9.35 vs. 5.0) [49], EAE (septin-8, 5.7 vs. 6.4 and cytochrome c oxidase, 9.2 vs. 5.8) [100] and MS (Ig kappa chain NIG 93 precursor, 8.1 vs. 6.5 and albumin, 5.5 vs. 9) [159,160]. Naturally, none of this key data, upon which to

better design future studies to identify critical proteoforms (rather than just amino acid sequences), would be routinely available using any other current approach.

Within the demyelinated regions, the hypertrophy of astrocytes and microglia, compounded by increased microglia numbers, may intensify the local energy imbalance and further compromise the function of OLG. Moreover, hypertrophied microglia and astrocytes may diminish the supportive roles played by glia at synapses leading to a pre-disposition to excitotoxicity [161–163]—a disturbance further implicated by changes in other synaptic proteoforms identified in this study.

The abundance of synaptic-regulatory proteoforms was either decreased (rab GDP dissociation inhibitor-α/β and vesicle-fusing ATPase), elevated (charged multivesicular body protein) or displayed opposing changes (syntaxin-binding protein 1) across the two time points—changes in synaptic function that may contribute to alteration of mood or behaviour in humans or animal models [164–166]. Likewise, the changes of abundance of proteins such as calcineurin, calbindin 2 and parvalbumin-α, involved in neurotransmitter release, has also been reported in EAE [100]. Although CPZ-feeding induce a wide range of behavioural deficits including motor, anxiety and cognition [reviewed by 2]; the present proteome analysis did not seek correlation with behavioural phenotypes, other studies have argued that CPZ-induced alteration of proteoforms involved in neurotransmitter release can result in cognitive decline [166] or increased climbing, rearing and ambulatory behaviours [99,108,109]. This study also revealed a marked change in neuronal and glial structural proteoforms, including Gfap, neurofilament light polypeptide, actin-related protein 2/3 complex subunit 5, and septins-2 and -5, at both time points, indicating axonal and glial remodelling. Consistent with the capacity for CPZ to induce the hypertrophy of astrocytes and increase microglia in the innate immune system (Figure 2a; Supplementary Figures S1–3), a marked increase in proteoforms involved in structural (Gfap), signalling, and inflammatory pathways were observed.

For some proteoforms, breaching the BBB negated the effects of 5 weeks of CPZ-feeding (e.g., septin-5, creatine kinase U-type and 14-3-3 protein epsilon). The effects of PT alone, or in combination with CPZ, indicate that PT did have an effect on the brain proteome, likely, in part at least, by altering the capacity of the BBB to regulate access to the CNS [60,113,167]. This is the first study to document the effects of giving PT alone on the $CD4/8^{+}$ cell migration and the whole brain proteome. In EAE, when PT is given together with adjuvant (CFA) and antigen stimulation (e.g., MOG), increased disruption of tight junctions at sites of perivascular inflammation and demyelination occurs [63]. In addition, increased rates of relapsing-remitting episodes [60], increased infiltration of serum albumin in the spinal cord [131] and suppression of the anti-inflammatory interleukin-10 [168] are observed. However, the extent to which these changes are attributable to PT alone, or the combined treatments used to induce EAE, remains un-documented. However, other studies have shown that PT alone evokes changes in BBB function leading to increased protein infiltration into the brain (~15 days; [169]), or disruption of G-protein function (~40 days; [170]) following PT administration. In the present study, repeated injections of PT during the second and third weeks of CPZ-feeding resulted in proteoform changes after 5 or 12 weeks indicating that PT injections alone have long-term effects at least on the brain proteome. Moreover, the proteomic analysis highlighted proteoform differences between the CPZ vs. EAE models; specifically, CPZ-feeding resulted in increased guanine nucleotide-binding protein G(o) subunit-α, glutamate dehydrogenase 1 and malate dehydrogenase, which decrease in EAE [88,94,105], perhaps reflecting the different underlying aetiologies (potentially including changes in specific proteoforms). Whether these opposing changes result specifically from the use of peripherally administered exogenous myelin antigens (e.g., MBP, PLP and MOG) in EAE or endogenously generated antigens (i.e., myelin debris) in the brain of CPZ-fed mice remains unclear but would seem likely.

Despite our rigorous efforts to minimize the experimental variables, we acknowledge certain inherent limitations in the analytical approach. This study relied on only two time points (i.e., 5 and 12 weeks) of CPZ-feeding(±PT), which did not allow us to determine if or when the identified proteoforms returned to baseline nor to correlate proteome changes with the initiation of oligodendrocytosis, demyelination and gliosis. Moreover, the sub-femtomole in-gel detection sensitivity may well have missed significant changes in very low abundance species, although these remain a substantial issue with all available analytical approaches if high quality final identifications are a serious expectation [78]. Furthermore, reliance on existing databases that address only amino acid sequences, as well as an apparent developing reliance in the field for online bioinformatics platforms that also largely address only what is known about canonical proteins [171–173], tends to further emphasize the fundamental importance of developing even more sensitive analytical approaches to routinely quantifying and fully characterizing proteoforms in order to provide the most direct understanding of the molecular mechanism underlying human diseases like MS.

5. Conclusions

This study confirmed that CPZ-feeding(±PT) in mice induced dose- and time-dependent oligodendrocytosis, demyelination and gliosis, but was not associated with any detectable invasion of peripheral adaptive (CD4/8) immune cells into the CNS. In the periphery, CPZ-feeding induced a dose-dependent suppression of splenic CD4/8 and organ mass, suggesting that this peripheral action of CPZ was a major impediment to studying the role of the peripheral immune system following demyelination and disruption of the BBB. Notably, oligodendrocytosis, demyelination and gliosis with the low dose of CPZ for 5 weeks resulted in minimal splenic atrophy and less severe adaptive immune system suppression, indicating that this might be a better model to test the 'inside-out' theory of MS. Moreover, using a highly sensitive 'top-down' proteomic approach, changes in 33 brain proteoforms were identified in the CPZ-fed mice, the majority of which were found to be associated with mitochondrial function. This strongly suggests that mitochondrial perturbations may elicit oligodendrocytosis and demyelination.

Supplementary Materials: The following are available online at http://www.mdpi.com/2073-4409/8/11/1314/s1. The Stereology and LC/MS/MS files associated with this article can be found in the following link http:$\delimiter"026E30F$$\delimiter"026E30F$galen.uws.edu.au$\delimiter"026E30F$mmrg$\delimiter"026E30F$sen.

Author Contributions: M.K.S., E.G., S.J.M., P.J.S., D.A.M. and J.R.C. conceived the study and provided all resources. Lab work and preliminary analysis were carried out by M.K.S. and M.S.M.A. All authors reviewed the analyses and draft manuscripts, and approved the final version.

Funding: This study was supported by funding from the Rotary Club of Narellan.

Acknowledgments: The authors acknowledge the Western Sydney University School of Medicine Animal Care and Mass Spectrometry Facilities for their help with this project. MKS was the recipient of a WSU-International Postgraduate Research Scholarship. MSMA was the recipient of a PhD sponsorship from the Higher Committee for Education Development in Iraq.

Conflicts of Interest: All authors declare no conflict of interest.

References

1. Partridge, M.A.; Myers, S.J.; Gopinath, S.; Coorssen, J.R. Proteomics of a conundrum: Thoughts on addressing the aetiology versus progression of multiple sclerosis. *Proteom. Clin. Appl.* **2015**, *9*, 838–843. [CrossRef] [PubMed]
2. Sen, M.K.; Mahns, D.A.; Coorssen, J.R.; Shortland, P.J. Behavioural phenotypes in the cuprizone model of central nervous system demyelination. *Neurosci. Biobehav. Rev.* **2019**, *107*, 23–46. [CrossRef] [PubMed]
3. Stys, P.K. Pathoetiology of multiple sclerosis: are we barking up the wrong tree? *F1000Prime Rep.* **2013**, *5*, 20. [CrossRef]
4. Stys, P.K.; Zamponi, G.W.; van Minnen, J.; Geurts, J.J. Will the real multiple sclerosis please stand up? *Nat. Rev. Neurosci.* **2012**, *13*, 507–514. [CrossRef] [PubMed]

5. Constantinescu, C.S.; Farooqi, N.; O'Brien, K.; Gran, B. Experimental autoimmune encephalomyelitis (EAE) as a model for multiple sclerosis (MS). *Br. J. Pharm.* **2011**, *164*, 1079–1106. [CrossRef] [PubMed]
6. Gold, R.; Linington, C.; Lassmann, H. Understanding pathogenesis and therapy of multiple sclerosis via animal models: 70 years of merits and culprits in experimental autoimmune encephalomyelitis research. *Brain* **2006**, *129*, 1953–1971. [CrossRef] [PubMed]
7. Glatigny, S.; Bettelli, E. Experimental Autoimmune Encephalomyelitis (EAE) as Animal Models of Multiple Sclerosis (MS). *Cold Spring Harb. Perspect. Med.* **2018**, *8*. [CrossRef]
8. Bittner, S.; Afzali, A.M.; Wiendl, H.; Meuth, S.G. Myelin oligodendrocyte glycoprotein (MOG35-55) induced experimental autoimmune encephalomyelitis (EAE) in C57BL/6 mice. *J. Vis. Exp.* **2014**. [CrossRef]
9. Patel, J.; Balabanov, R. Molecular mechanisms of oligodendrocyte injury in multiple sclerosis and experimental autoimmune encephalomyelitis. *Int. J. Mol. Sci.* **2012**, *13*, 10647–10659. [CrossRef]
10. Lu, J.; Kurejova, M.; Wirotanseng, L.N.; Linker, R.A.; Kuner, R.; Tappe-Theodor, A. Pain in experimental autoimmune encephalitis: a comparative study between different mouse models. *J. Neuroinflammation.* **2012**, *9*, 233. [CrossRef]
11. Evonuk, K.S.; Baker, B.J.; Doyle, R.E.; Moseley, C.E.; Sestero, C.M.; Johnston, B.P.; De Sarno, P.; Tang, A.; Gembitsky, I.; Hewett, S.J.; et al. Inhibition of System Xc(-) Transporter Attenuates Autoimmune Inflammatory Demyelination. *J. Immunol.* **2015**, *195*, 450–463. [CrossRef]
12. Hart, B.A.; Gran, B.; Weissert, R. EAE: imperfect but useful models of multiple sclerosis. *Trends Mol. Med.* **2011**, *17*, 119–125. [CrossRef] [PubMed]
13. Trapp, B.D.; Nave, K.A. Multiple sclerosis: an immune or neurodegenerative disorder? *Annu. Rev. Neurosci.* **2008**, *31*, 247–269. [CrossRef] [PubMed]
14. Lassmann, H.; Bradl, M. Multiple sclerosis: experimental models and reality. *Acta Neuropathol.* **2017**, *133*, 223–244. [CrossRef] [PubMed]
15. Lovett-Racke, A.E. Contribution of EAE to understanding and treating multiple sclerosis. *J. Neuroimmunol.* **2017**, *304*, 40–42. [CrossRef]
16. Krishnamoorthy, G.; Wekerle, H. EAE: an immunologist's magic eye. *Eur. J. Immunol.* **2009**, *39*, 2031–2035. [CrossRef]
17. Sriram, S.; Steiner, I. Experimental allergic encephalomyelitis: a misleading model of multiple sclerosis. *Ann. Neurol.* **2005**, *58*, 939–945. [CrossRef]
18. Behan, P.O.; Chaudhuri, A. EAE is not a useful model for demyelinating disease. *Mult. Scler. Relat. Disord.* **2014**, *3*, 565–574. [CrossRef]
19. Flugel, A.; Berkowicz, T.; Ritter, T.; Labeur, M.; Jenne, D.E.; Li, Z.; Ellwart, J.W.; Willem, M.; Lassmann, H.; Wekerle, H. Migratory activity and functional changes of green fluorescent effector cells before and during experimental autoimmune encephalomyelitis. *Immunity* **2001**, *14*, 547–560. [CrossRef]
20. Lassmann, H.; van Horssen, J. The molecular basis of neurodegeneration in multiple sclerosis. *FEBS Lett.* **2011**, *585*, 3715–3723. [CrossRef]
21. Friese, M.A.; Fugger, L. Autoreactive CD8+ T cells in multiple sclerosis: a new target for therapy? *Brain* **2005**, *128*, 1747–1763. [CrossRef] [PubMed]
22. Hauser, S.L.; Bhan, A.K.; Gilles, F.; Kemp, M.; Kerr, C.; Weiner, H.L. Immunohistochemical analysis of the cellular infiltrate in multiple sclerosis lesions. *Ann. Neurol.* **1986**, *19*, 578–587. [CrossRef]
23. Babbe, H.; Roers, A.; Waisman, A.; Lassmann, H.; Goebels, N.; Hohlfeld, R.; Friese, M.; Schroder, R.; Deckert, M.; Schmidt, S.; et al. Clonal expansions of CD8(+) T cells dominate the T cell infiltrate in active multiple sclerosis lesions as shown by micromanipulation and single cell polymerase chain reaction. *J. Exp. Med.* **2000**, *192*, 393–404. [CrossRef] [PubMed]
24. Ransohoff, R.M. Animal models of multiple sclerosis: the good, the bad and the bottom line. *Nat. Neurosci.* **2012**, *15*, 1074–1077. [CrossRef] [PubMed]
25. Gilmore, C.P.; Donaldson, I.; Bo, L.; Owens, T.; Lowe, J.; Evangelou, N. Regional variations in the extent and pattern of grey matter demyelination in multiple sclerosis: a comparison between the cerebral cortex, cerebellar cortex, deep grey matter nuclei and the spinal cord. *J. Neurol. Neurosurg. Psychiatry.* **2009**, *80*, 182–187. [CrossRef]
26. Day, M.J. Histopathology of EAE. In *Experimental Models of Multiple Sclerosis*; Lavi, E., Constantinescu, C.S., Eds.; Springer US: Boston, MA, USA, 2005; pp. 25–43.

27. Tanuma, N.; Shin, T.; Matsumoto, Y. Characterization of acute versus chronic relapsing autoimmune encephalomyelitis in DA rats. *J. Neuroimmunol.* **2000**, *108*, 171–180. [CrossRef]
28. Broadwater, L.; Pandit, A.; Clements, R.; Azzam, S.; Vadnal, J.; Sulak, M.; Yong, V.W.; Freeman, E.J.; Gregory, R.B.; McDonough, J. Analysis of the mitochondrial proteome in multiple sclerosis cortex. *BBA* **2011**, *1812*, 630–641. [CrossRef]
29. Rosenling, T.; Attali, A.; Luider, T.M.; Bischoff, R. The experimental autoimmune encephalomyelitis model for proteomic biomarker studies: from rat to human. *Clin. Chim. Acta.* **2011**, *412*, 812–822. [CrossRef] [PubMed]
30. Vargas, D.L.; Tyor, W.R. Update on disease-modifying therapies for multiple sclerosis. *J. Investig. Med.* **2017**, *65*, 883–891. [CrossRef] [PubMed]
31. Caprariello, A.V.; Rogers, J.A.; Morgan, M.L.; Hoghooghi, V.; Plemel, J.R.; Koebel, A.; Tsutsui, S.; Dunn, J.F.; Kotra, L.P.; Ousman, S.S.; et al. Biochemically altered myelin triggers autoimmune demyelination. *PNAS* **2018**, *115*, 5528–5533. [CrossRef]
32. Barnett, M.H.; Prineas, J.W. Relapsing and remitting multiple sclerosis: pathology of the newly forming lesion. *Ann. Neurol.* **2004**, *55*, 458–468. [CrossRef] [PubMed]
33. Henderson, A.P.; Barnett, M.H.; Parratt, J.D.; Prineas, J.W. Multiple sclerosis: distribution of inflammatory cells in newly forming lesions. *Ann. Neurol.* **2009**, *66*, 739–753. [CrossRef] [PubMed]
34. Lucchinetti, C.; Bruck, W.; Parisi, J.; Scheithauer, B.; Rodriguez, M.; Lassmann, H. Heterogeneity of multiple sclerosis lesions: implications for the pathogenesis of demyelination. *Ann. Neurol.* **2000**, *47*, 707–717. [CrossRef]
35. Lucchinetti, C.F.; Bruck, W.; Rodriguez, M.; Lassmann, H. Distinct patterns of multiple sclerosis pathology indicates heterogeneity on pathogenesis. *Brain Pathol.* **1996**, *6*, 259–274. [CrossRef] [PubMed]
36. Rodriguez, M.; Scheithauer, B. Ultrastructure of multiple sclerosis. *Ultrastruct. Pathol.* **1994**, *18*, 3–13. [CrossRef] [PubMed]
37. Traka, M.; Podojil, J.R.; McCarthy, D.P.; Miller, S.D.; Popko, B. Oligodendrocyte death results in immune-mediated CNS demyelination. *Nat. Neurosci.* **2016**, *19*, 65–74. [CrossRef]
38. Carlton, W.W. Studies on the induction of hydrocephalus and spongy degeneration by cuprizone feeding and attempts to antidote the toxicity. *Life Sci.* **1967**, *6*, 11–19. [CrossRef]
39. Matsushima, G.K.; Morell, P. The neurotoxicant, cuprizone, as a model to study demyelination and remyelination in the central nervous system. *Brain Pathol.* **2001**, *11*, 107–116. [CrossRef]
40. Komoly, S.; Jeyasingham, M.D.; Pratt, O.E.; Lantos, P.L. Decrease in oligodendrocyte carbonic anhydrase activity preceding myelin degeneration in cuprizone induced demyelination. *J. Neurol. Sci.* **1987**, *79*, 141–148. [CrossRef]
41. Zatta, P.; Raso, M.; Zambenedetti, P.; Wittkowski, W.; Messori, L.; Piccioli, F.; Mauri, P.L.; Beltramini, M. Copper and zinc dismetabolism in the mouse brain upon chronic cuprizone treatment. *Cell. Mol. Life Sci.* **2005**, *62*, 1502–1513. [CrossRef]
42. Moldovan, N.; Al-Ebraheem, A.; Lobo, L.; Park, R.; Farquharson, M.J.; Bock, N.A. Altered transition metal homeostasis in the cuprizone model of demyelination. *Neurotoxicol* **2015**, *48*, 1–8. [CrossRef] [PubMed]
43. Varga, E.; Pandur, E.; Abraham, H.; Horvath, A.; Acs, P.; Komoly, S.; Miseta, A.; Sipos, K. Cuprizone Administration Alters the Iron Metabolism in the Mouse Model of Multiple Sclerosis. *Cell. Mol. Neurobiol.* **2018**, *38*, 1081–1097. [CrossRef] [PubMed]
44. Venturini, G. Enzymic activities and sodium, potassium and copper concentrations in mouse brain and liver after cuprizone treatment in vivo. *J. Neurochem.* **1973**, *21*, 1147–1151. [CrossRef] [PubMed]
45. McTigue, D.M.; Tripathi, R.B. The life, death, and replacement of oligodendrocytes in the adult CNS. *J. Neurochem.* **2008**, *107*, 1–19. [CrossRef]
46. McLaurin, J.A.; Yong, V.W. Oligodendrocytes and myelin. *Neurol. Clin.* **1995**, *13*, 23–49. [CrossRef]
47. Liblau, R.; Fontaine, B.; Baron-Van Evercooren, A.; Wekerle, H.; Lassmann, H. Demyelinating diseases: from pathogenesis to repair strategies. *Trends Neurosci.* **2001**, *24*, 134–135. [CrossRef]
48. Tejedor, L.S.; Wostradowski, T.; Gingele, S.; Skripuletz, T.; Gudi, V.; Stangel, M. The Effect of Stereotactic Injections on Demyelination and Remyelination: a Study in the Cuprizone Model. *J. Mol. Neurosci.* **2017**, *61*, 479–488. [CrossRef]
49. Partridge, M.A.; Gopinath, S.; Myers, S.J.; Coorssen, J.R. An initial top-down proteomic analysis of the standard cuprizone mouse model of multiple sclerosis. *J. Chem. Biol.* **2016**, *9*, 9–18. [CrossRef]

50. Solti, I.; Kvell, K.; Talaber, G.; Veto, S.; Acs, P.; Gallyas, F.; Illes, Z.; Fekete, K.; Zalan, P.; Szanto, A.; et al. Thymic Atrophy and Apoptosis of CD4+CD8+ Thymocytes in the Cuprizone Model of Multiple Sclerosis. *PLoS ONE* **2015**, *10*, e0129217. [CrossRef]
51. Butt, R.H.; Coorssen, J.R. Postfractionation for enhanced proteomic analyses: routine electrophoretic methods increase the resolution of standard 2D-PAGE. *J. Proteome Res.* **2005**, *4*, 982–991. [CrossRef]
52. Wright, E.P.; Partridge, M.A.; Padula, M.P.; Gauci, V.J.; Malladi, C.S.; Coorssen, J.R. Top-down proteomics: enhancing 2D gel electrophoresis from tissue processing to high-sensitivity protein detection. *Proteomics* **2014**, *14*, 872–889. [CrossRef] [PubMed]
53. D'Silva, A.M.; Hyett, J.A.; Coorssen, J.R. Proteomic analysis of first trimester maternal serum to identify candidate biomarkers potentially predictive of spontaneous preterm birth. *J. Proteom.* **2018**, *178*, 31–42. [CrossRef]
54. Oliveira, B.M.; Coorssen, J.R.; Martins-de-Souza, D. 2DE: the phoenix of proteomics. *J. Proteom.* **2014**, *104*, 140–150. [CrossRef] [PubMed]
55. Coorssen, J.R.; Yergey, A.L. Proteomics Is Analytical Chemistry: Fitness-for-Purpose in the Application of Top-Down and Bottom-Up Analyses. *Proteomes* **2015**, *3*, 440–453. [CrossRef] [PubMed]
56. Kurgan, N.; Noaman, N.; Pergande, M.R.; Cologna, S.M.; Coorssen, J.R.; Klentrou, P. Changes to the Human Serum Proteome in Response to High Intensity Interval Exercise: A Sequential Top-Down Proteomic Analysis. *Front. Physiol.* **2019**, *10*. [CrossRef]
57. Kipp, M.; Clarner, T.; Dang, J.; Copray, S.; Beyer, C. The cuprizone animal model: new insights into an old story. *Acta Neuropathol.* **2009**, *118*, 723–736. [CrossRef]
58. Gudi, V.; Gingele, S.; Skripuletz, T.; Stangel, M. Glial response during cuprizone-induced de- and remyelination in the CNS: lessons learned. *Front. Cell. Neurosci.* **2014**, *8*, 73. [CrossRef]
59. Hiremath, M.M.; Saito, Y.; Knapp, G.W.; Ting, J.P.; Suzuki, K.; Matsushima, G.K. Microglial/macrophage accumulation during cuprizone-induced demyelination in C57BL/6 mice. *J. Neuroimmunol.* **1998**, *92*, 38–49. [CrossRef]
60. Mohajeri, M.; Sadeghizadeh, M.; Javan, M. Pertussis toxin promotes relapsing-remitting experimental autoimmune encephalomyelitis in Lewis rats. *J. Neuroimmunol.* **2015**, *289*, 105–110. [CrossRef]
61. Hofstetter, H.H.; Shive, C.L.; Forsthuber, T.G. Pertussis toxin modulates the immune response to neuroantigens injected in incomplete Freund's adjuvant: induction of Th1 cells and experimental autoimmune encephalomyelitis in the presence of high frequencies of Th2 cells. *J. Immunol.* **2002**, *169*, 117–125. [CrossRef]
62. Gao, Z.; Nissen, J.C.; Ji, K.; Tsirka, S.E. The experimental autoimmune encephalomyelitis disease course is modulated by nicotine and other cigarette smoke components. *PLoS ONE* **2014**, *9*, e107979. [CrossRef] [PubMed]
63. Bennett, J.; Basivireddy, J.; Kollar, A.; Biron, K.E.; Reickmann, P.; Jefferies, W.A.; McQuaid, S. Blood-brain barrier disruption and enhanced vascular permeability in the multiple sclerosis model EAE. *J. Neuroimmunol.* **2010**, *229*, 180–191. [CrossRef] [PubMed]
64. Almuslehi, M.S.M.; Sen, M.K.; Mahns, D.A.; Shortland, P.J.; Coorssen, J.R. Blood Brain Barrier Disruption Facilitates CD8 T Cells infiltration into the CNS of Orchiectomized Cuprizone Treated Mice. In Proceedings of the Australasian Neuroscience Society, Brisbane Convention & Exhibition Centre, Brisbane, Australia, 3–6 December 2018; p. 163.
65. Gyengesi, E.; Liang, H.; Millington, C.; Sonego, S.; Sirijovski, D.; Gunawardena, D.; Dhananjayan, K.; Venigalla, M.; Niedermayer, G.; Munch, G. Investigation Into the Effects of Tenilsetam on Markers of Neuroinflammation in GFAP-IL6 Mice. *Pharm. Res.* **2018**, *35*, 22. [CrossRef] [PubMed]
66. Gyengesi, E.; Calabrese, E.; Sherrier, M.C.; Johnson, G.A.; Paxinos, G.; Watson, C. Semi-automated 3D segmentation of major tracts in the rat brain: comparing DTI with standard histological methods. *Brain Struct. Funct.* **2014**, *219*, 539–550. [CrossRef]
67. Pistorio, A.L.; Hendry, S.H.; Wang, X. A modified technique for high-resolution staining of myelin. *J. Neurosci. Methods.* **2006**, *153*, 135–146. [CrossRef]
68. Paxinos, G.; Franklin, K. *Paxinos and Franklin's the Mouse Brain in Stereotaxic Coordinates*, Fourth ed.; Academic Press: Cambridge, MA, USA, 2012.
69. Taylor, L.C.; Gilmore, W.; Matsushima, G.K. SJL mice exposed to cuprizone intoxication reveal strain and gender pattern differences in demyelination. *Brain Pathol.* **2009**, *19*, 467–479. [CrossRef]

70. Gumusoglu, S.B.; Fine, R.S.; Murray, S.J.; Bittle, J.L.; Stevens, H.E. The role of IL-6 in neurodevelopment after prenatal stress. *Brain Behav. Immun.* **2017**, *65*, 274–283. [CrossRef]
71. Butt, R.H.; Coorssen, J.R. Pre-extraction sample handling by automated frozen disruption significantly improves subsequent proteomic analyses. *J. Proteome Res.* **2006**, *5*, 437–448. [CrossRef]
72. Butt, R.H.; Pfeifer, T.A.; Delaney, A.; Grigliatti, T.A.; Tetzlaff, W.G.; Coorssen, J.R. Enabling coupled quantitative genomics and proteomics analyses from rat spinal cord samples. *Mol. Cell. Proteom.* **2007**, *6*, 1574–1588. [CrossRef]
73. Wright, E.P.; Prasad, K.A.; Padula, M.P.; Coorssen, J.R. Deep imaging: how much of the proteome does current top-down technology already resolve? *PLoS ONE* **2014**, *9*, e86058. [CrossRef]
74. Gauci, V.J.; Padula, M.P.; Coorssen, J.R. Coomassie blue staining for high sensitivity gel-based proteomics. *J. Proteom.* **2013**, *90*, 96–106. [CrossRef] [PubMed]
75. Noaman, N.; Coorssen, J.R. Coomassie does it (better): A Robin Hood approach to total protein quantification. *Anal. Biochem.* **2018**, *556*, 53–56. [CrossRef] [PubMed]
76. Butt, R.H.; Coorssen, J.R. Coomassie blue as a near-infrared fluorescent stain: a systematic comparison with Sypro Ruby for in-gel protein detection. *Mol. Cell. Proteom.* **2013**, *12*, 3834–3850. [CrossRef] [PubMed]
77. Harris, L.R.; Churchward, M.A.; Butt, R.H.; Coorssen, J.R. Assessing detection methods for gel-based proteomic analyses. *J. Proteome Res.* **2007**, *6*, 1418–1425. [CrossRef]
78. Noaman, N.; Abbineni, P.S.; Withers, M.; Coorssen, J.R. Coomassie staining provides routine (sub)femtomole in-gel detection of intact proteoforms: Expanding opportunities for genuine Top-down Proteomics. *Electrophoresis* **2017**, *38*, 3086–3099. [CrossRef]
79. D'Silva, A.M.; Hyett, J.A.; Coorssen, J.R. A Routine 'Top-Down' Approach to Analysis of the Human Serum Proteome. *Proteomes* **2017**, *5*, 13. [CrossRef]
80. Stimpson, S.E.; Coorssen, J.R.; Myers, S.J. Mitochondrial protein alterations in a familial peripheral neuropathy caused by the V144D amino acid mutation in the sphingolipid protein, SPTLC1. *J. Chem. Biol.* **2015**, *8*, 25–35. [CrossRef]
81. Stroud, L.J.; Slapeta, J.; Padula, M.P.; Druery, D.; Tsiotsioras, G.; Coorssen, J.R.; Stack, C.M. Comparative proteomic analysis of two pathogenic Tritrichomonas foetus genotypes: there is more to the proteome than meets the eye. *Int. J. Parasitol.* **2017**, *47*, 203–213. [CrossRef]
82. UniProt Consortium, T. UniProt: the universal protein knowledgebase. *Nucleic Acids Res.* **2018**, *46*, 2699. [CrossRef]
83. Sharma, S.; Ray, S.; Moiyadi, A.; Sridhar, E.; Srivastava, S. Quantitative proteomic analysis of meningiomas for the identification of surrogate protein markers. *Sci. Rep.* **2014**, *4*, 7140. [CrossRef]
84. Szklarczyk, D.; Franceschini, A.; Wyder, S.; Forslund, K.; Heller, D.; Huerta-Cepas, J.; Simonovic, M.; Roth, A.; Santos, A.; Tsafou, K.P.; et al. STRING v10: protein-protein interaction networks, integrated over the tree of life. *Nucleic Acids Res.* **2015**, *43*, D447–D452. [CrossRef] [PubMed]
85. Hossain, M.U.; Khan, M.A.; Hashem, A.; Islam, M.M.; Morshed, M.N.; Keya, C.A.; Salimullah, M. Finding Potential Therapeutic Targets against Shigella flexneri through Proteome Exploration. *Front. Microbiol.* **2016**, *7*, 1817. [CrossRef] [PubMed]
86. De Las Rivas, J.; Fontanillo, C. Protein-protein interactions essentials: key concepts to building and analyzing interactome networks. *PLoS Comput. Biol.* **2010**, *6*, e1000807. [CrossRef] [PubMed]
87. De Riccardis, L.; Ferramosca, A.; Danieli, A.; Trianni, G.; Zara, V.; De Robertis, F.; Maffia, M. Metabolic response to glatiramer acetate therapy in multiple sclerosis patients. *BBA* **2016**, *6*, 131–137. [CrossRef] [PubMed]
88. Farias, A.S.; Martins-de-Souza, D.; Guimaraes, L.; Pradella, F.; Moraes, A.S.; Facchini, G.; Novello, J.C.; Santos, L.M. Proteome analysis of spinal cord during the clinical course of monophasic experimental autoimmune encephalomyelitis. *Proteomics* **2012**, *12*, 2656–2662. [CrossRef]
89. Menon, K.N.; Steer, D.L.; Short, M.; Petratos, S.; Smith, I.; Bernard, C.C. A novel unbiased proteomic approach to detect the reactivity of cerebrospinal fluid in neurological diseases. *Mol. Cell. Proteom.* **2011**, *10*, M110.000042. [CrossRef] [PubMed]
90. Almeras, L.; Lefranc, D.; Drobecq, H.; de Seze, J.; Dubucquoi, S.; Vermersch, P.; Prin, L. New antigenic candidates in multiple sclerosis: identification by serological proteome analysis. *Proteomics* **2004**, *4*, 2184–2194. [CrossRef]

91. Gat-Viks, I.; Geiger, T.; Barbi, M.; Raini, G.; Elroy-Stein, O. Proteomics-level analysis of myelin formation and regeneration in a mouse model for Vanishing White Matter disease. *J. Neurochem.* **2015**, *134*, 513–526. [CrossRef]
92. Noben, J.P.; Dumont, D.; Kwasnikowska, N.; Verhaert, P.; Somers, V.; Hupperts, R.; Stinissen, P.; Robben, J. Lumbar cerebrospinal fluid proteome in multiple sclerosis: characterization by ultrafiltration, liquid chromatography, and mass spectrometry. *J. Proteome Res.* **2006**, *5*, 1647–1657. [CrossRef]
93. Jastorff, A.M.; Haegler, K.; Maccarrone, G.; Holsboer, F.; Weber, F.; Ziemssen, T.; Turck, C.W. Regulation of proteins mediating neurodegeneration in experimental autoimmune encephalomyelitis and multiple sclerosis. *Proteom. Clin. Appl.* **2009**, *3*, 1273–1287. [CrossRef]
94. Linker, R.A.; Brechlin, P.; Jesse, S.; Steinacker, P.; Lee, D.H.; Asif, A.R.; Jahn, O.; Tumani, H.; Gold, R.; Otto, M. Proteome profiling in murine models of multiple sclerosis: identification of stage specific markers and culprits for tissue damage. *PLoS ONE* **2009**, *4*, e7624. [CrossRef] [PubMed]
95. Werner, P.; Pitt, D.; Raine, C.S. Multiple sclerosis: altered glutamate homeostasis in lesions correlates with oligodendrocyte and axonal damage. *Ann. Neurol.* **2001**, *50*, 169–180. [CrossRef] [PubMed]
96. Newcombe, J.; Eriksson, B.; Ottervald, J.; Yang, Y.; Franzen, B. Extraction and proteomic analysis of proteins from normal and multiple sclerosis postmortem brain. *J. Chromatogr. B Anal. Technol. Biomed. Life Sci.* **2005**, *815*, 191–202. [CrossRef] [PubMed]
97. Martin, N.A.; Molnar, V.; Szilagyi, G.T.; Elkjaer, M.L.; Nawrocki, A.; Okarmus, J.; Wlodarczyk, A.; Thygesen, E.K.; Palkovits, M.; Gallyas, F., Jr.; et al. Experimental Demyelination and Axonal Loss Are Reduced in MicroRNA-146a Deficient Mice. *Front. Immunol.* **2018**, *9*, 490. [CrossRef]
98. Liu, T.; Donahue, K.C.; Hu, J.; Kurnellas, M.P.; Grant, J.E.; Li, H.; Elkabes, S. Identification of differentially expressed proteins in experimental autoimmune encephalomyelitis (EAE) by proteomic analysis of the spinal cord. *J. Proteome Res.* **2007**, *6*, 2565–2575. [CrossRef]
99. Werner, S.R.; Saha, J.K.; Broderick, C.L.; Zhen, E.Y.; Higgs, R.E.; Duffin, K.L.; Smith, R.C. Proteomic analysis of demyelinated and remyelinating brain tissue following dietary cuprizone administration. *J. Mol. Neurosci.* **2010**, *42*, 210–225. [CrossRef]
100. Fazeli, A.S.; Nasrabadi, D.; Pouya, A.; Mirshavaladi, S.; Sanati, M.H.; Baharvand, H.; Salekdeh, G.H. Proteome analysis of post-transplantation recovery mechanisms of an EAE model of multiple sclerosis treated with embryonic stem cell-derived neural precursors. *J. Proteom.* **2013**, *94*, 437–450. [CrossRef]
101. Axelsson, M.; Malmestrom, C.; Nilsson, S.; Haghighi, S.; Rosengren, L.; Lycke, J. Glial fibrillary acidic protein: a potential biomarker for progression in multiple sclerosis. *J. Neurol.* **2011**, *258*, 882–888. [CrossRef]
102. Jain, M.R.; Bian, S.; Liu, T.; Hu, J.; Elkabes, S.; Li, H. Altered proteolytic events in experimental autoimmune encephalomyelitis discovered by iTRAQ shotgun proteomics analysis of spinal cord. *Proteome Sci.* **2009**, *7*, 25. [CrossRef]
103. Gresle, M.M.; Butzkueven, H.; Shaw, G. Neurofilament proteins as body fluid biomarkers of neurodegeneration in multiple sclerosis. *Mult. Scler. Int.* **2011**, *2011*, 315406. [CrossRef]
104. De Masi, R.; Vergara, D.; Pasca, S.; Acierno, R.; Greco, M.; Spagnolo, L.; Blasi, E.; Sanapo, F.; Trianni, G.; Maffia, M. PBMCs protein expression profile in relapsing IFN-treated multiple sclerosis: A pilot study on relation to clinical findings and brain atrophy. *J. Neuroimmunol.* **2009**, *210*, 80–86. [CrossRef] [PubMed]
105. Fazeli, A.S.; Nasrabadi, D.; Sanati, M.H.; Pouya, A.; Ibrahim, S.M.; Baharvand, H.; Salekdeh, G.H. Proteome analysis of brain in murine experimental autoimmune encephalomyelitis. *Proteomics* **2010**, *10*, 2822–2832. [CrossRef] [PubMed]
106. Ni Fhlathartaigh, M.; McMahon, J.; Reynolds, R.; Connolly, D.; Higgins, E.; Counihan, T.; Fitzgerald, U. Calreticulin and other components of endoplasmic reticulum stress in rat and human inflammatory demyelination. *Acta Neuropathol. Commun.* **2013**, *1*, 37. [CrossRef] [PubMed]
107. Colucci, M.; Roccatagliata, L.; Capello, E.; Narciso, E.; Latronico, N.; Tabaton, M.; Mancardi, G.L. The 14-3-3 protein in multiple sclerosis: a marker of disease severity. *Mult. Scler.* **2004**, *10*, 477–481. [CrossRef]
108. Chang, H.; Liu, J.; Zhang, Y.; Wang, F.; Wu, Y.; Zhang, L.; Ai, H.; Chen, G.; Yin, L. Increased central dopaminergic activity might be involved in the behavioral abnormality of cuprizone exposure mice. *Behav. Brain Res.* **2017**, *331*, 143–150. [CrossRef]
109. Franco-Pons, N.; Torrente, M.; Colomina, M.T.; Vilella, E. Behavioral deficits in the cuprizone-induced murine model of demyelination/remyelination. *Toxicol. Lett.* **2007**, *169*, 205–213. [CrossRef]

110. Lampron, A.; Larochelle, A.; Laflamme, N.; Prefontaine, P.; Plante, M.M.; Sanchez, M.G.; Yong, V.W.; Stys, P.K.; Tremblay, M.E.; Rivest, S. Inefficient clearance of myelin debris by microglia impairs remyelinating processes. *J. Exp. Med.* **2015**, *212*, 481–495. [CrossRef]
111. Coorssen, J.R.; Blank, P.S.; Albertorio, F.; Bezrukov, L.; Kolosova, I.; Backlund, P.S., Jr.; Zimmerberg, J. Quantitative femto- to attomole immunodetection of regulated secretory vesicle proteins critical to exocytosis. *Anal. Biochem.* **2002**, *307*, 54–62. [CrossRef]
112. Remington, L.T.; Babcock, A.A.; Zehntner, S.P.; Owens, T. Microglial recruitment, activation, and proliferation in response to primary demyelination. *Am. J. Pathol.* **2007**, *170*, 1713–1724. [CrossRef]
113. Kugler, S.; Bocker, K.; Heusipp, G.; Greune, L.; Kim, K.S.; Schmidt, M.A. Pertussis toxin transiently affects barrier integrity, organelle organization and transmigration of monocytes in a human brain microvascular endothelial cell barrier model. *Cell. Microbiol.* **2007**, *9*, 619–632. [CrossRef]
114. Praet, J.; Guglielmetti, C.; Berneman, Z.; Van der Linden, A.; Ponsaerts, P. Cellular and molecular neuropathology of the cuprizone mouse model: clinical relevance for multiple sclerosis. *Neurosci. Biobehav. Rev.* **2014**, *47*, 485–505. [CrossRef] [PubMed]
115. Cesta, M.F. Normal structure, function, and histology of the spleen. *Toxicol. Pathol.* **2006**, *34*, 455–465. [CrossRef] [PubMed]
116. Pearse, G. Normal structure, function and histology of the thymus. *Toxicol. Pathol.* **2006**, *34*, 504–514. [CrossRef] [PubMed]
117. Emerson, M.R.; Biswas, S.; LeVine, S.M. Cuprizone and piperonyl butoxide, proposed inhibitors of T-cell function, attenuate experimental allergic encephalomyelitis in SJL mice. *J. Neuroimmunol.* **2001**, *119*, 205–213. [CrossRef]
118. Herder, V.; Hansmann, F.; Stangel, M.; Schaudien, D.; Rohn, K.; Baumgartner, W.; Beineke, A. Cuprizone inhibits demyelinating leukomyelitis by reducing immune responses without virus exacerbation in an infectious model of multiple sclerosis. *J. Neuroimmunol.* **2012**, *244*, 84–93. [CrossRef]
119. Mana, P.; Fordham, S.A.; Staykova, M.A.; Correcha, M.; Silva, D.; Willenborg, D.O.; Linares, D. Demyelination caused by the copper chelator cuprizone halts T cell mediated autoimmune neuroinflammation. *J. Neuroimmunol.* **2009**, *210*, 13–21. [CrossRef]
120. Schwartz, R.H. T cell anergy. *Annu. Rev. Immunol.* **2003**, *21*, 305–334. [CrossRef]
121. Macián, F.; Im, S.-H.; García-Cózar, F.J.; Rao, A. T-cell anergy. *Curr. Opin. Immunol.* **2004**, *16*, 209–216. [CrossRef]
122. Nelson, B.H. IL-2, regulatory T cells, and tolerance. *J. Immunol.* **2004**, *172*, 3983–3988. [CrossRef]
123. Bala, S.; Failla, M.L. Copper deficiency reversibly impairs DNA synthesis in activated T lymphocytes by limiting interleukin 2 activity. *PNAS* **1992**, *89*, 6794–6797. [CrossRef]
124. Hopkins, R.G.; Failla, M.L. Transcriptional regulation of interleukin-2 gene expression is impaired by copper deficiency in Jurkat human T lymphocytes. *J. Nutr.* **1999**, *129*, 596–601. [CrossRef] [PubMed]
125. Lin, M.Y.; Zal, T.; Ch'en, I.L.; Gascoigne, N.R.; Hedrick, S.M. A pivotal role for the multifunctional calcium/calmodulin-dependent protein kinase II in T cells: from activation to unresponsiveness. *J. Immunol.* **2005**, *174*, 5583–5592. [CrossRef] [PubMed]
126. Bui, J.D.; Calbo, S.; Hayden-Martinez, K.; Kane, L.P.; Gardner, P.; Hedrick, S.M. A role for CaMKII in T cell memory. *Cell* **2000**, *100*, 457–467. [CrossRef]
127. Weyer, A.D.; Stucky, C.L. Repurposing a leukocyte elastase inhibitor for neuropathic pain. *Nat. Med.* **2015**, *21*, 429–430. [CrossRef] [PubMed]
128. Kang, K.; Park, B.; Oh, C.; Cho, K.; Ahn, K. A role for protein disulfide isomerase in the early folding and assembly of MHC class I molecules. *Antioxid. Redox Signal.* **2009**, *11*, 2553–2561. [CrossRef]
129. Desdin-Mico, G.; Soto-Heredero, G.; Mittelbrunn, M. Mitochondrial activity in T cells. *Mitochondrion* **2018**, *41*, 51–57. [CrossRef]
130. Sukumar, M.; Liu, J.; Mehta, G.U.; Patel, S.J.; Roychoudhuri, R.; Crompton, J.G.; Klebanoff, C.A.; Ji, Y.; Li, P.; Yu, Z.; et al. Mitochondrial Membrane Potential Identifies Cells with Enhanced Stemness for Cellular Therapy. *Cell. Metab.* **2016**, *23*, 63–76. [CrossRef]
131. Farias, A.S.; Pradella, F.; Schmitt, A.; Santos, L.M.; Martins-de-Souza, D. Ten years of proteomics in multiple sclerosis. *Proteomics.* **2014**, *14*, 467–480. [CrossRef]

132. Dagley, L.F.; Croft, N.P.; Isserlin, R.; Olsen, J.B.; Fong, V.; Emili, A.; Purcell, A.W. Discovery of novel disease-specific and membrane-associated candidate markers in a mouse model of multiple sclerosis. *Mol. Cell. Proteom.* **2014**, *13*, 679–700. [CrossRef]
133. Elkabes, S.; Li, H. Proteomic strategies in multiple sclerosis and its animal models. *Proteom. Clin. Appl.* **2007**, *1*, 1393–1405. [CrossRef]
134. Zhan, X.; Yang, H.; Peng, F.; Li, J.; Mu, Y.; Long, Y.; Cheng, T.; Huang, Y.; Li, Z.; Lu, M.; et al. How many proteins can be identified in a 2DE gel spot within an analysis of a complex human cancer tissue proteome? *Electrophoresis* **2018**, *39*, 965–980. [CrossRef] [PubMed]
135. Oveland, E.; Nystad, A.; Berven, F.; Myhr, K.M.; Torkildsen, O.; Wergeland, S. 1,25-Dihydroxyvitamin-D3 induces brain proteomic changes in cuprizone mice during remyelination involving calcium proteins. *Neurochem. Int.* **2018**, *112*, 267–277. [CrossRef] [PubMed]
136. Berggard, T.; Linse, S.; James, P. Methods for the detection and analysis of protein-protein interactions. *Proteomics* **2007**, *7*, 2833–2842. [CrossRef] [PubMed]
137. Turvey, M.E.; Koudelka, T.; Comerford, I.; Greer, J.M.; Carroll, W.; Bernard, C.C.; Hoffmann, P.; McColl, S.R. Quantitative proteome profiling of CNS-infiltrating autoreactive CD4+ cells reveals selective changes during experimental autoimmune encephalomyelitis. *J. Proteome Res.* **2014**, *13*, 3655–3670. [CrossRef] [PubMed]
138. Puntarulo, S. Iron, oxidative stress and human health. *Mol. Asp. Med.* **2005**, *26*, 299–312. [CrossRef] [PubMed]
139. Faizi, M.; Salimi, A.; Seydi, E.; Naserzadeh, P.; Kouhnavard, M.; Rahimi, A.; Pourahmad, J. Toxicity of cuprizone a Cu(2+) chelating agent on isolated mouse brain mitochondria: a justification for demyelination and subsequent behavioral dysfunction. *Toxicol. Mech. Methods.* **2016**, *26*, 276–283. [CrossRef] [PubMed]
140. Youle, R.J.; van der Bliek, A.M. Mitochondrial fission, fusion, and stress. *Science* **2012**, *337*, 1062–1065. [CrossRef]
141. Acs, P.; Komoly, S. Selective ultrastructural vulnerability in the cuprizone-induced experimental demyelination. *Ideggyogy Sz.* **2012**, *65*, 266–270.
142. Biancotti, J.C.; Kumar, S.; de Vellis, J. Activation of inflammatory response by a combination of growth factors in cuprizone-induced demyelinated brain leads to myelin repair. *Neurochem. Res.* **2008**, *33*, 2615–2628. [CrossRef]
143. Harris, J.J.; Attwell, D. The energetics of CNS white matter. *J. Neurosci.* **2012**, *32*, 356–371. [CrossRef]
144. Bradl, M.; Lassmann, H. Oligodendrocytes: biology and pathology. *Acta Neuropathol.* **2010**, *119*, 37–53. [CrossRef] [PubMed]
145. Carvalho, A.N.; Lim, J.L.; Nijland, P.G.; Witte, M.E.; Van Horssen, J. Glutathione in multiple sclerosis: more than just an antioxidant? *Mult. Scler.* **2014**, *20*, 1425–1431. [CrossRef]
146. Kang, Y.J. Metallothionein redox cycle and function. *Exp. Biol. Med.* **2006**, *231*, 1459–1467. [CrossRef] [PubMed]
147. Pinteaux, E.; Perraut, M.; Tholey, G. Distribution of mitochondrial manganese superoxide dismutase among rat glial cells in culture. *Glia* **1998**, *22*, 408–414. [CrossRef]
148. Lassmann, H.; van Horssen, J. Oxidative stress and its impact on neurons and glia in multiple sclerosis lesions. *BBA.* **2016**, *1862*, 506–510. [CrossRef] [PubMed]
149. Stone, S.; Lin, W. The unfolded protein response in multiple sclerosis. *Front. Neurosci.* **2015**, *9*, 264. [CrossRef] [PubMed]
150. Cwiklinska, H.; Mycko, M.P.; Luvsannorov, O.; Walkowiak, B.; Brosnan, C.F.; Raine, C.S.; Selmaj, K.W. Heat shock protein 70 associations with myelin basic protein and proteolipid protein in multiple sclerosis brains. *Int. Immunol.* **2003**, *15*, 241–249. [CrossRef] [PubMed]
151. Mycko, M.P.; Papoian, R.; Boschert, U.; Raine, C.S.; Selmaj, K.W. Microarray gene expression profiling of chronic active and inactive lesions in multiple sclerosis. *Clin. Neurol. Neurosurg.* **2004**, *106*, 223–229. [CrossRef]
152. Michaels, T.C.; Lazell, H.W.; Arosio, P.; Knowles, T.P. Dynamics of protein aggregation and oligomer formation governed by secondary nucleation. *J. Chem. Phys.* **2015**, *143*, 054901. [CrossRef]
153. Choi, M.L.; Gandhi, S. Crucial role of protein oligomerization in the pathogenesis of Alzheimer's and Parkinson's diseases. *FEBS J.* **2018**, *285*, 3631–3644. [CrossRef]

154. Dasgupta, A.; Zheng, J.; Perrone-Bizzozero, N.I.; Bizzozero, O.A. Increased carbonylation, protein aggregation and apoptosis in the spinal cord of mice with experimental autoimmune encephalomyelitis. *ASN Neuro.* **2013**, *5*, e00111. [CrossRef] [PubMed]
155. David, M.A.; Tayebi, M. Detection of Protein Aggregates in Brain and Cerebrospinal Fluid Derived from Multiple Sclerosis Patients. *Front. Neurol.* **2014**, *5*. [CrossRef] [PubMed]
156. Frohlich, C.; Grabiger, S.; Schwefel, D.; Faelber, K.; Rosenbaum, E.; Mears, J.; Rocks, O.; Daumke, O. Structural insights into oligomerization and mitochondrial remodelling of dynamin 1-like protein. *EMBO J.* **2013**, *32*, 1280–1292. [CrossRef]
157. Clinton, R.W.; Francy, C.A.; Ramachandran, R.; Qi, X.; Mears, J.A. Dynamin-related Protein 1 Oligomerization in Solution Impairs Functional Interactions with Membrane-anchored Mitochondrial Fission Factor. *J. Biol. Chem.* **2016**, *291*, 478–492. [CrossRef] [PubMed]
158. Jorgensen, C.S.; Ryder, L.R.; Steino, A.; Hojrup, P.; Hansen, J.; Beyer, N.H.; Heegaard, N.H.; Houen, G. Dimerization and oligomerization of the chaperone calreticulin. *Eur. J. Biochem.* **2003**, *270*, 4140–4148. [CrossRef] [PubMed]
159. Hammack, B.N.; Fung, K.Y.; Hunsucker, S.W.; Duncan, M.W.; Burgoon, M.P.; Owens, G.P.; Gilden, D.H. Proteomic analysis of multiple sclerosis cerebrospinal fluid. *Mult. Scler.* **2004**, *10*, 245–260. [CrossRef] [PubMed]
160. Lehmensiek, V.; Sussmuth, S.D.; Tauscher, G.; Brettschneider, J.; Felk, S.; Gillardon, F.; Tumani, H. Cerebrospinal fluid proteome profile in multiple sclerosis. *Mult. Scler.* **2007**, *13*, 840–849. [CrossRef]
161. Ziegler-Waldkirch, S.; Meyer-Luehmann, M. The Role of Glial Cells and Synapse Loss in Mouse Models of Alzheimer's Disease. *Front. Cell. Neurosci.* **2018**, *12*, 473. [CrossRef]
162. Bisht, K.; Sharma, K.P.; Lecours, C.; Sanchez, M.G.; El Hajj, H.; Milior, G.; Olmos-Alonso, A.; Gomez-Nicola, D.; Luheshi, G.; Vallieres, L.; et al. Dark microglia: A new phenotype predominantly associated with pathological states. *Glia* **2016**, *64*, 826–839. [CrossRef]
163. Matute, C.; Alberdi, E.; Ibarretxe, G.; Sanchez-Gomez, M.V. Excitotoxicity in glial cells. *Eur. J. Pharm.* **2002**, *447*, 239–246. [CrossRef]
164. Hanin, I. Central neurotransmitter function and its behavioral correlates in man. *Env. Health Perspect.* **1978**, *26*, 135–141. [CrossRef] [PubMed]
165. Dutta, R.; Chang, A.; Doud, M.K.; Kidd, G.J.; Ribaudo, M.V.; Young, E.A.; Fox, R.J.; Staugaitis, S.M.; Trapp, B.D. Demyelination causes synaptic alterations in hippocampi from multiple sclerosis patients. *Ann. Neurol.* **2011**, *69*, 445–454. [CrossRef] [PubMed]
166. Dutta, R.; Chomyk, A.M.; Chang, A.; Ribaudo, M.V.; Deckard, S.A.; Doud, M.K.; Edberg, D.D.; Bai, B.; Li, M.; Baranzini, S.E.; et al. Hippocampal demyelination and memory dysfunction are associated with increased levels of the neuronal microRNA miR-124 and reduced AMPA receptors. *Ann. Neurol.* **2013**, *73*, 637–645. [CrossRef] [PubMed]
167. Schellenberg, A.E.; Buist, R.; Del Bigio, M.R.; Toft-Hansen, H.; Khorooshi, R.; Owens, T.; Peeling, J. Blood-brain barrier disruption in CCL2 transgenic mice during pertussis toxin-induced brain inflammation. *Fluids Barriers CNS* **2012**, *9*, 10. [CrossRef] [PubMed]
168. Arimoto, H.; Tanuma, N.; Jee, Y.; Miyazawa, T.; Shima, K.; Matsumoto, Y. Analysis of experimental autoimmune encephalomyelitis induced in F344 rats by pertussis toxin administration. *J. Neuroimmunol.* **2000**, *104*, 15–21. [CrossRef]
169. Amiel, S.A. The effects of Bordetella pertussis vaccine on cerebral vascular permeability. *Br. J. Exp. Pathol.* **1976**, *57*, 653–662.
170. Shah, S.; Breivogel, C.; Selly, D.; Munirathinam, G.; Childers, S.; Yoburn, B.C. Time-dependent effects of in vivo pertussis toxin on morphine analgesia and G-proteins in mice. *Pharm. Biochem. Behav.* **1997**, *56*, 465–469. [CrossRef]
171. Armirotti, A.; Damonte, G. Achievements and perspectives of top-down proteomics. *Proteomics* **2010**, *10*, 3566–3576. [CrossRef]

172. Kachuk, C.; Doucette, A.A. The benefits (and misfortunes) of SDS in top-down proteomics. *J. Proteom.* **2018**, *175*, 75–86. [CrossRef]
173. Perkel, J.M. Tearing the top off 'Top-Down' Proteomics. *Biotechniques* **2012**, *53*, 75–78. [CrossRef]

Suppression of the peripheral immune system limits the central immune response following cuprizone-feeding: Relevance to modelling Multiple Sclerosis

Monokesh K. Sen[1], Mohammed S.M. Almuslehi[1,2], Erika Gyengesi[1], Simon J. Myers[3], Peter J. Shortland[3], David A. Mahns[1*], and Jens R. Coorssen[4*]

[1]School of Medicine, Western Sydney University, Locked Bag 1797, Penrith, NSW 2751, Australia; monokesh.sen@westernsydney.edu.au.
[1,2]School of Medicine, Western Sydney University, Locked Bag 1797, Penrith, NSW 2751, Australia and [2]Department of Physiology, College of Veterinary Medicine, Diyala University, Diyala, Iraq; m.almuslehi@westernsydney.edu.au.
[1]School of Medicine, Western Sydney University, Locked Bag 1797, Penrith, NSW 2751, Australia; e.gyengesi@westernsydney.edu.au.
[1]School of Medicine, Western Sydney University, Locked Bag 1797, Penrith, NSW 2751, Australia; d.mahns@westernsydney.edu.au.
[3]School of Science and Health, Western Sydney University, Locked Bag 1797, Penrith, NSW 2751, Australia; s.myers@westernsydney.edu.au.
[3]School of Science and Health, Western Sydney University, Locked Bag 1797, Penrith, NSW 2751, Australia; p.shortland@westernsydney.edu.au.
[4]Department of Health Sciences, Faculty of Applied Health Sciences, and Department of Biological Sciences, Faculty of Mathematics and Science, Brock University, St. Catharines, Ontario, ON L2S 3A1, Canada; jcoorssen@brocku.ca

***Co-corresponding authors**
[1]School of Medicine, Western Sydney University, Locked Bag 1797, Penrith, NSW 2751, Australia; d.mahns@westernsydney.edu.au.

[4]Department of Health Sciences, Faculty of Applied Health Sciences, and Department of Biological Sciences, Faculty of Mathematics and Science, Brock University, St. Catharines, Ontario, ON L2S 3A1, Canada; jcoorssen@brocku.ca.

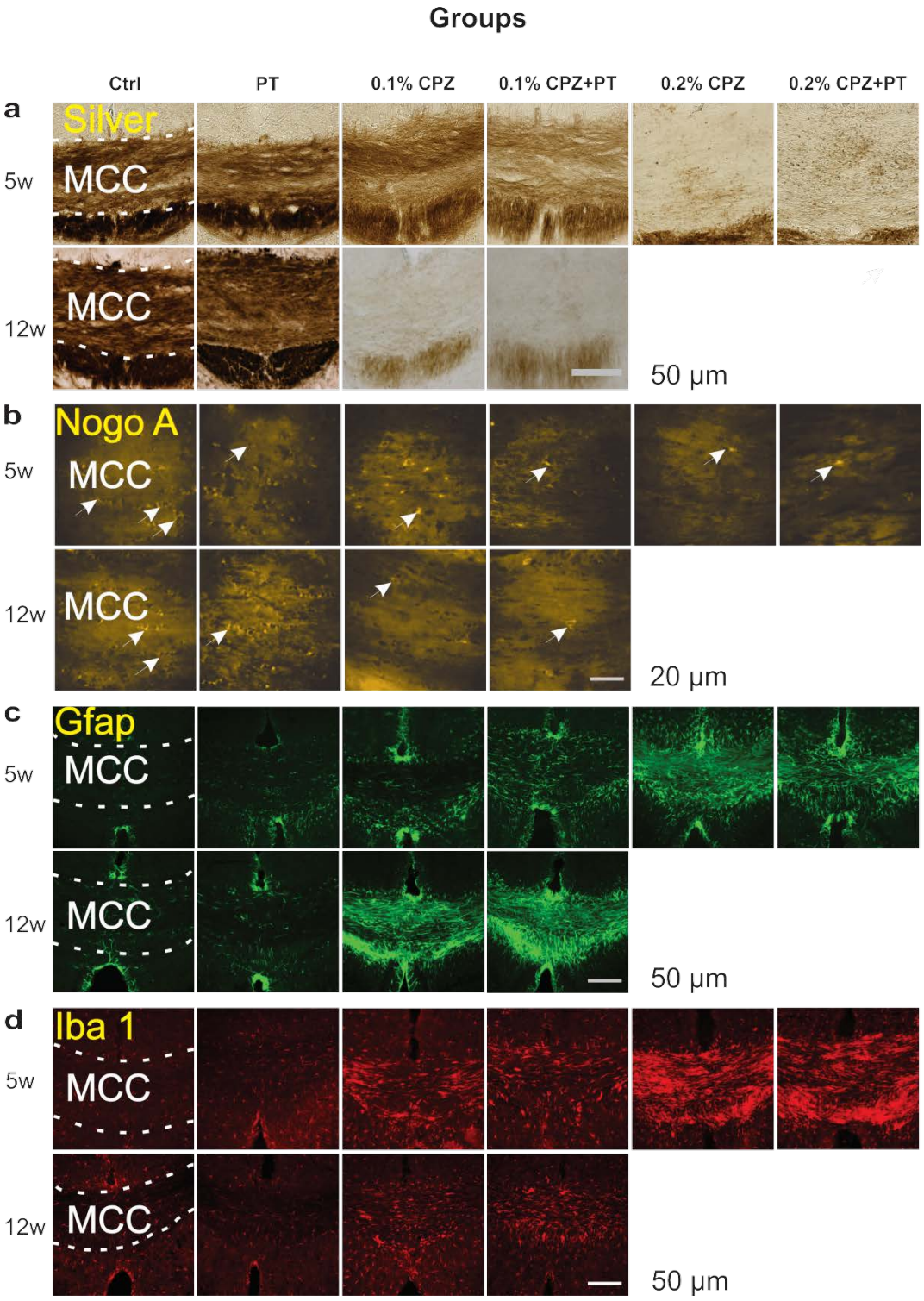

Figure 1: Histological effects of different treatments on the midline corpus callosum
Representative images of silver-stained brain sections from 5- and 12- week experimental groups to assess demyelination (**a**), or immunohistochemistry to identify the cell bodies of mature oligodendrocytes using Nogo A (**b**), astrocytes using Gfap (**c**) or microglia using Iba 1 (**d**) antibodies. Dashed lines represent the upper and lower borders of the MCC. Arrows indicate Nogo A positive cells.

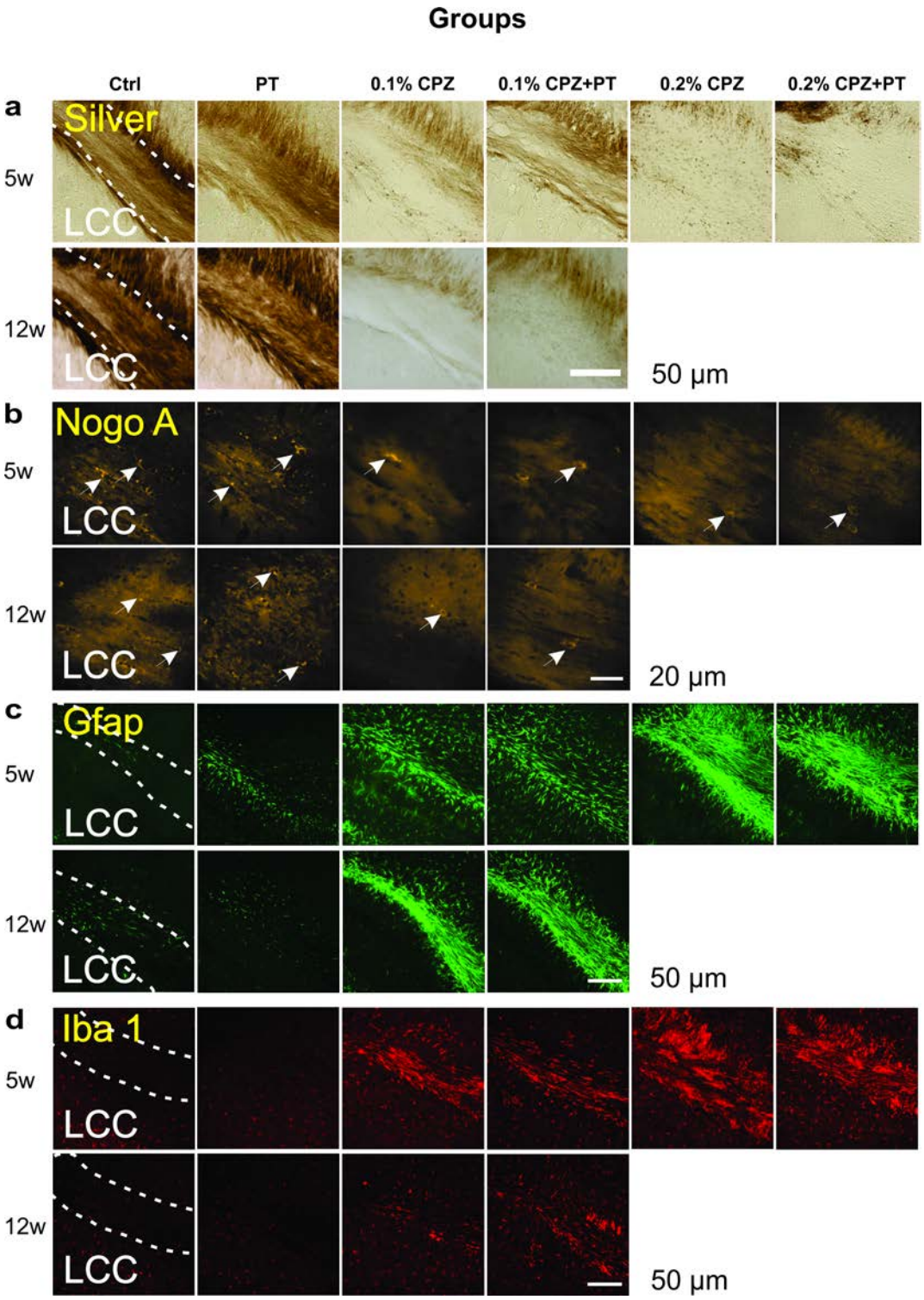

Figure 2: Histological effects of different treatments on the lateral corpus callosum
Representative images of silver-stained brain sections from 5- and 12- week experimental groups to assess demyelination (**a**), or immunohistochemistry to identify the cell bodies of mature oligodendrocytes using Nogo A (**b**), astrocytes using Gfap (**c**) or microglia using Iba 1 (**d**) antibodies. Dashed lines represent the upper and lower borders of the LCC. Arrows indicate Nogo A positive cells.

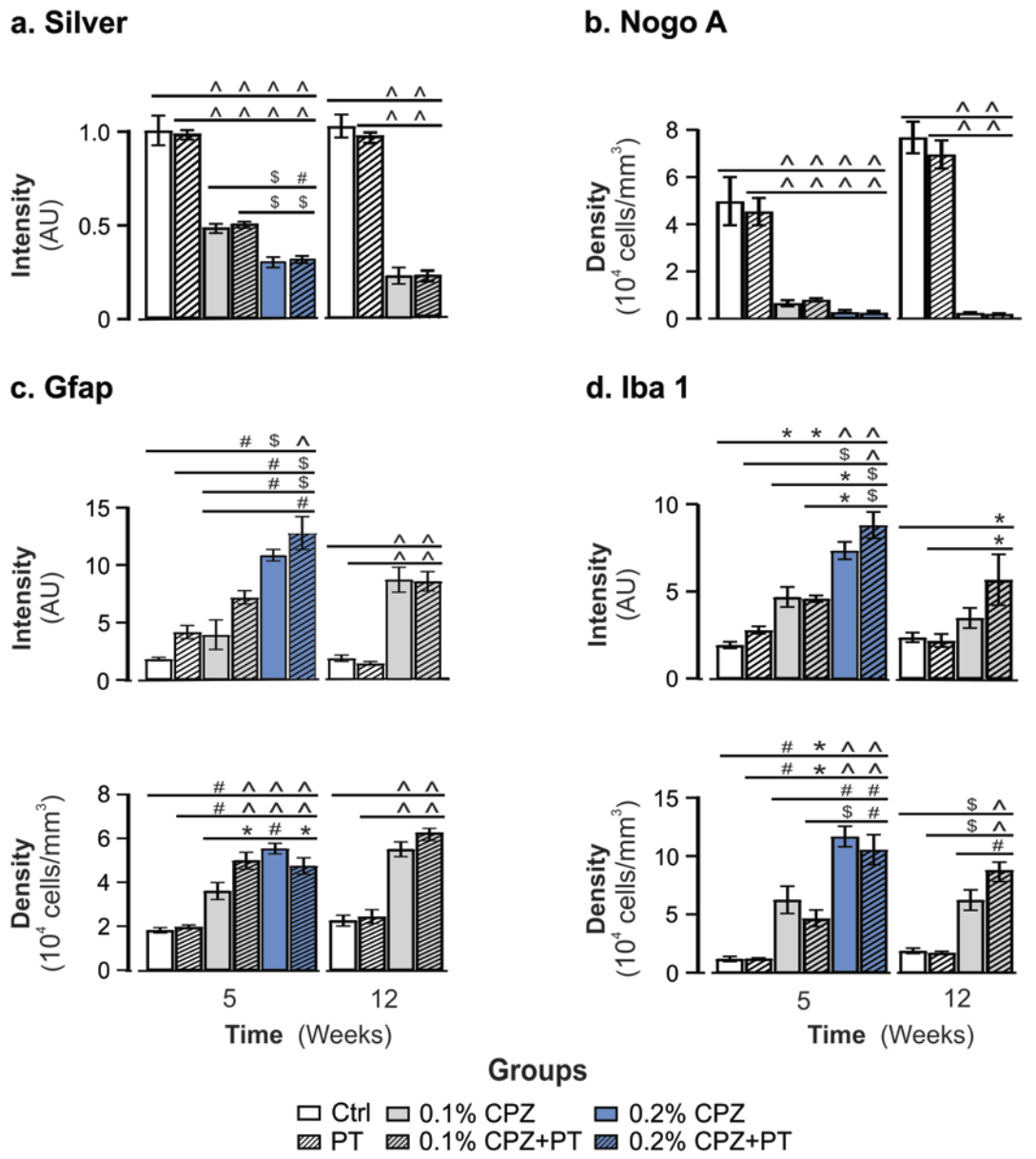

Figure 3: Quantification of demyelination, cell death and gliosis in lateral corpus callosum

a) Silver staining. CPZ-feeding(±PT) led to significant demyelination and reduced silver staining intensity at 5 and 12 weeks in the LCC. PT alone had no effect. Feeding 0.1% CPZ for longer (12 weeks) produced a comparable demyelination to that seen with 0.2% for 5 weeks. **b**) Nogo A. CPZ-feeding(±PT) led to significant oligodendrocytosis with 0.1% CPZ as effective as 0.2% CPZ at either time point. PT alone had no effect. **c**) Gfap. Staining intensity increased in a dose dependent fashion the CPZ(±PT) treated groups and this was associated with an increase the number of Gfap positive astrocytes at both time points. PT only did not evoke a Gfap response. **d**) Iba 1. Increased Iba 1 fluorescence intensity and number of Iba 1 positive microglia were seen in both 5-and 12-week groups. Significant effects were best seen at the highest doses used at each time point. PT only produced no microglial response. Data are presented as mean ± SEM. One-way ANOVA and Tukey post hoc analysis was used to determine differences among groups (*p<0.05, #p<0.01, \$$p$<0.001 and ^$p$<0.0001). Quantitation based on analysis of 5-9 sections/animal, 3-5 animals/group.

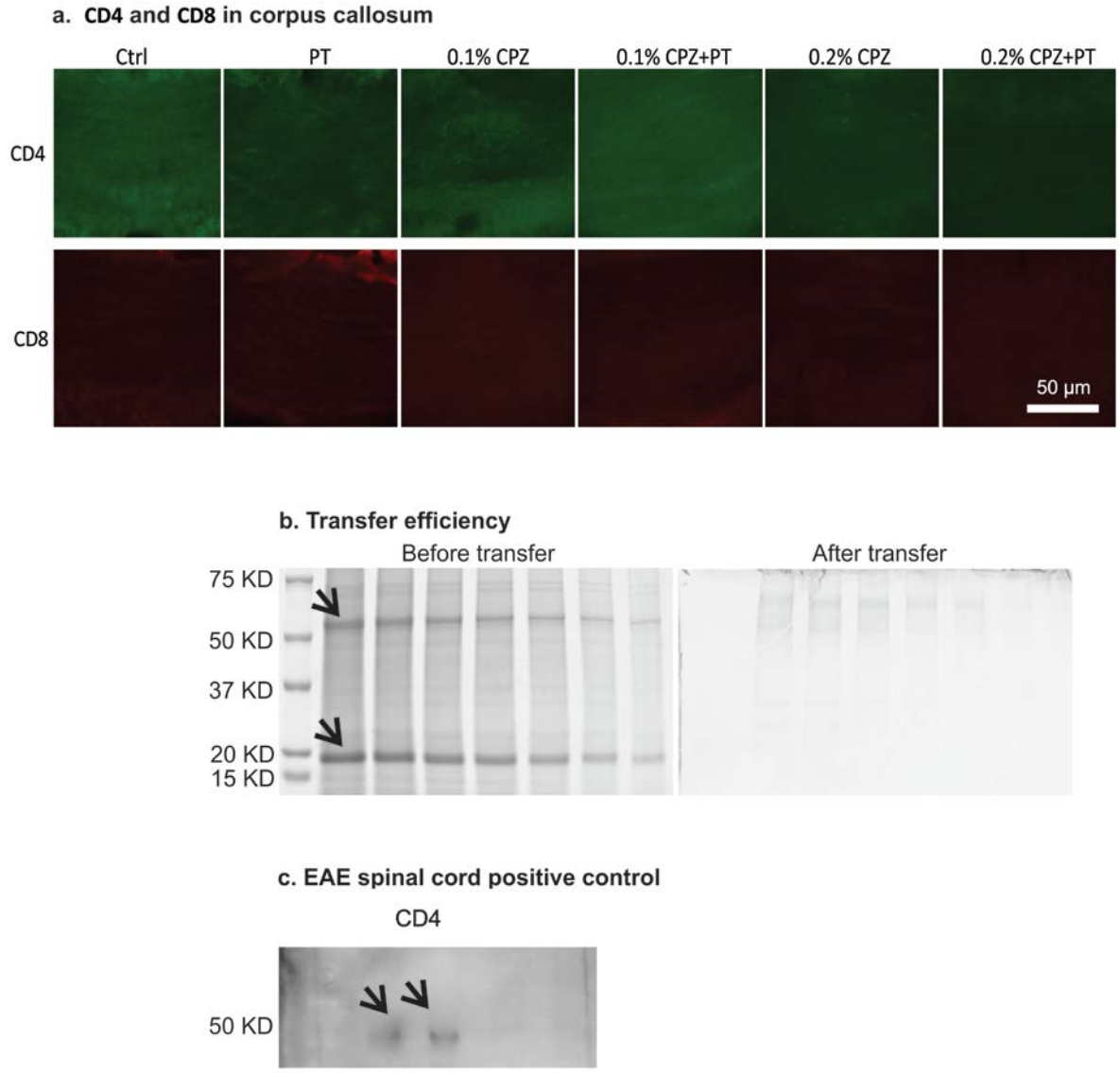

Figure 4: Immune staining and transfer efficiency

a) Immunofluorescence staining of CD4 and CD8 in the corpus callosum from the 5-week study (n=5 sections/animal, n=3 animals/group). No positive cells were detected. **b**) 1D gels used to quantify the transfer efficiency of respective regions of CD4 (50 KD) and CD8 (30 KD) proteins from gel to PVDF membrane (n=3 bands/gel, n=2 gels). Arrows indicate the bands quantified. **c**) 40 µg spinal cord homogenate was used to detect CD4 signal from EAE (n=2 animals, n=3 gels). Arrows indicate the CD4 band.

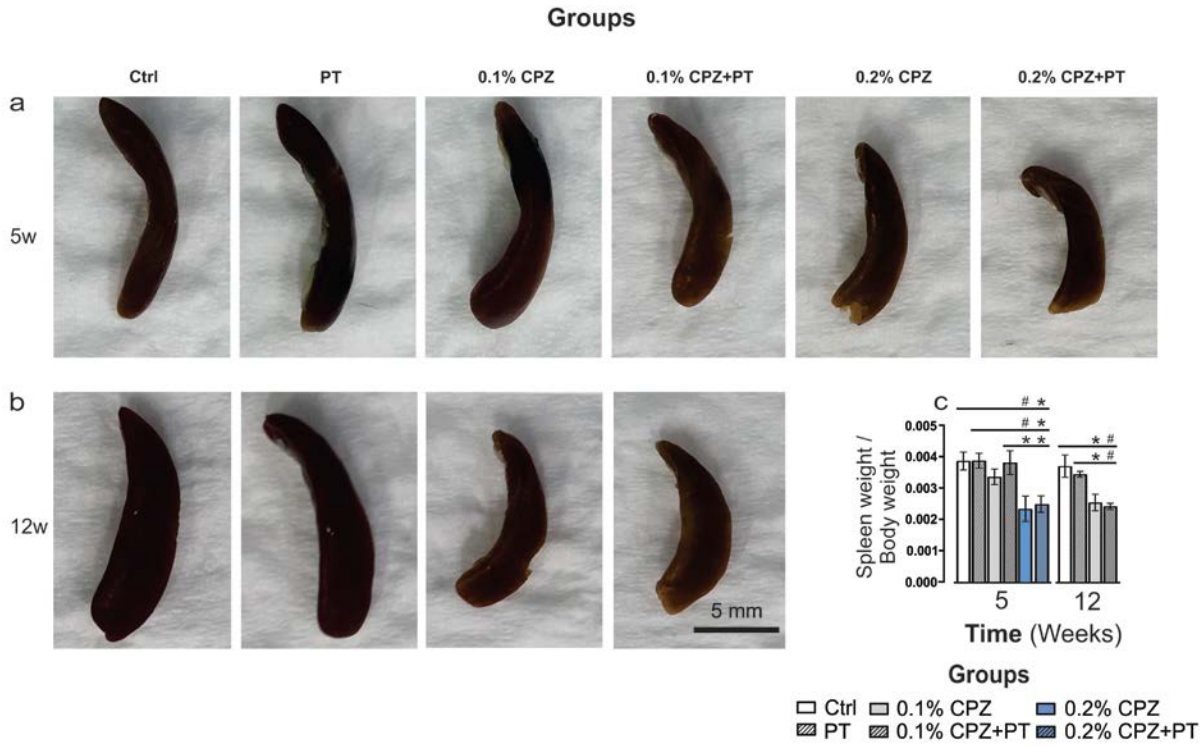

Figure 5: Dose and time dependent splenic atrophy

Representative images (**a** and **b**) of spleen from 5- and 12-week studies, respectively. Scale bar is 5 mm. Normalized (spleen tissue mass/body weight) splenic mass is shown in **c**. Feeding with 0.2% CPZ(±PT) for 5 weeks or 0.1% CPZ(±PT) for 12 weeks resulted in a significant reduction of splenic mass. Data are presented as mean ± SEM. One-way ANOVA and Tukey post hoc analysis was used to determine differences among groups (*p<0.05 and #p<0.01). Quantitation based on analysis of 3 and 5 spleens from 5 and 12 weeks, respectively.

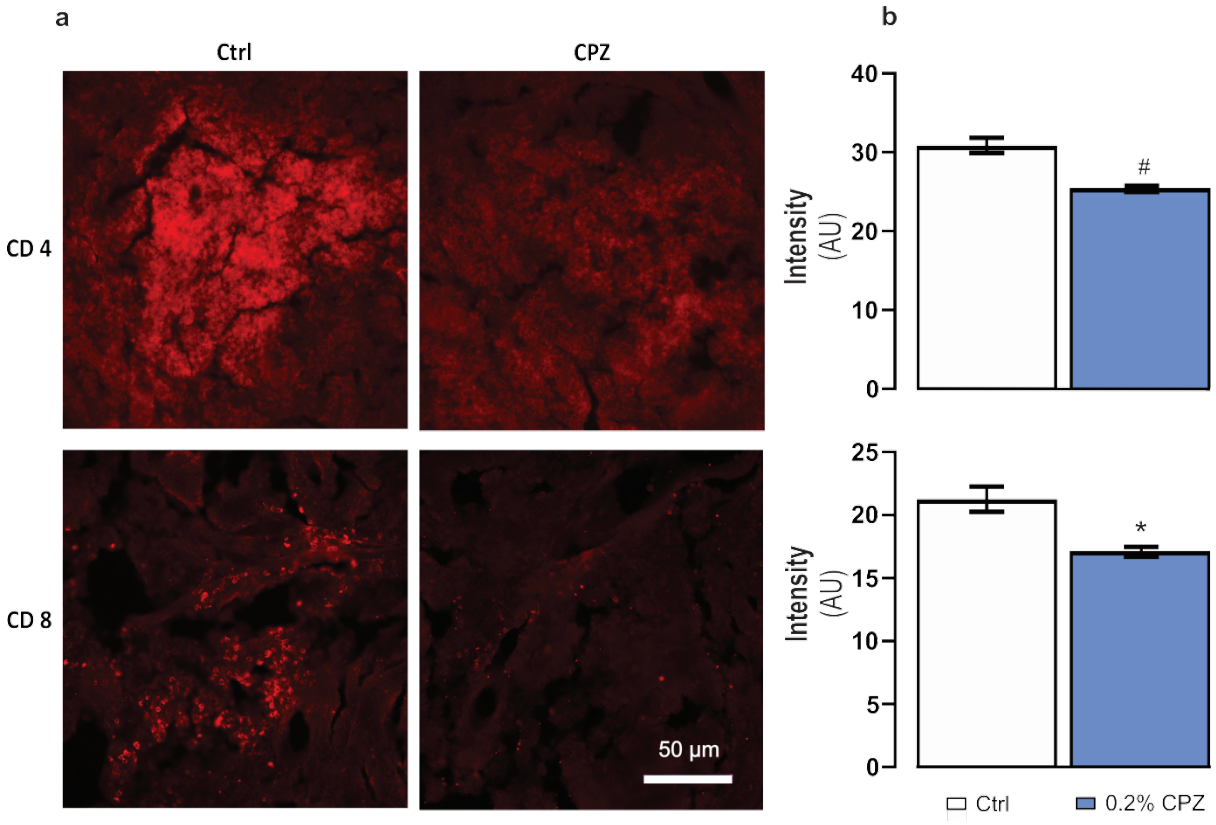

Figure 6: Reduction of T-cell fluorescence intensity

Representative images of spleen (**a)** and quantification (**b**) of CD4 and CD8 from Ctrl and 0.2% CPZ, respectively. Scale bar is 50 µm. Feeding with 0.2% CPZ showed a significant reduction of splenic CD4 and CD8 T-cells. Data are presented as mean ± SEM. Unpaired two-tailed t test was used to determine differences between groups (*p<0.05 and #p<0.01). Quantitation based on analysis of 3 spleens/group and 10 sections/spleen.

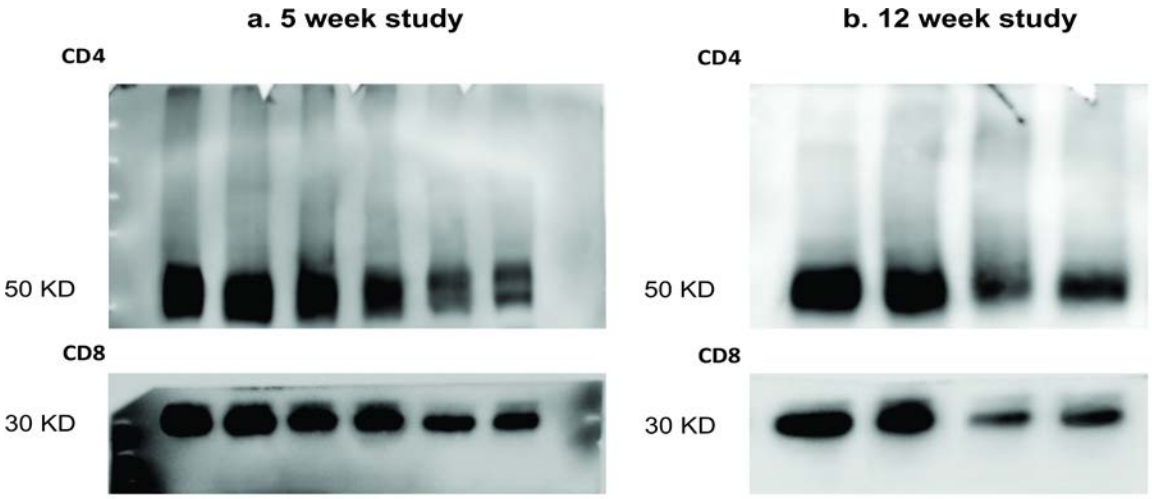

Figure 7: Western blot images of CD4 and CD8 from spleen samples from both 5- and 12-week studies

Table 1: Quantification of the total number of protein spots in 2D gels of whole brain soluble and membrane proteomes

Tissue fraction	Ctrl	PT	0.1% CPZ	0.1% CPZ +PT	0.2% CPZ	0.2% CPZ + PT	Feeding duration
SP	829±6	830±15	866±12	871±19	860±12	841±12	5 weeks
MP	766±10	802±12	798±15	835±21	779±13	778±16	
SP	808±6	802±2	791±5	789±4	-	-	12 weeks
MP	719±2	708 ±5	716 ±4	727±5	-	-	

Key: Soluble protein (SP) and membrane protein (MP), (n=5 animals/group, n=15 gels/fraction).

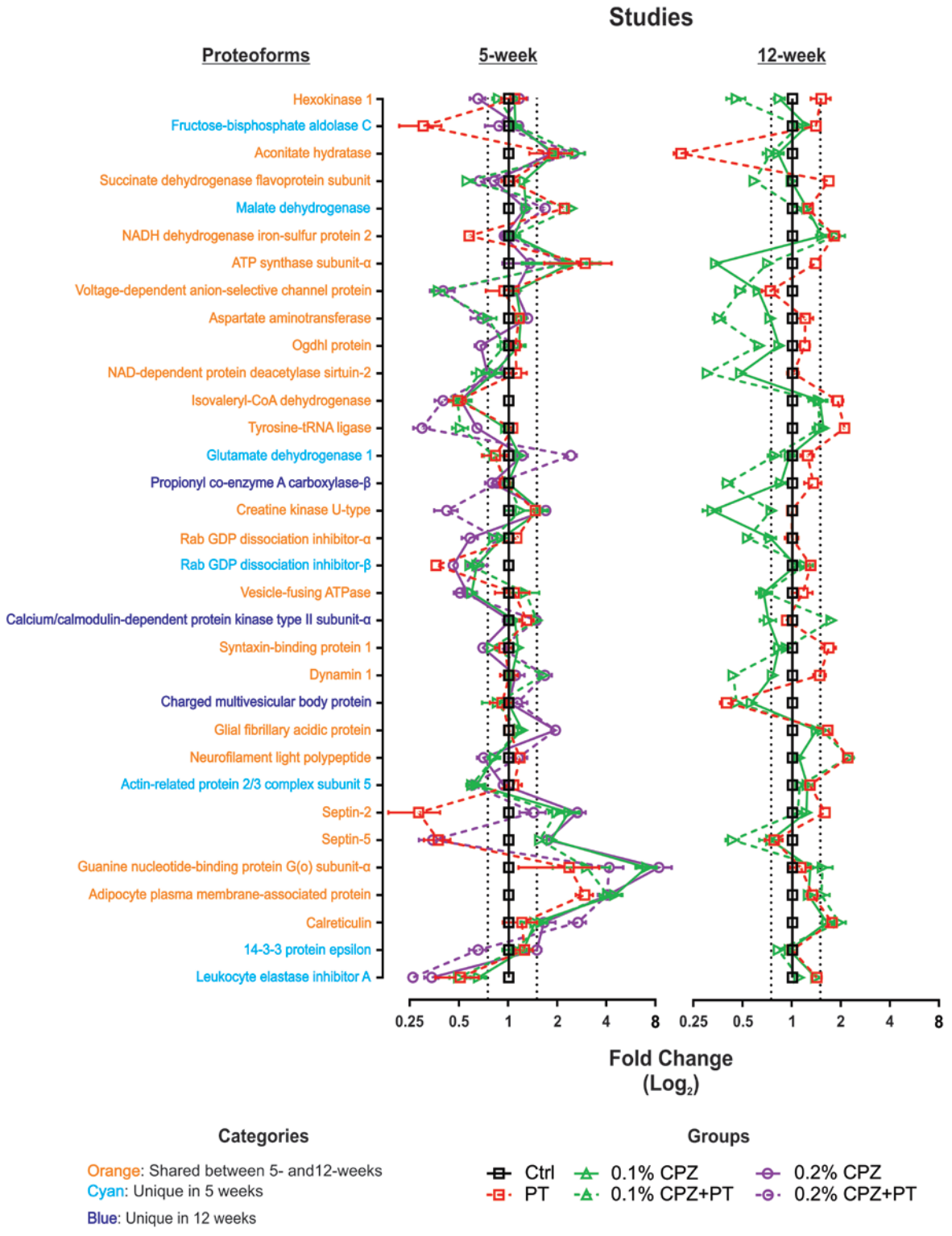

Figure 8: Pattern of proteoform change

Log2 fold changes in abundance for 33 proteoforms relative to Ctrl showing the pattern of changes (colour marked in left Y-axis) at both time points. Changes (increase or decrease) in abundance (≥1.5 fold) shared at both 5 and 12 weeks are shown in orange. Abundance changes observed following 5 weeks (≥1.5 fold) but not 12 weeks (<1.5 fold) of CPZ-feeding are shown in cyan. Proteoforms unchanged at 5 weeks (<1.5 fold) but changed after 12 weeks (≥1.5 fold) are shown in blue.

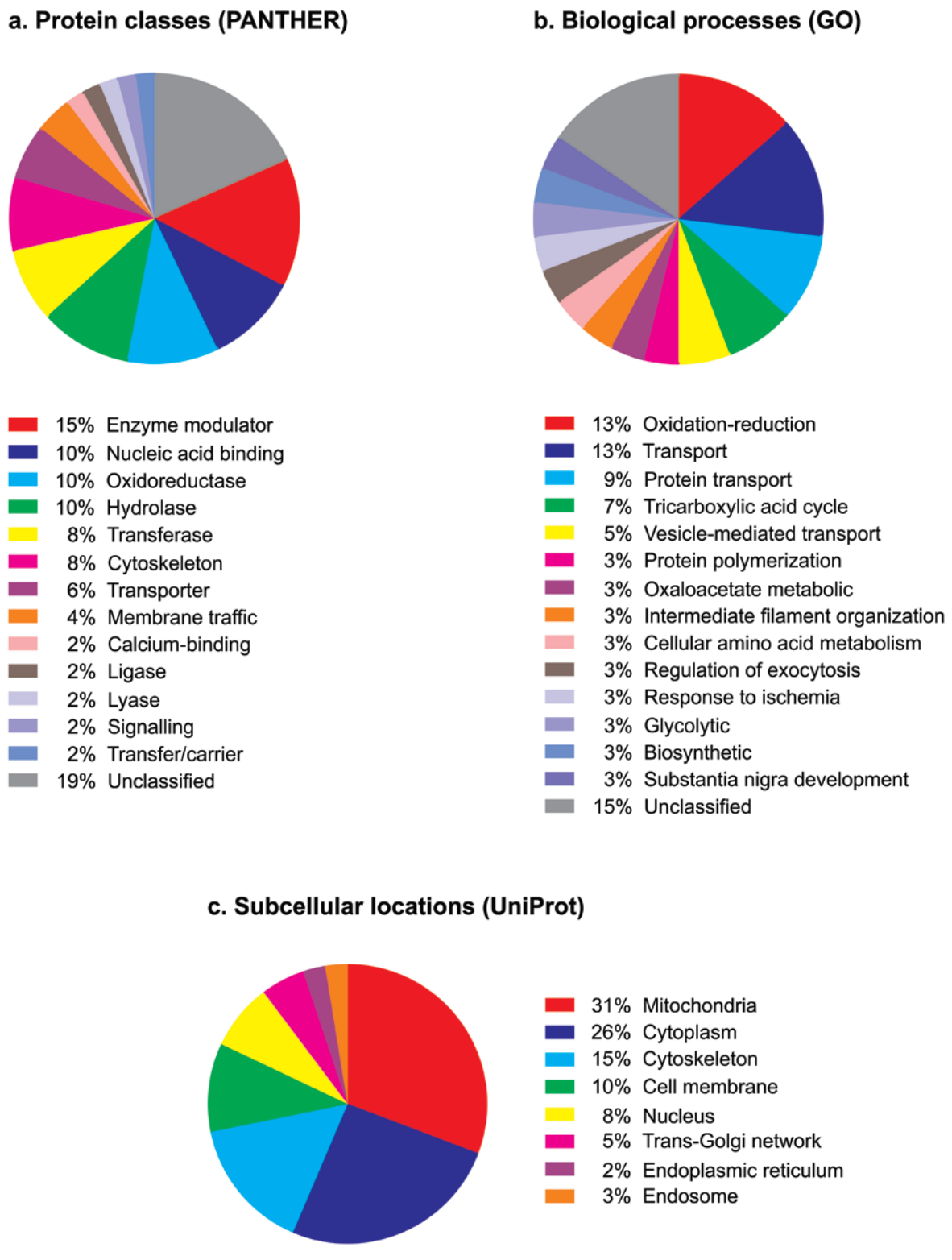

Figure 9: Functional clustering

Pie charts show the distribution of proteins according to **a**) Protein classes (characterized using PANTHER), **b**) Biological processes (categorised using GO) and **c**) Subcellular locations (categorised using UniProt).

a

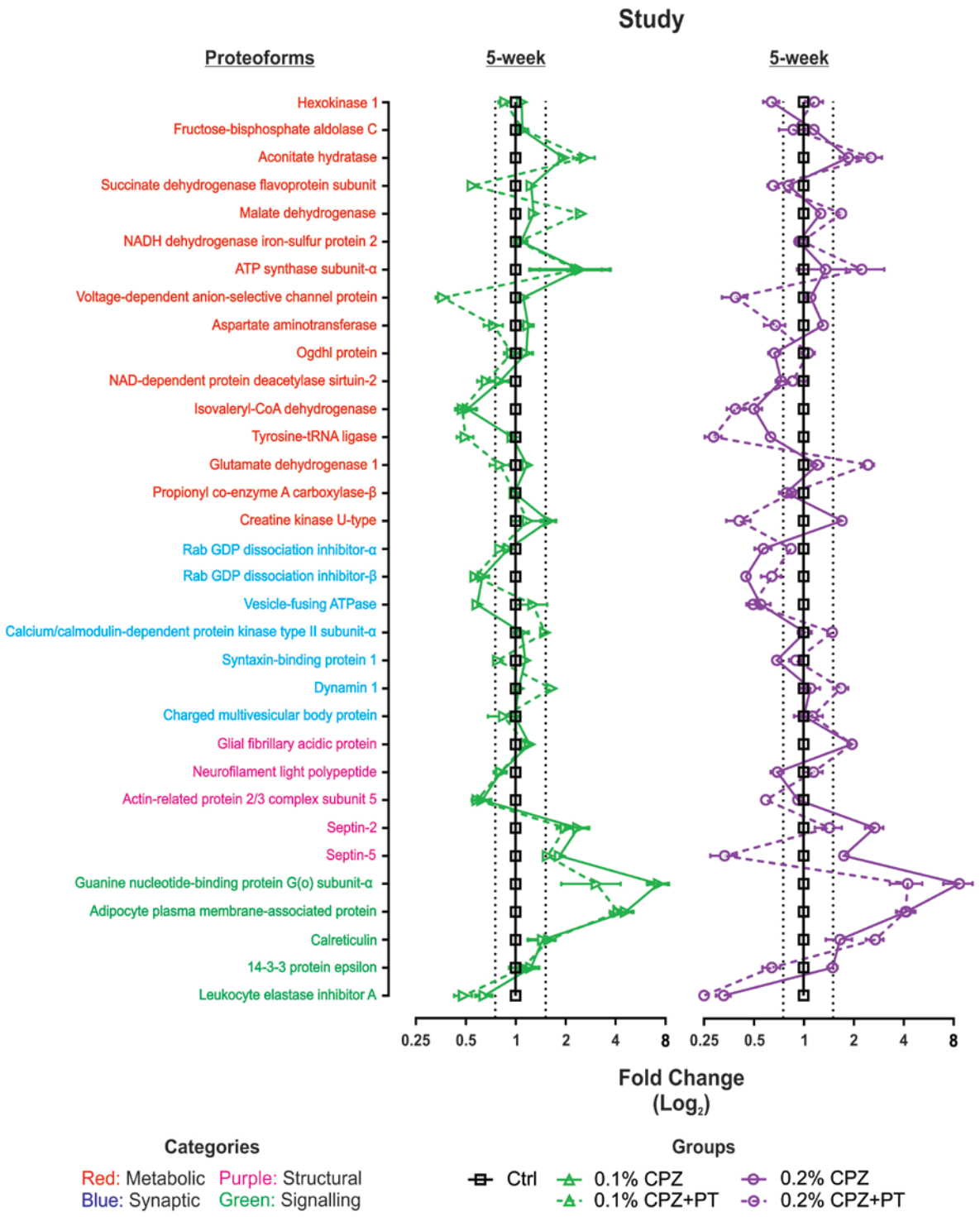
Study
Proteoforms
5-week
5-week
Hexokinase 1
Fructose-bisphosphate aldolase C
Aconitate hydratase
Succinate dehydrogenase flavoprotein subunit
Malate dehydrogenase
NADH dehydrogenase iron-sulfur protein 2
ATP synthase subunit-α
Voltage-dependent anion-selective channel protein
Aspartate aminotransferase
Ogdhl protein
NAD-dependent protein deacetylase sirtuin-2
Isovaleryl-CoA dehydrogenase
Tyrosine-tRNA ligase
Glutamate dehydrogenase 1
Propionyl co-enzyme A carboxylase-β
Creatine kinase U-type
Rab GDP dissociation inhibitor-α
Rab GDP dissociation inhibitor-β
Vesicle-fusing ATPase
Calcium/calmodulin-dependent protein kinase type II subunit-α
Syntaxin-binding protein 1
Dynamin 1
Charged multivesicular body protein
Glial fibrillary acidic protein
Neurofilament light polypeptide
Actin-related protein 2/3 complex subunit 5
Septin-2
Septin-5
Guanine nucleotide-binding protein G(o) subunit-α
Adipocyte plasma membrane-associated protein
Calreticulin
14-3-3 protein epsilon
Leukocyte elastase inhibitor A
0.25 0.5 1 2 4 8
0.25 0.5 1 2 4 8
Fold Change (Log2)
Categories
Red: Metabolic Purple: Structural
Blue: Synaptic Green: Signalling
Groups
Ctrl
0.1% CPZ
0.1% CPZ+PT
0.2% CPZ
0.2% CPZ+PT

b

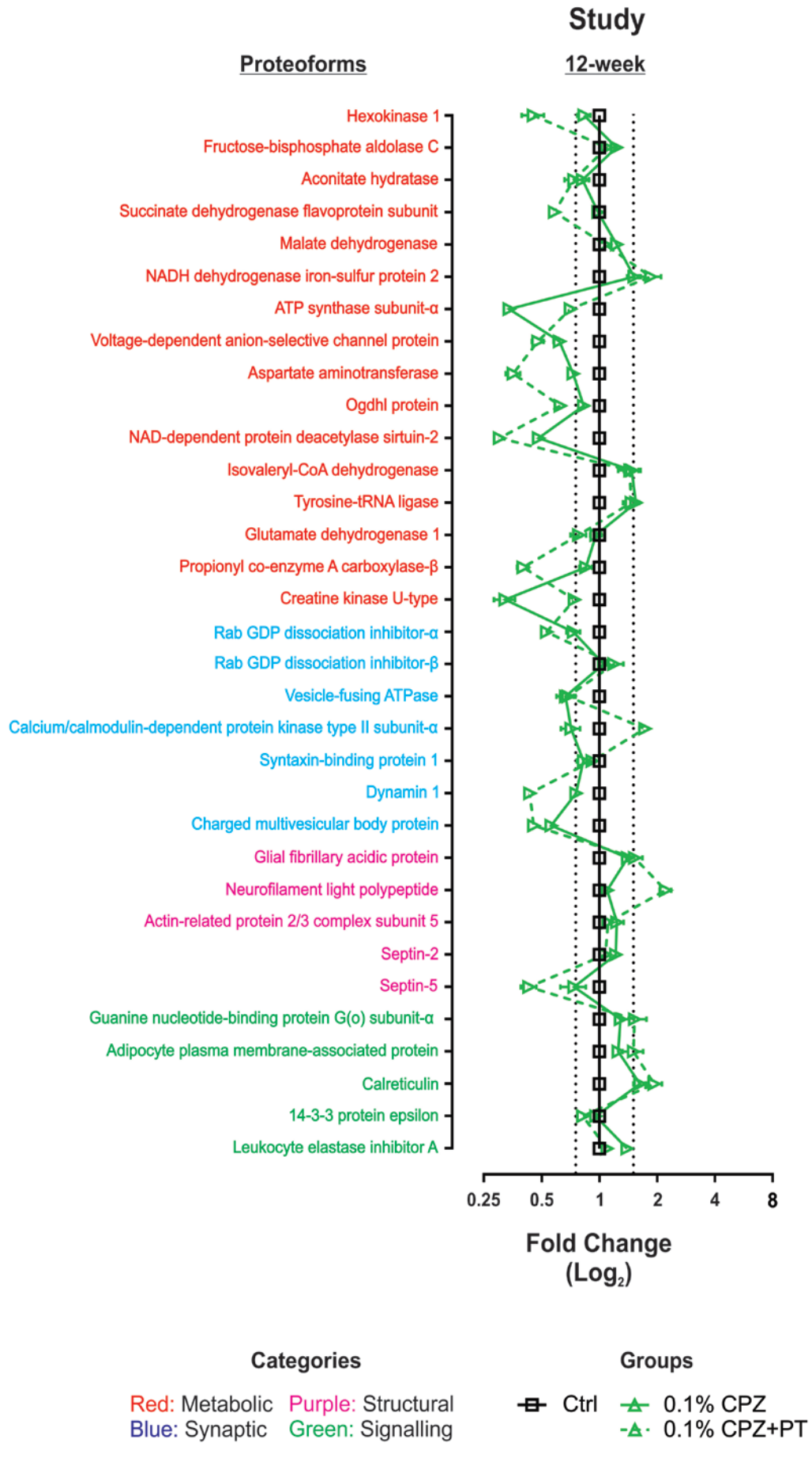
Study
Proteoforms
12-week
Hexokinase 1
Fructose-bisphosphate aldolase C
Aconitate hydratase
Succinate dehydrogenase flavoprotein subunit
Malate dehydrogenase
NADH dehydrogenase iron-sulfur protein 2
ATP synthase subunit-α
Voltage-dependent anion-selective channel protein
Aspartate aminotransferase
Ogdhl protein
NAD-dependent protein deacetylase sirtuin-2
Isovaleryl-CoA dehydrogenase
Tyrosine-tRNA ligase
Glutamate dehydrogenase 1
Propionyl co-enzyme A carboxylase-β
Creatine kinase U-type
Rab GDP dissociation inhibitor-α
Rab GDP dissociation inhibitor-β
Vesicle-fusing ATPase
Calcium/calmodulin-dependent protein kinase type II subunit-α
Syntaxin-binding protein 1
Dynamin 1
Charged multivesicular body protein
Glial fibrillary acidic protein
Neurofilament light polypeptide
Actin-related protein 2/3 complex subunit 5
Septin-2
Septin-5
Guanine nucleotide-binding protein G(o) subunit-α
Adipocyte plasma membrane-associated protein
Calreticulin
14-3-3 protein epsilon
Leukocyte elastase inhibitor A
0.25
0.5
1
2
4
8
Fold Change
(Log2)
Categories
Red: Metabolic
Purple: Structural
Blue: Synaptic
Green: Signalling
Groups
Ctrl
0.1% CPZ
0.1% CPZ+PT

c

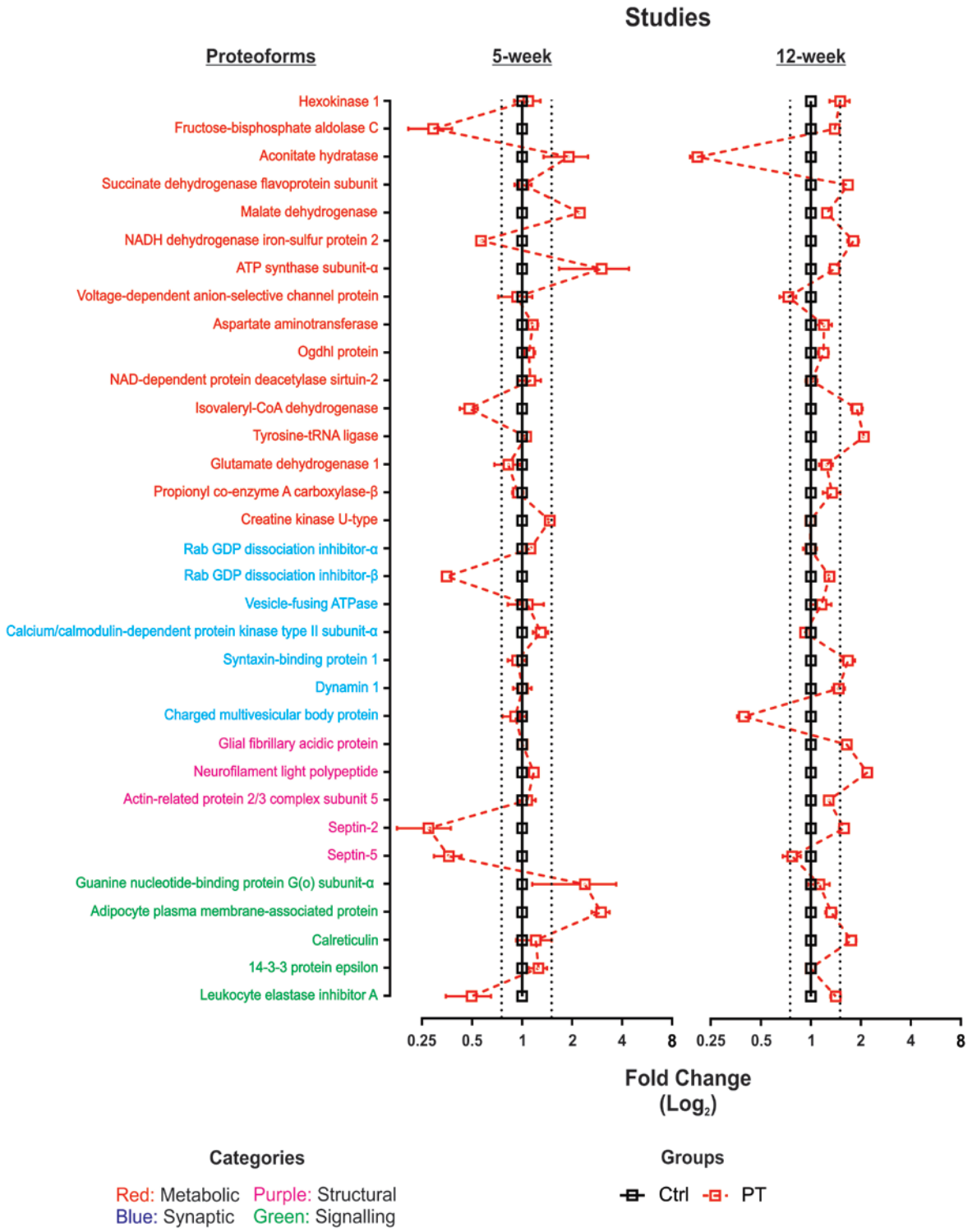

Figure 10: Duration and treatment-dependent proteoform changes

Log2 fold changes in abundance for 33 proteoforms relative to Ctrl showing the changes with CPZ (±PT) in the **a**) 5 week study or **b**) 12 week study. Changes only in PT groups at both 5 and 12 weeks are shown in **c**).

Table 2: Comparison of PT group to the PT+CPZ groups only

Protein name	5 weeks	12 weeks
Hexokinase 1	0.1PT=PT=0.2PT	0.1PT<PT
Fructose-bisphosphate aldolase C	0.1PT>PT<0.2PT	0.1PT=PT
Aconitate hydratase	0.1PT>PT<0.2PT	0.1PT>PT
Succinate dehydrogenase flavoprotein subunit	0.1PT<PT>0.2PT	0.1PT<PT
Malate dehydrogenase	0.1PT=PT>0.2PT	0.1PT=PT
NADH dehydrogenase iron-sulfur protein 2	0.1PT>PT<0.2PT	0.1PT=PT
ATP synthase subunit-α	0.1PT=PT=0.2PT	0.1PT<PT
Voltage-dependent anion-selective channel protein	0.1PT<PT>0.2PT	0.1PT=PT
Aspartate aminotransferase	0.1PT<PT>0.2PT	0.1PT<PT
Ogdhl protein	0.1PT=PT=0.2PT	0.1PT<PT
NAD-dependent protein deacetylase sirtuin-2	0.1PT>PT=0.2PT	0.1PT<PT
Isovaleryl-CoA dehydrogenase	0.1PT=PT=0.2PT	0.1PT<PT
Tyrosine-tRNA ligase	0.1PT<PT>0.2PT	0.1PT<PT
Glutamate dehydrogenase 1	0.1PT=PT<0.2PT	0.1PT<PT
Propionyl co-enzyme A carboxylase-β	0.1PT=PT=0.2PT	0.1PT<PT
Creatine kinase U-type	0.1PT=PT>0.2PT	0.1PT=PT
Rab GDP dissociation inhibitor-α	0.1PT<PT>0.2PT	0.1PT<PT
Rab GDP dissociation inhibitor-β	0.1PT=PT=0.2PT	0.1PT=PT
Vesicle-fusing ATPase	0.1PT=PT>0.2PT	0.1PT<PT
Calcium/calmodulin-dependent protein kinase type II subunit-α	0.1PT=PT<0.2PT	0.1PT=PT
Syntaxin-binding protein 1	0.1PT=PT=0.2PT	0.1PT<PT
Dynamin 1	0.1PT>PT<0.2PT	0.1PT<PT
Charged multivesicular body protein	0.1PT=PT=0.2PT	0.1PT=PT
Glial fibrillary acidic protein	0.1PT=PT<0.2PT	0.1PT=PT
Neurofilament light polypeptide	0.1PT<PT=0.2PT	0.1PT=PT
Actin-related protein 2/3 complex subunit 5	0.1PT<PT>0.2PT	0.1PT=PT
Septin-2	0.1PT>PT<0.2PT	0.1PT<PT
Septin-5	0.1PT>PT=0.2PT	0.1PT<PT
Guanine nucleotide-binding protein G(o) subunit-α	0.1PT=PT<0.2PT	0.1PT>PT
Adipocyte plasma membrane-associated protein	0.1PT>PT<0.2PT	0.1PT=PT
Calreticulin	0.1PT=PT<0.2PT	0.1PT=PT
14-3-3 protein epsilon	0.1PT=PT=0.2PT	0.1PT=PT
Leukocyte elastase inhibitor A	0.1PT=PT=0.2PT	0.1PT<PT

Key: Significant (p<0.05) increases and decreases relative to PT are indicated by < and > symbols, respectively. =, no significant difference; 0.1% CPZ+PT abbreviated to 0.1PT and 0.2% CPZ+PT to 0.2PT.

Behaviour

In the behavioural tests, there were no detectable differences (p>0.05) between any groups in the latency to fall from the rotarod (**Figure 1a**) or inverted screen apparatus (**Figure 1b**).

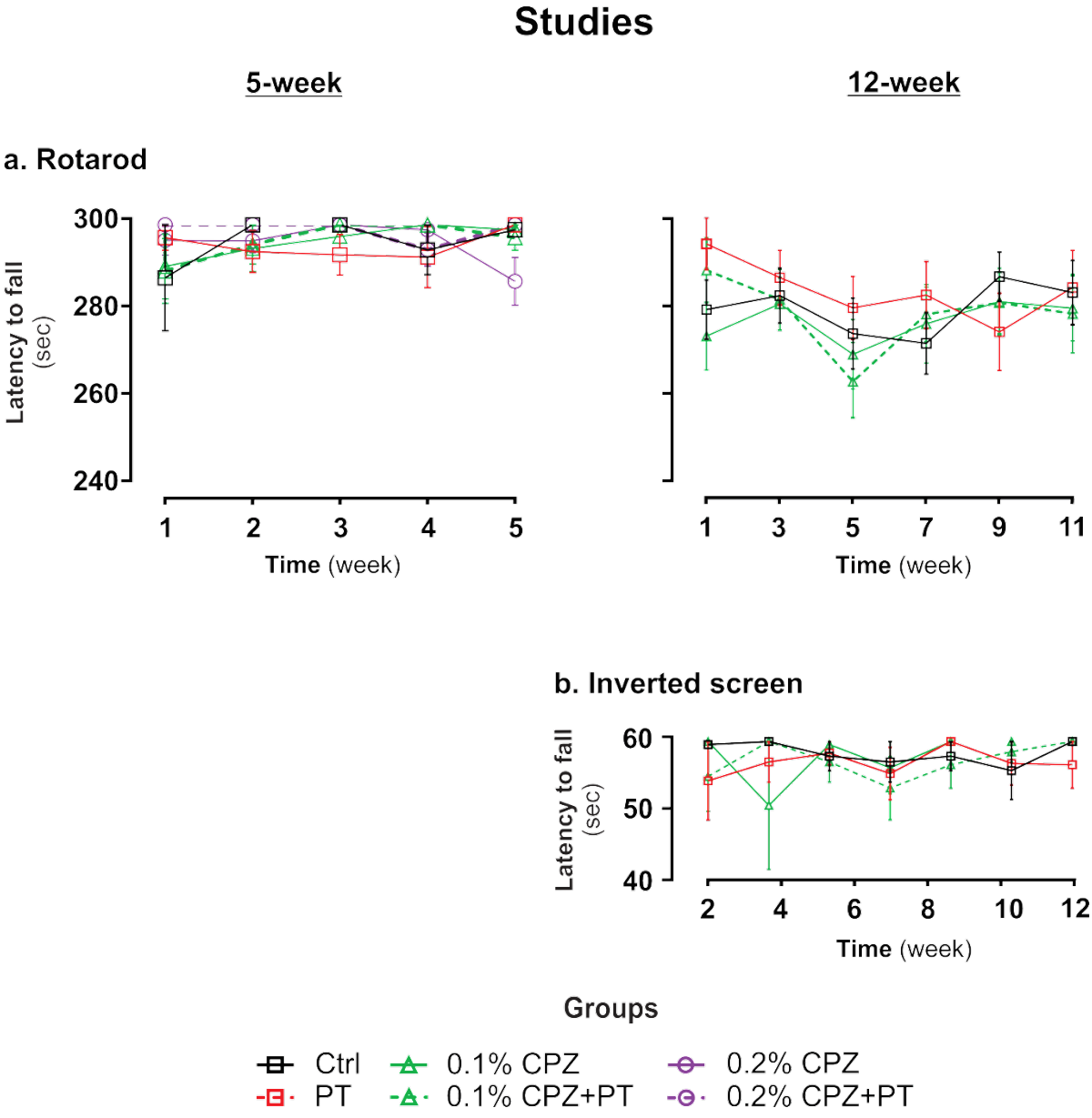

Figure 1: Behavioural changes induced by CPZ-feeding

There were no significant differences between groups in the latency to fall using the rotarod (**a**) or inverted screen (**b**) tests in either study. Data are expressed as mean ± SEM. Two-way ANOVA and Tukey post hoc analysis were used to determine differences among groups (5-week study, n=10 animals/group; 12-week study n=12 animals/group).

Chapter-4 (Paper II)

This chapter has been published in Neuroscience & Biobehavioral Reviews, 107:23-46. doi: 10.1016/j.neubiorev.2019.08.008.

Neuroscience and Biobehavioral Reviews 107 (2019) 23–46

Contents lists available at ScienceDirect

Neuroscience and Biobehavioral Reviews

journal homepage: www.elsevier.com/locate/neubiorev

Behavioural phenotypes in the cuprizone model of central nervous system demyelination

Monokesh K. Sen[a], David A. Mahns[a], Jens R. Coorssen[b,**], Peter J. Shortland[c,*]

[a] School of Medicine, Western Sydney University, New South Wales, Australia
[b] Departments of Health Sciences and Biological Sciences, Faculties of Applied Health Sciences and Mathematics & Science, Brock University, Ontario, Canada
[c] Science and Health, Western Sydney University, New South Wales, Australia

ARTICLE INFO

Keywords:
Behavioural assays
Cuprizone
Oligodendrocytosis
Multiple sclerosis
Clinical symptoms
Animal models

ABSTRACT

The feeding of cuprizone (CPZ) to animals has been extensively used to model the processes of demyelination and remyelination, with many papers adopting a narrative linked to demyelinating conditions like multiple sclerosis (MS), the aetiology of which is unknown. However, no current animal model faithfully replicates the myriad of symptoms seen in the clinical condition of MS. CPZ ingestion causes mitochondrial and endoplasmic reticulum stress and subsequent apoptosis of oligodendrocytes leads to central nervous system demyelination and glial cell activation. Although there are a wide variety of behavioural tests available for characterizing the functional deficits in animal models of disease, including that of CPZ-induced deficits, they have focused on a narrow subset of outcomes such as motor performance, cognition, and anxiety. The literature has not been systematically reviewed in relation to these or other symptoms associated with clinical MS. This paper reviews these tests and makes recommendations as to which are the most important in order to better understand the role of this model in examining aspects of demyelinating diseases like MS.

1. Introduction

Demyelination in the human central nervous system (CNS) and the resulting inflammatory responses are hallmarks of multiple sclerosis (MS; Barnett and Prineas, 2004; Frischer et al., 2009; Stys et al., 2012). MS is an incurable and chronic disease, often initiating in young adults (Abe et al., 2000; Sivaraman and Moodley, 2016), that results in life-long health, psychological, economic as well as social and healthcare burdens (Compston and Coles, 2008; Constantinescu et al., 2011; Hemmer et al., 2015). It affects approximately 2–3 million people worldwide and is 2–3 times more prevalent in women than men (Compston and Coles, 2008; Filippi et al., 2018). Patients with MS suffer from a wide range of clinical symptoms which include motor dysfunctions, pain, cognitive complications, depression, visual disturbances, fatigue, sleep disorders and anxiety, all of which have a detrimental effect on quality of life (Braley and Chervin, 2010; Cattaneo et al., 2002; Goldenberg, 2012; Haussleiter et al., 2009; Jongen et al., 2012; Kister et al., 2013; Larocca, 2011; O'Connor et al., 2008; Rahn et al., 2012). Despite extensive research on MS since its first description by the French neurologist Jean-Martin Charcot in 1868, the underlying aetiology remains enigmatic (Clanet, 2008). The sheer number of research publications on MS patients and animal models highlights the significant effort invested to understand the disease process and develop new medications. As of July 2018 there were over 79,584 published articles on MS, with 12,629 on experimental autoimmune encephalomyelitis (EAE) and 694 on cuprizone (CPZ) intoxication, the two most widely used 'animal models of MS', listed in PubMed (https://www.ncbi.nlm.nih.gov/pubmed/).

Approximately 85% of newly diagnosed patients, three-quarters of whom are young women, have the relapsing remitting (RRMS) form of

Abbreviations: B6, C57Bl/6 mouse strain; MS, Multiple sclerosis; BBB, Blood brain barrier; OLG, Oligodendrocytes; CFA, Complete Freund's adjuvant; OPC, Oligodendrocyte progenitor cells; CNS, Central nervous system; PLP, Proteolipid protein; CPZ, Cuprizone; PT, Pertussis toxin; EAE, Experimental autoimmune encephalomyelitis; PPMS, Primary progressive MS; ER, Endoplasmic reticulum; PRMS, Progressive relapsing MS; MAG, Myelin associated glycoprotein; RRMS, Relapsing remitting MS; MBP, Myelin basic protein; SPMS, Secondary progressive MS; MOG, Myelin oligodendrocyte glycoprotein

* Corresponding author at: Department of Medical Sciences, School of Science & Health, Western Sydney University, Locked Bag 1797, Penrith NSW 2751, Australia.

** Corresponding author at: Department of Health Sciences, Faculty of Applied Health Sciences and Department of Biological Sciences, Faculty of Mathematics & Science, Brock University, St. Catharines, ON L2S 3A1, Canada.

E-mail addresses: jcoorssen@brocku.ca (J.R. Coorssen), p.shortland@westernsydney.edu.au (P.J. Shortland).

https://doi.org/10.1016/j.neubiorev.2019.08.008
Received 2 May 2019; Received in revised form 1 August 2019; Accepted 12 August 2019
Available online 21 August 2019

MS, characterized by the disruption of the blood brain barrier (BBB) and recurring episodes of focal demyelination in the brain, spinal cord and/or optic nerve that result in neurological dysfunction followed by spontaneous partial or complete remission (Compston and Coles, 2008; Harbo et al., 2013; Partridge et al., 2015; Stys et al., 2012). After 8–20 years, the majority of RRMS patients (65–75%) transition to a secondary slow progressive form of MS (SPMS, non-relapsing) with less inflammation but continuous neurological decline and atrophy in the CNS (Compston and Coles, 2008; Kamm et al., 2014; Rovaris et al., 2006; Stys et al., 2012; Trapp and Nave, 2008). A further 10% of patients suffer primary progressive MS (PPMS) that presents as a gradual increase in neurological disability over time (Abdelhak et al., 2017; Goldenberg, 2012). Compared with RRMS, PPMS onset appears later in life and is more prevalent (~70%) in men (Miller and Leary, 2007; Nakahara et al., 2012). The fourth form is progressive relapsing MS (PRMS), a relatively rare variant that affects only a small percentage of MS patients (~5%). PRMS is characterized by early disease onset with an unpredictable combination of relapses and progression (Kremenchutzky et al., 1999; Rovaris et al., 2006; Tullman et al., 2004). Depending upon the severity of MS, it can also be divided into acute and/or chronic stages. When patients die within a few years (~1-2) of disease onset, this is termed acute (i.e. very aggressive, Marburg type), whereas long term ongoing disability is referred to as chronic (Lucchinetti et al., 2000; Stys et al., 2012; Tievsky et al., 1999; Wood et al., 1996).

Many studies have considered MS as an autoreactive, 'outside-in' peripheral immune cell (T and/or B-cells) mediated attack on the CNS components (e.g. myelin) that results in demyelination and an inflammatory response (Bernard and Kerlero de Rosbo, 1992; Compston and Coles, 2008; Constantinescu et al., 2011; McFarland and Martin, 2007). However, others have focused on whether the aetiology is an initial CNS oligodendrocytosis (i.e. degeneration and death of oligodendrocytes) that leads to subsequent activation (and invasion) of peripheral immune cells. Consequently, demyelination followed by an autoimmune response in the CNS has been termed the 'inside-out' hypothesis (Caprariello et al., 2018; Chaudhuri and Behan, 2004; Gulcher et al., 1994; Partridge et al., 2015; Stys, 2013; Stys et al., 2012; Traka et al., 2016; Trapp and Nave, 2008).

2. Multiple sclerosis (MS) patients and animal models

Detailed histological analyses of biopsy and autopsy samples from MS patients have revealed a heterogeneous pattern of demyelination and inflammation. Active lesions are categorized into four types (I-IV) that share common features such as a reduction in myelin basic protein (MBP), proteolipid protein (PLP), myelin oligodendrocyte glycoprotein (MOG), or myelin associated glycoprotein (MAG) and an infiltration of T-lymphocytes and macrophages. Type I and II lesions are defined by the involvement of immunoglobulin G/complement complexes, with limited oligodendrocyte (OLG) dystrophy, whereas type III and IV lesions are defined by marked apoptosis and depletion of mature OLG and an intact BBB (Lassmann et al., 2001; Lucchinetti et al., 2000, 1996; Popescu and Lucchinetti, 2012). The progression of pathological changes appears as hyper-intense focal demyelination which is diagnosed clinically using magnetic resonance imaging (Hemond and Bakshi, 2018).

In many fields of biomedical research animal models are used in an effort to better understand disease pathophysiology and thus facilitate biomarker identification and drug development (Perlman, 2016; Rosenthal and Brown, 2007; Rust, 1982). The original observation that repeated intramuscular injection of naïve rabbit brain extracts (derived using Locke's solution with alcohol or alcohol/ether) resulted in weakness, ataxia, weight loss in naïve monkeys and histological changes including gliosis and perivascular demyelination in the CNS demonstrated that demyelinating diseases can be modelled in animals (Rivers et al., 1933). Extending this approach, peripheral injections (e.g. peritoneal) of 'myelin antigens' into rodents has been widely used to induce a state of experimental autoimmune encephalomyelitis (EAE). In EAE, animals are injected with exogenous CNS antigens: either in MBP, MOG, PLP or MAG plus complete Freund's adjuvant (CFA) that activates and boosts peripheral immune cells (e.g. T and/or B-cells). Upon subsequent breach of the BBB using pertussis toxin (PT), peripheral autoreactive immune cells migrate into the CNS resulting in demyelination. Approximately 6–10 days post immunization animals begin to exhibit subtle motor deficits (e.g. a limp tail and hind limb weakness) termed 'early EAE' and after 15–20 days ('later EAE'), more advanced symptoms of motor deterioration (e.g. hind limb paralysis) are observed (Bjelobaba et al., 2018; Constantinescu et al., 2011; Croxford et al., 2011; Jorgensen et al., 2007; Procaccini et al., 2015; Terry et al., 2016). Although EAE is very heterogeneous in terms of the induction and clinical presentation (Constantinescu et al., 2011), it is the model of choice for immunologists as it is involving important cellular immune mechanisms such as regulation of autoimmunity (Krishnamoorthy and Wekerle, 2009). In contrast, in toxin-induced models, such as CPZ, primary progressive oligodendrocytosis leads to gliosis and demyelination in the apparent absence of autoimmunity and/or BBB disruption (Partridge et al., 2016, 2015; Praet et al., 2014; Skripuletz et al., 2011). Withdrawing CPZ results in the regeneration of mature OLG from proliferating oligodendrocyte progenitor cells (OPC) followed by remyelination (Bjelobaba et al., 2018; Kipp et al., 2009; Mason et al., 2000; Praet et al., 2014; Skripuletz et al., 2011; Vega-Riquer et al., 2017).

The extent to which behavioural and histological features of experimental models mimic the clinical features of human MS varies according to the animal model used. In EAE, key features such as T-cell invasion of the CNS, emergence of type I and II lesions (most notably in the spinal cord), and the decline of motor functions, mimic those observed in MS (Bjelobaba et al., 2018; Constantinescu et al., 2011) whereas other clinical features such as oligodendrocytosis, demyelination, microglia/ macrophage activation and the emergence of type III and IV lesions are observed in the CPZ model (Acs and Komoly, 2012; Kipp et al., 2009; Torkildsen et al., 2008). The concordance and discordance (highlighted in bold black and bold grey, respectively, in Table 1) in the pathological and functional features of MS with those observed in EAE and CPZ animal models are summarised in Table 1.

The EAE animal model has proven useful to investigate autoimmune mechanisms potentially involved in MS and the C57Bl/6 (B6) mouse EAE model is the favoured paradigm to examine gene effects on autoimmunity and T-cell responsiveness in transgenic/knockout mice (Krishnamoorthy and Wekerle, 2009). This model has provided a platform for preclinical assessment of therapeutics (e.g. Mitoxantrone, Interferon-β and Fingolimod) which are now used as disease modifying agents for MS patients (Constantinescu et al., 2011; Farooqi et al., 2010; Vargas and Tyor, 2017). However, as EAE only and perhaps indirectly mimics some aspects of the human disease, there is a need for alternate animal models to better understand disease aetiology and develop more broadly effective therapeutics (Table 1). The best alternative animal model is CPZ due to its capacity to model demyelination and remyelination in the absence of a peripheral immune response. CPZ may therefore be more useful to study the early, initiating events associated with demyelinating diseases.

Feeding CPZ to rodents has been used extensively since the 1960s to model and understand the processes underlying CNS oligodendrocytosis, demyelination, remyelination and glial cell activation; however, very little is known regarding the resulting behavioural deficits. Behavioural assessments using animal models are particularly important to understanding the pathophysiology of a disease and identifying potential therapeutics (Sukoff Rizzo and Crawley, 2017). There are more than 100 behavioural assays, including for motor function, pain, anxiety, cognition, fatigue and depression-like phenotypes that have been developed for assessing animal models of disease (Crawley, 2008; Crawley and Paylor, 1997; Hanell and Marklund, 2014; Karl et al., 2003; Puzzo et al., 2014; Taylor et al., 2010; Van Meer

Table 1
Pathological and functional features of two commonly used animal models of MS.

Deficits	Features	MS	EAE	CPZ
Pathological	Proposed hypothesis	Unknown (Stys et al., 2012)	Outside-in? (Peterson and Fujinami, 2007; Stys et al., 2012)	Inside-out? (Caprariello et al., 2018; Stys et al., 2012)
	Lesion subtypes	I-IV (Lucchinetti et al., 2000; Popescu et al., 2013)	**I** and **II**? (Constantinescu et al., 2011)	**III** and **IV**? (Acs and Komoly, 2012; Kipp et al., 2009; Torkildsen et al., 2008)
	Presentation	PPMS, SPMS, RRMS, PRMS, acute and chronic (Compston and Coles, 2008; Stys et al., 2012)	**RRMS**, **acute** and **chronic**? (t Hart et al., 2011)	**PPMS** and **SPMS**? (Caprariello et al., 2018; Stys et al., 2012)
	Mode of initiation	Unknown (Compston and Coles, 2008; Stys et al., 2012)	T-cell mediated autoimmune attack (Constantinescu et al., 2011; Gold et al., 2006)	Metabolic disturbance causes preferential OLG apoptosis? (Gudi et al., 2014; Praet et al., 2014)
	Mode of induction	Unknown (Compston and Coles, 2008; Stys et al., 2012)	Peripheral Injections of myelin antigens, CFA and PT (Constantinescu et al., 2011; Gold et al., 2006)	Oral feeding of CPZ (Gudi et al., 2014; Vega-Riquer et al., 2017)
	Myelin protein suppression	Brain > spinal cord (Gilmore et al., 2009; Lassmann and Bradl, 2017; Sriram and Steiner, 2005)	**Spinal cord** > **brain** (Constantinescu et al., 2011; Gold et al., 2006)	**Brain** > **spinal cord** (Acs et al., 2013; Herder et al., 2011; Vega-Riquer et al., 2017)
	Remyelination	Continuous but depending on factors such as MS subtype and patient age (Franklin, 2002; Lucchinetti et al., 2000)	**Discontinuous**, cannot be well studied due to progressive loss of myelin (Lassmann and Bradl, 2017; Ransohoff, 2012)	Cessation of CPZ feeding results in remyelination and easy to study (Gudi et al., 2014; Lassmann and Bradl, 2017)
	CD4/8 infiltration	CD8 > CD4 (Hauser et al., 1986; Sriram and Steiner, 2005)	**CD4** > **CD8** (Lassmann and van Horssen, 2011)	**Undetectable** (Remington et al., 2007; Tejedor et al., 2017)
	B-cell involvement	Detectable (Disanto et al., 2012)	**Detectable** (Pierson et al., 2014)	**Undetectable** (Tejedor et al., 2017)
	Glial activation	Brain > spinal cord (Chu et al., 2018; Ponath et al., 2018)	Spinal cord > brain (Brambilla et al., 2014; Luo et al., 2017)	**Brain** > **spinal cord** (Gudi et al., 2014; Herder et al., 2011)
Functional	Motor function	↓ (Comber et al., 2017)	↓ (Heckman et al., 2013)	↓ (Hibbits et al., 2009; Ray et al., 2017)
	Pain	↑ (Khan et al., 2018)	↑ (Lu et al., 2012)	↑ (Tsukahara et al., 2018)
	Fatigue	↑ (Mills and Young, 2011)	↑ (Grace et al., 2017)	**X** (Bolcskei et al., 2018)
	Cognition	↓ (Jongen et al., 2012)	↓ (Acharjee et al., 2013)	↓ (Li et al., 2015; Tezuka et al., 2013)
	Vision	↓ (Sanchez-Dalmau et al., 2018)	↓ (Guo et al., 2009)	↓ (Namekata et al., 2014)
	Depression	↑ (Sukoff Rizzo and Crawley, 2017)	↑ (Ayatollahi et al., 2017)	**X** (Kondo et al., 2016)
	Sleep	↓ (Fleming and Pollak, 2005)	↓ (He et al., 2014a)	–
	Anxiety	↑ (Zorzon et al., 2001)	↑ (Piras et al., 2013)	↑ (Serra-de-Oliveira et al., 2015; Xu et al., 2009)
	Epileptic seizure	↑ (Allen et al., 2013)	–	↑ (Hoffmann et al., 2008)

Key: Increase: ↑, Decrease: ↓, No change: ×, Not applicable/reported/performed: -.

Table 2
Comparison of clinical symptoms of MS vs. behavioural assessment used in CPZ studies. The frequency of MS was measured from clinical prevalence whereas CPZ was measured by the number of publications.

Clinical symptoms	MS frequency (%)	CPZ papers (%)
Motor	80	32
Pain	29-86	4
Fatigue	75	1
Cognition	40-65	29
Optic neuritis	50	1
Depression	50	1
Sleep	50	0
Anxiety	35	30
Epileptic seizure	2-3	2

and Raber, 2005). These are used as surrogate indicators of disease states. Surprisingly, behavioural studies in the CPZ model are quite limited and only concentrate on a small subset of outcomes such as anxiety, motor functions and cognition (summarised in Table 2). Although clinical MS includes a wide range of other symptoms such as pain, depression, fatigue, visual and sleeping disturbances, these have not been well characterized or reviewed systematically in the CPZ model. Here, we critically review the CPZ behavioural literature appearing in PubMed from 1960 to 2018, and recommend better strategies to improve understanding of the behavioural consequences of CPZ-feeding in terms of clinical MS.

3. Search strategy and selection criteria

A PubMed literature search was carried out for papers published in the English language between 1960 and July 2018 with the main focus on studies published in the last 10 years due to the increasing number of publications reporting behavioural testing in the CPZ model (Fig. 1).

3.1. Inclusion criteria

The search was carried out by combining the terms 'MS and clinical symptoms (motor, pain, fatigue, cognition, vision, depression, sleep, anxiety and epileptic seizure), animal model of MS, CPZ animal model, EAE animal model, behaviour and CPZ, behaviour and EAE'. The reference lists associated with the identified publications were also assessed and considered in preparing this review. In total, the present literature search identified in total 694 publications listed from 1966 to July 2018, of which 60 were behavioural studies and 24 were reviews (Fig. 1).

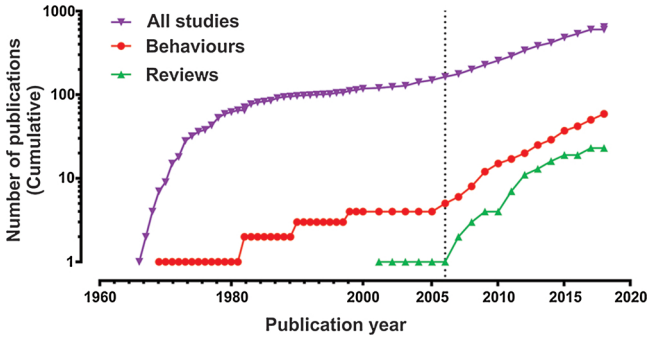

Fig. 1. Timeline of publications using the CPZ model.
Studies after 2000 are plotted on an expanded time scale. The vertical dashed line denotes the start of publications reporting quantitative behavioural testing in CPZ.

3.2. Exclusion criteria

CPZ is also used to model Schizophrenia due to some similarities in the changes of brain pathology and cognitive function (Praet et al., 2014). In the assessment of the literature the analysis of 'Schizophrenia-like behaviour and therapeutics' was limited by the small number of relevant papers (Herring and Konradi, 2011; Sun et al., 2017; Wang et al., 2013, 2015; Xiao et al., 2008; Xu et al., 2010, 2009). These were considered to the extent that they examined the link between demyelination behaviour.

4. Cuprizone (CPZ) model

4.1. A brief history of the CPZ animal model

CPZ is an organic compound synthesized by reacting cyclohexanone with oxaldyhydrazone (Carlton, 1967; Messori et al., 2007). It is commonly used to investigate the mechanisms of demyelination and remyelination in an effort to model human diseases such as MS (Kipp et al., 2009; Matsushima and Morell, 2001; Praet et al., 2014; Skripuletz et al., 2011; Vega-Riquer et al., 2017). The first observations of the demyelinating properties of CPZ was reported in the mid-1960s (Carlton, 1966, 1967; Carlton, 1969). From 1960–2000, papers largely described the formation of mega-mitochondria in liver and CNS, oligodendrocytosis, inflammatory (especially innate immunity) responses, demyelination and remyelination (Blakemore, 1972, 1973; Blakemore, 1974; Blakemore and Irvine, 2008; Hiremath et al., 1998; Hoppel and Tandler, 1973; Mason et al., 2000; Morell et al., 1998; Petronilli and Zoratti, 1990; Suzuki, 1969). A key study by Hiremath et al. (Hiremath et al., 1998) characterized the optimal CPZ dose in B6 mice (the most frequently used strain) to study de- and remyelination. From 2001 onwards, a substantial increase in the number of papers appearing in PubMed (Fig. 1) reflected the increasing importance of CPZ in MS research as this model was used to study the dynamics of oligodendrocytosis, demyelination and remyelination (Caprariello et al., 2018; Gudi et al., 2014; Kipp et al., 2009; Tejedor et al., 2017; Traka et al., 2016). Initially, changes in animal wellbeing, including weakness, weight loss and lethargy, were assessed qualitatively using only unsubstantiated visual observations (De and Subramanian, 1982; Petronilli and Zoratti, 1990; Suzuki and Kikkawa, 1969). However, the first quantitative behavioural assessment was reported in 2006 (Liebetanz and Merkler, 2006) and coincided with the onset of a second wave of publications (Fig. 1) examining CPZ-induced changes in behaviour (Franco-Pons et al., 2007). By comparing the histopathology and apparent behavioural changes induced by CPZ, the first therapeutic intervention trial, using a 'Salmon diet', showed decreased demyelination coupled with reduction of anxiety-like behavioural deficits (Torkildsen et al., 2009).

4.2. Mode of induction and mechanism(s) of action of CPZ

To study behavioural deficits thought to model the different phases of human MS, 0.2% (w/w) CPZ is fed to mice for 5–6 weeks resulting in progressive, dose-dependent and highly reproducible demyelination in CNS structures such as the corpus callosum, hippocampus, thalamus and cerebellum (Goldberg et al., 2015; Hibbits et al., 2009; Kipp et al., 2009; Praet et al., 2014; Skripuletz et al., 2010a; Vega-Riquer et al., 2017; Yang et al., 2009). Within the first 1–3 weeks of CPZ-feeding oligodendrocytosis is initiated and robust demyelination occurs by 4–5 weeks with the appearance of a glial (e.g. microglia and astrocytes) response (summarized in Fig. 2; Gudi et al., 2014; Hiremath et al., 1998) and this is termed the 'acute phase'. Resolution of gliosis and remyelination occurs when new mature OLG regenerate from OPC following cessation of CPZ-feeding at this early time point (Gudi et al., 2014, 2009; Hiremath et al., 1998; Mason et al., 2000). Prolonged feeding of CPZ for 12–14 weeks produces a 'chronic response' thought

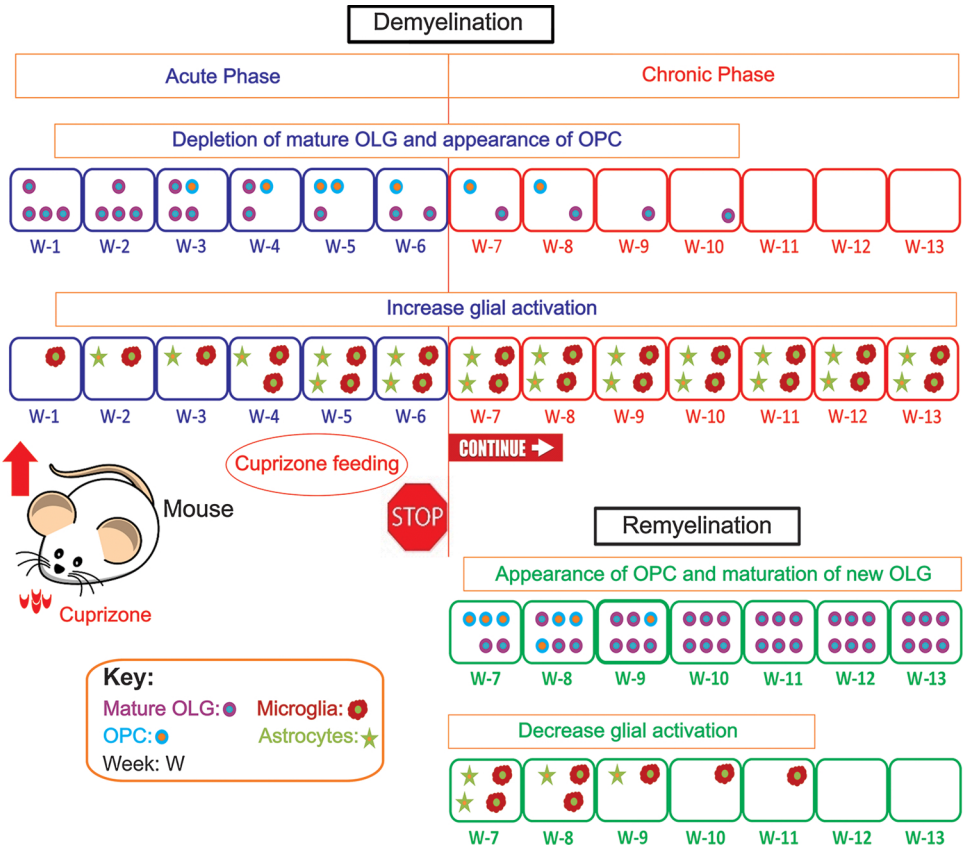

Fig. 2. Schematic representation of CPZ-induced demyelination and remyelination in the corpus callosum.
CPZ-feeding causes depletion of mature OLG that starts within 1 week and results in continuous demyelination until the cessation of CPZ-feeding or death. The appearance of OPC occurs simultaneously with the degeneration of mature OLG leading to remyelination. Glial (microglia and astrocytes) activation is *inversely proportional* to mature OLG damage; increasing degeneration of mature OLG accelerates the activation of glial reactivity. Commonly, 7–8 week old B6 mice are fed 0.2% CPZ for 5–6 weeks in order to develop 'acute' demyelination. Feeding for 10–15 weeks causes 'chronic' demyelination. Greater than 0.2% CPZ or prolonged feeding induces 'severe' demyelination and increases mortality rates.

to model the later stages of MS. This prolonged feeding results in long-term demyelination, extensive gliosis, a marked decrease of the normal age related weight gain and increased mortality (Hibbits et al., 2009, 2012; Kipp et al., 2009; Lindner et al., 2009; Skripuletz et al., 2011).

The aetiology of CPZ-induced demyelination is incompletely understood. Studies have defined CPZ as an 'oligotoxic' compound, somewhat selectively affecting mature OLG, both in vitro and in vivo, leading to demyelination (Benardais et al., 2013; Cammer, 1999; Gudi et al., 2014; Mason et al., 2000; Matsushima and Morell, 2001). CPZ causes copper chelation (Matsushima and Morell, 2001) that may subsequently lead to other metal ion imbalances (e.g. iron, zinc, sodium and manganese) in different parts of the body such as the brain and liver (Moldovan et al., 2015; Varga et al., 2018; Venturini, 1973; Zatta et al., 2005). Consequently, mitochondrial (Acs et al., 2013; Benardais et al., 2013; Hoppel and Tandler, 1973; Partridge et al., 2016; Pasquini et al., 2007; Solti et al., 2015; Werner et al., 2010) and endoplasmic reticulum (ER; Abe et al., 2015; Hemm et al., 1971; Lin et al., 2006; Love, 1988; Partridge et al., 2016; Praet et al., 2014; Stone and Lin, 2015; Suzuki and Kikkawa, 1969) stress occur. This then results in reduced adenosine triphosphate production, the unfolded protein response and increased production of reactive oxygen and nitrogen species (Faizi et al., 2016; Praet et al., 2014; Wagner and Rafael, 1977). OLG stress results due to the reduced energy supply from mitochondria and reduced levels of detoxifying enzymes such as manganese superoxide dismutase and glutathione peroxidase (Liblau et al., 2001; McLaurin and Yong, 1995; McTigue and Tripathi, 2008; Omotoso et al., 2018). The cumulative result is oligodendrocytosis resulting in the loss of myelin from axons (Gudi et al., 2014; Kipp et al., 2009; Matsushima and Morell, 2001; Praet et al., 2014). Microglia and astrocytes are activated to facilitate clearance of myelin debris. Inadequate clearance of myelin debris and extensive gliosis are associated with the secretion of toxic substances such as nitric oxide that exacerbate oligodendrocytosis and demyelination (summarized in Fig. 3; Gudi et al., 2014; Lampron et al., 2015; Linares et al., 2006; Skripuletz et al., 2013). All of these processes can contribute to axonal damage (see below).

As well as causing white matter axonal damage (Clarner et al., 2015; Hoflich et al., 2016; Schultz et al., 2017; Slowik et al., 2015), CPZ can also induce axonal damage identified by the histological accumulation of amyloid precursor protein along axons in grey matter regions such as the thalamus (Wagenknecht et al., 2016). This persists even after remyelination occurs (Lindner et al., 2009; Manrique-Hoyos et al., 2012). Axonal damage can evoke Wallerian degeneration of the distal axon and loss of synaptic contacts, and so can contribute to the prolonged disability and functional deficits (reviewed by Nyamoya et al., 2017). Although both in vitro and in vivo studies have argued that CNS neurons are resistant to CPZ-induced injury (Acs and Komoly, 2012; Benardais et al., 2013; Benetti et al., 2010; Namekata et al., 2014; Sun et al., 2016). CPZ has been reported to induce glutamate excitotoxicity / synaptotoxicity (Azami Tameh et al., 2013; Dutta et al., 2013) via differential effects on the expression of glutamate receptor subunits. For example, CPZ-feeding produced upregulation of the NR2A subunit of the N-methyl-D-aspartate receptor in the corpus callosum and down regulation of the metabotropic glutamate receptor subunit mGluR2 in the cortex (Azami Tameh et al., 2013). Similarly, reduced expression of ionotropic amino-3-hydroxy-5-methyl-4-isoxazole propionic acid glutamate receptors was found in hippocampal neurons (Dutta et al., 2013). These events were associated with reduced spatial memory functions suggesting that synaptotoxicity, in addition to demyelination, contributes to altered behavioural outcomes (Dutta et al., 2013).

The BBB remains intact following CPZ-feeding restricts peripheral adaptive immune cell (i.e. T or B-cell) infiltration into the CNS (McMahon et al., 2002), whereas reactive adaptive immune cells predominate in human MS. Thus, the CPZ model may be useful to explore the underlying mechanisms involved in both the earliest as well as the later progressive stages of MS that are not dependent on the infiltration of adaptive immune cells into the CNS. However, T-cell infiltration into the CNS in the CPZ model has recently been reported when BBB disruption was combined with an 'immune booster' to investigate the

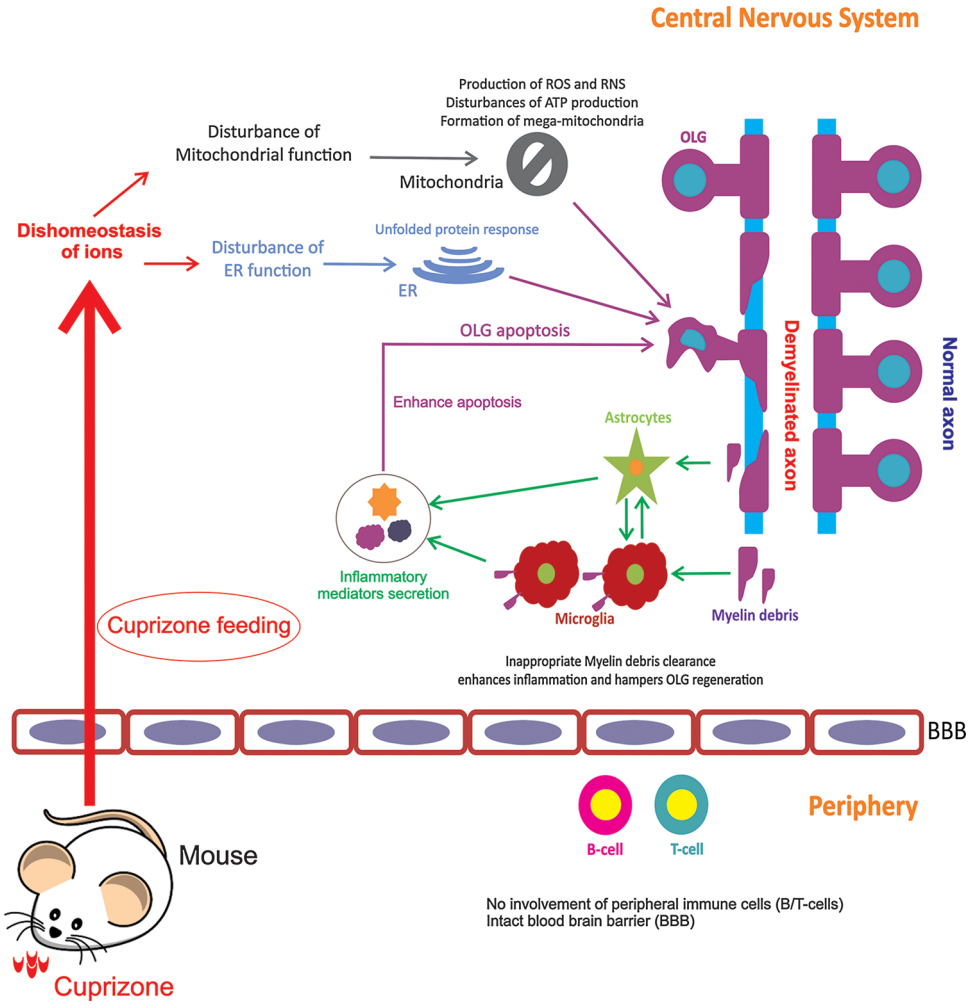

Fig. 3. Schematic representation of the proposed mechanism of action underlying CPZ-induced OLG stress and demyelination.
Oral ingestion of CPZ in rodents leads to a dysregulation of ER and mitochondrial functions resulting in apoptosis of OLG and subsequent formation of myelin debris that, in turn, activates glial cells such as microglia and astrocytes that produce inflammatory molecules, further exacerbating the OLG degeneration process. The intact BBB limits peripheral B or T-cell entry into the CNS.

'inside-out' hypothesis of MS (Caprariello et al., 2018), suggesting that human MS may well start via a CNS dysregulation that then leads to infiltration by peripheral cells.

5. Behaviour

5.1. Behavioural phenotypes

Although MS is considered a highly debilitating neurological disorder, there are many aspects of health that remain relatively normal despite the emergence of symptoms linked to different parts of the CNS (e.g. brain and spinal cord). For example, comparing the age and weight of MS patients with healthy matched controls, only small differences in total life span (Compston and Coles, 2008) and weight gain are observed (Markianos et al., 2013). However, EAE animals are lethargic and show weight loss, presumably as a consequence of motor paralysis restricting their ability to eat (Jorgensen et al., 2007; Xin et al., 2015). Qualitative observations between 1969–1990 suggested that CPZ ingestion produced 'sickness-like behaviour,' and increased mental weakness in juvenile mice (De and Subramanian, 1982; Morell et al., 1998; Petronilli and Zoratti, 1990; Suzuki and Kikkawa, 1969). In contrast, since 1998, young (7–8 weeks old) B6 mice are widely used, and quantitative assessment documented reduced weight gain and increased activities such as locomotion, climbing and rearing but without muscle paralysis (Chang et al., 2017; Franco-Pons et al., 2007; Morell et al., 1998; Stidworthy et al., 2003; Yang et al., 2009).

Quantitative measurements of aspects of CPZ-induced behavioural deficits have been investigated with a preferential focus on motor, anxiety and cognitive behaviours. However, there is a clear mismatch between the prevalence of clinical symptoms observed in human MS and the application of relevant behavioural assessments in CPZ-fed animals (see Table 2). This was most notable for the more prevalent symptoms of pain and visual disturbances, for which there are well validated animal behavioural tests (Deuis et al., 2017; Karl et al., 2003; Namekata et al., 2014). A limited number of recent CPZ studies have also assessed animals for depression and epileptic seizures (Hoffmann et al., 2008; Kondo et al., 2016; Lapato et al., 2017). The general parameters for the various quantitative behavioural tests assessing changes in motor function, pain, fatigue, cognition, vision, depression, sleep, seizure and anxiety in animal models are documented in Table 3.

5.2. Motor phenotypes in CPZ studies

Around 80% of MS patients have disturbances in motor functions including difficulties in maintaining balance, reduced walking speed and impaired dexterity of the hands and feet (Benedict et al., 2011; Cattaneo et al., 2002; Larocca, 2011; Pellegrino et al., 2018). Human studies show demyelination in different CNS structures including the

Table 3
Summary of general parameters for different behavioural tests in animal models.

Behavioural phenotypes	Behavioural tests in rodents	Basic principles	Parameters	Examples of tested strain (mice) '*' CPZ study	Examples of tested strain (rat) '*' CPZ study
General activity	Body weight	Ability to restrict weight loss	Measurement	*B6 (Franco-Pons et al., 2007)	*Wistar (Oakden et al., 2017)
	Physical examination	Natural appearance	Tremor, abnormal walking and abnormal posture	*B6 (Nunes et al., 2012)	SCA17 (Kelp et al., 2013)
	Functional observation battery	Natural appearance	Mobility, gait and touch	*B6 (Franco-Pons et al., 2007)	*Lewis (Serra-de-Oliveira et al., 2015)
Motor	Rotarod	Ability to hold	Latency to fall and number of flip/fall	*B6 (Yamamoto et al., 2014)	Wistar (Haddadi et al., 2014)
	Walking beam	Ability to maintain balance and walk	Time to cross and foot slip	*B6 (Hagemeyer et al., 2012)	Lewis (Merkler et al., 2001)
	Complex wheel	Ability to walk	Maximum velocity among daily run, maximum run interval, time to cross and foot slip	*B6 (Hibbits et al., 2009)	Sprague-Dawley (Chomiak et al., 2016)
	Walking ladder	Ability to maintain balance and walk	Time to cross and foot slips	B6 (Pollak et al., 2012)	Sprague-Dawley (Kim et al., 2013)
	Pole	Ability to hold	Time to T-turn, time to reach bottom and time to fall/slip	*B6 (Zheng et al., 2017)	Wistar (Mattiasson et al., 2000)
	Negative geotaxis	Ability to maintain balance and walk	Time to reorientate and incline	* Gas6-/- Axl-/- DKO (Ray et al., 2017)	Sprague-Dawley (Unger et al., 2007)
	Hanging steel wire	Ability to hold	Latency to fall	*B6 (Elbaz et al., 2018)	–
	Forelimb reaching	Ability to hold	Success rate and time to reach	B6 (Whishaw et al., 2017)	Long-Evans (Gharbawie et al., 2005)
Pain	Electronic von Frey	Response to stimulus	Latency to withdraw paw	*TRPA1-KO (Bolcskei et al., 2018)	Long-Evans (Samour et al., 2017)
	Manual von Frey filament	Response to stimulus	Latency to withdraw paw	*TRPA1-KO (Bolcskei et al., 2018)	Sprague-Dawley (Su et al., 2015)
	Tail flick	Response to stimulus	Latency to withdraw tail	*B6 (Vakilzadeh et al., 2016)	Sprague-Dawley (Zhou et al., 2014)
	Cold plate	Response to stimulus	Latency to withdraw paw	B6 (Draxler et al., 2014)	Sprague-Dawley (Yalcin et al., 2009)
	Hargraves	Response to stimulus	Latency to withdraw paw	Hph-1 (Nasser et al., 2013)	Long-Evans (Samour et al., 2017)
	Air puff	Response to stimulus	Latency to dead withdraw and forepaw swipe	B6 (Thorburn et al., 2016)	Sprague-Dawley (Ahn et al., 2004)
	Grimace scale	Spontaneous pain	Altered facial expression	B6 (Duffy et al., 2016)	Wistar (Sotocinal et al., 2011)
Fatigue	Voluntary wheel running	Ability to walk	Time spend in voluntary movement	B6 (Hicks et al., 2016)	Agouti (Grace et al., 2017)
	Upside down grid	Ability to hold and hang	Latency to fall	*TRPA1-KO (Bolcskei et al., 2018)	Wistar (Golli et al., 2016)
Cognition	Y-maze	Exploring and recognizing environment	Exploration of new or old environments	*B6 (Makinodan et al., 2009)	Sprague-Dawley (Wang et al., 2017b)
	Social interaction	Exploring environment and interact with peers	Interaction time and distance	*B6 (Hibbits et al., 2009)	Wistar (Nam et al., 2014)
	Novel objective recognition	Exploring and recognizing object	Time to explore objects and ratio of exploring new/old objects	*B6 (Makinodan et al., 2009)	*Lewis (Serra-de-Oliveira et al., 2015)
	Morris water maze	Ability to navigate and recognize location	Latency to escape, duration in goal quadrant	*B6 (Aryanpour et al., 2017)	Sprague-Dawley (Mu et al., 2014)
	Fear conditioning	Learning the neutral conditional stimulus	Freezing, reflex expression and internal change	*B6 (Kondo et al., 2016)	Sprague-Dawley (Joels and Lamprecht, 2014)
Vision	Multifocal electroretinogram	Electrical activity	Visual response amplitude	*B6 (Namekata et al., 2014)	Albino (Ball and Petry, 2000)
	Running wheel	Ability to visualize	Decrease vision	B6 (Thompson et al., 2008)	–
	Modified Y-maze	Ability to recognize colour	Decrease vision	S334terline-3 (Thomas et al., 2007)	–
Depression	Forced swim	Ability to swim	Time spend in swimming and immobility	*B6 (Kondo et al., 2016)	Wistar (Serra-de-Oliveira et al., 2015) –
	Tail suspension	Ability to move	Latency to escape	*B6 (Kondo et al., 2016)	Wistar (Castagne et al., 2011)
	Sucrose preference	Ability to enjoy	Decrease sucrose uptake	SJL/J (Pollak et al., 2000)	Sprague-Dawley (Sobrian et al., 2003)
Sleep	Chamber	Pattern of sleeping	Abnormal patterns of posture, breathing and sleeping	β-hydroxylase (-/-) (Mitchell et al., 2008)	Sprague-Dawley (McKenna et al., 2008)
	Electromyography	Pattern of electrical amplitude	Electric activity	B6 (Bastianini et al., 2017)	Sprague-Dawley (Pagliardini et al., 2012)

(*continued on next page*)

Table 3 (*continued*)

Behavioural phenotypes	Behavioural tests in rodents	Basic principles	Parameters	Examples of tested strain (mice) '*' CPZ study	Examples of tested strain (rat) '*' CPZ study
Anxiety	Open field	Spontaneous activity	Total running time, running frequency in perimeter, running frequency in centre, rearing and grooming	*B6 (Franco-Pons et al., 2007)	*Lewis (Serra-de-Oliveira et al., 2015)
	Elevated plus maze	Spontaneous activity	Running frequency open arms, running frequency closed in arms, rearing and grooming	*B6 (Zimmermann et al., 2018)	*Lewis (Serra-de-Oliveira et al., 2015)
	Hole board	Spontaneous activity	Distance travel, hole-poking, rearing and grooming	*B6 (Skripuletz et al., 2010b)	Sprague-Dawley (Wernecke and Fendt, 2015)
	Light dark	Spontaneous activity	Latency to enter dark, time spend in each chamber, number of rearing and head dipping	*B6 (Kondo et al., 2016)	Sprague-Dawley (Arrant et al., 2013)
Epileptic seizure	Electroencephalography	Pattern of electrical amplitude	Electric activity	*B6 (Hoffmann et al., 2008)	Sprague-Dawley (Bergstrom et al., 2013)

Key: C57Bl/6: B6; not investigated/found: -.

cerebellum and spinal cord (Cameron et al., 2008; Gilmore et al., 2006) which have been associated with these motor deficits (D'Ambrosio et al., 2017; Parmar et al., 2018; Wilkins, 2017). In animal models, deficits in motor function can be investigated using a wide range of behavioural tools including rotarod, complex wheel, walking beam, walking ladder, pole, negative geotaxis, hanging steel wire and forelimb reaching tests (Elbaz et al., 2018; Hibbits et al., 2009; Karl et al., 2003; Klein and Dunnett, 2012; Ray et al., 2017; Schaar et al., 2010; Soblosky et al., 2001).

The rotarod apparatus is one of the most widely used tools to measure motor phenotypes in CPZ-fed mice (Abakumova et al., 2015; Bolcskei et al., 2018; Chang et al., 2017; Elbaz et al., 2018; Faizi et al., 2016; Franco-Pons et al., 2007; Hagemeyer et al., 2012; Hashimoto et al., 2017; Iwasa et al., 2014; Kondo et al., 2016; Kumar et al., 2018; Sanadgol et al., 2018; Wang et al., 2016; Yamamoto et al., 2014, 2017; Ye et al., 2013; Yoshikawa et al., 2011; Zhang et al., 2016). In this test, rodents are placed on a rotating drum that progressively increases its speed (from 4 to 40 rpm) over the course of the testing period (˜300 s). Animals with motor and/or coordination impairment show a decreased capacity to remain on the rod (latency to fall), decreased time to first rolling and increased number of rotations/flips (i.e. the animal rotates freely with the rod, but does not fall off; Bolcskei et al., 2018; Chang et al., 2017; Franco-Pons et al., 2007; Hagemeyer et al., 2012; Kondo et al., 2016). For example, in the EAE model, the latency to fall from the rod correlated with the severity of the clinical motor score (Miller and Karpus, 2007; van den Berg et al., 2016). In CPZ studies, while some groups reported decreased latency to fall (Abakumova et al., 2015; Elbaz et al., 2018; Faizi et al., 2016; Franco-Pons et al., 2007; Hashimoto et al., 2017; Iwasa et al., 2014; Kumar et al., 2018; Sanadgol et al., 2018; Wang et al., 2016; Yamamoto et al., 2017; Yoshikawa et al., 2011; Zhang et al., 2016) others reported no change in rotarod performance (Bolcskei et al., 2018; Chang et al., 2017; Hagemeyer et al., 2012; Kondo et al., 2016). Conflicting reports by different groups using the same instrument highlight the need for comprehensive reporting of all test parameters; for instance, when the latency to fall was reported with a duration of 300 s results were variable, whereas attention to other parameters, such as the number of flips (Yamamoto et al., 2014) or increasing the duration of the test to 600 s revealed changes in motor function (Iwasa et al., 2014). Alternatively, the demands of the test may be insufficient to detect subtle changes in coordination. Such arguments are supported by the capacity of the complex wheel (complex wheel; see below) apparatus to detect changes within 2 weeks of CPZ-feeding and consistent results in the walking beam test within 5 weeks of CPZ-feeding (see below). There have been attempts to account for this variability by relating changes in motor performance with the presence of demyelination within the corpus callosum (Franco-Pons et al., 2007; Hagemeyer et al., 2012; Liebetanz and Merkler, 2006; Manrique-Hoyos et al., 2012; Skripuletz et al., 2015, 2010b; Yoshikawa et al., 2011); however, these analyses did not include an animal-by-animal correlation between motor performance and the extent of demyelination.

Four studies used the complex wheel to test for changes in motor performance and deficits were found within 2–3 weeks of CPZ-feeding (Hibbits et al., 2009; Liebetanz and Merkler, 2006; Manrique-Hoyos et al., 2012; Mierzwa et al., 2013). In this test, animals are familiarized and trained on a freely accessible, automated running wheel (˜38 regularly spaced rungs) in their home cage. During the testing session the wheel is made complex by randomly removing rungs (˜10 rungs) thus creating variable step intervals. Changes in the total distance run, maximum velocity during daily runs, number of runs and maximum run interval are used to quantify motor performance (Hibbits et al., 2009; Liebetanz and Merkler, 2006; Manrique-Hoyos et al., 2012; Mierzwa et al., 2013). The presence of a comprehensive suite of variables (Table 3) such as running speed, distance run in a day and the ability to assess foot placement precision (motor coordination) suggest that this test is superior to the rotarod in assessing the impact of CPZ-induced demyelination on motor function.

If, as indicated above, subtle motor changes can be detected with increasing task complexity, it is equally plausible that a more detailed assessment of normal locomotor function can provide increased sensitivity and thus detect earlier changes in motor behaviour. For example, when the capacity of animals to cross an elevated (˜40-50 cm) horizontal walking beam that becomes progressively narrower at one end (e.g. decreasing from 10 to 11 mm to 7–8 mm over a length of 70–80 cm - the walking beam test) was quantified, CPZ-fed animals took longer to cross the beam and showed more foot slips (mainly hind limbs) than controls (Hagemeyer et al., 2012; Ray et al., 2017; Skripuletz et al., 2015, 2010b; Zheng et al., 2017). However, even using this test, inconsistent and/or unclear observations were found. For example, in some cases, only the time to cross the narrowing beam was measured, without assessing foot slips (Skripuletz et al., 2015, 2010b; Zheng et al., 2017) or which limbs slipped (Ray et al., 2017). Moreover, the studies were conducted only once or twice during the 5–6 weeks of CPZ-feeding, and thus did not describe the progression of motor decline during CPZ-feeding (Ray et al., 2017; Skripuletz et al., 2015, 2010b; Zheng et al., 2017), nor did they provide behavioural baseline data prior to CPZ-feeding (i.e. animals were learning the test during the experimental period). It is recommended that all parameters (e.g. crossing time, number of fore- and hind foot slips) be assessed in order to detect any possible motor deficits in the CPZ model.

Another complex locomotor task is the walking ladder (or grid walk) test. This enables the measurement of fore- and hind-limb coordination and accuracy of paw placement on the rungs. The apparatus is constructed as an elevated (13–16 cm) horizontal walk-way 60–70 cm long, in which the width of the walkway approximates the girth of the test animal (e.g. ˜3–4 cm for mice and 8–10 cm for rats). A lamp is placed at the start to encourage the animal to cross the narrow and confined corridor with evenly spaced rungs along the base. The complexity of the task can be increased by withdrawing rungs from the base of the walkway. The time to cross the ladder and the number of foot slips are recorded (Table 3). Deficits in motor function correlate with increased foot slips and longer crossing times (Jacobi et al., 2015; Kim et al., 2013; Pollak et al., 2012; Schaar et al., 2010). The main advantage of the walking ladder over instruments such as the rotarod or walking beam is that the walking ladder apparatus can readily detect foot placement errors and that fore limb impairment is easier to measure. Therefore, it can be hypothesised that due to the complexity of the walking ladder the foot misplacement of CPZ-fed animals will increase, which remains to be tested.

In contrast to the walking beam and walking ladder tests, the pole test assesses the ability of an animal to descend a vertical pole. In this test, animals are placed head-up on the top of a vertical pole (generally 50–60 cm long, ˜1 cm^2 diameter) with the base typically located in their home cage. Again, the complexity of the test can be increased by placing regular (or irregular) windings around the circumference to vary the capacity of the animal to grip the pole during its descent. The time to turn head downward (T-turn) and total time to descend to the base are recorded. Animals with impaired coordination take more time to T-turn and to descend (Matsuura et al., 1997; Rommelfanger et al., 2007; Zieba et al., 2015). Only one publication has used this test, showing that CPZ-fed animals took longer to descend the pole, thus suggesting impaired motor function (Zheng et al., 2017).

In the negative geotaxis test, animals are placed head facing down on an inclined (30-45°) platform; the greater the time taken to reorientate the head to an upward direction and to reach the top of the inclined platform, the greater the presumed deficits in motor function (Heier and DiDonato, 2009; Thiessen and Lindzey, 1967). In a single study, CPZ-fed mice took more time to reach the top of the platform suggesting diminished motor function (Ray et al., 2017). Likewise, a single study used a hanging steel wire (2 mm in diameter and 35 cm long) to measure strength/motor function of CPZ-fed mice. When mice were allowed to hang using their forepaws, the duration time to release was reduced in CPZ-fed animals suggesting decreased muscle strength and/or motor functions (Elbaz et al., 2018).

The forelimb reaching is a sensitive test used to evaluate fine, voluntary motor function after stroke, spinal cord injury or unilateral brain damage (Klein and Dunnett, 2012; Schaar et al., 2010; Streijger et al., 2013). In this test, rodents are placed in a clear plexiglass box with a narrow slit through which to grab a food pellet placed outside. The animals are first trained in the task, followed by actual test sessions. To motivate pellet retrieval, animals can be deprived of food (e.g. overnight) prior to testing (Chen et al., 2014; Schaar et al., 2010). The frame-by-frame assessment of the actual grasping movement includes quantification of the time to reach the pellet, success rate, paw preference, and number of pellets consumed in a given time is recorded. Animals with compromised motor function show a reduced success rate to grasp food. The unique advantage of this task is that the capacity of the fore limb can be easily assessed (Klein and Dunnett, 2012; Schaar et al., 2010). For example, following brain or spinal cord injury in rodents, a reduced success rate of reaching for a food pellet is seen, suggesting motor impairment (Gharbawie et al., 2005; Metz et al., 2005; Streijger et al., 2013). Unfortunately, this test has never been used in the CPZ model.

In summary, a wide variety of tests exist to assess motor function. Whilst the rotarod is the most commonly used test, it is the least sensitive and reliable. Subtle deficits (e.g. decreased walking speed and increased limb misplacement) that arise from CPZ-feeding become evident as the complexity of the test is increased. For instance, the walking beam and complex wheel tests detected changes in motor coordination activity (Hagemeyer et al., 2012; Hibbits et al., 2009; Skripuletz et al., 2010b; Yokoi et al., 2011). Moreover, most published CPZ motor studies only used a single motor test, the rotarod. Only three papers used two motor tests in the same study and these produced conflicting results depending on the test used i.e. deficits were detected in walking beam, pole and negative geotaxis tests but not with the rotarod (Hagemeyer et al., 2012; Ray et al., 2017; Zheng et al., 2017). Indeed, the more complex tasks appear to measure quite different aspects of motor performance: whereas the rotarod assesses the capacity of a quadruped to maintain their centre of gravity over a rotating beam (i.e. not fall off), a task that may be equally well resolved by poorly coordinated foot placement or holding onto and rotating with the rod. In contrast, the walking beam, walking ladder and complex wheel measure the capacity of animals to make coordinated limb placements when challenged by a narrow walkway or the complex/varying foot placements demanded by the complex wheel, conditions that reveal functional deficits not detected by the rotarod (Table 3).

Since the complex wheel has the capacity to measure multiple parameters and animals are free to engage in the task within their home cage without experimenter intervention, this test is able to discern early, developing deficits (i.e. within 2–3 weeks of CPZ-feeding) and provide reproducible results across different labs; this would thus appear to be one of the best available tools to measure motor performance (Hibbits et al., 2009; Liebetanz and Merkler, 2006; Manrique-Hoyos et al., 2012; Mierzwa et al., 2013). However, the attribution of deficits to motor functions may be confounded when cognitive function is also compromised (Cui et al., 2018; Dutta et al., 2013; Li et al., 2015; Murakami et al., 2017; Omotoso et al., 2018; Shao et al., 2015; Tezuka et al., 2013) due to demyelination and gliosis in cortical memory circuits and cerebellar systems (Goldberg et al., 2015; Koutsoudaki et al., 2009; Norkute et al., 2009; Skripuletz et al., 2010a). Therefore, it becomes difficult, if not impossible, to separate the contribution of the cognitive versus motor systems based only on behavioral readouts.

Importantly, pathological changes in the areas/pathways responsible for behavioural motor deficits in the CPZ model have been poorly studied. Many papers use demyelination of the corpus callosum as a proxy for demyelination of the CNS as a whole, rather than focusing on demyelination in CNS regions relevant to, for example, motor function, making correlations to causality less reliable (Abakumova et al., 2015; Bolcskei et al., 2018; Chang et al., 2017; Faizi et al., 2016;

Franco-Pons et al., 2007; Hagemeyer et al., 2012; Hashimoto et al., 2017; Hibbits et al., 2009; Iwasa et al., 2014; Kumar et al., 2018; Liebetanz and Merkler, 2006; Manrique-Hoyos et al., 2012; Sanadgol et al., 2018; Wang et al., 2016; Yamamoto et al., 2014, 2017; Yu et al., 2018). In this context, it is essential to point out that current reports have failed to show spinal cord demyelination and gliosis with CPZ (Acs et al., 2013; Herder et al., 2011; Love, 1988; Ray et al., 2017). This is unlike the EAE animal model in which the major site of demyelination and gliosis is the spinal cord white matter (Table 1), and at least correlates with the severe difficulty in walking that occurs ~10-14 days after induction (Duffy et al., 2016; Dutra et al., 2013; Heckman et al., 2013). Further, far more detailed studies are required to closely examine CPZ-induced changes in the ascending and descending pathways involved in motor behaviour.

5.3. Pain-like symptoms

Many MS patients (29–86%) report pain-related symptoms such as mechanical, heat and/or cold hyperalgesia (Table 2; Hadjimichael et al., 2007; Kenner et al., 2007; Khan et al., 2018; Khan and Smith, 2014; Svendsen et al., 2003). The mechanism(s) of neuropathic pain in MS is not clearly understood. In the context of MS, the mechanisms involved in pain-like behaviours have been inferred from animal studies on peripheral nerve injury (Wang et al., 2017a), oligodendrocytosis (Gritsch et al., 2014), and inflammation in the spinal cord (Duffy et al., 2016; Lu et al., 2012) and brain stem (Duffy et al., 2016; Thorburn et al., 2016). Given the marked incidence of painful sensations in MS patients, it is surprising that only a few studies have assessed pain-related behaviour in the CPZ model (Table 3). Pain-like behaviours in animals are most often measured using flexion withdrawal reflexes evoked by electrical, mechanical and heat or cold stimuli (Barrot, 2012; Deuis et al., 2017; Deuis and Vetter, 2016; Duffy et al., 2016; Savage and Ma, 2015; Thorburn et al., 2016).

Mechanical stimuli can be measured using manual von Frey filament or electronic devices such as the Dynamic plantar aesthesiometer apparatus (Chew et al., 2013; Deuis et al., 2017; Shaikh et al., 2016). The use of manual von Frey filament commonly involves the use of the 'up-down' method (Chaplan et al., 1994) to determine the withdrawal threshold. This is subject to inter-experimenter variability as well as differential application of filament bending strength (on a logarithmic scale) to the paw (i.e. not a true reflection of the applied force). The electronic von Frey filament uses a linear, increasing force to elicit withdrawal in an automated controlled manner. However, in some test areas, such as the face, it is more practical to use manual von Frey filament to examine threshold changes than electronic von Frey filament (Duffy et al., 2016). Only one study has evaluated mechanical threshold changes in CPZ-fed animals (Bolcskei et al., 2018). Both manual and electronic von Frey filaments stimuli have been applied to the hind paws of mice. The results showed no differences between CPZ and control mice with either method; however, more consistent and reliable results were obtained using electronic than manual von Frey filaments (Bolcskei et al., 2018). In EAE, studies using both electronic (Rodrigues et al., 2009) and manual von Frey filaments (Duffy et al., 2016; Lu et al., 2012; Serizawa et al., 2018) indicated mechanical hypersensitivity in the early stage (i.e. prior to motor paralysis), suggesting increased pain-like behavioural deficits.

Similar flexion withdrawal responses to heat sources are measured using the Hargraves apparatus, or the tail flick test in which a heat source is applied to the tail or paw with a set cut-off time to avoid tissue burn and the time taken to elicit a withdrawal reflex is recorded (Deuis and Vetter, 2016; Samour et al., 2017). In a single study using the tail flick response to immersion in hot water (50–60 °C), no difference between control and CPZ-fed animals was observed (Vakilzadeh et al., 2016). In contrast, development of thermal hyperalgesia occurs during the early (Lu et al., 2012; Thibault et al., 2011) and later stages of the EAE model (Lu et al., 2012; Schmitz et al., 2014). Histological examination of EAE mice revealed a reduction in abundance of neuronal nuclei (a neuron-specific nuclear protein), gliosis (Duffy et al., 2016; Lu et al., 2012; Schmitz et al., 2014), demyelination, and T-cell infiltration (Duffy et al., 2016; Schmitz et al., 2014) mainly in the lumbar spinal cord. However, in CPZ, the single study examining gliosis did not identify an effect in the spinal cord (Herder et al., 2011), consistent with other studies that have shown no evidence of CPZ-induced demyelination in this area (Herder et al., 2011; Love, 1988; Ray et al., 2017). In contrast, a recent study using electrical activation of peripheral nerves revealed a decrease in the electrical threshold to evoke a withdrawal response following 2 weeks of CPZ-feeding suggesting that sensory information may be subtly altered even at this early stage (Tsukahara et al., 2018).

Sensitivity to cold in rodents is measured using the cold plantar, temperature preference, cold plate or acetone evaporation tests (Deuis et al., 2017; Shaikh et al., 2016). In these tests, animals are placed on a cold plate (or exposed to focal cooling stimuli) and the emergence of nociceptive responses such as jumping, shaking, flinching or licking are taken to be indicative of pain-like symptoms (Deuis et al., 2017; Shaikh et al., 2016). The emergence of pain-like behaviours to cool stimuli (that do not normally evoke pain-like behaviours) is referred to as cold allodynia and appears to be a more sensitive measure of changes in sensory function (Samour et al., 2017; Shaikh et al., 2016). No studies have evaluated cold hypersensitivity in CPZ-treated animals whereas increased paw withdrawal responses are found early in EAE animals (Table 3; Schmitz et al., 2014; Thibault et al., 2011).

Trigeminal neuralgia, sudden and sharp episodes of facial pain, is more prevalent in patients with MS (Fallata et al., 2017; Khan and Smith, 2014). It is suggested that facial pain in rodents can be measured using the air puff or manual von Frey filament tests, although the potential relationship to trigeminal neuralgia (or an animal correlate) has not been directly established (Duffy et al., 2016; Thorburn et al., 2016). In the air puff test, facial hypersensitivity is quantified by measuring parameters such withdrawal of head from the stimulus probe and/or forepaw swipes down the snout. The increased frequency of these activities is suggested to indicate pain-like symptoms such as allodynia and hyperalgesia. One study using EAE showed that during the early and late (i.e. motor decline stage) stages air puff scores increased suggesting facial pain sensitivity (Thorburn et al., 2016). In addition, spontaneous pain can be measured by quantifying changes in facial expression using a grimace scale that includes orbital tightening, nose bulge, cheek bulge, ear position and whisker change, with scores of 'not present' to 'severe' (Langford et al., 2010; Sotocinal et al., 2011). During the later stages of EAE, changes in facial expression were also found, further suggesting increased pain-like behaviour (Duffy et al., 2016). T-cell recruitment, glial activation and demyelination in the trigeminal primary afferent pathway, trigeminal sensory root and the spinal trigeminal tract have been suggested to trigger facial hypersensitivity in EAE (Duffy et al., 2016; Thorburn et al., 2016). However, no studies have assessed facial sensitivity in CPZ animals.

In summary, limited studies in CPZ-fed animals have not provided reliable evidence of changes in nociceptive reflex thresholds. In addition, as with motor behaviour, histological investigations in these studies were conducted only in the corpus callosum (Bolcskei et al., 2018; Tsukahara et al., 2018; Vakilzadeh et al., 2016) rather than in relevant regions of the pain matrix such as the dorsal root ganglia, spinal cord or trigeminal grey and white matter, thalamus, somatosensory and limbic cortices. Therefore, further studies are necessary to draw clearer conclusions about nociceptive behavioural deficits in the CPZ model.

5.4. Fatigue

Exhaustion, physical tiredness and insomnia are common clinical symptoms reported by ~75% of MS patients (Table 2), commonly coalescing as a sense of fatigue (Braley and Chervin, 2010; Lerdal et al., 2007; Mills and Young, 2011). The mechanisms leading to increased

fatigue in MS are poorly understood but have been loosely attributed to neurochemical imbalances (i.e. of dopamine, serotonin (Dobryakova et al., 2015; Newland et al., 2016) or melatonin (Melamud et al., 2012)) or thalamic (Minagar et al., 2013) and hypothalamic (Burfeind et al., 2016) demyelination. Interestingly, in animal models, the behavioural focus has been on tests of physical endurance such as the upside down grid (Bolcskei et al., 2018; Ruiz et al., 2015) and voluntary wheel running (Grace et al., 2017; Hicks et al., 2016) to measure fatigue-like behaviour (Table 3).

The upside down grid test is used to quantify fatigue-like behaviour and strength (Bolcskei et al., 2018; Ruiz et al., 2015). Briefly, test animals are placed on a wire mesh which is inverted and the time taken to release their grasp is measured, with decreased time representing fatigue-like behaviour (Bolcskei et al., 2018; Deacon, 2013; Meinen et al., 2012; Ruiz et al., 2015). CPZ-fed mice displayed responses indistinguishable from controls in this test (Bolcskei et al., 2018). The voluntary wheel running test lacks the complexity of complex wheel but does allow individually housed animals unrestricted access; total running time, distance travelled and speed parameters can be recorded (Grace et al., 2017; Hicks et al., 2016). The advantage of voluntary wheel running over the upside down grid is the autonomous nature of the instrument which allows animals to move freely and spontaneous activities over time can be observed. Decreased voluntary movement in EAE animals indicates fatigue-like symptoms in the early and later stages (Grace et al., 2017). However, in EAE animals, many behavioural tests are limited to the early phase as the later phase is confounded by progressive motor paralysis. In CPZ-fed animals, the usefulness of the voluntary wheel running test has not yet been determined. In addition, results of fatigue studies may be confounded by sensorimotor deficits, sleep disturbances or depression. For example, people with MS have high rates of fatigue, depression, and sleep disturbances coupled with decreased motor function (Attarian et al., 2004; Pardini et al., 2013; Pokryszko-Dragan et al., 2013). Whether such motor and sleep deficits, or depression also affect fatigue measures in CPZ-fed animals remain to be investigated.

5.5. Cognitive deficits

MS patients (40–65%) experience cognitive impairment (Table 2) that manifests as decreased memory, language, executive functions and social interactions (Jongen et al., 2012; Rahn et al., 2012). The extent of demyelination and inflammation processes in the CNS, especially in the limbic system (e.g. hippocampus, fornix and cingulum; Damjanovic et al., 2017; Keser et al., 2018; Rocca et al., 2018; Sacco et al., 2015), and cerebellum (Valentino et al., 2009; Weier et al., 2014; Wilkins, 2017) have been suggested to have a role in the cognitive decline. Cognitive behaviour in animals can be assessed using the Y-maze, novel object recognition, social interaction, Morris water maze and fear conditioning tests (Table 3; Campos et al., 2013; Karl et al., 2003; Taylor et al., 2010; Webster et al., 2014; Zhang et al., 2012; Zieba et al., 2015). CPZ-fed animals showed decreased memory functions and impaired social interaction as assessed by these tests (Abakumova et al., 2015; Adilijiang et al., 2015; Aryanpour et al., 2017; Chang et al., 2017; Cui et al., 2018; Dutta et al., 2013; Hibbits et al., 2009; Kondo et al., 2016; Li et al., 2015; Makinodan et al., 2009; Murakami et al., 2017; Omotoso et al., 2018; Ray et al., 2017; Serra-de-Oliveira et al., 2015; Shao et al., 2015; Sun et al., 2017; Tezuka et al., 2013; Valeiras et al., 2014; Wang et al., 2015; Xiao et al., 2008; Xu et al., 2010, 2011; Xu et al., 2009).

The Y-maze test is used to measure the exploration of novelty which infers potential deficits in spatial memory function, using a three arm 'maze' (Makinodan et al., 2009; Wolf et al., 2016). Animals are placed at the end of the 'start' arm and allowed to explore the new environment. Reduced exploration/alteration frequency, but increase frequency of entry into the other arms indicates declining cognitive function and this has been observed in CPZ-fed animals (Adilijiang et al., 2015; Kondo et al., 2016; Li et al., 2015; Makinodan et al., 2009; Murakami et al., 2017; Omotoso et al., 2018; Sun et al., 2017; Tezuka et al., 2013; Wang et al., 2015; Xiao et al., 2008; Xu et al., 2010, 2011). In contrast, two studies reported no changes compared to naïve controls using the Y-maze test after 0.4% CPZ-feeding for 3 weeks or 0.2% CPZ for 1 week (Chang et al., 2017; Shao et al., 2015) and correlative histological examination showed no demyelination in the hippocampus (Shao et al., 2015), suggesting that short term (1–3 week) exposure to CPZ did not evoke memory dysregulation; complete demyelination of this region takes 5–6 weeks (Koutsoudaki et al., 2009; Norkute et al., 2009).

In the social interaction test, animals are allowed to meet one another in an open environment. The number of close contacts (e.g. ˜5 cm, 0.2 s) are scored as a measure of social interaction for rodents (Thanos et al., 2017; Wilson and Koenig, 2014). Less interaction with another animal has been documented in CPZ-fed animals, indicating impaired social interaction (Abakumova et al., 2015; Adilijiang et al., 2015; Hibbits et al., 2009; Makinodan et al., 2009; Mierzwa et al., 2013; Valeiras et al., 2014; Wang et al., 2015; Xu et al., 2010, 2011; Xu et al., 2009).

The novel object recognition test is used to assess recognition memory tasks. It consists of three phases: habituation, familiarization and the test phase. In the habituation phase, each animal is allowed to freely explore in an open-field arena. During the familiarization phase, a single animal is placed in the open-field arena containing two identical sample objects for a brief period of time. During testing, the ratio of the time spent exploring novel vs. old items is measured (Broadbent et al., 2010; Leger et al., 2013). CPZ-fed animals invested more time exploring the familiar object, with less preference for exploring new objects, suggesting decreased cognitive function (Chang et al., 2017; Kondo et al., 2016; Murakami et al., 2017; Ray et al., 2017; Serra-de-Oliveira et al., 2015; Shao et al., 2015; Tezuka et al., 2013). In contrast, 0.2% CPZ-feeding for 4 weeks and testing for 6–10 weeks after CPZ-feeding was stopped revealed no memory deficit, most probably because of remyelination (Makinodan et al., 2009), suggesting that pathways for recognition memory depend to some extent on myelination.

The Morris water maze is used to investigate spatial memory and learning. The test depends on the ability of animals to find a submerged platform. A round pool about 90–100 cm in diameter and 30–40 cm high, filled with cloudy water (25–26 °C) is used. The test comprises two phases: training and testing. In the training phase, animals learn to locate a visible platform (e.g. 1–1.5 cm above the water); during the test phase the platform is submerged (by 1–1.5 cm below the water) and the time (and path) taken to locate the platform is recorded (Anisman and McIntyre, 2002; Barnhart et al., 2015; Vorhees and Williams, 2006). In CPZ-fed animals, an increased distance travelled and increased time to reach the goal quadrant was indicative of decreased memory and learning function (Aryanpour et al., 2017; Cui et al., 2018; Dutta et al., 2013; Omotoso et al., 2018; Zhang et al., 2016).

To measure associative learning skills related to aversive experience or environmental cues, the fear conditioning test is used. In this test, fear responses, such as defensive activity (immobility/freezing), startle reflex response and stress-induced hormones such as corticosterone and renin secretion (LeDoux, 2000; Van de Kar et al., 1991) are measured in response to an external stimulus such as an electric shock (Campos et al., 2013; Webster et al., 2014). Lower scores (e.g. less freezing) suggest hippocampus-dependent memory deficits and learning. For example, fractalkine ($CX3CL1^{-/-}$) knockout mice showed reduced freezing responses, suggestive of deficits in associative learning behaviour (Rogers et al., 2011). Likewise, in the early stage of EAE, decreased freezing reflects reduced hippocampal function and learning skills (Acharjee et al., 2013). A single study using the fear conditioning test in animals fed 0.2% CPZ for 1 week showed no significant difference in freezing responses compared to controls suggesting no deficit in associative learning and memory (Kondo et al., 2016), likely due to the

lack of demyelination in the hippocampus after this short period of CPZ-feeding (Koutsoudaki et al., 2009; Norkute et al., 2009). Whether, the increase in duration and/or dose of CPZ-feeding changes the fear response remains untested.

Thus, cognitive deficits are prominent in CPZ-fed animals with regard to well-established tests such as the novel object recognition, Morris water maze, Y-maze and social interaction (Abakumova et al., 2015; Adilijiang et al., 2015; Aryanpour et al., 2017; Chang et al., 2017; Cui et al., 2018; Dutta et al., 2013; Hibbits et al., 2009; Kondo et al., 2016; Li et al., 2015; Makinodan et al., 2009; Murakami et al., 2017; Omotoso et al., 2018; Ray et al., 2017; Serra-de-Oliveira et al., 2015; Shao et al., 2015; Sun et al., 2017; Tezuka et al., 2013; Valeiras et al., 2014; Wang et al., 2015; Xiao et al., 2008; Xu et al., 2010, 2011; Xu et al., 2009), with the Y-maze test being the most frequently used (Adilijiang et al., 2015; Chang et al., 2017; Kondo et al., 2016; Li et al., 2015; Makinodan et al., 2009; Murakami et al., 2017; Omotoso et al., 2018; Shao et al., 2015; Sun et al., 2017; Tezuka et al., 2013; Wang et al., 2015; Xiao et al., 2008; Xu et al., 2010, 2011). However, task selection during study design is a critical aspect in cognitive testing due to the existence of multiple paradigms of cognition (e.g. spatial memory, social interaction and recognition memory) and the lack of a single instrument that measures all aspects of cognition (Karl et al., 2003; Taylor et al., 2010). For example, social impairment of the animal is tested using the social interaction test (Abakumova et al., 2015; Adilijiang et al., 2015; Hibbits et al., 2009; Mierzwa et al., 2013; Valeiras et al., 2014; Wang et al., 2015; Xu et al., 2010, 2011; Xu et al., 2009) whereas spatial learning and memory function can be assessed using the Morris water maze (Aryanpour et al., 2017; Cui et al., 2018; Dutta et al., 2013; Omotoso et al., 2018) and Y-maze (Adilijiang et al., 2015; Kondo et al., 2016; Li et al., 2015; Makinodan et al., 2009; Murakami et al., 2017; Omotoso et al., 2018; Sun et al., 2017; Tezuka et al., 2013; Wang et al., 2015; Xiao et al., 2008; Xu et al., 2010, 2011) tests. Likewise, in order to test recognition memory, the novel object recognition test is used (Chang et al., 2017; Kondo et al., 2016; Murakami et al., 2017; Ray et al., 2017; Serra-de-Oliveira et al., 2015; Shao et al., 2015; Tezuka et al., 2013). This suggests that in order to get a better indication of cognitive decline, multiple tests are required (Adilijiang et al., 2015; Chang et al., 2017; Kondo et al., 2016; Makinodan et al., 2009; Murakami et al., 2017; Omotoso et al., 2018; Shao et al., 2015; Tezuka et al., 2013; Wang et al., 2015; Xu et al., 2010, 2011). Additionally, results may be confounded by the internal environment of the test set-up. For example, the Morris water maze test may be confounded by inherent fear/anxiety responses to water (Ehninger and Kempermann, 2006; Harrison et al., 2009) or severe deficits in motor function, as observed in EAE animals (Dutra et al., 2013). Lastly, the fear conditioning test can be confounded by declining motor function or fatigue. For example, physical tests (e.g. wheel running), followed by the fear conditioning test lead to increased tendency for freezing responses (Hopkins and Bucci, 2010).

In summary, the use of two tests together such as Y-maze (spatial memory) and novel object recognition (recognition memory) might be the best choices in order to achieve a better indication of cognitive deficit as shown in the work of different labs using CPZ (Kondo et al., 2016; Murakami et al., 2017; Tezuka et al., 2013). Histological analyses in cognition-based behavioural studies of CPZ were conducted mainly in corpus callosum (Abakumova et al., 2015; Aryanpour et al., 2017; Chang et al., 2017; Ray et al., 2017; Serra-de-Oliveira et al., 2015; Sun et al., 2017), hippocampus (Cui et al., 2018; Dutta et al., 2013; Li et al., 2015; Murakami et al., 2017; Omotoso et al., 2018; Shao et al., 2015; Tezuka et al., 2013; Xu et al., 2010), cortex (e.g. prefrontal; Makinodan et al., 2009; Xu et al., 2010) and basal ganglia (Tezuka et al., 2013; Wang et al., 2015; Xu et al., 2009; Zhang et al., 2016) whereas other relevant regions associated with cognitive function such as the fornix, cingulum and amygdala (Keser et al., 2018; Pessoa, 2010) remain to be investigated, suggesting more detailed examination of functionally relevant regions is required when attempting to explain the outcomes of cognitive tests in the CPZ model.

5.6. Visual disturbances/optic neuritis

Visual disturbances including blurred vision, reduced perception of colour, loss of visual fields and pain in the eye are the most frequent initial manifestations of human MS (˜50%, Table 2; Costello, 2016; Kale, 2016; Sakai et al., 2011) but are less common in the progressive (less inflammatory) variants (Confavreux et al., 2003; Henderson et al., 2008). Demyelination and inflammation in the optic nerve also extends to the loss of ganglion cells in ˜80% of MS patients (Balcer et al., 2015; Bermel and Balcer, 2013). In animals, visual disturbances are measured using multifocal electroretinograms or are inferred based on changed performance in running wheel or Y-maze tests (which depend upon visual cues, Table 3; Namekata et al., 2014; Thomas et al., 2007; Thompson et al., 2008).

A multifocal electroretinogram records the bioelectric potential of eye. In this system an electrode placed on the corneal surface (at the limbus, bordering the cornea and the sclera of eye) and response to a light stimulus is recorded. Typically, light is delivered to the full visual field in which the spectral composition, duration and light intensity are defined and varied (Dutescu et al., 2013; Guo et al., 2010; Namekata et al., 2014). In Olig $1^{-/-}$ (a transcription factor of mature OLG) knockout mice subjected to EAE, visual dysfunction was observed using a multifocal electroretinogram, correlating with demyelination and cellular infiltration in optic nerve (Guo et al., 2010). Likewise, CPZ-feeding produced a reduction in the multifocal electroretinogram amplitude indicative of disturbances in visual function (Namekata et al., 2014). Changes in the multifocal electroretinogram are associated with demyelination in the optic nerve (Bagchi et al., 2014; Namekata et al., 2014) and subcortical visual system (Araujo et al., 2017) following 0.2% CPZ-feeding for 12 (Namekata et al., 2014), 8 (Bagchi et al., 2014) and 5 (Araujo et al., 2017) weeks respectively. Interestingly, the optic tract and optic nerve have not been found to be demyelinated in the acute phase of CPZ-feeding (Araujo et al., 2017; Goldberg et al., 2015; Yang et al., 2009) whereas chronic feeding does result in optic nerve demyelination, suggesting time dependent effects of CPZ in the visual system (Namekata et al., 2014).

5.7. Depression

Depression-like symptoms including insomnia, suicidal ideation, sad mood and feelings of guilt affect ˜50% of the MS patients during their lifetime (Table 2; Siegert and Abernethy, 2005; Sukoff Rizzo and Crawley, 2017). The pathophysiology of depression is not clearly understood; however, like other clinical manifestations of the disease, many have suggested that the demyelination and neuro-inflammation processes in the CNS are causative factors (Brenner et al., 2018; Byatt et al., 2011; Rossi et al., 2017). It has been suggested that MS patients with demyelinating lesions in the brain (Rabins et al., 1986), particularly in the temporal lobe (Ron and Logsdail, 1989), hippocampus (Gold et al., 2014; Rocca et al., 2018) or arcuate fasciculus of the left hemisphere (Pujol et al., 1997), rather than in the spinal cord have more depression. Depression-like behaviour in animals can be measured using the forced swim, tail suspension or sucrose preference tests (Ayatollahi et al., 2017; Fukui et al., 2007; Kondo et al., 2016; Krishnan and Nestler, 2011; Porsolt et al., 2001; Strekalova et al., 2011).

In the forced swim test, rodents are placed individually in a clear plastic/glass cylinder (typically 25–30 cm high and 10 cm diameter) half-filled with water at 21–23 °C and activities like swimming, floating, climbing or mobility are scored. A decreased level of activity correlates with a depression-like phenotype (Krishnan and Nestler, 2011; Porsolt et al., 2001). Studies with EAE mice showed increased immobility in the early stage, suggesting depression (Acharjee et al., 2013; Ayatollahi et al., 2017). In contrast, a single study using the forced swim test with CPZ-fed animals detected no differences from controls (Kondo et al.,

2016).

In the tail suspension test, rodents are suspended above an experimental surface (typically 25–30 cm) and escape-oriented activities and mobility are recorded. Decreased activity indicated depression-like behaviour. For example, mice deficient in a transmembrane protein responsible for transporting cytoplasmic monoamines into secretory vesicles, showed decreased mobility in the tail suspension (and forced swim) test, suggesting depression-like behaviour (Fukui et al., 2007). In EAE animals, decreased mobility in the early stage suggested the induction of a depression-like behaviour phenotype (Majidi-Zolbanin et al., 2015). In contrast, a single study using the tail suspension test did not find evidence of a depressive phenotype following 1 week of CPZ-feeding (in 8 week old B6 mice), a result attributed to the limited demyelination and inflammation in the CNS at that stage (Kondo et al., 2016). Whether such phenotypes become more evident with continued CPZ-feeding and thus at latter time points remains untested.

Anhedonia is measured using the sucrose preference test (Liu et al., 2018). In this test, animals have free access to sucrose solution and depressed and non-depressed animals are identified on the basis of the amount of sucrose consumed at a given time (Liu et al., 2018; Strekalova et al., 2011). Healthy animals drink more sucrose as the sweet taste is desirable whereas animals exhibiting a depressive phenotype consume less (Skalisz et al., 2002). In both the earlier and later stages of EAE, animals showed a reduced preference for sucrose, suggesting increased depression (Pollak et al., 2000). Currently, no study has assessed depression-like behaviour in CPZ-fed animals using the sucrose preference test (Table 3).

The physical acts of swimming or tail mobilization, assessed by the forced swim or tail suspension tests respectively, may be confounded by diminished motor functions or increased fatigue/tiredness. For example, the usefulness of the forced swim test is limited in the later stages of EAE due to limb or tail paralysis and so may not reflect depressive behaviour, rather motor decline (Majidi-Zolbanin et al., 2015). In contrast, the sucrose preference test can be used as a simple primary screening tool as animals can freely access the sucrose solution and it is not confounded by a foreign environment (e.g. water), handling, or stress-inducing activity (e.g. climbing; Liu et al., 2018). Since these factors make depression difficult to assess in animals, it is imperative to recognise the limitations of the tests when designing behavioural studies. Importantly, due to the role of stress-induced hormones (e.g. corticosterone) and neurotransmitters (e.g. dopamine) in the regulation of affect (e.g. depression and fatigue) the measurement of these hormones during behavioural testing is important to overall interpretation of the data. For example, a reduction of dopamine release has been associated with depression and fatigue in MS and other neurological diseases while increased dopaminergic activity contributes to hyperactivity or excitement (Diehl and Gershon, 1992; Dobryakova et al., 2015). CPZ-feeding increases the concentration of dopamine in the prefrontal cortex (Chang et al., 2017; Valeiras et al., 2014; Xu et al., 2010) and dopamine transporter expression in the cerebral cortex (Chang et al., 2017). In addition, an elevated level of corticosterone was found in the serum of CPZ-fed animals (Serra-de-Oliveira et al., 2015; Yu et al., 2018). These may provide an explanation for increased activities such as climbing (Chang et al., 2017; Franco-Pons et al., 2007; Werner et al., 2010; Xu et al., 2009), locomotion (Bolcskei et al., 2018; Chang et al., 2017; Faizi et al., 2016; Franco-Pons et al., 2007; Sun et al., 2017; Tezuka et al., 2013; Zhang et al., 2013) or rearing (Bolcskei et al., 2018; Franco-Pons et al., 2007) in CPZ-fed animals. Therefore, CPZ animals may not be depressed or fatigued (since fatigue often co-occurs with depression) and further studies are needed to provide more refined understanding of this behavioural parameter.

5.8. Sleep disorders

Sleep abnormalities are seen in ~50% of MS patients (Table 2), with effects including restless leg syndrome, periodic limb movement disorders, sleep-related breathing disorders and disruptions of normal sleep patterns (Fleming and Pollak, 2005; Tachibana et al., 1994; Veauthier, 2015) that are markedly detrimental to quality of life (Brass et al., 2010). Furthermore, the disruption of night-time sleep leads to increased daytime sleepiness (Carnicka et al., 2015). Sleep disorders thus correlate strongly with non-motor symptoms such as fatigue, cognition, anxiety and depression (Attarian et al., 2004; Braley et al., 2014; Ghajarzadeh et al., 2012; Nagaraj et al., 2013). While the mechanisms are unclear, the presence of demyelinating lesions (Veauthier, 2015) and dysregulation of hormone function (e.g. melatonin; Melamud et al., 2012) have been implicated in the sleep disturbances suffered by MS patients. Given the marked abnormalities of sleeping patterns in human MS, it is surprising that these have not been investigated in the CPZ model.

To evaluate sleep abnormalities, spontaneous activities in an open field chamber and electrophysiological measurements such as electromyography are used (Taylor et al., 2010; Toth and Bhargava, 2013). In the open field test, animals are quantitatively assessed with regard to their posture, breathing and sleeping patterns (e.g. interrupted/uninterrupted, Table 3). If sleep is uninterrupted for 2 min then it is recorded as sleep, with a 'good sleep pattern' being defined by ~75% of a 10 min period spent sleeping (Taylor et al., 2010). Electromyography measures the pattern of activation in muscles that should be supressed in the deeper (slow wave) phases of sleep (Toth and Bhargava, 2013). In electromyography, electrodes are placed into the muscle to record electrical activity; data are scored as epochs in different categories representing wakefulness, slow wave sleep or paradoxical sleep (Bastianini et al., 2017; Tobler et al., 1997). In the early stage of EAE increased waking and decreased non-rapid eye movement were associated with disruption of sleep (He et al., 2014a, b).

Notably, functional deficits such as disturbances in sleep pattern, anxiety, cognitive decline and fatigue are all interlinked. For example, studies with MS patients showed a significant increase in sleep disturbances among those reporting high rates of fatigue whereas matched healthy controls had natural sleep cycles (Attarian et al., 2004; Pokryszko-Dragan et al., 2013). Moreover, sleep disturbances affect memory function (e.g. attention, working, decision and long-term memory; Alhola and Polo-Kantola, 2007; Braley et al., 2014). Thus, the normalization of good sleep patterns may manage fatigue and memory loss, although the causes of sleep disruption in MS are not known. Since CPZ-fed animals are suggested to have cognitive deficits (see above), it can be hypothesised that these animals may have disturbed sleeping patterns, but this remains to be investigated.

5.9. Anxiety-like behaviour

Anxiety is found in ~35% of MS patients (Table 2; Haussleiter et al., 2009; Riether, 1999) and there is a significant association with other common symptoms such as pain, fatigue and depression (Beiske et al., 2008; Janssens et al., 2006; Korostil and Feinstein, 2007). The pathophysiology of increasing anxiety in MS is not well understood. Human studies have indicated that cortical demyelination (Burns et al., 2014; Riether, 1999), reactive response to psychosocial pressures (Zorzon et al., 2001) or escalating symptoms such as motor deficits, fatigue and depression (Marrie et al., 2015; Zorzon et al., 2001) are associated with increasing anxiety.

Anxiety-like behaviour in rodents can be measured using the open field, elevated plus maze, hole board and light dark tests (Table 3; Campos et al., 2013; Karl et al., 2003; Ramos, 2008; Taylor et al., 2010). Spontaneous activities including walking, rearing (i.e. vertical activity) and grooming (i.e. fur licking and limb scratching) are typical behaviours associated with normal activities such as food foraging, social communication and hygiene (Kalueff et al., 2016; Tanaka et al., 2012). However, alterations of spontaneous activities and natural behaviour (e.g. activity in light vs. dark conditions) in response to fear/stress can be used as a maker of anxiety-like behaviour (Karl et al.,

2003; Ramos, 2008; Taylor et al., 2010).

The open field test is a basic technique to measure locomotion and anxiety-like behaviours of rodents. In this test, rodents are allowed to explore in a circular or square open environment and the locomotion (e.g. total distance travel and velocity) and exploratory (curiosity-like) activities (e.g. rearing) are documented (Karl et al., 2003; Ramos, 2008; Taylor et al., 2010). Increased activity in the perimeter, compared to the centre, suggests an attempt to find a safe, 'enclosed' environment (i.e. at the perimeter, in an effort to escape the open central field) due to inherent fear of an open, 'unsafe' place; this is regarded as anxiety-like behaviour (Karl et al., 2003; Ramos, 2008; Taylor et al., 2010). A similar phenomenon has been reported in some CPZ studies, suggesting anxiety like behaviour in CPZ-fed animal (Li et al., 2015; Makinodan et al., 2009; Sanadgol et al., 2018; Serra-de-Oliveira et al., 2015; Wang et al., 2013, 2016; Ye et al., 2013; Yu et al., 2018; Zhang et al., 2016).

In total, 20 publications were found to use open field to measure locomotion and anxiety-like behaviours in the CPZ model (Bolcskei et al., 2018; Cui et al., 2018; Elbaz et al., 2018; Faizi et al., 2016; Franco-Pons et al., 2007; Li et al., 2015; Makinodan et al., 2009; Sanadgol et al., 2017; Serra-de-Oliveira et al., 2015; Shao et al., 2015; Sun et al., 2017; Vakilzadeh et al., 2016; Valeiras et al., 2014; Wang et al., 2013, 2015; Xu et al., 2009; Ye et al., 2013; Yu et al., 2018; Zhang et al., 2015, 2016). However, in these studies inconsistent and contradictory results were often found: some groups reported that CPZ-feeding increased locomotion (Bolcskei et al., 2018; Shao et al., 2015; Sun et al., 2017; Valeiras et al., 2014) whereas, others reported decreased locomotion (Faizi et al., 2016; Sanadgol et al., 2017; Vakilzadeh et al., 2016; Wang et al., 2016; Ye et al., 2013; Yu et al., 2018; Zhang et al., 2015). Interestingly, others reported no change in locomotion even though a similar study design was followed (Cui et al., 2018; Franco-Pons et al., 2007; Li et al., 2015; Makinodan et al., 2009; Wang et al., 2013; Xu et al., 2009). In addition, decreased running frequency in the centre, considered as anxiety-like behaviour, was reported in some studies (Li et al., 2015; Makinodan et al., 2009; Sanadgol et al., 2018; Serra-de-Oliveira et al., 2015; Wang et al., 2013, 2016; Ye et al., 2013; Yu et al., 2018; Zhang et al., 2016) whereas others found increased frequency in the centre (Franco-Pons et al., 2007; Valeiras et al., 2014). These contradictory observations using the same test raise serious issues concerning the acceptability of using open field to measure anxiety and highlight the need to use alternative tests to assess anxiety.

To better assess anxiety-like behaviour, specialized tests such as the elevated plus maze or light dark tests can be used (Bourin and Hascoet, 2003; Ramos, 2008; Walf and Frye, 2007). In the elevated plus maze test, rodents are placed in a plus-shaped apparatus with two open and two closed arms for a fixed period of time (e.g. 8–10 min) with the time spent exploring, rearing and grooming on the arms and central area, as well as inspection of the space beneath the platform (head dipping) being measured (Campos et al., 2013; Paine et al., 2002; Walf and Frye, 2007). In the early stage of EAE, the decreased percentage of time spent in the open arms is taken as an indication of anxiety (Kocovski et al., 2018). Likewise, mice that received bilateral injection of 6-hydroxydopamine toxin (used to model Parkinson disease) showed a decreased amount of time in the open space, suggesting less exploratory behaviour and thus increased anxiety (Bonito-Oliva et al., 2014). In CPZ-fed animals, inconsistent results have been reported when the elevated plus maze test was used. For example, increased time in the open arms which does not reflect anxiety was found in some (Torkildsen et al., 2009; Xu et al., 2011, 2009; Zimmermann et al., 2018), but not other (Abakumova et al., 2015; Serra-de-Oliveira et al., 2015) studies, whereas two studies found no differences relative to controls using the elevated plus maze test (Cui et al., 2018; Makinodan et al., 2009). These inconsistencies arise, in part due to the reliance on different parameters: one study (Cui et al., 2018) reported exploration time in both arms and centre whereas others focused on the time spent in the arms alone (Abakumova et al., 2015; Makinodan et al., 2009; Serra-de-Oliveira et al., 2015; Torkildsen et al., 2009; Xu et al., 2011, 2009; Zimmermann et al., 2018). None of the studies investigated head dipping, rearing and grooming behaviours with elevated plus maze in CPZ studies. Such conflicting observations highlight the need for additional elevated plus maze studies using a consistent approach based on measuring all parameters in order to obtain a far clearer understanding of potential anxiety in CPZ model.

The innate aversion of animals to light can be measured using the light dark test. In this task animals are allowed to explore freely in two compartments, either the 'unsafe' illuminated side or the 'safe' dark side (Bourin and Hascoet, 2003; Campos et al., 2013). This test measures time in the light arena, time spent between the two areas and head dipping as surrogate measures of anxiety (Chaouloff et al., 1997; Taylor et al., 2010). For example, loss of Parkin function (an E3 ubiquitin--protein ligase mutation causing early-onset Parkinson's disease) in mice resulted in less exploration time in the light side and decreased transition between light and dark compartments suggesting increased anxiety-like behaviour (Zhu et al., 2007). Likewise, in the acute stages of EAE, mice spend less time in the light compartment reflecting less exploratory behaviour and thus increased anxiety-like behaviour (Gentile et al., 2016; Peruga et al., 2011). Anxiety in EAE has been associated with demyelination and inflammation in CNS structures such as spinal cord and hippocampus (Gentile et al., 2015; Peruga et al., 2011). One light dark study has shown that following 1 week of 0.2% CPZ-feeding there was less exploration in the illuminated compartment, suggesting anxiety-like behaviour (Kondo et al., 2016). This is well before marked demyelination occurs in this model (Hiremath et al., 1998), suggesting that the early events leading to oligodendrocytosis can result in measurable behavioural changes even before demyelination becomes evident. However, no significant differences were found in terms of latency to enter the boxes (Kondo et al., 2016), and other parameters including head dipping or rearing associated with CPZ-feeding remain untested.

The hole board is the least used test in CPZ experiments to measure anxiety and the exploration of novelty. It was developed as a more complex variant of the open field in which novel recesses or holes are added to the open field and anxiety and exploratory behaviours are documented. In this test, animals are placed, for a defined period of time, in a large, clean box with equally distributed holes (e.g. 16). Activities including distance travelled, number of hole-poking/exploring attempts, rearing and grooming are measured over a 5-minute period. Increased frequency of activities is interpreted to indicate increased exploratory behaviour to find a 'safe' place to escape/hide and is thus regarded as an indicator of an anxiety-like phenotype (Crawley, 1985; Karl et al., 2003; van Gaalen and Steckler, 2000). However, the hole board test has also been suggested to measure cognitive function by assessing the capacity to locate food pellet rewards. In this procedure, a reward is provided in the holes during a training session and rodents are allowed to search freely, whereas during the test session the reward holes are altered or left empty. Increased error numbers are taken to indicate deficits in working or reference memory (Feyissa et al., 2017; Kuc et al., 2006). In CPZ-fed animals no changes in hole-poke frequency were observed relative to naïve controls (Skripuletz et al., 2010b); however, there have been no investigations reporting on all the test parameters (e.g. rearing, grooming and distance travelled).

The open field and hole board tests are more useful to screen locomotion in rodents since they consist of an increased open area to move within (Gellért and Varga, 2016; Tanaka et al., 2012). Reduced ambulation in the centre of the open field and increased escape-like behaviour (e.g. rearing) are considered indications of anxiety but the results are often confounded by the drivers of locomotion. Also, exploration requires a choice and the open field, which is always brightly lit, has no choice other than to stay in the centre (i.e. generally disliked by rodents) or move towards the edge (Mitra et al., 2016; Wang et al., 2013). In contrast, tests such as elevated plus maze or light dark are thus recommended to more selectively measure anxiety-like phenotypes. A key aspect of these tests is the use of heightened natural

conflict wherein rodents must choose between the tendency to explore an unsafe open (light) environment and a safe (dark) environment. 'Anxious' animals are expected to spend less time exploring the open space but may increase the number of times they move between open and closed spaces in an attempt to ensure that they are in the safest possible place (Bourin and Hascoet, 2003; Karl et al., 2003; Pellow et al., 1985; Pellow and File, 1986; Walf and Frye, 2007; Zimmermann et al., 2018). The elevated plus maze test, when combined with detailed quantification of exploration in multiple compartments with differing environments (Bourin and Hascoet, 2003; Carola et al., 2002; Ramos, 2008) provides a better, more detailed account of anxiety-like behaviours.

Interestingly, as in other CPZ behavioural studies, most histological analyses of demyelination were assessed in the corpus callosum (Abakumova et al., 2015; Bolcskei et al., 2018; Faizi et al., 2016; Franco-Pons et al., 2007; Sanadgol et al., 2018; Serra-de-Oliveira et al., 2015; Skripuletz et al., 2010b; Sun et al., 2017; Torkildsen et al., 2009; Vakilzadeh et al., 2016; Valeiras et al., 2014; Wang et al., 2013; Xu et al., 2011; Ye et al., 2013; Yu et al., 2018; Zhang et al., 2015; Zimmermann et al., 2018), some in the cerebral cortex, hippocampus, basal ganglia (Cui et al., 2018; Elbaz et al., 2018; Li et al., 2015; Shao et al., 2015; Valeiras et al., 2014; Wang et al., 2015; Xu et al., 2011, 2009; Ye et al., 2013; Zhang et al., 2016) but none in limbic regions associated with anxiety such as cingulum and amygdala (Martin et al., 2009). Moreover, anxiety has been associated with the increased secretion of modulatory neurotransmitters such as dopamine and serotonin (Martin et al., 2009; Zarrindast and Khakpai, 2015). In CPZ studies increased levels of brain dopamine were found in some studies suggestive of anxiety-like behaviour (Chang et al., 2017; Valeiras et al., 2014; Xu et al., 2010). Therefore, further examination of functionally relevant regions and biochemical analyses are needed to better interpret anxiety-like behavioural responses in the CPZ model.

In summary, all tests that assess anxiety-like behavioural deficits are based on changes in normal, spontaneous activities. Unfortunately, analysis of the conflicting and disparate results due to widely varying test parameters makes it hard to draw clear conclusions about the presence of anxiety-like behaviours in CPZ mice. Moreover, there is clearly no 'ideal' test of anxiety as each has its limitations, so systematic testing and comprehensive reporting of all parameters should be considered essential for effective interpretations. Moreover, appropriate histological and biochemical analyses of relevant CNS regions should always be included so as to better draw correlations of potential anxiety behaviour associated with CPZ ingestion.

5.10. Epileptic seizures

An epileptic seizure is a transient, abnormal, excessive or synchronous bout of neuronal activity in the brain (Fisher et al., 2005). The prevalence of epilepsy in the MS patients is 2–3%, six times higher than the general population (Table 2; Allen et al., 2013; Poser and Brinar, 2003). Demyelination and inflammation in the cortical and subcortical areas including cerebral cortex and hippocampus, have been associated with the aetiology of increased epileptic seizure in MS patients (Calabrese et al., 2017; Hoffmann et al., 2008). However, this hypothetical view of frequency and progression is yet to be clearly elucidated (Kelley and Rodriguez, 2009). In animals, epileptic seizure can be measured using electroencephalography (Table 3), which records spontaneous electric activity of the brain. In electroencephalography, recording electrodes are fixed to the skull or directly to the underlying cortex (Bergstrom et al., 2013; Hoffmann et al., 2008; Lapato et al., 2017). In CPZ-fed animals, epileptic seizure were characterized as high-amplitude discharges in electroencephalography that were associated with generalized tonic-clonic seizures and loss of righting reflexes, suggesting demyelination in the hippocampus and cortex may underlie these events (Hoffmann et al., 2008; Lapato et al., 2017).

6. Other factors contributing to the variability of CPZ-induced behavioural outcomes

6.1. Strain and gender

C57Bl/6 (B6) mice are used widely in CPZ behavioural studies (~77% by publication numbers) due the high reproducibility of demyelination and gliosis (Hiremath et al., 1998). Although the B6 strain is 'gender indifferent' in inducing demyelination and glial activation, surprisingly the majority (84%) of the studies were carried out with males. However, studies in other strains of mice (e.g. BALB/cJ, CD1 and SJL) revealed strain specific patterns of pathological changes (Herder et al., 2011; Skripuletz et al., 2008; Taylor et al., 2009; Yu et al., 2017). For example, differential levels of demyelination in cortical and callosal regions have been described in these other strains suggesting the genetic background of the inbred strain may be important (Mahajan et al., 2016; Skripuletz et al., 2008; Taylor et al., 2009; Yu et al., 2017). However, no single study using CPZ has systematically compared the histological changes between strains, their underlying genetic make-up, and associated behavioural deficits. In addition, whether these fundamental factors are also at play in MS and could potentially explain the heterogeneity observed in disease progression remains to be determined.

6.2. Age, species, dose and duration

The effects of to OLG and demyelination are more marked in juvenile (3–4 weeks) compared to older (6–8 months old) animals (Doucette et al., 2010; Makinodan et al., 2009; Pfeifenbring et al., 2015; Wang et al., 2013). Demyelination in the juvenile period leads to long lasting behavioural deficits (e.g. in cognition) relative to older mice, suggesting age dependent vulnerability to behavioural recovery (Makinodan et al., 2009). This age-related effect is also evident when the responses to low (0.1%) and high (≥0.2%) doses of CPZ are compared at different time points; low doses produced marked demyelination in 3–4 week old animals whereas the same dose was ineffective when administered to 7–8 week old mice, where higher doses are required to elicit a comparable response (Blakemore, 1972; Hiremath et al., 1998; Suzuki and Kikkawa, 1969). Likewise, increasing the duration of CPZ-feeding increases the severity of demyelination and behavioural outcomes. For example, dose dependent vulnerability was found with regard to demyelination in the optic nerve where visual disturbances were evident only when feeding was continued over 5–6 weeks (Namekata et al., 2014). Rat studies have suggested that increased doses (0.5–2%) of CPZ are required to produce comparable pathological (e.g. demyelination and gliosis) and behavioural changes than those are seen in mice (Adamo et al., 2006; Love, 1988; Oakden et al., 2017; Serra-de-Oliveira et al., 2015). Similarly, in guinea pigs, 1% CPZ caused demyelination in brain and cerebellum following 20 weeks of feeding (Carlton, 1969) whereas no behavioural changes, demyelination, or inflammation were observed in cynomolgus monkeys when treated with 3% CPZ for 18 weeks (Chen et al., 2015). Whether such variations in dose response and the extent of demyelination, which would seem to correlate with animal size, would persist if CPZ was administered as a fixed dose (e.g. oral gavage) based on body weight remains untested.

6.3. Regional variabilities in CPZ-induced demyelination and behavioural outcomes

The magnitude of CPZ-mediated oligodendrocytosis is not equally distributed in the CNS. CPZ causes extensive oligodendrocytosis and demyelination in different parts of the cerebrum (e.g. corpus callosum, cerebral cortex, basal ganglia and hippocampus) and cerebellum (Goldberg et al., 2015; Groebe et al., 2009; Gudi et al., 2014, 2009; Skripuletz et al., 2010a; Yang et al., 2009) with limited, if any, evidence

in the brainstem (Jurevics et al., 2002) and spinal cord (Herder et al., 2011). Clearly, this regional variability may affect behavioural phenotypes. For example, it has been shown that the demyelination and gliosis in the spinal cord after induction of EAE is associated with neuropathic pain symptoms (Duffy et al., 2016; Lu et al., 2012; Schmitz et al., 2014) whereas only one paper has reported limited pathological changes in the spinal cord of CPZ-fed animals (Herder et al., 2011). The causes of such regional variability are unknown. Despite equivalent CPZ-induced inhibition of mitochondrial functions in both corpus callosum and spinal cord, the spinal cord is not demyelinated whereas the corpus callosum is highly affected (Acs et al., 2013), suggesting that additional factors determine the sensitivity of these structures in relation to oligodendrocytosis (Sperber et al., 2001; Vallstedt et al., 2005). One such factor may be the uneven distribution of different OLG subtypes in the CNS which could contribute to the regional variability of OLG loss. Amongst the four different subtypes of OLG, types I and II are most abundant in cerebrum and cerebellum whereas types III and IV are mainly found in the brainstem and spinal cord (Butt et al., 1995; Ferrer, 2018; Simons and Nave, 2015). Perhaps CPZ is highly toxic to type I and II OLG but less so to III and IV. In one study, the increased degeneration of type I OLG was reported in the cortex suggesting toxicity in this select subpopulation (Blakemore, 1972). However, the effect on other subtypes, especially OLG types III and IV which are mainly present in the brainstem and spinal cord, remains untested. Likewise, type IV is more Schwann cell-like and there is no evidence of CPZ affecting peripheral neurons. Moreover, age and regional variabilities of the distribution of OPC in the CNS may contribute to the de- and remyelination pattern during and following CPZ toxicity (Spitzer et al., 2019). Furthermore, altered gene expression may increase the susceptibility of one area over another to injury. For example, the reduction of expression of the Fyn gene, a member of the Src non-receptor tyrosine protein kinase family, promotes oligodendrocytosis. Fyn knockout mice showed a massive loss of OLG in the corpus callosum and optic nerve whereas the spinal cord remained unaffected (Sperber et al., 2001) suggesting regional differences in the regulation of OLG that underpins their susceptibility to CPZ.

6.4. Sample size, time and frequency of tests

Adequate power calculations to determine the correct sample size for an experiment is an important factor which is often overlooked in order to reduce the inherent variability between individuals (Charan and Kantharia, 2013; Crawley and Paylor, 1997; Dell et al., 2002). In CPZ studies, sample sizes varied from 4 to 20, with most studies using 10–15 mice/group (Chang et al., 2017; Hagemeyer et al., 2012; Hibbits et al., 2009; Liebetanz and Merkler, 2006; Makinodan et al., 2009; Tezuka et al., 2013; Xu et al., 2011). Likewise, the choice of the correct statistical test is also important. Variables between two groups require a simple unpaired *t*-test whereas in the case of multiple variables (e.g. age, gender, strain and different time points), analysis of variance or multivariate analysis of variance should be used with appropriate post hoc tests, such as Newman-Keuls or Tukey, which correct for multiple comparisons between groups based on parametric or non-parametric variables. In addition, experimental blinding (i.e. the analyst is unaware of the identity of the different experimental groups) during behavioural testing is essential to avoid experimental bias and to increase the reliability of data acquisition and analysis (Hånell and Marklund, 2014). Moreover, behavioural studies should report baseline data prior to CPZ-feeding to gauge any potential differences between animals assigned to the experimental vs. the naïve age-matched controls. In some CPZ studies, acquisition of base line data (Abakumova et al., 2015; Hibbits et al., 2009; Mierzwa et al., 2013) and a blinded strategy (Cui et al., 2018; Franco-Pons et al., 2007; Hagemeyer et al., 2012; Omotoso et al., 2018; Serra-de-Oliveira et al., 2015) were followed whereas the remaining behavioural studies did not report these details (Adilijiang et al., 2015; Chang et al., 2017; Dutta et al., 2013; Elbaz et al., 2018; Faizi et al., 2016; Hashimoto et al., 2017; Iwasa et al., 2014; Li et al., 2015; Liebetanz and Merkler, 2006; Makinodan et al., 2009; Manrique-Hoyos et al., 2012; Murakami et al., 2017; Ray et al., 2017; Sanadgol et al., 2018; Shao et al., 2015; Skripuletz et al., 2015; Skripuletz et al., 2010b; Sun et al., 2017; Tezuka et al., 2013; Torkildsen et al., 2009; Vakilzadeh et al., 2016; Wang et al., 2013, 2015; Wang et al., 2016; Xiao et al., 2008; Xu et al., 2010, 2009; Yamamoto et al., 2014, 2017; Ye et al., 2013; Yu et al., 2018; Zhang et al., 2016; Zheng et al., 2017; Zimmermann et al., 2018).

Behaviour experiments in laboratory rodents are usually carried out in day time. Rodents are nocturnal animals and so training during the day may influence behavioural results, especially if behaviour is not performed at the same time in each trial. For example, Dilute, Brown and non-Agouti mice showed reductions in activities such as rearing, locomotion and food foraging, and increased cognitive deficits during day time vs. night time testing (Roedel et al., 2006). However, testing behaviour early or late in the day might create variability due to waking up or tiredness/preparation for sleep. With CPZ, some tests (e.g. complex wheel) were conducted over the entire light-dark cycle (Hibbits et al., 2009; Liebetanz and Merkler, 2006; Manrique-Hoyos et al., 2012; Mierzwa et al., 2013) or confined to either of the dark (Makinodan et al., 2009) or light phase (Franco-Pons et al., 2007). However, these differences have not been systematically addressed in the CPZ model.

Lastly, multiple tests can affect the physical condition of the test animals and so influence results (Hånell and Marklund, 2014). For example, physical tests (e.g. wheel running and open field) followed by fear conditioning resulted in increased freezing/immobility behaviour compared to naïve fear conditioning, suggesting tiredness/fatigue of the animal (Hopkins and Bucci, 2010). It is recommended either to extend the time between tests or perform tests in the order of least stressful to most stressful. Moreover, instead of using multiple instruments, multiple behaviours can be measured using one instrument. For example, a modified hole board method can be used in which moveable lids cover the holes to make flat central areas similar to the open field apparatus. The measurement of anxiety, cognition and locomotion can then be carried out using one instrument (Ohl and Keck, 2003). This seems never to have been assessed in CPZ or EAE studies.

7. Conclusions

In addition to demyelination and gliosis in the CNS, there are a variety of clinical symptoms associated with human MS including problems with motor function, pain, fatigue, cognition, vision, depression, sleep, anxiety and seizures. To translate neuroscience research from 'bench-to-bedside-to-community,' appropriate animal behavioural assays are critical to identifying early markers of disease onset and to evaluate the effectiveness of therapeutics in preventing disease or resolving established disease states. This review highlights the similarities and differences between behavioural assessments and histopathology in CPZ-fed animal models versus the clinical symptoms seen in MS patients, with reference also to the EAE model. Despite the apparent tendency in the literature to anthropomorphize such test results to human clinical symptoms, one must remain cognizant of species differences and thus the inherent assumptions and limitations of such assessments in animal models. However, since CPZ is extensively used to model demyelination and remyelination, events commonly associated with MS, the detailed behavioural phenotypes associated with this model must be examined rigorously using appropriate quantitative tests. Therefore, from the current review we conclude that:

- Although CPZ-feeding has been used to investigate demyelination and gliosis in the CNS since the 1960s surprisingly few studies have assessed its effects on behaviour and these not been systematically, or critically, reviewed.
- Motor behaviour is the most commonly assessed parameter (and the

most common MS symptom) during CPZ-feeding, but the choice of test is important in order to identify potential changes. Complexity allows subtle deficits to be detected earlier, in otherwise pre-symptomatic animals and so tests like the ladder crossing and complex wheel tests are recommended. However, these tests are subject to cognitive confounders and it may not be possible to fully separate the apparent motor deficits from cognitive impairment purely on the basis of current behavioural criteria.

- There is a clear mismatch between the most commonly reported symptoms in MS such as pain and fatigue and the most commonly used behavioural tests of CPZ-fed animals (e.g. anxiety and cognition, see **Table 2**).
- Anxiety is the second most commonly measured behavioural parameter in CPZ-fed animals (Table 2). However, due to the multiple aspects inherent to anxiety, the selection of an appropriate test and the assessment of multiple parameters are important. The open field test is recommended for the initial screening for anxiety-like behaviour and locomotor deficits followed by assessment of multiple parameters using the elevated plus maze apparatus (see Table 3).
- Assessment of cognitive function is the third most common behavioural test. The Y-maze and novel object recognition tests are recommended due to their reproducibility across different labs, measurement of multiple parameters (e.g. spatial and recognition memory), and that they are not confounded by other factors such as water-induced stress such as associated with the Morris water maze.
- Since CPZ-fed animals are more active (e.g. increased locomotion, climbing and rearing) and have increased levels of stress hormones (e.g. corticosterone) and neurotransmitters (e.g. dopamine), these confound the use of current tests such as forced swim, tail suspension, sucrose preference, upside down grid and voluntary wheel running for assessing depression and fatigue-like behaviour.
- A better understanding of the interactions between multiple symptoms (e.g. depression, fatigue, pain, visual disturbances, sleep and epileptic seizure) is needed to determine whether there is a direct effect of CPZ-feeding on specific systems or whether these conditions are secondary to its broad range of action.
- In order to resolve the contributions of CPZ-induced demyelination to possible behavioural deficits, quantitative histopathological and/or biochemical assays of functionally relevant CNS areas and pathways are crucial to clarify their individual contributions rather than just using the corpus callosum as a proxy of dysfunction.

Author's contribution

MKS, DAM, JRC and PJS designed the scope of the review. MKS drafted the original manuscript, designed tables and figures. DAM, JRC and PJS critically reviewed the drafts. All authors approved the final version.

Declaration of Competing Interest

The authors have declared no conflict of interest.

Acknowledgements

We thank to the Rotary Club of Narellan for funding the Western Sydney University-Multiple Sclerosis Research Project.

References

Abakumova, T.O., Kuz'kina, A.A., Zharova, M.E., Pozdeeva, D.A., Gubskii, I.L., Shepeleva, I.I., Antonova, O.M., Nukolova, N.V., Kekelidze, Z.I., Chekhonin, V.P., 2015. Cuprizone model as a tool for preclinical studies of the efficacy of multiple sclerosis diagnosis and therapy. Bull. Exp. Biol. Med. 159, 111–115.

Abdelhak, A., Weber, M.S., Tumani, H., 2017. Primary progressive multiple sclerosis: putting together the puzzle. Front. Neurol. 8, 234.

Abe, H., Tanaka, T., Kimura, M., Mizukami, S., Saito, F., Imatanaka, N., Akahori, Y., Yoshida, T., Shibutani, M., 2015. Cuprizone decreases intermediate and late-stage progenitor cells in hippocampal neurogenesis of rats in a framework of 28-day oral dose toxicity study. Toxicol. Appl. Pharmacol. 287, 210–221.

Abe, M., Tsuchiya, K., Kurosa, Y., Nakai, O., Shinomiya, K., 2000. Multiple sclerosis with very late onset: a report of a case with onset at age 82 years and review of the literature. J. Spinal Disord. 13, 545–549.

Acharjee, S., Nayani, N., Tsutsui, M., Hill, M.N., Ousman, S.S., Pittman, Q.J., 2013. Altered cognitive-emotional behavior in early experimental autoimmune encephalitis–cytokine and hormonal correlates. Brain Behav. Immun. 33, 164–172.

Acs, P., Komoly, S., 2012. Selective ultrastructural vulnerability in the cuprizone-induced experimental demyelination. Ideggyogy. Sz. 65, 266–270.

Acs, P., Selak, M.A., Komoly, S., Kalman, B., 2013. Distribution of oligodendrocyte loss and mitochondrial toxicity in the cuprizone-induced experimental demyelination model. J. Neuroimmunol. 262, 128–131.

Adamo, A.M., Paez, P.M., Escobar Cabrera, O.E., Wolfson, M., Franco, P.G., Pasquini, J.M., Soto, E.F., 2006. Remyelination after cuprizone-induced demyelination in the rat is stimulated by apotransferrin. Exp. Neurol. 198, 519–529.

Adilijiang, A., Guan, T., He, J., Hartle, K., Wang, W., Li, X., 2015. The protective effects of Areca catechu extract on cognition and social interaction deficits in a cuprizone-induced demyelination model. Evidence-based complementary and alternative medicine: eCAM 2015, 426092.

Ahn, D.K., Jung, C.Y., Lee, H.J., Choi, H.S., Ju, J.S., Bae, Y.C., 2004. Peripheral glutamate receptors participate in interleukin-1beta-induced mechanical allodynia in the orofacial area of rats. Neurosci. Lett. 357, 203–206.

Alhola, P., Polo-Kantola, P., 2007. Sleep deprivation: impact on cognitive performance. Neuropsychiatr. Dis. Treat. 3, 553–567.

Allen, A.N., Seminog, O.O., Goldacre, M.J., 2013. Association between multiple sclerosis and epilepsy: large population-based record-linkage studies. BMC Neurol. 13, 189.

Anisman, H., McIntyre, D.C., 2002. Conceptual, spatial, and cue learning in the Morris water maze in fast or slow kindling rats: attention deficit comorbidity. The Journal of neuroscience: the official journal of the Society for Neuroscience 22, 7809–7817.

Araujo, S.E.S., Mendonca, H.R., Wheeler, N.A., Campello-Costa, P., Jacobs, K.M., Gomes, F.C.A., Fox, M.A., Fuss, B., 2017. Inflammatory demyelination alters subcortical visual circuits. J. Neuroinflammation 14, 162.

Arrant, A.E., Schramm-Sapyta, N.L., Kuhn, C.M., 2013. Use of the light/dark test for anxiety in adult and adolescent male rats. Behav. Brain Res. 256, 119–127.

Aryanpour, R., Pasbakhsh, P., Zibara, K., Namjoo, Z., Beigi Boroujeni, F., Shahbeigi, S., Kashani, I.R., Beyer, C., Zendehdel, A., 2017. Progesterone therapy induces an M1 to M2 switch in microglia phenotype and suppresses NLRP3 inflammasome in a cuprizone-induced demyelination mouse model. Int. Immunopharmacol. 51, 131–139.

Attarian, H.P., Brown, K.M., Duntley, S.P., Carter, J.D., Cross, A.H., 2004. The relationship of sleep disturbances and fatigue in multiple sclerosis. Arch. Neurol. 61, 525–528.

Ayatollahi, A.M., Haji Molla Hoseini, M., Ghanadian, S.M., Kosari-Nasab, M., Mami, F., Yazdiniapoure, Z., Zolfaghari, B., Salari, A.A., 2017. TAMEC: a new analogue of cyclomyrsinol diterpenes decreases anxiety- and depression-like behaviors in a mouse model of multiple sclerosis. Neurol. Res. 39, 1056–1065.

Azami Tameh, A., Clarner, T., Beyer, C., Atlasi, M.A., Hassanzadeh, G., Naderian, H., 2013. Regional regulation of glutamate signaling during cuprizone-induced demyelination in the brain. Ann. Anat. 195, 415–423.

Bagchi, B., Al-Sabi, A., Kaza, S., Scholz, D., O'Leary, V.B., Dolly, J.O., Ovsepian, S.V., 2014. Disruption of myelin leads to ectopic expression of K(V)1.1 channels with abnormal conductivity of optic nerve axons in a cuprizone-induced model of demyelination. PLoS One 9, e87736.

Balcer, L.J., Miller, D.H., Reingold, S.C., Cohen, J.A., 2015. Vision and vision-related outcome measures in multiple sclerosis. Brain 138, 11–27.

Ball, S.L., Petry, H.M., 2000. Noninvasive assessment of retinal function in rats using multifocal electroretinography. Invest. Ophthalmol. Vis. Sci. 41, 610–617.

Barnett, M.H., Prineas, J.W., 2004. Relapsing and remitting multiple sclerosis: pathology of the newly forming lesion. Ann. Neurol. 55, 458–468.

Barnhart, C.D., Yang, D., Lein, P.J., 2015. Using the Morris water maze to assess spatial learning and memory in weanling mice. PLoS One 10, e0124521.

Barrot, M., 2012. Tests and models of nociception and pain in rodents. Neuroscience 211, 39–50.

Bastianini, S., Alvente, S., Berteotti, C., Lo Martire, V., Silvani, A., Swoap, S.J., Valli, A., Zoccoli, G., Cohen, G., 2017. Accurate discrimination of the wake-sleep states of mice using non-invasive whole-body plethysmography. Sci. Rep. 7, 41698.

Beiske, A.G., Svensson, E., Sandanger, I., Czujko, B., Pedersen, E.D., Aarseth, J.H., Myhr, K.M., 2008. Depression and anxiety amongst multiple sclerosis patients. Eur. J. Neurol. 15, 239–245.

Benardais, K., Kotsiari, A., Skuljec, J., Koutsoudaki, P.N., Gudi, V., Singh, V., Vulinovic, F., Skripuletz, T., Stangel, M., 2013. Cuprizone [bis(cyclohexylidenehydrazide)] is selectively toxic for mature oligodendrocytes. Neurotox. Res. 24, 244–250.

Benedict, R.H., Holtzer, R., Motl, R.W., Foley, F.W., Kaur, S., Hojnacki, D., Weinstock-Guttman, B., 2011. Upper and lower extremity motor function and cognitive impairment in multiple sclerosis. Journal of the International Neuropsychological Society: JINS 17, 643–653.

Benetti, F., Ventura, M., Salmini, B., Ceola, S., Carbonera, D., Mammi, S., Zitolo, A., D'Angelo, P., Urso, E., Maffia, M., Salvato, B., Spisni, E., 2010. Cuprizone neurotoxicity, copper deficiency and neurodegeneration. Neurotoxicology 31, 509–517.

Bergstrom, R.A., Choi, J.H., Manduca, A., Shin, H.S., Worrell, G.A., Howe, C.L., 2013. Automated identification of multiple seizure-related and interictal epileptiform event types in the EEG of mice. Sci. Rep. 3, 1483.

Bermel, R.A., Balcer, L.J., 2013. Optic neuritis and the evaluation of visual impairment in multiple sclerosis. Continuum (Minneapolis, Minn.) 19, 1074–1086.

Bernard, C.C., Kerlero de Rosbo, N., 1992. Multiple sclerosis: an autoimmune disease of

multifactorial etiology. Curr. Opin. Immunol. 4, 760–765.
Bjelobaba, I., Begovic-Kupresanin, V., Pekovic, S., Lavrnja, I., 2018. Animal models of multiple sclerosis: focus on experimental autoimmune encephalomyelitis. J. Neurosci. Res. 96, 1021–1042.
Blakemore, W.F., 1972. Observations on oligodendrocyte degeneration, the resolution of status spongiosus and remyelination in cuprizone intoxication in mice. J. Neurocytol. 1, 413–426.
Blakemore, W.F., 1973. Demyelination of the superior cerebellar peduncle in the mouse induced by cuprizone. J. Neurol. Sci. 20, 63–72.
Blakemore, W.F., 1974. Remyelination of the superior cerebellar peduncle in old mice following demyelination induced by cuprizone. J. Neurol. Sci. 22, 121–126.
Blakemore, W.F., Irvine, K.A., 2008. Endogenous or exogenous oligodendrocytes for remyelination. J. Neurol. Sci. 265, 43–46.
Bolcskei, K., Kriszta, G., Saghy, E., Payrits, M., Sipos, E., Vranesics, A., Berente, Z., Abraham, H., Acs, P., Komoly, S., Pinter, E., 2018. Behavioural alterations and morphological changes are attenuated by the lack of TRPA1 receptors in the cuprizone-induced demyelination model in mice. J. Neuroimmunol. 320, 1–10.
Bonito-Oliva, A., Masini, D., Fisone, G., 2014. A mouse model of non-motor symptoms in Parkinson's disease: focus on pharmacological interventions targeting affective dysfunctions. Front. Behav. Neurosci. 8.
Bourin, M., Hascoet, M., 2003. The mouse light/dark box test. Eur. J. Pharmacol. 463, 55–65.
Braley, T.J., Chervin, R.D., 2010. Fatigue in multiple sclerosis: mechanisms, evaluation, and treatment. Sleep 33, 1061–1067.
Braley, T.J., Segal, B.M., Chervin, R.D., 2014. Obstructive sleep apnea and fatigue in patients with multiple sclerosis. J. Clin. Sleep Med. 10, 155–162.
Brambilla, R., Morton, P.D., Ashbaugh, J.J., Karmally, S., Lambertsen, K.L., Bethea, J.R., 2014. Astrocytes play a key role in EAE pathophysiology by orchestrating in the CNS the inflammatory response of resident and peripheral immune cells and by suppressing remyelination. Glia 62, 452–467.
Brass, S.D., Duquette, P., Proulx-Therrien, J., Auerbach, S., 2010. Sleep disorders in patients with multiple sclerosis. Sleep Med. Rev. 14, 121–129.
Brenner, P., Granqvist, M., Konigsson, J., Al Nimer, F., Piehl, F., Jokinen, J., 2018. Depression and fatigue in multiple sclerosis: relation to exposure to violence and cerebrospinal fluid immunomarkers. Psychoneuroendocrinology 89, 53–58.
Broadbent, N.J., Gaskin, S., Squire, L.R., Clark, R.E., 2010. Object recognition memory and the rodent hippocampus. Learn. Mem. 17, 5–11.
Burfeind, K.G., Yadav, V., Marks, D.L., 2016. Hypothalamic dysfunction and multiple sclerosis: implications for fatigue and weight dysregulation. Curr. Neurol. Neurosci. Rep. 16, 98.
Burns, M.N., Nawacki, E., Kwasny, M.J., Pelletier, D., Mohr, D.C., 2014. Do positive or negative stressful events predict the development of new brain lesions in people with multiple sclerosis? Psychol. Med. 44, 349–359.
Butt, A.M., Ibrahim, M., Ruge, F.M., Berry, M., 1995. Biochemical subtypes of oligodendrocyte in the anterior medullary velum of the rat as revealed by the monoclonal antibody Rip. Glia 14, 185–197.
Byatt, N., Rothschild, A.J., Riskind, P., Ionete, C., Hunt, A.T., 2011. Relationships between multiple sclerosis and depression. J. Neuropsychiatry Clin. Neurosci. 23, 198–200.
Calabrese, M., Castellaro, M., Bertoldo, A., De Luca, A., Pizzini, F.B., Ricciardi, G.K., Pitteri, M., Zimatore, S., Magliozzi, R., Benedetti, M.D., Manganotti, P., Montemezzi, S., Reynolds, R., Gajofatto, A., Monaco, S., 2017. Epilepsy in multiple sclerosis: the role of temporal lobe damage. Mult. Scler. 23, 473–482.
Cameron, M.H., Horak, F.B., Herndon, R.R., Bourdette, D., 2008. Imbalance in multiple sclerosis: a result of slowed spinal somatosensory conduction. Somatosens. Mot. Res. 25, 113–122.
Cammer, W., 1999. The neurotoxicant, cuprizone, retards the differentiation of oligodendrocytes in vitro. J. Neurol. Sci. 168, 116–120.
Campos, A.C., Fogaca, M.V., Aguiar, D.C., Guimaraes, F.S., 2013. Animal models of anxiety disorders and stress. Revista brasileira de psiquiatria (Sao Paulo, Brazil: 1999) 35 (Suppl. 2), S101–111.
Caprariello, A.V., Rogers, J.A., Morgan, M.L., Hoghooghi, V., Plemel, J.R., Koebel, A., Tsutsui, S., Dunn, J.F., Kotra, L.P., Ousman, S.S., Wee Yong, V., Stys, P.K., 2018. Biochemically altered myelin triggers autoimmune demyelination. Proc. Natl. Acad. Sci. U.S.A. 115, 5528–5533.
Carlton, W.W., 1966. Response of mice to the chelating agents sodium diethyldithiocarbamate, alpha-benzoinoxime, and biscyclohexanone oxaldihydrazone. Toxicol. Appl. Pharmacol. 8, 512–521.
Carlton, W.W., 1967. Studies on the induction of hydrocephalus and spongy degeneration by cuprizone feeding and attempts to antidote the toxicity. Life Sci. 6, 11–19.
Carlton, W.W., 1969. Spongiform encephalopathy induced in rats and guinea pigs by cuprizone. Exp. Mol. Pathol. 10, 274–287.
Carnicka, Z., Kollar, B., Siarnik, P., Krizova, L., Klobucnikova, K., Turcani, P., 2015. Sleep disorders in patients with multiple sclerosis. J. Clin. Sleep Med. 11, 553–557.
Carola, V., D'Olimpio, F., Brunamonti, E., Mangia, F., Renzi, P., 2002. Evaluation of the elevated plus-maze and open-field tests for the assessment of anxiety-related behaviour in inbred mice. Behav. Brain Res. 134, 49–57.
Castagne, V., Moser, P., Roux, S., Porsolt, R.D., 2011. Rodent models of depression: forced swim and tail suspension behavioral despair tests in rats and mice. Curr. Protoc. Neurosci Chapter 8: Unit 8 10A.
Cattaneo, D., De Nuzzo, C., Fascia, T., Macalli, M., Pisoni, I., Cardini, R., 2002. Risks of falls in subjects with multiple sclerosis. Arch. Phys. Med. Rehabil. 83, 864–867.
Chang, H., Liu, J., Zhang, Y., Wang, F., Wu, Y., Zhang, L., Ai, H., Chen, G., Yin, L., 2017. Increased central dopaminergic activity might be involved in the behavioral abnormality of cuprizone exposure mice. Behav. Brain Res. 331, 143–150.
Chaouloff, F., Durand, M., Mormede, P., 1997. Anxiety- and activity-related effects of diazepam and chlordiazepoxide in the rat light/dark and dark/light tests. Behav. Brain Res. 85, 27–35.
Chaplan, S.R., Bach, F.W., Pogrel, J.W., Chung, J.M., Yaksh, T.L., 1994. Quantitative assessment of tactile allodynia in the rat paw. J. Neurosci. Methods 53, 55–63.
Charan, J., Kantharia, N.D., 2013. How to calculate sample size in animal studies? J. Pharmacol. Pharmacother. 4, 303–306.
Chaudhuri, A., Behan, P.O., 2004. Multiple sclerosis is not an autoimmune disease. Arch. Neurol. 61, 1610–1612.
Chen, C.C., Gilmore, A., Zuo, Y., 2014. Study motor skill learning by single-pellet reaching tasks in mice. Journal of visualized experiments: JoVE.
Chen, Z., Chen, J.T., Johnson, M., Gossman, Z.C., Hendrickson, M., Sakaie, K., Martinez-Rubio, C., Gale, J.T., Trapp, B.D., 2015. Cuprizone does not induce CNS demyelination in nonhuman primates. Ann. Clin. Transl. Neurol. 2, 208–213.
Chew, D.J., Murrell, K., Carlstedt, T., Shortland, P.J., 2013. Segmental spinal root avulsion in the adult rat: a model to study avulsion injury pain. J. Neurotrauma 30, 160–172.
Chomiak, T., Block, E.W., Brown, A.R., Teskey, G.C., Hu, B., 2016. Development and testing of a new system for assessing wheel-running behaviour in rodents. BMC Res. Notes 9, 262.
Chu, F., Shi, M., Zheng, C., Shen, D., Zhu, J., Zheng, X., Cui, L., 2018. The roles of macrophages and microglia in multiple sclerosis and experimental autoimmune encephalomyelitis. J. Neuroimmunol. 318, 1–7.
Clanet, M., 2008. Jean-Martin Charcot. 1825 to 1893. Int. MS J. 15, 59–61.
Clarner, T., Janssen, K., Nellessen, L., Stangel, M., Skripuletz, T., Krauspe, B., Hess, F.M., Denecke, B., Beutner, C., Linnartz-Gerlach, B., Neumann, H., Vallieres, L., Amor, S., Ohl, K., Tenbrock, K., Beyer, C., Kipp, M., 2015. CXCL10 triggers early microglial activation in the cuprizone model. Journal of immunology (Baltimore, Md.: 1950) 194, 3400–3413.
Comber, L., Galvin, R., Coote, S., 2017. Gait deficits in people with multiple sclerosis: a systematic review and meta-analysis. Gait Posture 51, 25–35.
Compston, A., Coles, A., 2008. Multiple sclerosis. Lancet (London, England) 372, 1502–1517.
Confavreux, C., Vukusic, S., Adeleine, P., 2003. Early clinical predictors and progression of irreversible disability in multiple sclerosis: an amnesic process. Brain: a journal of neurology 126, 770–782.
Constantinescu, C.S., Farooqi, N., O'Brien, K., Gran, B., 2011. Experimental autoimmune encephalomyelitis (EAE) as a model for multiple sclerosis (MS). Br. J. Pharmacol. 164, 1079–1106.
Costello, F., 2016. Vision disturbances in multiple sclerosis. Semin. Neurol. 36, 185–195.
Crawley, J.N., 1985. Exploratory behavior models of anxiety in mice. Neurosci. Biobehav. Rev. 9, 37–44.
Crawley, J.N., 2008. Behavioral phenotyping strategies for mutant mice. Neuron 57, 809–818.
Crawley, J.N., Paylor, R., 1997. A proposed test battery and constellations of specific behavioral paradigms to investigate the behavioral phenotypes of transgenic and knockout mice. Horm. Behav. 31, 197–211.
Croxford, A.L., Kurschus, F.C., Waisman, A., 2011. Mouse models for multiple sclerosis: historical facts and future implications. Biochim. Biophys. Acta 1812, 177–183.
Cui, C., Wang, J., Mullin, A.P., Caggiano, A.O., Parry, T.J., Colburn, R.W., Pavlopoulos, E., 2018. The antibody rHIgM22 facilitates hippocampal remyelination and ameliorates memory deficits in the cuprizone mouse model of demyelination. Brain Res. 1694, 73–86.
D'Ambrosio, A., Pagani, E., Riccitelli, G.C., Colombo, B., Rodegher, M., Falini, A., Comi, G., Filippi, M., Rocca, M.A., 2017. Cerebellar contribution to motor and cognitive performance in multiple sclerosis: an MRI sub-regional volumetric analysis. Mult. Scler. 23, 1194–1203.
Damjanovic, D., Valsasina, P., Rocca, M.A., Stromillo, M.L., Gallo, A., Enzinger, C., Hulst, H.E., Rovira, A., Muhlert, N., De Stefano, N., Bisecco, A., Fazekas, F., Arevalo, M.J., Yousry, T.A., Filippi, M., 2017. Hippocampal and deep gray matter nuclei atrophy is relevant for explaining cognitive impairment in MS: a multicenter study. AJNR Am. J. Neuroradiol. 38, 18–24.
De, A.K., Subramanian, M., 1982. Effect of cuprizone feeding on hepatic superoxide dismutase and cytochrome oxidase activities in mice. Experientia 38, 784–785.
Deacon, R.M., 2013. Measuring motor coordination in mice. Journal of visualized experiments: JoVE e2609.
Dell, R.B., Holleran, S., Ramakrishnan, R., 2002. Sample size determination. ILAR J. 43, 207–213.
Deuis, J.R., Dvorakova, L.S., Vetter, I., 2017. Methods used to evaluate pain behaviors in rodents. Front. Mol. Neurosci. 10, 284.
Deuis, J.R., Vetter, I., 2016. The thermal probe test: a novel behavioral assay to quantify thermal paw withdrawal thresholds in mice. Temperature Austin (Austin) 3, 199–207.
Diehl, D.J., Gershon, S., 1992. The role of dopamine in mood disorders. Compr. Psychiatry 33, 115–120.
Disanto, G., Morahan, J.M., Barnett, M.H., Giovannoni, G., Ramagopalan, S.V., 2012. The evidence for a role of B cells in multiple sclerosis. Neurology 78, 823–832.
Dobryakova, E., Genova, H.M., DeLuca, J., Wylie, G.R., 2015. The dopamine imbalance hypothesis of fatigue in multiple sclerosis and other neurological disorders. Front. Neurol. 6, 52.
Doucette, J.R., Jiao, R., Nazarali, A.J., 2010. Age-related and cuprizone-induced changes in myelin and transcription factor gene expression and in oligodendrocyte cell densities in the rostral corpus callosum of mice. Cell. Mol. Neurobiol. 30, 607–629.
Draxler, P., Honsek, S.D., Forsthuber, L., Hadschieff, V., Sandkuhler, J., 2014. VGluT3(+) primary afferents play distinct roles in mechanical and cold hypersensitivity depending on pain etiology. J. Neurosci. 34, 12015–12028.
Duffy, S.S., Perera, C.J., Makker, P.G., Lees, J.G., Carrive, P., Moalem-Taylor, G., 2016.

Peripheral and central neuroinflammatory changes and pain behaviors in an animal model of multiple sclerosis. Front. Immunol. 7, 369.
Dutescu, R.M., Skosyrski, S., Kociok, N., Semkova, I., Mergler, S., Atorf, J., Joussen, A.M., Strauss, O., Kremers, J., 2013. Multifocal ERG recordings under visual control of the stimulated fundus in mice. Invest. Ophthalmol. Vis. Sci. 54, 2582–2589.
Dutra, R.C., Moreira, E.L., Alberti, T.B., Marcon, R., Prediger, R.D., Calixto, J.B., 2013. Spatial reference memory deficits precede motor dysfunction in an experimental autoimmune encephalomyelitis model: the role of kallikrein-kinin system. Brain Behav. Immun. 33, 90–101.
Dutta, R., Chomyk, A.M., Chang, A., Ribaudo, M.V., Deckard, S.A., Doud, M.K., Edberg, D.D., Bai, B., Li, M., Baranzini, S.E., Fox, R.J., Staugaitis, S.M., Macklin, W.B., Trapp, B.D., 2013. Hippocampal demyelination and memory dysfunction are associated with increased levels of the neuronal microRNA miR-124 and reduced AMPA receptors. Ann. Neurol. 73, 637–645.
Ehninger, D., Kempermann, G., 2006. Paradoxical effects of learning the Morris water maze on adult hippocampal neurogenesis in mice may be explained by a combination of stress and physical activity. Genes Brain Behav. 5, 29–39.
Elbaz, E.M., Senousy, M.A., El-Tanbouly, D.M., Sayed, R.H., 2018. Neuroprotective effect of linagliptin against cuprizone-induced demyelination and behavioural dysfunction in mice: a pivotal role of AMPK/SIRT1 and JAK2/STAT3/NF-kappaB signalling pathway modulation. Toxicol. Appl. Pharmacol. 352, 153–161.
Faizi, M., Salimi, A., Seydi, E., Naserzadeh, P., Kouhnavard, M., Rahimi, A., Pourahmad, J., 2016. Toxicity of cuprizone a Cu(2+) chelating agent on isolated mouse brain mitochondria: a justification for demyelination and subsequent behavioral dysfunction. Toxicol. Mech. Methods 26, 276–283.
Fallata, A., Salter, A., Tyry, T., Cutter, G.R., Marrie, R.A., 2017. Trigeminal neuralgia commonly precedes the diagnosis of multiple sclerosis. Int. J. MS Care 19, 240–246.
Farooqi, N., Gran, B., Constantinescu, C.S., 2010. Are current disease-modifying therapeutics in multiple sclerosis justified on the basis of studies in experimental autoimmune encephalomyelitis? J. Neurochem. 115, 829–844.
Ferrer, I., 2018. Oligodendrogliopathy in neurodegenerative diseases with abnormal protein aggregates: the forgotten partner. Prog. Neurobiol. 169, 24–54.
Feyissa, D.D., Aher, Y.D., Engidawork, E., Hoger, H., Lubec, G., Korz, V., 2017. Individual differences in male rats in a behavioral test battery: a multivariate statistical approach. Front. Behav. Neurosci. 11, 26.
Filippi, M., Bar-Or, A., Piehl, F., Preziosa, P., Solari, A., Vukusic, S., Rocca, M.A., 2018. Multiple sclerosis. Nat. Rev. Dis. Primers 4, 43.
Fisher, R.S., van Emde Boas, W., Blume, W., Elger, C., Genton, P., Lee, P., Engel Jr., J., 2005. Epileptic seizures and epilepsy: definitions proposed by the International League Against Epilepsy (ILAE) and the International Bureau for Epilepsy (IBE). Epilepsia 46, 470–472.
Fleming, W.E., Pollak, C.P., 2005. Sleep disorders in multiple sclerosis. Semin. Neurol. 25, 64–68.
Franco-Pons, N., Torrente, M., Colomina, M.T., Vilella, E., 2007. Behavioral deficits in the cuprizone-induced murine model of demyelination/remyelination. Toxicol. Lett. 169, 205–213.
Franklin, R.J., 2002. Why does remyelination fail in multiple sclerosis? Nat. Rev. Neurosci. 3, 705–714.
Frischer, J.M., Bramow, S., Dal-Bianco, A., Lucchinetti, C.F., Rauschka, H., Schmidbauer, M., Laursen, H., Sorensen, P.S., Lassmann, H., 2009. The relation between inflammation and neurodegeneration in multiple sclerosis brains. Brain: a journal of neurology 132, 1175–1189.
Fukui, M., Rodriguiz, R.M., Zhou, J., Jiang, S.X., Phillips, L.E., Caron, M.G., Wetsel, W.C., 2007. Vmat2 heterozygous mutant mice display a depressive-like phenotype. J. Neurosci. 27, 10520–10529.
Gellért, L., Varga, D., 2016. Locomotion activity measurement in an open field for mice. Bioprotocol 6, e1857.
Gentile, A., De Vito, F., Fresegna, D., Musella, A., Buttari, F., Bullitta, S., Mandolesi, G., Centonze, D., 2015. Exploring the role of microglia in mood disorders associated with experimental multiple sclerosis. Front. Cell. Neurosci. 9.
Gentile, A., Fresegna, D., Musella, A., Sepman, H., Bullitta, S., De Vito, F., Fantozzi, R., Usiello, A., Maccarrone, M., Mercuri, N.B., Lutz, B., Mandolesi, G., Centonze, D., 2016. Interaction between interleukin-1beta and type-1 cannabinoid receptor is involved in anxiety-like behavior in experimental autoimmune encephalomyelitis. J. Neuroinflammation 13, 231.
Ghajarzadeh, M., Sahraian, M.A., Fateh, R., Daneshmand, A., 2012. Fatigue, depression and sleep disturbances in Iranian patients with multiple sclerosis. Acta Med. Iran. 50, 244–249.
Gharbawie, O.A., Gonzalez, C.L., Whishaw, I.Q., 2005. Skilled reaching impairments from the lateral frontal cortex component of middle cerebral artery stroke: a qualitative and quantitative comparison to focal motor cortex lesions in rats. Behav. Brain Res. 156, 125–137.
Gilmore, C.P., Bo, L., Owens, T., Lowe, J., Esiri, M.M., Evangelou, N., 2006. Spinal cord gray matter demyelination in multiple sclerosis-a novel pattern of residual plaque morphology. Brain Pathol. 16, 202–208.
Gilmore, C.P., Donaldson, I., Bo, L., Owens, T., Lowe, J., Evangelou, N., 2009. Regional variations in the extent and pattern of grey matter demyelination in multiple sclerosis: a comparison between the cerebral cortex, cerebellar cortex, deep grey matter nuclei and the spinal cord. J. Neurol. Neurosurg. Psychiatr. 80, 182–187.
Gold, R., Linington, C., Lassmann, H., 2006. Understanding pathogenesis and therapy of multiple sclerosis via animal models: 70 years of merits and culprits in experimental autoimmune encephalomyelitis research. Brain 129, 1953–1971.
Gold, S.M., O'Connor, M.F., Gill, R., Kern, K.C., Shi, Y., Henry, R.G., Pelletier, D., Mohr, D.C., Sicotte, N.L., 2014. Detection of altered hippocampal morphology in multiple sclerosis-associated depression using automated surface mesh modeling. Hum. Brain Mapp. 35, 30–37.
Goldberg, J., Clarner, T., Beyer, C., Kipp, M., 2015. Anatomical distribution of cuprizone-induced lesions in C57BL6 mice. J. Mol. Neurosci. 57, 166–175.
Goldenberg, M.M., 2012. Multiple sclerosis review. P T 37, 175–184.
Golli, N.E., Dallagi, Y., Rahali, D., Rejeb, I., Fazaa, S.E., 2016. Neurobehavioral assessment following e-cigarette refill liquid exposure in adult rats. Toxicol. Mech. Methods 26, 435–442.
Grace, P.M., Loram, L.C., Christianson, J.P., Strand, K.A., Flyer-Adams, J.G., Penzkover, K.R., Forsayeth, J.R., van Dam, A.M., Mahoney, M.J., Maier, S.F., Chavez, R.A., Watkins, L.R., 2017. Behavioral assessment of neuropathic pain, fatigue, and anxiety in experimental autoimmune encephalomyelitis (EAE) and attenuation by interleukin-10 gene therapy. Brain Behav. Immun. 59, 49–54.
Gritsch, S., Lu, J., Thilemann, S., Wortge, S., Mobius, W., Bruttger, J., Karram, K., Ruhwedel, T., Blanfeld, M., Vardeh, D., Waisman, A., Nave, K.A., Kuner, R., 2014. Oligodendrocyte ablation triggers central pain independently of innate or adaptive immune responses in mice. Nat. Commun. 5, 5472.
Groebe, A., Clarner, T., Baumgartner, W., Dang, J., Beyer, C., Kipp, M., 2009. Cuprizone treatment induces distinct demyelination, astrocytosis, and microglia cell invasion or proliferation in the mouse cerebellum. Cerebellum 8, 163–174.
Gudi, V., Gingele, S., Skripuletz, T., Stangel, M., 2014. Glial response during cuprizone-induced de- and remyelination in the CNS: lessons learned. Front. Cell. Neurosci. 8, 73.
Gudi, V., Moharregh-Khiabani, D., Skripuletz, T., Koutsoudaki, P.N., Kotsiari, A., Skuljec, J., Trebst, C., Stangel, M., 2009. Regional differences between grey and white matter in cuprizone induced demyelination. Brain Res. 1283, 127–138.
Gulcher, J.R., Vartanian, T., Stefansson, K., 1994. Is multiple sclerosis an autoimmune disease? Clin. Neurosci. 2, 246–252.
Guo, X., Harada, C., Namekata, K., Kikushima, K., Mitamura, Y., Yoshida, H., Matsumoto, Y., Harada, T., 2009. Effect of geranylgeranylacetone on optic neuritis in experimental autoimmune encephalomyelitis. Neurosci. Lett. 462, 281–285.
Guo, X., Harada, C., Namekata, K., Mitamura, Y., Yoshida, H., Matsumoto, Y., Harada, T., 2010. Delayed onset of experimental autoimmune encephalomyelitis in Olig1 deficient mice. PLoS One 5.
Haddadi, R., Nayebi, A.M., Farajniya, S., Brooshghalan, S.E., Sharifi, H., 2014. Silymarin improved 6-OHDA-induced motor impairment in hemi-parkisonian rats: behavioral and molecular study. Daru: journal of Faculty of Pharmacy, Tehran University of Medical Sciences 22, 38.
Hadjimichael, O., Kerns, R.D., Rizzo, M.A., Cutter, G., Vollmer, T., 2007. Persistent pain and uncomfortable sensations in persons with multiple sclerosis. Pain 127, 35–41.
Hagemeyer, N., Boretius, S., Ott, C., Von Streitberg, A., Welpinghus, H., Sperling, S., Frahm, J., Simons, M., Ghezzi, P., Ehrenreich, H., 2012. Erythropoietin attenuates neurological and histological consequences of toxic demyelination in mice. Mol. Med. 18, 628–635.
Hanell, A., Marklund, N., 2014. Structured evaluation of rodent behavioral tests used in drug discovery research. Front. Behav. Neurosci. 8, 252.
Hånell, A., Marklund, N., 2014. Structured evaluation of rodent behavioral tests used in drug discovery research. Front. Behav. Neurosci. 8.
Harbo, H.F., Gold, R., Tintore, M., 2013. Sex and gender issues in multiple sclerosis. Ther. Adv. Neurol. Disord. 6, 237–248.
Harrison, F.E., Hosseini, A.H., McDonald, M.P., 2009. Endogenous anxiety and stress responses in water maze and Barnes maze spatial memory tasks. Behav. Brain Res. 198, 247–251.
Hashimoto, M., Yamamoto, S., Iwasa, K., Yamashina, K., Ishikawa, M., Maruyama, K., Bosetti, F., Yoshikawa, K., 2017. The flavonoid Baicalein attenuates cuprizone-induced demyelination via suppression of neuroinflammation. Brain Res. Bull. 135, 47–52.
Hauser, S.L., Bhan, A.K., Gilles, F., Kemp, M., Kerr, C., Weiner, H.L., 1986. Immunohistochemical analysis of the cellular infiltrate in multiple sclerosis lesions. Ann. Neurol. 19, 578–587.
Haussleiter, I.S., Brune, M., Juckel, G., 2009. Psychopathology in multiple sclerosis: diagnosis, prevalence and treatment. Ther. Adv. Neurol. Disord. 2, 13–29.
He, J., Hsuchou, H., He, Y., Kastin, A.J., Mishra, P.K., Fang, J., Pan, W., 2014a. Leukocyte infiltration across the blood-spinal cord barrier is modulated by sleep fragmentation in mice with experimental autoimmune encephalomyelitis. Fluids Barriers CNS 11, 27.
He, J., Wang, Y., Kastin, A.J., Pan, W., 2014b. Increased sleep fragmentation in experimental autoimmune encephalomyelitis. Brain Behav. Immun. 38, 53–58.
Heckman, K.L., DeCoteau, W., Estevez, A., Reed, K.J., Costanzo, W., Sanford, D., Leiter, J.C., Clauss, J., Knapp, K., Gomez, C., Mullen, P., Rathbun, E., Prime, K., Marini, J., Patchefsky, J., Patchefsky, A.S., Hailstone, R.K., Erlichman, J.S., 2013. Custom cerium oxide nanoparticles protect against a free radical mediated autoimmune degenerative disease in the brain. ACS Nano 7, 10582–10596.
Heier, C.R., DiDonato, C.J., 2009. Translational readthrough by the aminoglycoside geneticin (G418) modulates SMN stability in vitro and improves motor function in SMA mice in vivo. Hum. Mol. Genet. 18, 1310–1322.
Hemm, R.D., Carlton, W.W., Welser, J.R., 1971. Ultrastructural changes of cuprizone encephalopathy in mice. Toxicol. Appl. Pharmacol. 18, 869–882.
Hemmer, B., Kerschensteiner, M., Korn, T., 2015. Role of the innate and adaptive immune responses in the course of multiple sclerosis. Lancet Neurol. 14, 406–419.
Hemond, C.C., Bakshi, R., 2018. Magnetic resonance imaging in multiple sclerosis. Cold Spring Harb. Perspect. Med. 8.
Henderson, A.P., Trip, S.A., Schlottmann, P.G., Altmann, D.R., Garway-Heath, D.F., Plant, G.T., Miller, D.H., 2008. An investigation of the retinal nerve fibre layer in progressive multiple sclerosis using optical coherence tomography. *Brain: a journal of neurology* 131, 277–287.
Herder, V., Hansmann, F., Stangel, M., Skripuletz, T., Baumgartner, W., Beineke, A., 2011. Lack of cuprizone-induced demyelination in the murine spinal cord despite

oligodendroglial alterations substantiates the concept of site-specific susceptibilities of the central nervous system. Neuropathol. Appl. Neurobiol. 37, 676–684.
Herring, N.R., Konradi, C., 2011. Myelin, copper, and the cuprizone model of schizophrenia. Front. Biosci. Schol. Ed. (Schol Ed) 3, 23–40.
Hibbits, N., Pannu, R., Wu, T.J., Armstrong, R.C., 2009. Cuprizone demyelination of the corpus callosum in mice correlates with altered social interaction and impaired bilateral sensorimotor coordination. ASN Neuro 1.
Hibbits, N., Yoshino, J., Le, T.Q., Armstrong, R.C., 2012. Astrogliosis during acute and chronic cuprizone demyelination and implications for remyelination. ASN Neuro 4, 393–408.
Hicks, J.A., Hatzidis, A., Arruda, N.L., Gelineau, R.R., De Pina, I.M., Adams, K.W., Seggio, J.A., 2016. Voluntary wheel-running attenuates insulin and weight gain and affects anxiety-like behaviors in C57BL6/J mice exposed to a high-fat diet. Behav. Brain Res. 310, 1–10.
Hiremath, M.M., Saito, Y., Knapp, G.W., Ting, J.P., Suzuki, K., Matsushima, G.K., 1998. Microglial/macrophage accumulation during cuprizone-induced demyelination in C57BL/6 mice. J. Neuroimmunol. 92, 38–49.
Hoffmann, K., Lindner, M., Groticke, I., Stangel, M., Loscher, W., 2008. Epileptic seizures and hippocampal damage after cuprizone-induced demyelination in C57BL/6 mice. Exp. Neurol. 210, 308–321.
Hoflich, K.M., Beyer, C., Clarner, T., Schmitz, C., Nyamoya, S., Kipp, M., Hochstrasser, T., 2016. Acute axonal damage in three different murine models of multiple sclerosis: a comparative approach. Brain Res. 1650, 125–133.
Hopkins, M.E., Bucci, D.J., 2010. Interpreting the effects of exercise on fear conditioning: the influence of time of day. Behav. Neurosci. 124, 868–872.
Hoppel, C.L., Tandler, B., 1973. Biochemical effects of cuprizone on mouse liver and heart mitochondria. Biochem. Pharmacol. 22, 2311–2318.
Iwasa, K., Yamamoto, S., Takahashi, M., Suzuki, S., Yagishita, S., Awaji, T., Maruyama, K., Yoshikawa, K., 2014. Prostaglandin F2alpha FP receptor inhibitor reduces demyelination and motor dysfunction in a cuprizone-induced multiple sclerosis mouse model. Prostaglandins Leukot. Essent. Fatty Acids 91, 175–182.
Jacobi, A., Loy, K., Schmalz, A.M., Hellsten, M., Umemori, H., Kerschensteiner, M., Bareyre, F.M., 2015. FGF22 signaling regulates synapse formation during post-injury remodeling of the spinal cord. EMBO J. 34, 1231–1243.
Janssens, A.C., Buljevac, D., van Doorn, P.A., van der Meche, F.G., Polman, C.H., Passchier, J., Hintzen, R.Q., 2006. Prediction of anxiety and distress following diagnosis of multiple sclerosis: a two-year longitudinal study. Mult. Scler. 12, 794–801.
Joels, G., Lamprecht, R., 2014. Fear memory formation can affect a different memory: fear conditioning affects the extinction, but not retrieval, of conditioned taste aversion (CTA) memory. Front. Behav. Neurosci. 8, 324.
Jongen, P.J., Ter Horst, A.T., Brands, A.M., 2012. Cognitive impairment in multiple sclerosis. Minerva Med. 103, 73–96.
Jorgensen, S.H., Storm, N., Jensen, P.E., Laursen, H., Sorensen, P.S., 2007. IVIG enters the central nervous system during treatment of experimental autoimmune encephalomyelitis and is localised to inflammatory lesions. Exp. Brain Res. 178, 462–469.
Jurevics, H., Largent, C., Hostettler, J., Sammond, D.W., Matsushima, G.K., Kleindienst, A., Toews, A.D., Morell, P., 2002. Alterations in metabolism and gene expression in brain regions during cuprizone-induced demyelination and remyelination. J. Neurochem. 82, 126–136.
Kale, N., 2016. Optic neuritis as an early sign of multiple sclerosis. Eye Brain 8, 195–202.
Kalueff, A.V., Stewart, A.M., Song, C., Berridge, K.C., Graybiel, A.M., Fentress, J.C., 2016. Neurobiology of rodent self-grooming and its value for translational neuroscience. Nat. Rev. Neurosci. 17, 45–59.
Kamm, C.P., Uitdehaag, B.M., Polman, C.H., 2014. Multiple sclerosis: current knowledge and future outlook. Eur. Neurol. 72, 132–141.
Karl, T., Pabst, R., von Horsten, S., 2003. Behavioral phenotyping of mice in pharmacological and toxicological research. Exp. Toxicol. Pathol. 55, 69–83.
Kelley, B.J., Rodriguez, M., 2009. Seizures in patients with multiple sclerosis: ep iology, pathophysiology and management. CNS Drugs 23, 805–815.
Kelp, A., Koeppen, A.H., Petrasch-Parwez, E., Calaminus, C., Bauer, C., Portal, E., Yu-Taeger, L., Pichler, B., Bauer, P., Riess, O., Nguyen, H.P., 2013. A novel transgenic rat model for spinocerebellar ataxia type 17 recapitulates neuropathological changes and supplies in vivo imaging biomarkers. J. Neurosci. 33, 9068–9081.
Kenner, M., Menon, U., Elliott, D.G., 2007. Multiple sclerosis as a painful disease. Int. Rev. Neurobiol. 79, 303–321.
Keser, Z., Hasan, K.M., Mwangi, B., Younes, K., Khayat-Khoei, M., Kamali, A., Lincoln, J.A., Nelson, F.M., 2018. Quantitative limbic system mapping of main cognitive domains in multiple sclerosis. Front. Neurol. 9.
Khan, A., Kamran, S., Ponirakis, G., Akhtar, N., Khan, R., George, P., Babu, B.M., Ibrahim, F.M., Petropoulos, I.N., Canibano, B.G., Wilins, S.S., Deleu, D., Shuaib, A., Malik, R.A., 2018. Peripheral neuropathy in patients with multiple sclerosis. PLoS One 13, e0193270.
Khan, N., Smith, M.T., 2014. Multiple sclerosis-induced neuropathic pain: pharmacological management and pathophysiological insights from rodent EAE models. Inflammopharmacology 22, 1–22.
Kim, D., Zai, L., Liang, P., Schaffling, C., Ahlborn, D., Benowitz, L.I., 2013. Inosine enhances axon sprouting and motor recovery after spinal cord injury. PLoS One 8, e81948.
Kipp, M., Clarner, T., Dang, J., Copray, S., Beyer, C., 2009. The cuprizone animal model: new insights into an old story. Acta Neuropathol. 118, 723–736.
Kister, I., Bacon, T.E., Chamot, E., Salter, A.R., Cutter, G.R., Kalina, J.T., Herbert, J., 2013. Natural history of multiple sclerosis symptoms. Int. J. MS Care 15, 146–158.
Klein, A., Dunnett, S.B., 2012. Analysis of skilled forelimb movement in rats: the single pellet reaching test and staircase test. Curr. Protoc. Neurosci Chapter 8: Unit8, 28.
Kocovski, P., Dang, P.T., D'Souza, C.S., Stamper, C.E., Hale, M.W., Orian, J.M., 2018. Differential anxiety-like responses in NOD/ShiLtJ and C57BL/6J mice following experimental autoimmune encephalomyelitis induction and oral gavage. Lab. Anim. 52, 470–478.
Kondo, M.A., Fukudome, D., Smith, D.R., Gallagher, M., Kamiya, A., Sawa, A., 2016. Dimensional assessment of behavioral changes in the cuprizone short-term exposure model for psychosis. Neurosci. Res. 107, 70–74.
Korostil, M., Feinstein, A., 2007. Anxiety disorders and their clinical correlates in multiple sclerosis patients. Mult. Scler. 13, 67–72.
Koutsoudaki, P.N., Skripuletz, T., Gudi, V., Moharregh-Khiabani, D., Hildebrandt, H., Trebst, C., Stangel, M., 2009. Demyelination of the hippocampus is prominent in the cuprizone model. Neurosci. Lett. 451, 83–88.
Kremenchutzky, M., Cottrell, D., Rice, G., Hader, W., Baskerville, J., Koopman, W., Ebers, G.C., 1999. The natural history of multiple sclerosis: a geographically based study. 7. Progressive-relapsing and relapsing-progressive multiple sclerosis: a re-evaluation. Brain 122 (Pt 10), 1941–1950.
Krishnamoorthy, G., Wekerle, H., 2009. EAE: an immunologist's magic eye. Eur. J. Immunol. 39, 2031–2035.
Krishnan, V., Nestler, E.J., 2011. Animal models of depression: molecular perspectives. Curr. Top. Behav. Neurosci. 7, 121–147.
Kuc, K.A., Gregersen, B.M., Gannon, K.S., Dodart, J.C., 2006. Holeboard discrimination learning in mice. Genes Brain Behav. 5, 355–363.
Kumar, P., Sharma, G., Gupta, V., Kaur, R., Thakur, K., Malik, R., Kumar, A., Kaushal, N., Raza, K., 2018. Preclinical explorative assessment of dimethyl fumarate-based biocompatible nanolipoidal carriers for the management of multiple sclerosis. ACS Chem. Neurosci. 9, 1152–1158.
Lampron, A., Larochelle, A., Laflamme, N., Prefontaine, P., Plante, M.M., Sanchez, M.G., Yong, V.W., Stys, P.K., Tremblay, M.E., Rivest, S., 2015. Inefficient clearance of myelin debris by microglia impairs remyelinating processes. J. Exp. Med. 212, 481–495.
Langford, D.J., Bailey, A.L., Chanda, M.L., Clarke, S.E., Drummond, T.E., Echols, S., Glick, S., Ingrao, J., Klassen-Ross, T., Lacroix-Fralish, M.L., Matsumiya, L., Sorge, R.E., Sotocinal, S.G., Tabaka, J.M., Wong, D., van den Maagdenberg, A.M., Ferrari, M.D., Craig, K.D., Mogil, J.S., 2010. Coding of facial expressions of pain in the laboratory mouse. Nat. Methods 7, 447–449.
Lapato, A.S., Szu, J.I., Hasselmann, J.P.C., Khalaj, A.J., Binder, D.K., Tiwari-Woodruff, S.K., 2017. Chronic demyelination-induced seizures. Neuroscience 346, 409–422.
Larocca, N.G., 2011. Impact of walking impairment in multiple sclerosis: perspectives of patients and care partners. Patient 4, 189–201.
Lassmann, H., Bradl, M., 2017. Multiple sclerosis: experimental models and reality. Acta Neuropathol. 133, 223–244.
Lassmann, H., Bruck, W., Lucchinetti, C., 2001. Heterogeneity of multiple sclerosis pathogenesis: implications for diagnosis and therapy. Trends Mol. Med. 7, 115–121.
Lassmann, H., van Horssen, J., 2011. The molecular basis of neurodegeneration in multiple sclerosis. FEBS Lett. 585, 3715–3723.
LeDoux, J.E., 2000. Emotion circuits in the brain. Annu. Rev. Neurosci. 23, 155–184.
Leger, M., Quiedeville, A., Bouet, V., Haelewyn, B., Boulouard, M., Schumann-Bard, P., Freret, T., 2013. Object recognition test in mice. Nat. Protoc. 8, 2531–2537.
Lerdal, A., Celius, E.G., Krupp, L., Dahl, A.A., 2007. A prospective study of patterns of fatigue in multiple sclerosis. Eur. J. Neurol. 14, 1338–1343.
Li, Z., He, Y., Fan, S., Sun, B., 2015. Clemastine rescues behavioral changes and enhances remyelination in the cuprizone mouse model of demyelination. Neurosci. Bull. 31, 617–625.
Liblau, R., Fontaine, B., Baron-Van Evercooren, A., Wekerle, H., Lassmann, H., 2001. Demyelinating diseases: from pathogenesis to repair strategies. Trends Neurosci. 24, 134–135.
Liebetanz, D., Merkler, D., 2006. Effects of commissural de- and remyelination on motor skill behaviour in the cuprizone mouse model of multiple sclerosis. Exp. Neurol. 202, 217–224.
Lin, W., Kemper, A., Dupree, J.L., Harding, H.P., Ron, D., Popko, B., 2006. Interferon-gamma inhibits central nervous system remyelination through a process modulated by endoplasmic reticulum stress. Brain 129, 1306–1318.
Linares, D., Taconis, M., Mana, P., Correcha, M., Fordham, S., Staykova, M., Willenborg, D.O., 2006. Neuronal nitric oxide synthase plays a key role in CNS demyelination. J. Neurosci. 26, 12672–12681.
Lindner, M., Fokuhl, J., Linsmeier, F., Trebst, C., Stangel, M., 2009. Chronic toxic demyelination in the central nervous system leads to axonal damage despite remyelination. Neurosci. Lett. 453, 120–125.
Liu, M.Y., Yin, C.Y., Zhu, L.J., Zhu, X.H., Xu, C., Luo, C.X., Chen, H., Zhu, D.Y., Zhou, Q.G., 2018. Sucrose preference test for measurement of stress-induced anhedonia in mice. Nat. Protoc. 13, 1686–1698.
Love, S., 1988. Cuprizone neurotoxicity in the rat: morphologic observations. J. Neurol. Sci. 84, 223–237.
Lu, J., Kurejova, M., Wirotanseng, L.N., Linker, R.A., Kuner, R., Tappe-Theodor, A., 2012. Pain in experimental autoimmune encephalitis: a comparative study between different mouse models. J. Neuroinflammation 9, 233.
Lucchinetti, C., Bruck, W., Parisi, J., Scheithauer, B., Rodriguez, M., Lassmann, H., 2000. Heterogeneity of multiple sclerosis lesions: implications for the pathogenesis of demyelination. Ann. Neurol. 47, 707–717.
Lucchinetti, C.F., Bruck, W., Rodriguez, M., Lassmann, H., 1996. Distinct patterns of multiple sclerosis pathology indicates heterogeneity on pathogenesis. Brain Pathol. 6, 259–274.
Luo, C., Jian, C., Liao, Y., Huang, Q., Wu, Y., Liu, X., Zou, D., Wu, Y., 2017. The role of microglia in multiple sclerosis. Neuropsychiatr. Dis. Treat. 13, 1661–1667.
Mahajan, V.S., Demissie, E., Mattoo, H., Viswanadham, V., Varki, A., Morris, R., Pillai, S., 2016. Striking Immune Phenotypes in Gene-Targeted Mice Are Driven by a Copy-Number Variant Originating from a Commercially Available C57BL/6 Strain. Cell

Rep. 15, 1901–1909.
Majidi-Zolbanin, J., Doosti, M.H., Kosari-Nasab, M., Salari, A.A., 2015. Prenatal maternal immune activation increases anxiety- and depressive-like behaviors in offspring with experimental autoimmune encephalomyelitis. Neuroscience 294, 69–81.
Makinodan, M., Yamauchi, T., Tatsumi, K., Okuda, H., Takeda, T., Kiuchi, K., Sadamatsu, M., Wanaka, A., Kishimoto, T., 2009. Demyelination in the juvenile period, but not in adulthood, leads to long-lasting cognitive impairment and deficient social interaction in mice. Prog. Neuropsychopharmacol. Biol. Psychiatry 33, 978–985.
Manrique-Hoyos, N., Jurgens, T., Gronborg, M., Kreutzfeldt, M., Schedensack, M., Kuhlmann, T., Schrick, C., Bruck, W., Urlaub, H., Simons, M., Merkler, D., 2012. Late motor decline after accomplished remyelination: impact for progressive multiple sclerosis. Ann. Neurol. 71, 227–244.
Markianos, M., Evangelopoulos, M.E., Koutsis, G., Davaki, P., Sfagos, C., 2013. Body mass index in multiple sclerosis: associations with CSF neurotransmitter metabolite levels. ISRN Neurol. 2013, 981070.
Marrie, R.A., Reingold, S., Cohen, J., Stuve, O., Trojano, M., Sorensen, P.S., Cutter, G., Reider, N., 2015. The incidence and prevalence of psychiatric disorders in multiple sclerosis: a systematic review. Mult. Scler. 21, 305–317.
Martin, E.I., Ressler, K.J., Binder, E., Nemeroff, C.B., 2009. The neurobiology of anxiety disorders: brain imaging, genetics, and psychoneuroendocrinology. Psychiatr. Clin. North Am. 32, 549–575.
Mason, J.L., Jones, J.J., Taniike, M., Morell, P., Suzuki, K., Matsushima, G.K., 2000. Mature oligodendrocyte apoptosis precedes IGF-1 production and oligodendrocyte progenitor accumulation and differentiation during demyelination/remyelination. J. Neurosci. Res. 61, 251–262.
Matsushima, G.K., Morell, P., 2001. The neurotoxicant, cuprizone, as a model to study demyelination and remyelination in the central nervous system. Brain Pathol. 11, 107–116.
Matsuura, K., Kabuto, H., Makino, H., Ogawa, N., 1997. Pole test is a useful method for evaluating the mouse movement disorder caused by striatal dopamine depletion. J. Neurosci. Methods 73, 45–48.
Mattiasson, G.J., Philips, M.F., Tomasevic, G., Johansson, B.B., Wieloch, T., McIntosh, T.K., 2000. The rotating pole test: evaluation of its effectiveness in assessing functional motor deficits following experimental head injury in the rat. J. Neurosci. Methods 95, 75–82.
McFarland, H.F., Martin, R., 2007. Multiple sclerosis: a complicated picture of autoimmunity. Nat. Immunol. 8, 913–919.
McKenna, J.T., Cordeira, J.W., Christie, M.A., Tartar, J.L., McCoy, J.G., Lee, E., McCarley, R.W., Strecker, R.E., 2008. Assessing sleepiness in the rat: a multiple sleep latencies test compared to polysomnographic measures of sleepiness. J. Sleep Res. 17, 365–375.
McLaurin, J.A., Yong, V.W., 1995. Oligodendrocytes and myelin. Neurol. Clin. 13, 23–49.
McMahon, E.J., Suzuki, K., Matsushima, G.K., 2002. Peripheral macrophage recruitment in cuprizone-induced CNS demyelination despite an intact blood-brain barrier. J. Neuroimmunol. 130, 32–45.
McTigue, D.M., Tripathi, R.B., 2008. The life, death, and replacement of oligodendrocytes in the adult CNS. J. Neurochem. 107, 1–19.
Meinen, S., Lin, S., Ruegg, M.A., Punga, A.R., 2012. Fatigue and muscle atrophy in a mouse model of myasthenia gravis is paralleled by loss of sarcolemmal nNOS. PLoS One 7, e44148.
Melamud, L., Golan, D., Luboshitzky, R., Lavi, I., Miller, A., 2012. Melatonin dysregulation, sleep disturbances and fatigue in multiple sclerosis. J. Neurol. Sci. 314, 37–40.
Merkler, D., Metz, G.A., Raineteau, O., Dietz, V., Schwab, M.E., Fouad, K., 2001. Locomotor recovery in spinal cord-injured rats treated with an antibody neutralizing the myelin-associated neurite growth inhibitor Nogo-A. J. Neurosci. 21, 3665–3673.
Messori, L., Casini, A., Gabbiani, C., Sorace, L., Muniz-Miranda, M., Zatta, P., 2007. Unravelling the chemical nature of copper cuprizone. Dalton Trans. 2112–2114.
Metz, G.A., Antonow-Schlorke, I., Witte, O.W., 2005. Motor improvements after focal cortical ischemia in adult rats are mediated by compensatory mechanisms. Behav. Brain Res. 162, 71–82.
Mierzwa, A.J., Zhou, Y.X., Hibbits, N., Vana, A.C., Armstrong, R.C., 2013. FGF2 and FGFR1 signaling regulate functional recovery following cuprizone demyelination. Neurosci. Lett. 548, 280–285.
Miller, D.H., Leary, S.M., 2007. Primary-progressive multiple sclerosis. Lancet Neurol. 6, 903–912.
Miller, S.D., Karpus, W.J., 2007. Experimental autoimmune encephalomyelitis in the mouse. Curr. Protoc. Immunol Chapter 15: Unit 15.11.
Mills, R.J., Young, C.A., 2011. The relationship between fatigue and other clinical features of multiple sclerosis. Mult. Scler. 17, 604–612.
Minagar, A., Barnett, M.H., Benedict, R.H., Pelletier, D., Pirko, I., Sahraian, M.A., Frohman, E., Zivadinov, R., 2013. The thalamus and multiple sclerosis: modern views on pathologic, imaging, and clinical aspects. Neurology 80, 210–219.
Mitchell, H.A., Bogenpohl, J.W., Liles, L.C., Epstein, M.P., Bozyczko-Coyne, D., Williams, M., Weinshenker, D., 2008. Behavioral responses of dopamine beta-hydroxylase knockout mice to modafinil suggest a dual noradrenergic-dopaminergic mechanism of action. Pharmacol. Biochem. Behav. 91, 217–222.
Mitra, S., Sameer Kumar, G.S., Tiwari, V., Lakshmi, B.J., Thakur, S.S., Kumar, S., 2016. Implication of Genetic Deletion of Wdr13 in Mice: Mild Anxiety, Better Performance in Spatial Memory Task, with Upregulation of Multiple Synaptic Proteins. Front. Mol. Neurosci. 9, 73.
Moldovan, N., Al-Ebraheem, A., Lobo, L., Park, R., Farquharson, M.J., Bock, N.A., 2015. Altered transition metal homeostasis in the cuprizone model of demyelination. Neurotoxicology 48, 1–8.
Morell, P., Barrett, C.V., Mason, J.L., Toews, A.D., Hostettler, J.D., Knapp, G.W., Matsushima, G.K., 1998. Gene expression in brain during cuprizone-induced demyelination and remyelination. Mol. Cell. Neurosci. 12, 220–227.
Mu, S., Wang, J., Zhou, G., Peng, W., He, Z., Zhao, Z., Mo, C., Qu, J., Zhang, J., 2014. Transplantation of induced pluripotent stem cells improves functional recovery in Huntington's disease rat model. PLoS One 9, e101185.
Murakami, M., Nagahama, M., Abe, Y., Niikura, T., 2017. Humanin affects object recognition and gliosis in short-term cuprizone-treated mice. Neuropeptides 66, 90–96.
Nagaraj, K., Taly, A.B., Gupta, A., Prasad, C., Christopher, R., 2013. Depression and sleep disturbances in patients with multiple sclerosis and correlation with associated fatigue. J. Neurosci. Rural Pract. 4, 387–391.
Nakahara, J., Maeda, M., Aiso, S., Suzuki, N., 2012. Current concepts in multiple sclerosis: autoimmunity versus oligodendrogliopathy. Clin. Rev. Allergy Immunol. 42, 26–34.
Nam, H., Clinton, S.M., Jackson, N.L., Kerman, I.A., 2014. Learned helplessness and social avoidance in the Wistar-Kyoto rat. Front. Behav. Neurosci. 8, 109.
Namekata, K., Kimura, A., Harada, C., Yoshida, H., Matsumoto, Y., Harada, T., 2014. Dock3 protects myelin in the cuprizone model for demyelination. Cell Death Dis. 5, e1395.
Nasser, A., Bjerrum, O.J., Heegaard, A.M., Moller, A.T., Larsen, M., Dalboge, L.S., Dupont, E., Jensen, T.S., Moller, L.B., 2013. Impaired behavioural pain responses in hph-1 mice with inherited deficiency in GTP cyclohydrolase 1 in models of inflammatory pain. Mol. Pain 9, 5.
Newland, P., Starkweather, A., Sorenson, M., 2016. Central fatigue in multiple sclerosis: a review of the literature. J. Spinal Cord Med. 39, 386–399.
Norkute, A., Hieble, A., Braun, A., Johann, S., Clarner, T., Baumgartner, W., Beyer, C., Kipp, M., 2009. Cuprizone treatment induces demyelination and astrocytosis in the mouse hippocampus. J. Neurosci. Res. 87, 1343–1355.
Nunes, A.K., Raposo, C., Luna, R.L., Cruz-Hofling, M.A., Peixoto, C.A., 2012. Sildenafil (Viagra(R)) down regulates cytokines and prevents demyelination in a cuprizone-induced MS mouse model. Cytokine 60, 540–551.
Nyamoya, S., Schweiger, F., Kipp, M., Hochstrasser, T., 2017. Cuprizone as a model of myelin and axonal damage. Drug Discov. Today Dis. Models 25–26, 63–68.
O'Connor, A.B., Schwid, S.R., Herrmann, D.N., Markman, J.D., Dworkin, R.H., 2008. Pain associated with multiple sclerosis: systematic review and proposed classification. Pain 137, 96–111.
Oakden, W., Bock, N.A., Al-Ebraheem, A., Farquharson, M.J., Stanisz, G.J., 2017. Early regional cuprizone-induced demyelination in a rat model revealed with MRI. NMR Biomed. 30.
Ohl, F., Keck, M.E., 2003. Behavioural screening in mutagenised mice–in search for novel animal models of psychiatric disorders. Eur. J. Pharmacol. 480, 219–228.
Omotoso, G.O., Ukwubile, I.I., Arietarhire, L., Sulaimon, F., Gbadamosi, I.T., 2018. Kolaviron protects the brain in cuprizone-induced model of experimental multiple sclerosis via enhancement of intrinsic antioxidant mechanisms: Possible therapeutic applications? Pathophysiology.
Pagliardini, S., Greer, J.J., Funk, G.D., Dickson, C.T., 2012. State-dependent modulation of breathing in urethane-anesthetized rats. J. Neurosci. 32, 11259–11270.
Paine, T.A., Jackman, S.L., Olmstead, M.C., 2002. Cocaine-induced anxiety: alleviation by diazepam, but not buspirone, dimenhydrinate or diphenhydramine. Behav. Pharmacol. 13, 511–523.
Pardini, M., Bonzano, L., Roccatagliata, L., Mancardi, G.L., Bove, M., 2013. The fatigue-motor performance paradox in multiple sclerosis. Sci. Rep. 3, 2001.
Parmar, K., Stadelmann, C., Rocca, M.A., Langdon, D., D'Angelo, E., D'Souza, M., Burggraaff, J., Wegner, C., Sastre-Garriga, J., Barrantes-Freer, A., Dorn, J., Uitdehaag, B.M.J., Montalban, X., Wuerfel, J., Enzinger, C., Rovira, A., Tintore, M., Filippi, M., Kappos, L., Sprenger, T., 2018. The role of the cerebellum in multiple sclerosis-150 years after Charcot. Neurosci. Biobehav. Rev. 89, 85–98.
Partridge, M.A., Gopinath, S., Myers, S.J., Coorssen, J.R., 2016. An initial top-down proteomic analysis of the standard cuprizone mouse model of multiple sclerosis. J. Chem. Biol. 9, 9–18.
Partridge, M.A., Myers, S.J., Gopinath, S., Coorssen, J.R., 2015. Proteomics of a conundrum: thoughts on addressing the aetiology versus progression of multiple sclerosis. Proteomics Clin. Appl. 9, 838–843.
Pasquini, L.A., Calatayud, C.A., Bertone Una, A.L., Millet, V., Pasquini, J.M., Soto, E.F., 2007. The neurotoxic effect of cuprizone on oligodendrocytes depends on the presence of pro-inflammatory cytokines secreted by microglia. Neurochem. Res. 32, 279–292.
Pellegrino, L., Coscia, M., Muller, M., Solaro, C., Casadio, M., 2018. Evaluating upper limb impairments in multiple sclerosis by exposure to different mechanical environments. Sci. Rep. 8, 2110.
Pellow, S., Chopin, P., File, S.E., Briley, M., 1985. Validation of open:closed arm entries in an elevated plus-maze as a measure of anxiety in the rat. J. Neurosci. Methods 14, 149–167.
Pellow, S., File, S.E., 1986. Anxiolytic and anxiogenic drug effects on exploratory activity in an elevated plus-maze: a novel test of anxiety in the rat. Pharmacol. Biochem. Behav. 24, 525–529.
Perlman, R.L., 2016. Mouse models of human disease: an evolutionary perspective. Evol. Med. Public Health 2016, 170–176.
Peruga, I., Hartwig, S., Thone, J., Hovemann, B., Gold, R., Juckel, G., Linker, R.A., 2011. Inflammation modulates anxiety in an animal model of multiple sclerosis. Behav. Brain Res. 220, 20–29.
Pessoa, L., 2010. Emotion and cognition and the amygdala: from "what is it?" to "what's to be done?". Neuropsychologia 48, 3416–3429.
Peterson, L.K., Fujinami, R.S., 2007. Inflammation, demyelination, neurodegeneration and neuroprotection in the pathogenesis of multiple sclerosis. J. Neuroimmunol. 184, 37–44.
Petronilli, V., Zoratti, M., 1990. A characterization of cuprizone-induced giant mouse liver mitochondria. J. Bioenerg. Biomembr. 22, 663–677.
Pfeifenbring, S., Nessler, S., Wegner, C., Stadelmann, C., Bruck, W., 2015. Remyelination after cuprizone-induced demyelination is accelerated in juvenile mice. J.

Neuropathol. Exp. Neurol. 74, 756–766.
Pierson, E.R., Stromnes, I.M., Goverman, J.M., 2014. B cells promote induction of experimental autoimmune encephalomyelitis by facilitating reactivation of T cells in the central nervous system. J. Immunol. 192, 929–939.
Piras, G., Rattazzi, L., McDermott, A., Deacon, R., D'Acquisto, F., 2013. Emotional change-associated T cell mobilization at the early stage of a mouse model of multiple sclerosis. Front. Immunol. 4, 400.
Pokryszko-Dragan, A., Bilinska, M., Gruszka, E., Biel, L., Kaminska, K., Konieczna, K., 2013. Sleep disturbances in patients with multiple sclerosis. Neurol. Sci. 34, 1291–1296.
Pollak, J., Doyle, K.P., Mamer, L., Shamloo, M., Buckwalter, M.S., 2012. Stratification substantially reduces behavioral variability in the hypoxic-ischemic stroke model. Brain Behav. 2, 698–706.
Pollak, Y., Ovadia, H., Goshen, I., Gurevich, R., Monsa, K., Avitsur, R., Yirmiya, R., 2000. Behavioral aspects of experimental autoimmune encephalomyelitis. J. Neuroimmunol. 104, 31–36.
Ponath, G., Park, C., Pitt, D., 2018. The role of astrocytes in multiple sclerosis. Front. Immunol. 9, 217.
Popescu, B.F., Lucchinetti, C.F., 2012. Pathology of demyelinating diseases. Annu. Rev. Pathol. 7, 185–217.
Popescu, B.F., Pirko, I., Lucchinetti, C.F., 2013. Pathology of multiple sclerosis: where do we stand? Continuum Minneap. Minn (Minneap Minn) 19, 901–921.
Porsolt, R.D., Brossard, G., Hautbois, C., Roux, S., 2001. Rodent models of depression: forced swimming and tail suspension behavioral despair tests in rats and mice. Curr. Protoc. Neurosci Chapter 8: Unit 8 10A.
Poser, C.M., Brinar, V.V., 2003. Epilepsy and multiple sclerosis. Epilepsy Behav. 4, 6–12.
Praet, J., Guglielmetti, C., Berneman, Z., Van der Linden, A., Ponsaerts, P., 2014. Cellular and molecular neuropathology of the cuprizone mouse model: clinical relevance for multiple sclerosis. Neurosci. Biobehav. Rev. 47, 485–505.
Procaccini, C., De Rosa, V., Pucino, V., Formisano, L., Matarese, G., 2015. Animal models of multiple sclerosis. Eur. J. Pharmacol. 759, 182–191.
Pujol, J., Bello, J., Deus, J., Marti-Vilalta, J.L., Capdevila, A., 1997. Lesions in the left arcuate fasciculus region and depressive symptoms in multiple sclerosis. Neurology 49, 1105–1110.
Puzzo, D., Lee, L., Palmeri, A., Calabrese, G., Arancio, O., 2014. Behavioral assays with mouse models of Alzheimer's disease: practical considerations and guidelines. Biochem. Pharmacol. 88, 450–467.
Rabins, P.V., Brooks, B.R., O'Donnell, P., Pearlson, G.D., Moberg, P., Jubelt, B., Coyle, P., Dalos, N., Folstein, M.F., 1986. Structural brain correlates of emotional disorder in multiple sclerosis. Brain 109 (Pt 4), 585–597.
Rahn, K., Slusher, B., Kaplin, A., 2012. Cognitive impairment in multiple sclerosis: a forgotten disability remembered. Cerebrum 2012, 14.
Ramos, A., 2008. Animal models of anxiety: do I need multiple tests? Trends Pharmacol. Sci. 29, 493–498.
Ransohoff, R.M., 2012. Animal models of multiple sclerosis: the good, the bad and the bottom line. Nat. Neurosci. 15, 1074–1077.
Ray, A.K., DuBois, J.C., Gruber, R.C., Guzik, H.M., Gulinello, M.E., Perumal, G., Raine, C., Kozakiewicz, L., Williamson, J., Shafit-Zagardo, B., 2017. Loss of Gas6 and Axl signaling results in extensive axonal damage, motor deficits, prolonged neuroinflammation, and less remyelination following cuprizone exposure. Glia 65, 2051–2069.
Remington, L.T., Babcock, A.A., Zehntner, S.P., Owens, T., 2007. Microglial recruitment, activation, and proliferation in response to primary demyelination. Am. J. Pathol. 170, 1713–1724.
Riether, A.M., 1999. Anxiety in patients with multiple sclerosis. Semin. Clin. Neuropsychiatry 4, 103–113.
Rivers, T.M., Sprunt, D.H., Berry, G.P., 1933. Observations on attempts to produce acute disseminated encephalomyelitis in monkeys. J. Exp. Med. 58, 39–53.
Rocca, M.A., Barkhof, F., De Luca, J., Frisen, J., Geurts, J.J.G., Hulst, H.E., Sastre-Garriga, J., Filippi, M., 2018. The hippocampus in multiple sclerosis. Lancet Neurol. 17, 918–926.
Rodrigues, D.H., Sachs, D., Teixeira, A.L., 2009. Mechanical hypernociception in experimental autoimmune encephalomyelitis. Arq. Neuropsiquiatr. 67, 78–81.
Roedel, A., Storch, C., Holsboer, F., Ohl, F., 2006. Effects of light or dark phase testing on behavioural and cognitive performance in DBA mice. Lab. Anim. 40, 371–381.
Rogers, J.T., Morganti, J.M., Bachstetter, A.D., Hudson, C.E., Peters, M.M., Grimmig, B.A., Weeber, E.J., Bickford, P.C., Gemma, C., 2011. CX3CR1 deficiency leads to impairment of hippocampal cognitive function and synaptic plasticity. J. Neurosci. 31, 16241–16250.
Rommelfanger, K.S., Edwards, G.L., Freeman, K.G., Liles, L.C., Miller, G.W., Weinshenker, D., 2007. Norepinephrine loss produces more profound motor deficits than MPTP treatment in mice. Proc. Natl. Acad. Sci. U.S.A. 104, 13804–13809.
Ron, M.A., Logsdail, S.J., 1989. Psychiatric morbidity in multiple sclerosis: a clinical and MRI study. Psychol. Med. 19, 887–895.
Rosenthal, N., Brown, S., 2007. The mouse ascending: perspectives for human-disease models. Nat. Cell Biol. 9, 993–999.
Rossi, S., Studer, V., Motta, C., Polidoro, S., Perugini, J., Macchiarulo, G., Giovannetti, A.M., Pareja-Gutierrez, L., Calo, A., Colonna, I., Furlan, R., Martino, G., Centonze, D., 2017. Neuroinflammation drives anxiety and depression in relapsing-remitting multiple sclerosis. Neurology 89, 1338–1347.
Rovaris, M., Confavreux, C., Furlan, R., Kappos, L., Comi, G., Filippi, M., 2006. Secondary progressive multiple sclerosis: current knowledge and future challenges. Lancet Neurol. 5, 343–354.
Ruiz, L.M., Salazar, C., Jensen, E., Ruiz, P.A., Tiznado, W., Quintanilla, R.A., Barreto, M., Elorza, A.A., 2015. Quercetin affects erythropoiesis and heart mitochondrial function in mice. Oxid. Med. Cell. Longev. 2015, 836301.
Rust, J.H., 1982. Animal models for human diseases. Perspect. Biol. Med. 25, 662–672.
Sacco, R., Bisecco, A., Corbo, D., Della Corte, M., d'Ambrosio, A., Docimo, R., Gallo, A., Esposito, F., Esposito, S., Cirillo, M., Lavorgna, L., Tedeschi, G., Bonavita, S., 2015. Cognitive impairment and memory disorders in relapsing-remitting multiple sclerosis: the role of white matter, gray matter and hippocampus. J. Neurol. 262, 1691–1697.
Sakai, R.E., Feller, D.J., Galetta, K.M., Galetta, S.L., Balcer, L.J., 2011. Vision in multiple sclerosis: the story, structure-function correlations, and models for neuroprotection. J. Neuroophthalmol. 31, 362–373.
Samour, M.S., Shaikh, S.M., Mahns, D.A., Shortland, P.J., 2017. Noxious, but not innocuous, thermal stimuli evoke pERK expression in dorsal horn neurons after spared nerve injury in adult rats. Neurosci. Lett. 654, 49–55.
Sanadgol, N., Golab, F., Mostafaie, A., Mehdizadeh, M., Khalseh, R., Mahmoudi, M., Abdollahi, M., Vakilzadeh, G., Taghizadeh, G., Sharifzadeh, M., 2018. Low, but not high, dose triptolide controls neuroinflammation and improves behavioral deficits in toxic model of multiple sclerosis by dampening of NF-kappaB activation and acceleration of intrinsic myelin repair. Toxicol. Appl. Pharmacol. 342, 86–98.
Sanadgol, N., Golab, F., Tashakkor, Z., Taki, N., Moradi Kouchi, S., Mostafaie, A., Mehdizadeh, M., Abdollahi, M., Taghizadeh, G., Sharifzadeh, M., 2017. Neuroprotective effects of ellagic acid on cuprizone-induced acute demyelination through limitation of microgliosis, adjustment of CXCL12/IL-17/IL-11 axis and restriction of mature oligodendrocytes apoptosis. Pharm. Biol. 55, 1679–1687.
Sanchez-Dalmau, B., Martinez-Lapiscina, E.H., Pulido-Valdeolivas, I., Zubizarreta, I., Llufriu, S., Blanco, Y., Sola-Valls, N., Sepulveda, M., Guerrero, A., Alba, S., Andorra, M., Camos, A., Sanchez-Vela, L., Alfonso, V., Saiz, A., Villoslada, P., 2018. Predictors of vision impairment in Multiple Sclerosis. PLoS One 13, e0195856.
Savage, S., Ma, D., 2015. Experimental behaviour testing: pain. Br. J. Anaesth. 114, 721–724.
Schaar, K.L., Brenneman, M.M., Savitz, S.I., 2010. Functional assessments in the rodent stroke model. Exp. Transl. Stroke Med. 2, 13.
Schmitz, K., de Bruin, N., Bishay, P., Mannich, J., Haussler, A., Altmann, C., Ferreiros, N., Lotsch, J., Ultsch, A., Parnham, M.J., Geisslinger, G., Tegeder, I., 2014. R-flurbiprofen attenuates experimental autoimmune encephalomyelitis in mice. EMBO Mol. Med. 6, 1398–1422.
Schultz, V., van der Meer, F., Wrzos, C., Scheidt, U., Bahn, E., Stadelmann, C., Bruck, W., Junker, A., 2017. Acutely damaged axons are remyelinated in multiple sclerosis and experimental models of demyelination. Glia 65, 1350–1360.
Serizawa, K., Tomizawa-Shinohara, H., Magi, M., Yogo, K., Matsumoto, Y., 2018. Anti-IL-6 receptor antibody improves pain symptoms in mice with experimental autoimmune encephalomyelitis. J. Neuroimmunol. 319, 71–79.
Serra-de-Oliveira, N., Boilesen, S.N., Prado de Franca Carvalho, C., LeSueur-Maluf, L., Zollner Rde, L., Spadari, R.C., Medalha, C.C., Monteiro de Castro, G., 2015. Behavioural changes observed in demyelination model shares similarities with white matter abnormalities in humans. Behav. Brain Res. 287, 265–275.
Shaikh, S., Shortland, P., Lauto, A., Barton, M., Morley, J.W., Mahns, D.A., 2016. Sensory perturbations using suture and sutureless repair of transected median nerve in rats. Somatosens. Mot. Res. 33, 20–28.
Shao, Y., Peng, H., Huang, Q., Kong, J., Xu, H., 2015. Quetiapine mitigates the neuroinflammation and oligodendrocyte loss in the brain of C57BL/6 mouse following cuprizone exposure for one week. Eur. J. Pharmacol. 765, 249–257.
Siegert, R.J., Abernethy, D.A., 2005. Depression in multiple sclerosis: a review. J. Neurol. Neurosurg. Psychiatr. 76, 469–475.
Simons, M., Nave, K.A., 2015. Oligodendrocytes: myelination and axonal support. Cold Spring Harb. Perspect. Biol. 8, a020479.
Sivaraman, I., Moodley, M., 2016. Multiple sclerosis in the very young: a case report and review of the literature. Neurodegener. Dis. Manag. 6, 31–36.
Skalisz, L.L., Beijamini, V., Joca, S.L., Vital, M.A., Da Cunha, C., Andreatini, R., 2002. Evaluation of the face validity of reserpine administration as an animal model of depression–Parkinson's disease association. Prog. Neuropsychopharmacol. Biol. Psychiatry 26, 879–883.
Skripuletz, T., Bussmann, J.H., Gudi, V., Koutsoudaki, P.N., Pul, R., Moharregh-Khiabani, D., Lindner, M., Stangel, M., 2010a. Cerebellar cortical demyelination in the murine cuprizone model. Brain Pathol. 20, 301–312.
Skripuletz, T., Gudi, V., Hackstette, D., Stangel, M., 2011. De- and remyelination in the CNS white and grey matter induced by cuprizone: the old, the new, and the unexpected. Histol. Histopathol. 26, 1585–1597.
Skripuletz, T., Hackstette, D., Bauer, K., Gudi, V., Pul, R., Voss, E., Berger, K., Kipp, M., Baumgartner, W., Stangel, M., 2013. Astrocytes regulate myelin clearance through recruitment of microglia during cuprizone-induced demyelination. Brain 136, 147–167.
Skripuletz, T., Lindner, M., Kotsiari, A., Garde, N., Fokuhl, J., Linsmeier, F., Trebst, C., Stangel, M., 2008. Cortical demyelination is prominent in the murine cuprizone model and is strain-dependent. Am. J. Pathol. 172, 1053–1061.
Skripuletz, T., Manzel, A., Gropengiesser, K., Schafer, N., Gudi, V., Singh, V., Salinas Tejedor, L., Jorg, S., Hammer, A., Voss, E., Vulinovic, F., Degen, D., Wolf, R., Lee, D.H., Pul, R., Moharregh-Khiabani, D., Baumgartner, W., Gold, R., Linker, R.A., Stangel, M., 2015. Pivotal role of choline metabolites in remyelination. Brain 138, 398–413.
Skripuletz, T., Miller, E., Moharregh-Khiabani, D., Blank, A., Pul, R., Gudi, V., Trebst, C., Stangel, M., 2010b. Beneficial effects of minocycline on cuprizone induced cortical demyelination. Neurochem. Res. 35, 1422–1433.
Slowik, A., Schmidt, T., Beyer, C., Amor, S., Clarner, T., Kipp, M., 2015. The sphingosine 1-phosphate receptor agonist FTY720 is neuroprotective after cuprizone-induced CNS demyelination. Br. J. Pharmacol. 172, 80–92.
Soblosky, J.S., Song, J.H., Dinh, D.H., 2001. Graded unilateral cervical spinal cord injury in the rat: evaluation of forelimb recovery and histological effects. Behav. Brain Res.

119, 1–13.
Sobrian, S.K., Marr, L., Ressman, K., 2003. Prenatal cocaine and/or nicotine exposure produces depression and anxiety in aging rats. Prog. Neuropsychopharmacol. Biol. Psychiatry 27, 501–518.
Solti, I., Kvell, K., Talaber, G., Veto, S., Acs, P., Gallyas Jr., F., Illes, Z., Fekete, K., Zalan, P., Szanto, A., Bognar, Z., 2015. Thymic atrophy and apoptosis of CD4 + CD8 + thymocytes in the cuprizone model of multiple sclerosis. PLoS One 10, e0129217.
Sotocinal, S.G., Sorge, R.E., Zaloum, A., Tuttle, A.H., Martin, L.J., Wieskopf, J.S., Mapplebeck, J.C., Wei, P., Zhan, S., Zhang, S., McDougall, J.J., King, O.D., Mogil, J.S., 2011. The Rat Grimace Scale: a partially automated method for quantifying pain in the laboratory rat via facial expressions. Mol. Pain 7, 55.
Sperber, B.R., Boyle-Walsh, E.A., Engleka, M.J., Gadue, P., Peterson, A.C., Stein, P.L., Scherer, S.S., McMorris, F.A., 2001. A unique role for Fyn in CNS myelination. J. Neurosci. 21, 2039–2047.
Spitzer, S.O., Sitnikov, S., Kamen, Y., Evans, K.A., Kronenberg-Versteeg, D., Dietmann, S., de Faria Jr., O., Agathou, S., Karadottir, R.T., 2019. Oligodendrocyte progenitor cells become regionally diverse and heterogeneous with age. Neuron 101, 459–471 e455.
Sriram, S., Steiner, I., 2005. Experimental allergic encephalomyelitis: a misleading model of multiple sclerosis. Ann. Neurol. 58, 939–945.
Stidworthy, M.F., Genoud, S., Suter, U., Mantei, N., Franklin, R.J., 2003. Quantifying the early stages of remyelination following cuprizone-induced demyelination. Brain Pathol. 13, 329–339.
Stone, S., Lin, W., 2015. The unfolded protein response in multiple sclerosis. Front. Neurosci. 9, 264.
Streijger, F., Plunet, W.T., Lee, J.H., Liu, J., Lam, C.K., Park, S., Hilton, B.J., Fransen, B.L., Matheson, K.A., Assinck, P., Kwon, B.K., Tetzlaff, W., 2013. Ketogenic diet improves forelimb motor function after spinal cord injury in rodents. PLoS One 8, e78765.
Strekalova, T., Couch, Y., Kholod, N., Boyks, M., Malin, D., Leprince, P., Steinbusch, H.M., 2011. Update in the methodology of the chronic stress paradigm: internal control matters. Behav. Brain Funct. 7, 9.
Stys, P.K., 2013. Pathoetiology of multiple sclerosis: are we barking up the wrong tree? F1000Prime Rep. 5, 20.
Stys, P.K., Zamponi, G.W., van Minnen, J., Geurts, J.J., 2012. Will the real multiple sclerosis please stand up? Nat. Rev. Neurosci. 13, 507–514.
Su, C., D'Amour, J., Lee, M., Lin, H.Y., Manders, T., Xu, D., Eberle, S.E., Goffer, Y., Zou, A.H., Rahman, M., Ziff, E., Froemke, R.C., Huang, D., Wang, J., 2015. Persistent pain alters AMPA receptor subunit levels in the nucleus accumbens. Mol. Brain 8, 46.
Sukoff Rizzo, S.J., Crawley, J.N., 2017. Behavioral Phenotyping Assays for Genetic Mouse Models of Neurodevelopmental, Neurodegenerative, and Psychiatric Disorders. Annu. Rev. Anim. Biosci. 5, 371–389.
Sun, J., Zhou, H., Bai, F., Ren, Q., Zhang, Z., 2016. Myelin injury induces axonal transport impairment but not AD-like pathology in the hippocampus of cuprizone-fed mice. Oncotarget 7, 30003–30017.
Sun, Z.Y., Gu, H.S., Chen, X., Zhang, L., Li, X.M., Zhang, J.W., Li, L., 2017. A novel flavanone derivative ameliorates cuprizone-induced behavioral changes and white matter pathology in the brain of mice. Psychiatry Res. 257, 249–259.
Suzuki, K., 1969. Giant hepatic mitochondria: production in mice fed with cuprizone. Science 163, 81–82.
Suzuki, K., Kikkawa, Y., 1969. Status spongiosus of CNS and hepatic changes induced by cuprizone (biscyclohexanone oxalyldihydrazone). Am. J. Pathol. 54, 307–325.
Svendsen, K.B., Jensen, T.S., Overvad, K., Hansen, H.J., Koch-Henriksen, N., Bach, F.W., 2003. Pain in patients with multiple sclerosis: a population-based study. Arch. Neurol. 60, 1089–1094.
t Hart, B.A., Gran, B., Weissert, R., 2011. EAE: imperfect but useful models of multiple sclerosis. Trends Mol. Med. 17, 119–125.
Tachibana, N., Howard, R.S., Hirsch, N.P., Miller, D.H., Moseley, I.F., Fish, D., 1994. Sleep problems in multiple sclerosis. Eur. Neurol. 34, 320–323.
Tanaka, S., Young, J.W., Halberstadt, A.L., Masten, V.L., Geyer, M.A., 2012. Four factors underlying mouse behavior in an open field. Behav. Brain Res. 233, 55–61.
Taylor, L.C., Gilmore, W., Matsushima, G.K., 2009. SJL mice exposed to cuprizone intoxication reveal strain and gender pattern differences in demyelination. Brain Pathol. 19, 467–479.
Taylor, T.N., Greene, J.G., Miller, G.W., 2010. Behavioral phenotyping of mouse models of Parkinson's disease. Behav. Brain Res. 211, 1–10.
Tejedor, L.S., Wostradowski, T., Gingele, S., Skripuletz, T., Gudi, V., Stangel, M., 2017. The effect of stereotactic injections on demyelination and remyelination: a study in the cuprizone model. J. Mol. Neurosci. 61, 479–488.
Terry, R.L., Ifergan, I., Miller, S.D., 2016. Experimental autoimmune encephalomyelitis in mice. Methods Mol. Biol. 1304, 145–160.
Tezuka, T., Tamura, M., Kondo, M.A., Sakaue, M., Okada, K., Takemoto, K., Fukunari, A., Miwa, K., Ohzeki, H., Kano, S., Yasumatsu, H., Sawa, A., Kajii, Y., 2013. Cuprizone short-term exposure: astrocytic IL-6 activation and behavioral changes relevant to psychosis. Neurobiol. Dis. 59, 63–68.
Thanos, P.K., Restif, C., O'Rourke, J.R., Lam, C.Y., Metaxas, D., 2017. Mouse Social Interaction Test (MoST): a quantitative computer automated analysis of behavior. Journal of neural transmission (Vienna, Austria: 1996) 124, 3–11.
Thibault, K., Calvino, B., Pezet, S., 2011. Characterisation of sensory abnormalities observed in an animal model of multiple sclerosis: a behavioural and pharmacological study. Eur. J. Pain 15 (231), e231–216.
Thiessen, D.D., Lindzey, G., 1967. Negative geotaxis in mice: effect of balancing practice on incline behaviour in C57BL-6J male mice. Anim. Behav. 15, 113–116.
Thomas, B.B., Samant, D.M., Seiler, M.J., Aramant, R.B., Sheikholeslami, S., Zhang, K., Chen, Z., Sadda, S.R., 2007. Behavioral evaluation of visual function of rats using a visual discrimination apparatus. J. Neurosci. Methods 162, 84–90.
Thompson, S., Philp, A.R., Stone, E.M., 2008. Visual function testing: a quantifiable visually guided behavior in mice. Vision Res. 48, 346–352.
Thorburn, K.C., Paylor, J.W., Webber, C.A., Winship, I.R., Kerr, B.J., 2016. Facial hypersensitivity and trigeminal pathology in mice with experimental autoimmune encephalomyelitis. Pain 157, 627–642.
Tievsky, A.L., Ptak, T., Farkas, J., 1999. Investigation of apparent diffusion coefficient and diffusion tensor anisotrophy in acute and chronic multiple sclerosis lesions. AJNR Am. J. Neuroradiol. 20, 1491–1499.
Tobler, I., Deboer, T., Fischer, M., 1997. Sleep and sleep regulation in normal and prion protein-deficient mice. J. Neurosci. 17, 1869–1879.
Torkildsen, O., Brunborg, L.A., Milde, A.M., Mork, S.J., Myhr, K.M., Bo, L., 2009. A salmon based diet protects mice from behavioural changes in the cuprizone model for demyelination. Clin. Nutr. 28, 83–87.
Torkildsen, O., Brunborg, L.A., Myhr, K.M., Bo, L., 2008. The cuprizone model for demyelination. Acta Neurol. Scand., Suppl. 188, 72–76.
Toth, L.A., Bhargava, P., 2013. Animal models of sleep disorders. Comp. Med. 63, 91–104.
Traka, M., Podojil, J.R., McCarthy, D.P., Miller, S.D., Popko, B., 2016. Oligodendrocyte death results in immune-mediated CNS demyelination. Nat. Neurosci. 19, 65–74.
Trapp, B.D., Nave, K.A., 2008. Multiple sclerosis: an immune or neurodegenerative disorder? Annu. Rev. Neurosci. 31, 247–269.
Tsukahara, R., Yamamoto, S., Yoshikawa, K., Gotoh, M., Tsukahara, T., Neyama, H., Ishii, S., Akahoshi, N., Yanagida, K., Sumida, H., Araki, M., Araki, K., Yamamura, K.I., Murakami-Murofushi, K., Ueda, H., 2018. LPA5 signaling is involved in multiple sclerosis-mediated neuropathic pain in the cuprizone mouse model. J. Pharmacol. Sci. 136, 93–96.
Tullman, M.J., Oshinsky, R.J., Lublin, F.D., Cutter, G.R., 2004. Clinical characteristics of progressive relapsing multiple sclerosis. Mult. Scler. 10, 451–454.
Unger, E.L., Paul, T., Murray-Kolb, L.E., Felt, B., Jones, B.C., Beard, J.L., 2007. Early iron deficiency alters sensorimotor development and brain monoamines in rats. J. Nutr. 137, 118–124.
Vakilzadeh, G., Khodagholi, F., Ghadiri, T., Ghaemi, A., Noorbakhsh, F., Sharifzadeh, M., Gorji, A., 2016. The Effect of Melatonin on Behavioral, Molecular, and Histopathological Changes in Cuprizone Model of Demyelination. Mol. Neurobiol. 53, 4675–4684.
Valeiras, B., Rosato Siri, M.V., Codagnone, M., Reines, A., Pasquini, J.M., 2014. Gender influence on schizophrenia-relevant abnormalities in a cuprizone demyelination model. Glia 62, 1629–1644.
Valentino, P., Cerasa, A., Chiriaco, C., Nistico, R., Pirritano, D., Gioia, M., Lanza, P., Canino, M., Del Giudice, F., Gallo, O., Condino, F., Torchia, G., Quattrone, A., 2009. Cognitive deficits in multiple sclerosis patients with cerebellar symptoms. Mult. Scler. 15, 854–859.
Vallstedt, A., Klos, J.M., Ericson, J., 2005. Multiple dorsoventral origins of oligodendrocyte generation in the spinal cord and hindbrain. Neuron 45, 55–67.
Van de Kar, L.D., Piechowski, R.A., Rittenhouse, P.A., Gray, T.S., 1991. Amygdaloid lesions: differential effect on conditioned stress and immobilization-induced increases in corticosterone and renin secretion. Neuroendocrinology 54, 89–95.
van den Berg, R., Laman, J.D., van Meurs, M., Hintzen, R.Q., Hoogenraad, C.C., 2016. Rotarod motor performance and advanced spinal cord lesion image analysis refine assessment of neurodegeneration in experimental autoimmune encephalomyelitis. J. Neurosci. Methods 262, 66–76.
van Gaalen, M.M., Steckler, T., 2000. Behavioural analysis of four mouse strains in an anxiety test battery. Behav. Brain Res. 115, 95–106.
Van Meer, P., Raber, J., 2005. Mouse behavioural analysis in systems biology. Biochem. J. 389, 593–610.
Varga, E., Pandur, E., Abraham, H., Horvath, A., Acs, P., Komoly, S., Miseta, A., Sipos, K., 2018. Cuprizone administration alters the Iron metabolism in the mouse model of multiple sclerosis. Cell. Mol. Neurobiol. 38, 1081–1097.
Vargas, D.L., Tyor, W.R., 2017. Update on disease-modifying therapies for multiple sclerosis. J. Investig. Med. 65, 883–891.
Veauthier, C., 2015. Sleep disorders in multiple sclerosis. Review. Curr. Neurol. Neurosci. Rep. 15, 21.
Vega-Riquer, J.M., Mendez-Victoriano, G., Morales-Luckie, R.A., Gonzalez-Perez, O., 2017. Five decades of cuprizone, an updated model to replicate demyelinating diseases. Curr. Neuropharmacol.
Venturini, G., 1973. Enzymic activities and sodium, potassium and copper concentrations in mouse brain and liver after cuprizone treatment in vivo. J. Neurochem. 21, 1147–1151.
Vorhees, C.V., Williams, M.T., 2006. Morris water maze: procedures for assessing spatial and related forms of learning and memory. Nat. Protoc. 1, 848–858.
Wagenknecht, N., Becker, B., Scheld, M., Beyer, C., Clarner, T., Hochstrasser, T., Kipp, M., 2016. Thalamus degeneration and inflammation in two distinct multiple sclerosis animal models. J. Mol. Neurosci. 60, 102–114.
Wagner, T., Rafael, J., 1977. Biochemical properties of liver megamitochondria induced by chloramphenicol or cuprizone. Exp. Cell Res. 107, 1–13.
Walf, A.A., Frye, C.A., 2007. The use of the elevated plus maze as an assay of anxiety-related behavior in rodents. Nat. Protoc. 2, 322–328.
Wang, H., Li, C., Wang, H., Mei, F., Liu, Z., Shen, H.Y., Xiao, L., 2013. Cuprizone-induced demyelination in mice: age-related vulnerability and exploratory behavior deficit. Neurosci. Bull. 29, 251–259.
Wang, H.N., Liu, G.H., Zhang, R.G., Xue, F., Wu, D., Chen, Y.C., Peng, Y., Peng, Z.W., Tan, Q.R., 2015. Quetiapine ameliorates schizophrenia-like behaviors and protects myelin integrity in cuprizone intoxicated mice: the involvement of notch signaling pathway. Int. J. Neuropsychopharmacol. 19.
Wang, I.C., Chung, C.Y., Liao, F., Chen, C.C., Lee, C.H., 2017a. Peripheral sensory neuron injury contributes to neuropathic pain in experimental autoimmune encephalomyelitis. Sci. Rep. 7, 42304.
Wang, W., Shi, W., Qian, H., Deng, X., Wang, T., Li, W., 2017b. Stellate ganglion block attenuates chronic stress induced depression in rats. PLoS One 12, e0183995.

Wang, W.W., Lu, L., Bao, T.H., Zhang, H.M., Yuan, J., Miao, W., Wang, S.F., Xiao, Z.C., 2016. Scutellarin alleviates behavioral deficits in a mouse model of multiple sclerosis, possibly through protecting neural stem cells. J. Mol. Neurosci. 58, 210–220.
Webster, S.J., Bachstetter, A.D., Nelson, P.T., Schmitt, F.A., Van Eldik, L.J., 2014. Using mice to model Alzheimer's dementia: an overview of the clinical disease and the preclinical behavioral changes in 10 mouse models. Front. Genet. 5, 88.
Weier, K., Penner, I.K., Magon, S., Amann, M., Naegelin, Y., Andelova, M., Derfuss, T., Stippich, C., Radue, E.W., Kappos, L., Sprenger, T., 2014. Cerebellar abnormalities contribute to disability including cognitive impairment in multiple sclerosis. PLoS One 9, e86916.
Wernecke, K.E., Fendt, M., 2015. The olfactory hole-board test in rats: a new paradigm to study aversion and preferences to odors. Front. Behav. Neurosci. 9, 223.
Werner, S.R., Saha, J.K., Broderick, C.L., Zhen, E.Y., Higgs, R.E., Duffin, K.L., Smith, R.C., 2010. Proteomic analysis of demyelinated and remyelinating brain tissue following dietary cuprizone administration. J. Mol. Neurosci. 42, 210–225.
Whishaw, I.Q., Faraji, J., Kuntz, J., Mirza Agha, B., Patel, M., Metz, G.A.S., Mohajerani, M.H., 2017. Organization of the reach and grasp in head-fixed vs freely-moving mice provides support for multiple motor channel theory of neocortical organization. Exp. Brain Res. 235, 1919–1932.
Wilkins, A., 2017. Cerebellar dysfunction in multiple sclerosis. Front. Neurol. 8, 312.
Wilson, C.A., Koenig, J.I., 2014. Social interaction and social withdrawal in rodents as readouts for investigating the negative symptoms of schizophrenia. Eur. Neuropsychopharmacol. 24, 759–773.
Wolf, A., Bauer, B., Abner, E.L., Ashkenazy-Frolinger, T., Hartz, A.M., 2016. A comprehensive behavioral test battery to assess learning and memory in 129S6/Tg2576 mice. PLoS One 11, e0147733.
Wood, D.D., Bilbao, J.M., O'Connors, P., Moscarello, M.A., 1996. Acute multiple sclerosis (Marburg type) is associated with developmentally immature myelin basic protein. Ann. Neurol. 40, 18–24.
Xiao, L., Xu, H., Zhang, Y., Wei, Z., He, J., Jiang, W., Li, X., Dyck, L.E., Devon, R.M., Deng, Y., Li, X.M., 2008. Quetiapine facilitates oligodendrocyte development and prevents mice from myelin breakdown and behavioral changes. Mol. Psychiatry 13, 697–708.
Xin, Y.L., Yu, J.Z., Yang, X.W., Liu, C.Y., Li, Y.H., Feng, L., Chai, Z., Yang, W.F., Wang, Q., Jiang, W.J., Zhang, G.X., Xiao, B.G., Ma, C.G., 2015. FSD-C10: a more promising novel ROCK inhibitor than Fasudil for treatment of CNS autoimmunity. Biosci. Rep. 35.
Xu, H., Yang, H.J., McConomy, B., Browning, R., Li, X.M., 2010. Behavioral and neurobiological changes in C57BL/6 mouse exposed to cuprizone: effects of antipsychotics. Front. Behav. Neurosci. 4, 8.
Xu, H., Yang, H.J., Rose, G.M., Li, X.M., 2011. Recovery of behavioral changes and compromised white matter in C57BL/6 mice exposed to cuprizone: effects of antipsychotic drugs. Front. Behav. Neurosci. 5, 31.
Xu, H., Yang, H.J., Zhang, Y., Clough, R., Browning, R., Li, X.M., 2009. Behavioral and neurobiological changes in C57BL/6 mice exposed to cuprizone. Behav. Neurosci. 123, 418–429.
Yalcin, I., Charlet, A., Freund-Mercier, M.J., Barrot, M., Poisbeau, P., 2009. Differentiating thermal allodynia and hyperalgesia using dynamic hot and cold plate in rodents. J. Pain 10, 767–773.
Yamamoto, S., Gotoh, M., Kawamura, Y., Yamashina, K., Yagishita, S., Awaji, T., Tanaka, M., Maruyama, K., Murakami-Murofushi, K., Yoshikawa, K., 2014. Cyclic phosphatidic acid treatment suppress cuprizone-induced demyelination and motor dysfunction in mice. Eur. J. Pharmacol. 741, 17–24.
Yamamoto, S., Yamashina, K., Ishikawa, M., Gotoh, M., Yagishita, S., Iwasa, K., Maruyama, K., Murakami-Murofushi, K., Yoshikawa, K., 2017. Protective and therapeutic role of 2-carba-cyclic phosphatidic acid in demyelinating disease. J. Neuroinflammation 14, 142.
Yang, H.J., Wang, H., Zhang, Y., Xiao, L., Clough, R.W., Browning, R., Li, X.M., Xu, H., 2009. Region-specific susceptibilities to cuprizone-induced lesions in the mouse forebrain: implications for the pathophysiology of schizophrenia. Brain Res. 1270, 121–130.
Ye, J.N., Chen, X.S., Su, L., Liu, Y.L., Cai, Q.Y., Zhan, X.L., Xu, Y., Zhao, S.F., Yao, Z.X., 2013. Progesterone alleviates neural behavioral deficits and demyelination with reduced degeneration of oligodendroglial cells in cuprizone-induced mice. PLoS One 8, e54590.
Yokoi, F., Dang, M.T., Li, J., Standaert, D.G., Li, Y., 2011. Motor deficits and decreased striatal dopamine receptor 2 binding activity in the striatum-specific Dyt1 conditional knockout mice. PLoS One 6, e24539.
Yoshikawa, K., Palumbo, S., Toscano, C.D., Bosetti, F., 2011. Inhibition of 5-lipoxygenase activity in mice during cuprizone-induced demyelination attenuates neuroinflammation, motor dysfunction and axonal damage. Prostaglandins Leukot. Essent. Fatty Acids 85, 43–52.
Yu, H., Wu, M., Lu, G., Cao, T., Chen, N., Zhang, Y., Jiang, Z., Fan, H., Yao, R., 2018. Prednisone alleviates demyelination through regulation of the NLRP3 inflammasome in a C57BL/6 mouse model of cuprizone-induced demyelination. Brain Res. 1678, 75–84.
Yu, Q., Hui, R., Park, J., Huang, Y., Kusnecov, A.W., Dreyfus, C.F., Zhou, R., 2017. Strain differences in cuprizone induced demyelination. Cell Biosci. 7, 59.
Zarrindast, M.R., Khakpai, F., 2015. The modulatory role of dopamine in anxiety-like behavior. Arch. Iran. Med. 18, 591–603.
Zatta, P., Raso, M., Zambenedetti, P., Wittkowski, W., Messori, L., Piccioli, F., Mauri, P.L., Beltramini, M., 2005. Copper and zinc dismetabolism in the mouse brain upon chronic cuprizone treatment. Cell. Mol. Life Sci. 62, 1502–1513.
Zhang, H., Zhang, Y., Xu, H., Wang, L., Zhao, J., Wang, J., Zhang, Z., Tan, Q., Kong, J., Huang, Q., Li, X.M., 2013. Locomotor activity and anxiety status, but not spatial working memory, are affected in mice after brief exposure to cuprizone. Neurosci. Bull. 29, 633–641.
Zhang, M., Zhan, X.L., Ma, Z.Y., Chen, X.S., Cai, Q.Y., Yao, Z.X., 2015. Thyroid hormone alleviates demyelination induced by cuprizone through its role in remyelination during the remission period. Exp. Biol. Med. (Maywood) 240, 1183–1196.
Zhang, Q., Li, Z., Wu, S., Li, X., Sang, Y., Li, J., Niu, Y., Ding, H., 2016. Myricetin alleviates cuprizone-induced behavioral dysfunction and demyelination in mice by Nrf2 pathway. Food Funct. 7, 4332–4342.
Zhang, W., Zhang, W., Li, Z., Hao, J., Zhang, Z., Liu, L., Mao, N., Miao, J., Zhang, L., 2012. S14G-humanin improves cognitive deficits and reduces amyloid pathology in the middle-aged APPswe/PS1dE9 mice. Pharmacol. Biochem. Behav. 100, 361–369.
Zheng, J., Ding, W., Li, B., Yang, Y., 2017. Enriched environment promotes remyelination and motor function recovery through modulation of HDAC1/2 in mice. Neurosci. Lett. 655, 121–130.
Zhou, Q., Bao, Y., Zhang, X., Zeng, L., Wang, L., Wang, J., Jiang, W., 2014. Optimal interval for hot water immersion tail-flick test in rats. Acta Neuropsychiatr. 26, 218–222.
Zhu, X.R., Maskri, L., Herold, C., Bader, V., Stichel, C.C., Gunturkun, O., Lubbert, H., 2007. Non-motor behavioural impairments in parkin-deficient mice. Eur. J. Neurosci. 26, 1902–1911.
Zieba, J., Low, J.K., Purtell, L., Qi, Y., Campbell, L., Herzog, H., Karl, T., 2015. Behavioural characteristics of the Prader-Willi syndrome related biallelic Snord116 mouse model. Neuropeptides 53, 71–77.
Zimmermann, J., Emrich, M., Krauthausen, M., Saxe, S., Nitsch, L., Heneka, M.T., Campbell, I.L., Muller, M., 2018. IL-17A Promotes Granulocyte Infiltration, Myelin Loss, Microglia Activation, and Behavioral Deficits During Cuprizone-Induced Demyelination. Mol. Neurobiol. 55, 946–957.
Zorzon, M., de Masi, R., Nasuelli, D., Ukmar, M., Mucelli, R.P., Cazzato, G., Bratina, A., Zivadinov, R., 2001. Depression and anxiety in multiple sclerosis. A clinical and MRI study in 95 subjects. J. Neurol. 248, 416–421.

Chapter-5 (Paper III)

This chapter has been published in Brain, Behavior, and Immunity, https://doi.org/10.1016/j.bbi.2020.01.021.

Brain, Behavior, and Immunity xxx (xxxx) xxx–xxx

Contents lists available at ScienceDirect

Brain, Behavior, and Immunity

journal homepage: www.elsevier.com/locate/ybrbi

Behavioural and histological changes in cuprizone-fed mice

Monokesh K. Sen[a], Mohammed S.M. Almuslehi[a,b], Jens R. Coorssen[c], David A. Mahns[a], Peter J. Shortland[d,*]

[a] School of Medicine, Western Sydney University, Penrith, New South Wales, Australia
[b] Department of Physiology, College of Veterinary Medicine, Diyala University, Diyala, Iraq
[c] Departments of Health Sciences and Biological Sciences, Faculties of Applied Health Sciences and Mathematics & Science, Brock University, Ontario, Canada
[d] School of Science, Western Sydney University, Penrith, New South Wales, Australia

ARTICLE INFO

Keywords:
Motor incoordination
Ataxia
Sensory performance
Pain
Oligodendrocytosis
Demyelination
Gliosis

ABSTRACT

Feeding cuprizone (CPZ) to mice causes demyelination and reactive gliosis in the central nervous system (CNS), hallmarks of some neurodegenerative diseases like multiple sclerosis. However, relatively little is known regarding the behavioural deficits associated with CPZ-feeding and much of what is known is contradictory. This study investigated whether 37 days oral feeding of 0.2% CPZ to young adult mice evoked sensorimotor behavioural changes. Behavioural tests included measurements of nociceptive withdrawal reflex responses and locomotor tests. Additionally, these were compared to histological analysis of the relevant CNS regions by analysis of neuronal and glial cell components. CPZ-fed mice exhibited more foot slips in walking ladder and beam tests compared to controls. In contrast, no changes in nociceptive thresholds to thermal or mechanical stimuli occurred between groups. Histological analysis showed demyelination throughout the CNS, which was most prominent in white matter tracts in the cerebrum but was also elevated in areas such as the hippocampus, basal ganglia and diencephalon. Profound demyelination and gliosis was seen in the deep cerebellar nuclei and brain stem regions associated with the vestibular system. However, in the spinal cord changes were minimal. No loss of oligodendrocytes, neurons or motoneurons occurred but a significant increase in astrocyte staining ensued throughout the white matter of the spinal cord. The results suggest that CPZ differentially affects oligodendrocytes throughout the CNS and induces subtle motor changes such as ataxia. This is associated with deficits in CNS regions associated with motor and balance functions such as the cerebellum and brain stem.

1. Introduction

Feeding cuprizone (CPZ) to mice is commonly used to study demyelination (and remyelination) and gliosis in the central nervous system (CNS) in the absence of an adaptive immune response, because the blood brain barrier remains intact (Partridge et al., 2015; Sen et al., 2019a; Sen et al., 2019b). While the precise mechanism of CPZ-induced toxicity is unclear, it is thought to be because of metal ion imbalance causing mitochondrial and endoplasmic reticulum stress resulting in oligodendrocyte (OLG) loss (termed oligodendrocytosis). This causes demyelination and gliosis (reviewed in Sen et al., 2019b). Despite the extensive use of CPZ as a tool to study demyelination, there has been less emphasis on the neuropathological consequences within the CNS. Almost all studies reported demyelination of the corpus callosum as a proxy for CPZ efficacy (see Sen et al., 2019b). However, only a few investigated anatomical changes in the grey and white matter regions of the cerebrum (Goldberg et al., 2015; Yang et al., 2009), cerebellum (Groebe et al., 2009; Skripuletz et al., 2010), brain stem or spinal cord (Herder et al., 2011; Jurevics et al., 2002).

Demyelination and gliosis in the CNS are hallmarks of demyelinating diseases like multiple sclerosis (MS). The CPZ model is an accepted animal model of MS (Acs and Kalman, 2012; Kipp et al., 2017) since the histopathology caused closely resembles the oligodendropathology seen in type III and IV MS brain lesions (Lucchinetti et al., 2000; Lucchinetti et al., 1996). Clinically, the two most common symptoms of MS patients are motor deficits and pain (see Table 2 of Sen et al., 2019b). Motor deficits including difficulties in maintaining balance, reduced walking speed and impaired limb dexterity were reported in about 80% of MS patients (Benedict et al., 2011; Cattaneo et al., 2002; Larocca, 2011; Pellegrino et al., 2018). Using the CPZ model, motor performance was commonly assessed using the rotarod apparatus, with mixed results, due to the limitations of the test (reviewed in Sen et al., 2019b). That review suggested that increasing the complexity of the motor task and assessing the accuracy of foot placements when

* Corresponding author at: Department of Medical Sciences, School of Science, Western Sydney University, Locked Bag 1797, Penrith, NSW 2751, Australia.
E-mail address: p.shortland@westernsydney.edu.au (P.J. Shortland).

https://doi.org/10.1016/j.bbi.2020.01.021
Received 6 December 2019; Received in revised form 20 January 2020; Accepted 30 January 2020

traversing an elevated beam or ladder would detect subtle deficits in CPZ-fed animals, as the two tasks assess different aspects of locomotion such as foot placement accuracy, limb coordination and balance. Therefore, this study compared the walking ladder and beam tests to the rotarod test.

MS patients also show a marked prevalence for pain and paraesthesia (30–80%; Sen et al., 2019b). However, only a limited number of CPZ studies have investigated changes in sensory functions such as nociception (Bolcskei et al., 2018; Tsukahara et al., 2018; Vakilzadeh et al., 2016), with only one investigating changes in low threshold tactile and proprioceptive inputs (Bolcskei et al., 2018). None of these studies correlated behavioural changes with histological investigations of the relevant ascending or descending somatosensory pathways, making interpretation of the changes challenging (Sen et al., 2019b). Therefore, we tested whether CPZ-feeding caused reliable sensorimotor behavioural deficits using specific sensory and motor behavioural tests followed by histological examination of specific CNS regions associated with the relevant somatosensory systems for oligodendrocytosis, demyelination, gliosis and neuronal loss.

2. Materials and methods

2.1. Animals, feeding and monitoring

Four-week old male C57BL/6 mice (n = 20) were purchased from the Animal Resources Centre, Murdoch, WA, Australia (www.arc.wa.gov.au). Males were used because it was demonstrated that there was no gender difference in demyelination and gliosis with CPZ-feeding (Taylor et al., 2010). At 7 weeks of age, mice were allocated randomly into two groups: naïve controls (Ctrl, n = 10) or cuprizone-fed (CPZ, n = 10). Control mice received normal rodent chow whereas the CPZ group were fed 0.2% w/w CPZ (Sigma-Aldrich, St. Louis, MO, USA) mixed into standard rodent powder chow (Gordon's Specialty Stockfeeds, Yanderra, NSW, Australia) for 37 days to induce oligodendrocytosis, demyelination and gliosis (Sen et al., 2019a; Sen et al., 2019b). Mice were weighed every third day to monitor general growth and health. No obvious changes in posture, gait and body condition were apparent in either group. Research and animal care procedures were approved by the Western Sydney University animal ethics committee (A10394), in accordance with the Australian Code of Practice for the Care and Use of Animals for Scientific Purposes as laid out by the National Health and Medical Research Council of Australia.

2.2. Behavioural assessments

These were performed in a blinded manner by the same observer throughout. All tests occurred between 9 am – 1 pm at room temperature (RT, 21–23 °C), with normal lighting conditions in an isolated behavioural lab. On test days, animals were habituated to their surroundings for 30 min prior to testing. Baseline behavioural tests occurred four times every third day for 2 weeks prior to group allocation. The ladder, beam, rotarod and nociceptive tests were performed on separate days as indicated in Fig. 2.

2.3. Motor tests

Locomotor activity and balance were measured using the accelerating rotarod apparatus (Ugo Basile, Gemonio, VA, Italy) as described previously (Franco-Pons et al., 2007; Traka et al., 2016). Testing was performed weekly to minimize repeated test-induced tiredness of mice due to the physical demands of the task. After the habituation period, each mouse was placed on the rotating drum at an initial speed of 4 revolutions per minute (rpm) that accelerated up to 40 rpm over 300 s. On each test day, three trials were performed (with a 1-hour rest interval between each trial). The latency to fall off the apparatus, time to first flip (i.e. the mouse holds onto the rotating rod rather than walking), and the total number of flips were recorded for each mouse.

Custom-made walking ladder and beam apparatus were used to assess more complex motor functions. For the walking ladder test, (Supplementary Fig. 1A) a desk lamp was placed at the starting end to encourage mice to move toward the safety of the darker home cage. The cut-off time allowed for crossing the ladder was 1 min. On each test day, three trials were performed (with 30 min rest between each trial). All trials were filmed with a Logitech C525 HD Webcam and analysed offline. The time to cross the ladder was measured. In addition, the number of foot slips was quantified in two ways: 1) a complete foot slip when the entire foot missed the rung, which was quantified for both hind- and fore-limbs; and 2) a partial foot slip, when part of the foot slips from the rung from both hind- and fore-limbs on days 8, 18 and 32. During the ladder test, mice often stopped to perform exploratory behaviours such as rearing, grooming, defecation, urination and head dipping. The quantification of the number of exploration activities was assessed on days 8, 18 and 32.

In the walking beam test (Supplementary Fig. 1B) mice crossed the beam towards the narrow end connected to the home cage. A desk lamp was placed behind the starting side of the beam to encourage mice to walk towards the home cage. The cut-off time allowed for crossing the beam was 1 min. Each trial (n = 3 trials in total with 30 min rest between trials) was recorded with a Logitech C525 HD Webcam, and analysed offline. The time to cross the beam and the total number of hind limb 'complete foot slips' (right and left combined) were quantified every third day. In both tests, the number of times mice stopped to perform exploratory behaviours on days 8, 18 and 32 were counted to investigate whether this behaviour was a contributing factor to the time taken to cross the beam or ladder.

2.4. Nociceptive tests

Flexion withdrawal responses were measured every third day by observing the paw withdrawal thresholds to mechanical and thermal stimuli using the dynamic plantar aesthesiometer and Hargreaves apparatus (Bioseb, Vitrolles, France), respectively, as described previously (Samour et al., 2017; Shaikh et al., 2016). Briefly, mice were placed inside a chamber on a wire mesh or glass screen platform for mechanical and thermal tests, respectively. The mechanical stimulus was applied to either the right or the left hind paw at an increasing force rate of 2 g/second until a flexion withdrawal response was evoked or a maximal force of 20 g was achieved. The thermal stimulus was applied using an infrared heat source (power flux: 0.64 mW/cm^2) delivered to the right or left hind paw and the paw withdrawal latency (15 s cut-off) was recorded. On each trial day, five consecutive paw withdrawal latencies were measured (30 min rest between trials).

2.5. Histology

2.5.1. Tissue processing

Mice were anesthetized with isoflurane (2–3% in 100% oxygen; Cenvet, Blacktown, NSW, Australia) and perfused with 30 ml of 0.9% saline using a perfusion pump (Peri-Star, Shanghai, China) followed by 50 ml of ice-cold 4% paraformaldehyde (PFA, Sigma-Aldrich). The cerebrum, cerebellum, brain stem and spinal cord were removed and post fixed in 4% PFA at 4 °C for one week. Tissues were then stored in 0.01 M phosphate buffered saline (PBS, Sigma-Aldrich) containing 0.02% sodium azide (Amresco, Solon, OH, USA) to prevent bacterial growth at 4 °C for up to 1 month. Samples were cryoprotected in distilled water containing 30% sucrose (Coles, Hawthorn East, VIC, Australia) solution for 48 h at RT. Samples were embedded in 4% gelatine (Chem-Supply, Gillman, SA, Australia) in a cryo-mold (Sakura, Torrance, CA, USA) and sectioned coronally at 40 μm using a cryostat (Leica, Wetzlar, HE, Germany). Individual sections were transferred to either 6-well plates (Sakura) containing 5 ml of cold (5–6 °C) 0.01 M PBS for free floating staining or mounted onto 0.5% gelatine-coated

slides (Knittel Glass, Braunschweig, NI, Germany) for silver staining.

2.5.2. Silver myelin staining

This was carried out as previously described (Sen et al., 2019a). Briefly, 40 μm slide-mounted sections were air dried for 48 h and then immersed in 10% formalin (Sigma-Aldrich) for 2 weeks at RT to increase staining contrast. Sections from different animals in each group were stained in parallel to maintain the consistency of staining. Slides were washed with distilled water and pre-treated with a lipid solvent pyridine (VWR, Radnor, PA, USA):acetic anhydride (Merck, Darmstadt, HE, Germany) solution (ratio 2:1) for 30 min at RT. Sections were then rehydrated using serial ethanol washes of 80, 60, 40 and 20% for 20 s each, followed by two washes with distilled water. Washed slides were then immersed in freshly prepared ammonical silver nitrate (Chem-Supply) containing developing solution (0.2% ammonium nitrate, 0.2% silver nitrate and 5% sodium carbonate) for 45 min at RT. Unbound silver was removed by washing with 0.5% acetic acid for 3x3 minutes. Sections were then dehydrated with 20 s rinses of 20, 40, 60, 80 and 100% ethanol followed by immersion in xylene (VWR) for 5 min at RT. Finally, slides were sealed with glass cover slips (Knittel Glass) using 1 ml of Entellan® Mounting Medium (Merck), air dried for 72 h, and stored at RT until viewed under the microscope.

2.5.3. Immunofluorescence staining

Free-floating coronal sections (40 μm) were bathed in warm 0.01 M PBS for 3x5 minutes to remove residual gelatine. Non-specific antigen binding was blocked by immersion in 0.01 M PBS containing 10% normal goat serum (Sigma-Aldrich) at RT for 2 h on an orbital shaker (Fisher Biotec, Wembley, WA, Australia). For single labelling, sections were incubated with primary antibodies (Abs) dissolved in 0.1% Triton X100 (Tx100, Amresco) in 0.01 M PBS (Table 1) for 12 h at RT on an orbital shaker. Sections were washed thrice in 0.01 M PBS and then incubated for 2 h at RT with Alexa Fluor conjugated secondary Abs (Table 1), on an orbital shaker in the dark. Following three more washes in 0.01 M PBS, sections were mounted onto slides and sealed with cover-slips (Knittel Glass) using Vectashield™ plus 4′,6-diamidino-2-phenylindole (DAPI, 1.5 μg/ml, Vector Laboratories, Burlingame, CA, USA) to counterstain nuclei. For the negative control, the primary antibodies were omitted and all other steps carried out as described above. Slides were stored at 4 °C in the dark until viewed under the microscope (within 2 weeks of staining). Double staining using ionized calcium binding adaptor molecule 1 (IBA 1) and glial fibrillary acidic protein (GFAP) was performed by mixing the two primary antibodies (optimized for concentration to avoid bleed through). Blocking, washing, duration of incubation and mounting protocols were the same as used in single labelling tissue sections. Fluorescence intensity quantification was performed on the single stained sections and double-labelled images were used for illustrative purposes.

2.5.4. Image analysis

2.5.4.1. Silver myelin intensity. All images were captured using a brightfield microscope (Carl Zeiss, Jena, TH, Germany) using the same parameter settings for exposure time and illumination intensity. Images were analysed using ImageJ software (https://imagej.nih.gov/). The region of interest of an image was contoured and the mean optical density was quantified as mean grey value (0–256, back-white): sum of all the pixels in the region of interest divided by the number of pixels (range black). In silver-stained tissue sections, normal myelin sheaths appear darkly stained and demyelinated sheaths appear lightly stained, so the signal intensity *increases* as myelin stain *decreases*.

Significant differences were confirmed by comparing the light intensity in control and CPZ-fed animals in each region of interest. In order to show the extent CPZ-induced demyelination across regions of high (nuclear) and low (tract regions) light intensity under control conditions (where myelin staining can vary up to 10-fold) changes were plotted on a common linear scale as function of their respective control

Table 1
Antibodies used in the present study.

Target protein/antigen	Primary			Secondary			
	Antibody	Dilution	Catalogue/company	Antibody	Dilution	Catalogue/company
Astrocytes	Mouse anti-GFAP Alexa Fluor 488 conjugate	1:1000	MAB3402X, Merck-Millipore, Burlington, MA, USA	–	–	–
Microglia	Rabbit anti-IBA 1	1:1000	019–19741, Wako, Chuo-Ku, OSA, Japan	Alexa Fluor 594 conjugated goat anti-rabbit IgG	1:500	A-11007, Invitrogen, Norcross, GA, USA
Mature OLG	Rabbit anti-APC	1:500	AB5664P, Merck-Millipore	Alexa Fluor 488 conjugated goat anti-rabbit IgG	1:500	A-21428, Invitrogen
Clarke's nucleus	Moue anti-NeuN	1:500	MAB377, Merck-Millipore	Alexa Fluor 488 conjugated goat anti-mouse IgG	1:500	R-37120, Invitrogen
Motor neurons	Rabbit anti-ChAT Alexa Fluor 488 conjugate	1:100	ab192465, Abcam, Cambridge, UK	–	–	–
Purkinje neurons	Rabbit anti-Calb	1:1000	AB1778, Merck-Millipore	Alexa Fluor 594 conjugated goat anti-rabbit IgG	1:500	A-21428, Invitrogen

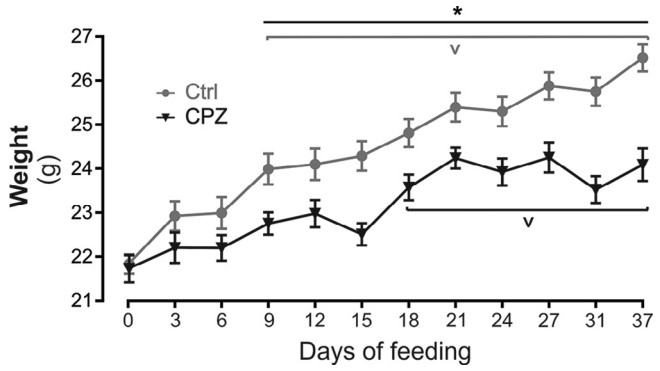

Fig. 1. Effects of CPZ on body weight. CPZ-fed mice gained weight more slowly compared to control mice. Two-way ANOVA was used to determine the effects of time. Tukey post hoc analysis was used to determine differences between groups (*$p < 0.05$) and the duration of feeding compared to baseline ($\dot{p} < 0.05$). Data is mean ± SEM (n = 10 animals/group). g = gram, Ctrl = control.

value (i.e. CPZ-fed/control, fold change) in each region of interest. In all histological quantification graphs, nuclear and *tract* regions were denoted by the use of black and grey colour coding respectively, on the x-axes labels. No change between CPZ-fed and control groups was detailed as a 1-fold change whereas a 2-fold change equated to doubling of the light intensity.

2.5.4.2. Immunofluorescence intensity measurement. All images were captured using a fluorescence microscope (Carl Zeiss, Germany) using the same parameters (exposure 100 ms at 20x magnification). Images were opened in ImageJ and fluorescence intensity was measured from each region of interest as described above. Data are presented as fold change relative to control.

2.5.4.3. Stereological quantification of cell numbers. Cells positively stained for adenomatous polyposis coli (APC) and neuronal nuclei (NeuN, co-stained with DAPI) were counted using the stereo investigator optical fractionator workflow software (www.mbfbioscience.com/stereology) as described previously (Sen et al., 2019a). At low magnification (10x or 20x objective), the region of interest was contoured and nucleated cells (DAPI positive) in every ninth section (360 μm apart) were quantified at high magnification (63x). To obtain the cell density, the total cell number was divided by the total measured volume and expressed as 10^4 cells/mm^3. Data are presented as fold change relative to control. The details of the parameters for stereology counting can be accessed at the following link (http:\\galen.uws.edu.au\mmrg\monokesh).

2.5.4.4. Manual counting. Choline acetyltransferase (ChAT) positive neurons in the spinal cord and calbindin (Calb) positive Purkinje neurons in the cerebellum were counted manually.

2.6. Anatomical structures

The different CNS regions were identified according to the mouse brain atlas and spinal cord landmarks (Gyengesi et al., 2014; Harrison et al., 2013; Paxinos and Franklin, 2012; Sengul et al., 2015).

2.7. Statistical analysis

Behavioural parameters and body weight analysis were performed using a Repeated Measures Two Way Analysis of Variance (RMANOVA) with post hoc tests to investigate individual differences between groups. For histological analysis, 3–5 sections per animal from 3 to 5 animals per group were quantified. Individual comparisons in histology used an unpaired two-tailed *t*-test to determine the consistency and difference between two groups. The regional (rostral-caudal) distribution of demyelination and gliosis in corpus callosum was analysed using two-way ANOVA. The relationship between gliosis and demyelination was evaluated in the corpus callosum, cerebellar nuclei, brain stem and spinal cord. The correlation coefficient R^2 was calculated by plotting the intensity values of GFAP and IBA 1 against the silver staining values (measuring demyelination) and linear correlation analysis was carried out at 95% confidence interval. Data were presented as fold change.

Data are presented as means ± standard error of the mean (SEM). Significant interaction effects are described in the figure legends. The criterion for statistical significance was set at $p < 0.05$. Statistical analyses were performed using GraphPad Prism (version 8.3, GraphPad Software, San Diego, CA, USA) software. All figures were constructed using CorelDRAW (version 2018, www.coreldraw.com, Ottawa, ON, Canada) and Adobe Photoshop CS5 (Adobe, San Jose, CA, USA).

3. Results

3.1. General behaviour

There were no obvious changes in posture, general locomotion or body fur condition, or obvious neurological deficits apparent in any of the mice. All mice gained weight over the course of the experiment but the CPZ group gained weight more slowly than controls ($F(11, 99) = 125$, $p < 0.05$), with the divergence beginning after 9 days of CPZ-feeding and persisting thereafter ($p < 0.05$, Fig. 1). By the end of the experiment, control mice had increased their body weight by 21% compared to 11% for CPZ-fed mice (Fig. 1, $p < 0.05$).

3.2. Locomotion and motor coordination tests

Using the rotarod apparatus, three different aspects of locomotion were measured on a weekly basis: latency to fall from the apparatus, time to first roll around cylinder and number of roll revolutions before the mouse fell off the apparatus (Fig. 2**A–C**). No significant differences were found between control and CPZ-fed mice for any parameter measured ($p > 0.05$, two-way ANOVA).

Using the ladder crossing test, it was observed that during the first two weeks, both control and CPZ-fed mice took significantly longer to cross the ladder compared to later time points (Fig. 2**D, F**$(9, 90) = 1.48$, $p < 0.05$). This was confirmed by analysis of the exploratory behaviour at selected time points (days 8, 18 and 32) which showed that mice in both groups spent more time stopping and exploring their local environment rather than crossing the ladder at earlier compared to later times (Fig. 2**E**, $p < 0.05$, RMANOVA). Between-group differences in the speed of crossing the ladder were observed only during the fourth week of CPZ-feeding. Further analysis of the number of foot slips revealed that after two weeks of CPZ-feeding, treated mice experienced significantly more forelimb foot slips (Fig. 2 **F, G,** $F(9, 81) = 11.71$, $p < 0.05$) that persisted thereafter. However, no such deficit was observed for the hind limbs (Fig. 2**H, I**).

In the walking beam test there was no significant difference between groups in the time taken to cross the beam (Fig. 2**J**). However, it was noted for both groups that it took progressively longer for the mice to complete the task which began after 3 weeks and was clearly evident during the 5th week ($F(9, 81) = 12.26$, $p < 0.05$). This increase was primarily due to increased exploratory behaviour (Fig. 2**K**). However, in the CPZ group, a significant increase in hindlimb foot faults occurred during week 5 of feeding whereas control mice rarely made foot faults, and this did not change over time (Fig. 2**L**).

3.3. Nociceptive thresholds

No differences in withdrawal latencies or thresholds were found at any time points within or between groups for either thermal or

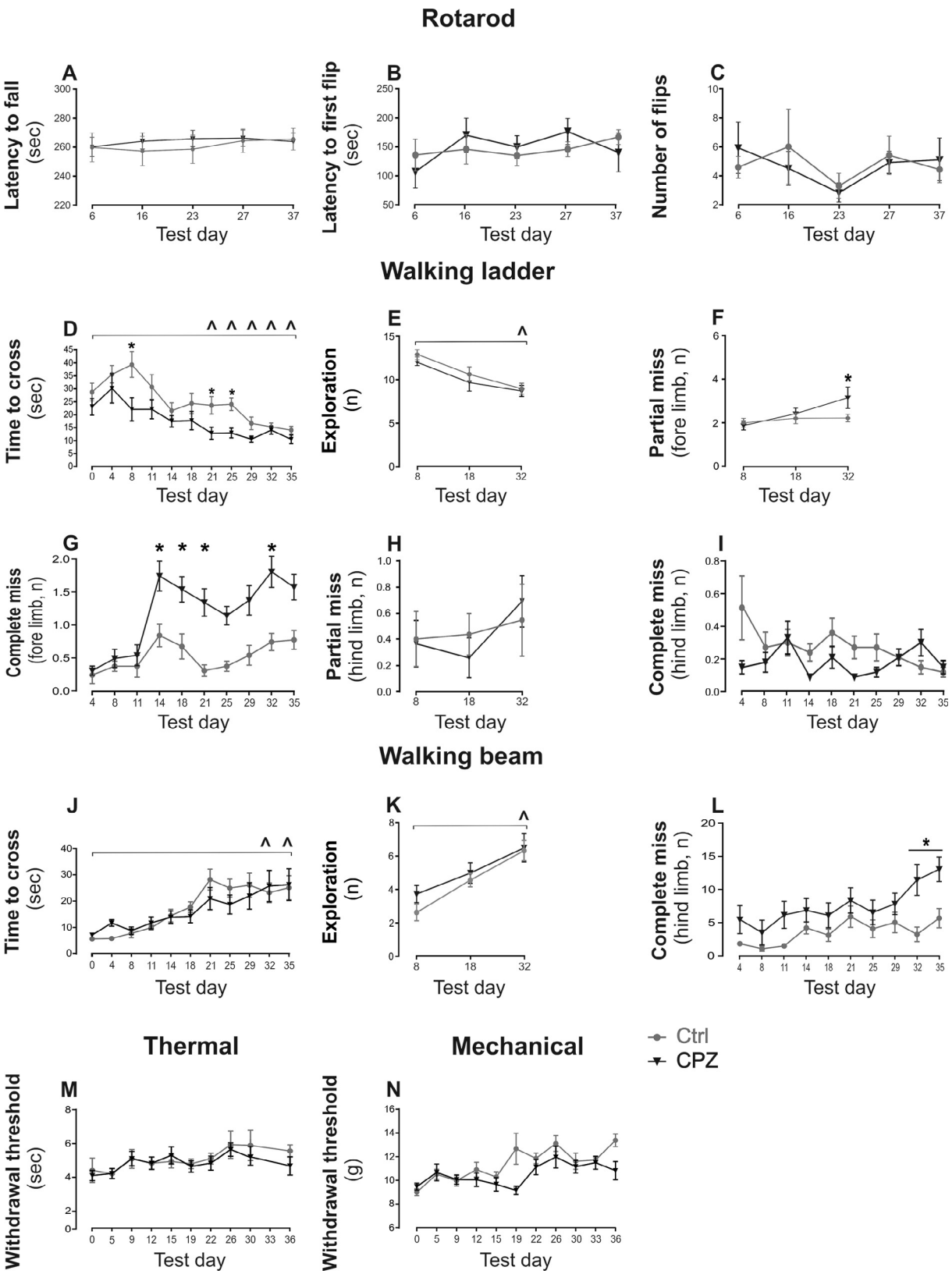

Fig. 2. Behavioural assessments. Rotarod measurements: (A) latency to fall off the apparatus, (**B**) time to first flip, and (**C**) number of flips before falling off. **Walking ladder test measurements**: time to cross ladder (**D**) number of stops for exploratory behaviour during ladder crossing **(E)** partial or complete forelimb (**F, G**) or hindlimb (**H, I**) foot slips. **Walking beam test measurements**: time to cross beam (**J**), number of complete hind limb foot slips (**K**) and number of stops for exploratory behaviour whilst crossing (**L**). **Measurements of thermal** (**M**) and **mechanical** (**N**) **nociceptive paw withdrawal thresholds**. Abbreviations: sec, seconds; n, number and g, grams force. Two-way ANOVA & Tukey post hoc analysis were used to determine between group differences and RMANOVA was used to determine individual group differences over time $*p < 0.05$. Data are expressed as mean ± SEM (n = 10 animals/group). $*p < 0.05$ (difference between groups) and $\hat{}p < 0.05$ (difference across time points compared to the first day of testing). Ctrl = control.

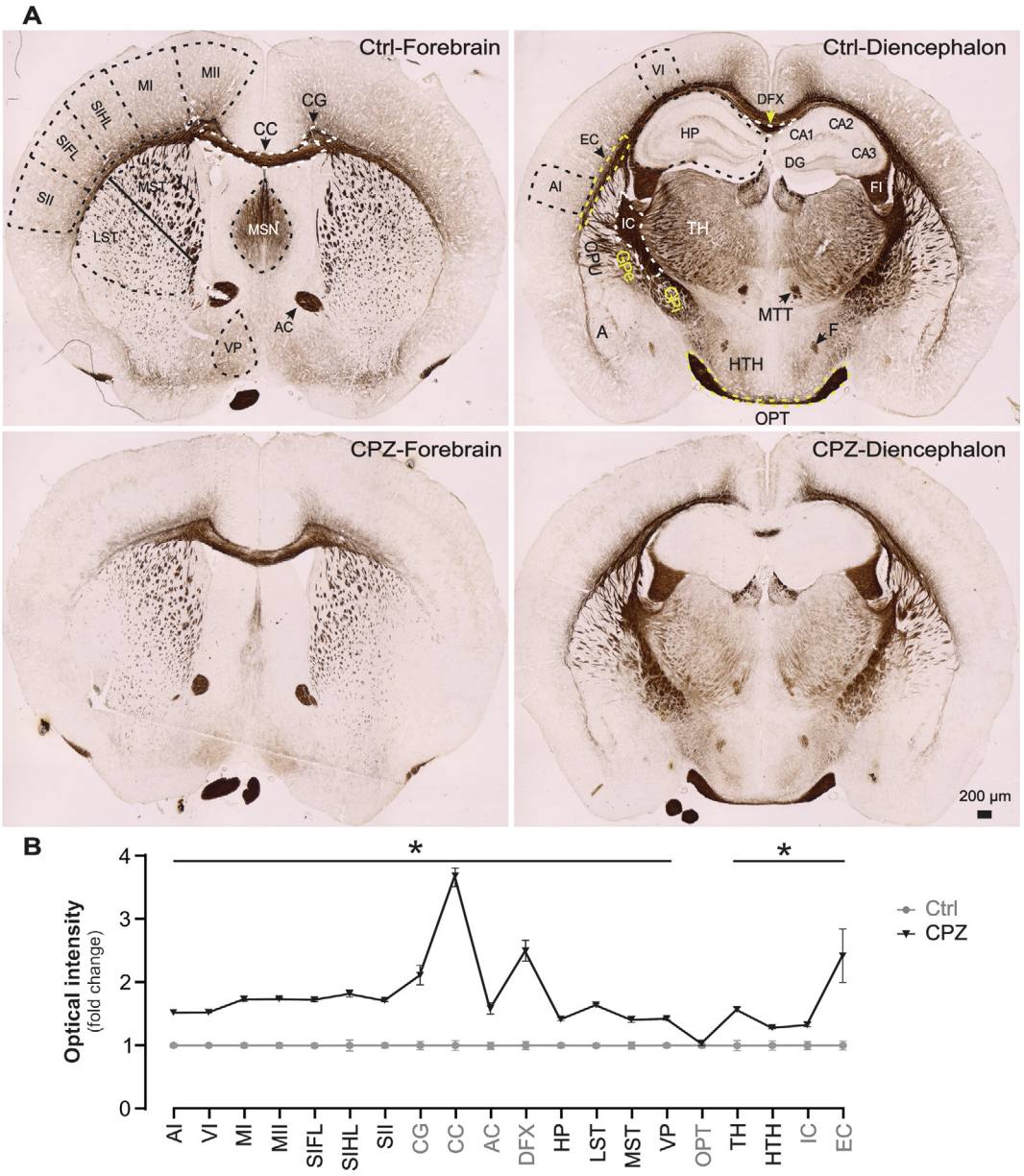

Fig. 3. Effects of CPZ on demyelination in the cerebrum. A). Representative examples of silver stained images of the grey and white matter regions of the forebrain and diencephalon. **B**). Quantification, (n = 5 animals/group and 3–5 sections/animal). Data are presented as the mean (± SEM). An unpaired two-tailed *t*-test was used to determine differences between groups. Significant differences amongst groups are indicated by $*p < 0.05$. Dashed lines show the regions either quantified or discussed in the text. Abbreviations: AC, anterior commissure; AI, primary auditory cortex; CC, corpus callosum; CG, cingulum; CPU, caudate putamen; Ctrl, control; DFX, dorsal fornix; DG, dentate gyrus; EC, external capsule; F, fornix; FI, fimbria; GPe, external globus pallidus; GPi, internal globus pallidus; HP, hippocampus; HTH, hypothalamus; IC, internal capsule; LST, lateral striatum; MST, middle striatum; MSN, middle septal nucleus; MI, primary motor cortex; MII, secondary motor cortex; MTT, mammillothalamic tract; OPT, optic tract; SIFL, primary somatosensory forelimb cortex; SIHL, primary somatosensory hindlimb cortex; SII, secondary somatosensory cortex; TH, thalamus; VI, primary visual cortex and VP, ventral pallidum.

mechanical sensitivity ($p > 0.05$, 2-way ANOVA, Fig. 2**M**, **N**).

3.4. Histology

3.4.1. Cerebrum

The cerebrum comprises the cerebral cortices, the underlying hippocampi and basal ganglia and associated white matter tracts. To confirm the effectiveness of CPZ, the amount of demyelination and loss of mature OLG cells were quantified using silver- and APC-staining, respectively, in the corpus callosum (Fig. 3; Supplementary Fig. 2). CPZ-fed mice showed a significant reduction ($p < 0.05$) in myelin staining and OLG numbers compared to control in the midline corpus callosum (Fig. 3). Further analysis revealed a regional difference in the rostro-caudal plane with regard to demyelination in the corpus callosum, with significantly more demyelination in caudal sections (Supplementary Fig. 3D). In addition, a differential demyelination between the corpus callosum and the underlying dorsal fornix as well as the adjacent cingulum was evident (Fig. 3). This prompted a more careful look at other white matter tracts in the forebrain. Demyelination occurred in the external capsule as well as the anterior commissure, but not in the optic nerve/tract (Fig. 3). In the cortical grey matter of control mice, silver staining was differentially distributed with strong staining in the deeper layers that became less intense toward the cortical surface (Fig. 3). Following CPZ-feeding, extensive demyelination was observed in areas such as the auditory, visual, primary motor, secondary motor, primary motor forelimb and hindlimb and secondary

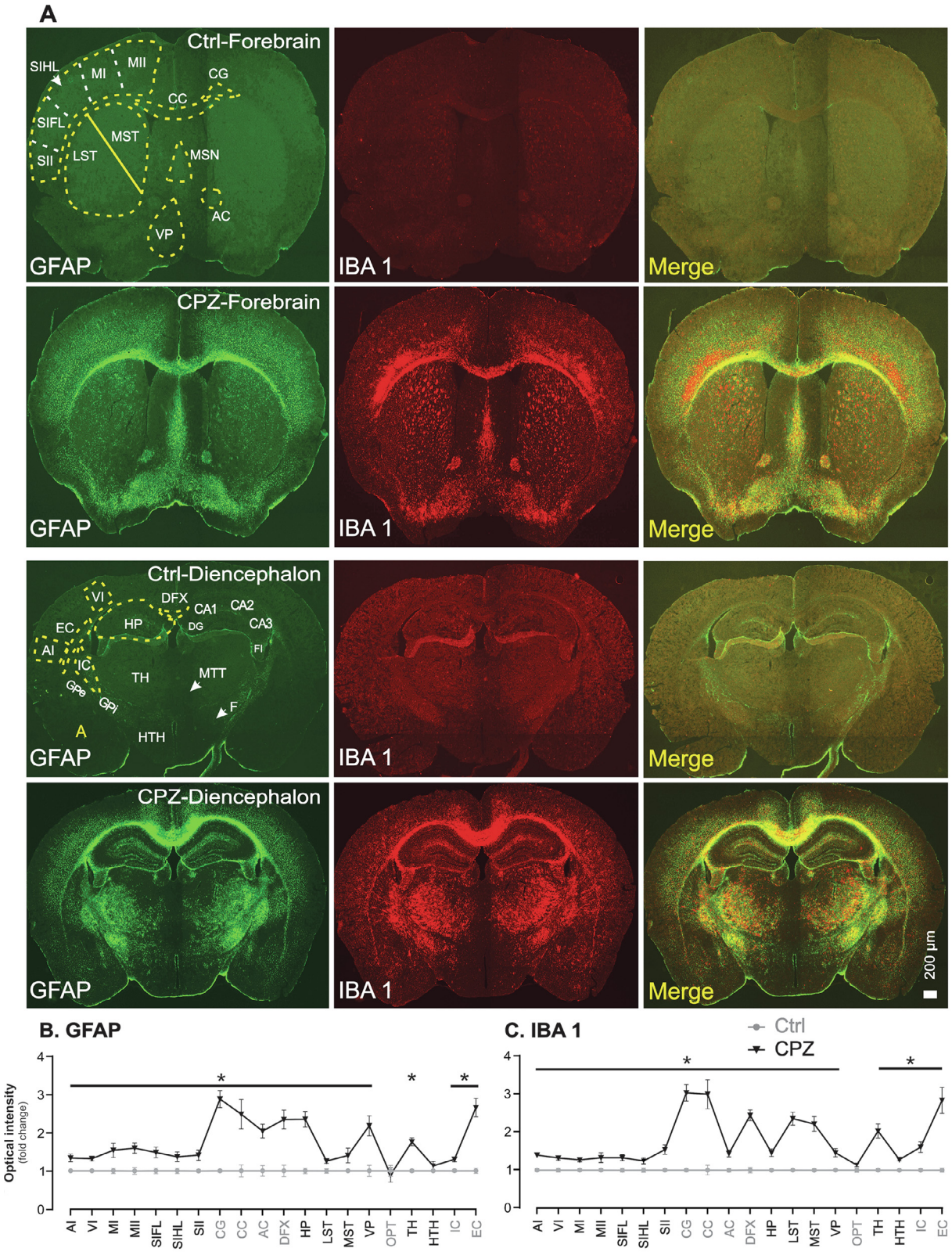

Fig. 4. Effects of CPZ on gliosis in the cerebrum. Representative images A (rostral, top and caudal, bottom) of GFAP, IBA 1 and merged staining and quantification of GFAP (**B**) and IBA 1 (**C**), respectively (n = 5 animals/group and 3–5 sections/animal) in the grey and white matter regions of the cerebrum. Data are presented as the mean (± SEM). An unpaired two-tailed *t*-test was used to determine differences between groups. Significant differences amongst groups are indicated by $*p < 0.05$. Dashed lines show the regions either quantified or discussed in the text. Abbreviations: AC, anterior commissure; AI, primary auditory cortex; CC, corpus callosum; CG, cingulum; Ctrl, control; DFX, dorsal fornix; DG, dentate gyrus; EC, external capsule; F, fornix; FI, fimbria; GPe, external globus pallidus; GPi, internal globus pallidus; HP, hippocampus; HTH, hypothalamus; IC, internal capsule; LST, lateral striatum; MST, medial striatum; MSN, medial septal nucleus; MI, primary motor cortex; MII, secondary motor cortex; MTT, mammillothalamic tract; SIFL, primary somatosensory forelimb cortex; SIHL, primary somatosensory hindlimb cortex; SII, secondary somatosensory cortex; TH, thalamus; VI, primary visual cortex and VP, ventral pallidum.

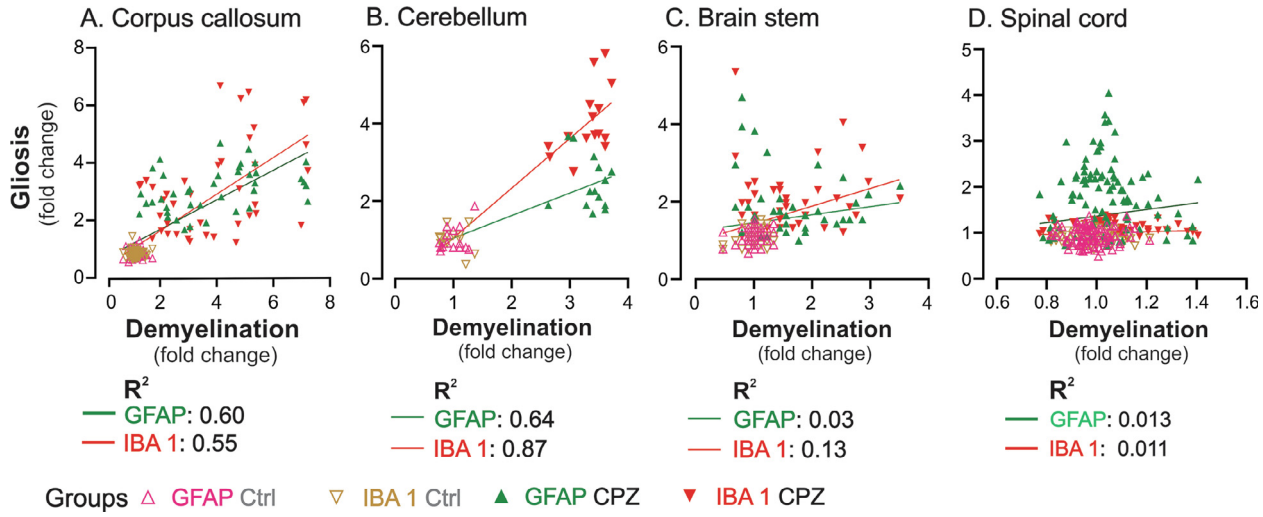

Fig. 5. Relationship of demyelination to gliosis in different regions of the CNS. Pearson's correlation coefficients for astro- and micro-gliosis as function of demyelination in the corpus callosum **A**), cerebellum **B**), brain stem **C**) and spinal cord **D**). Ctrl = control.

somatosensory cortical regions (Fig. 3). Gliosis was also a hallmark of CPZ-induced pathology in the demyelinated areas. In the cerebrum of CPZ-fed mice, there was a significant increase in IBA 1 and GFAP staining in all regions where silver staining was decreased (Fig. 4; Supplementary Fig. 3B, C, E, F). Correlation analysis in the corpus callosum demonstrated that the intensity of gliosis was proportional to the amount of demyelination (Fig. 5).

Given that the cingulum and fornix showed demyelination, an investigation of the hippocampus was performed. A generalised decrease in silver staining was observed with a concurrent decrease in APC number in the hippocampus (Fig. 3; Supplementary Fig. 2). GFAP staining increased in the fimbria of the fornix. In the hippocampal grey matter, increased staining occurred particularly in the dentate gyrus (granular region), the molecular layer of CA1-3, and the outer perimeter of the hippocampal complex (alveus and stratum oriens) compared to control mice (Fig. 4). Similarly, an increase in IBA 1 staining within the hippocampus was observed but with some differences e.g. no obvious increase in the dentate gyrus area (Fig. 4).

Analysis of the basal ganglia revealed demyelination in the lateral and medial striatal regions, globus pallidus external and internal segments, medial septal nucleus, ventral pallidum and substantia nigra (Fig. 3) regions. In the striatum, demyelination was more evident in the lateral region compared to the medial region, especially the ventrolateral area. Increased GFAP staining was more generalised throughout the striatum, whereas increased IBA 1 staining was seen particularly associated with the striosomes (fibres of passage) in the striatum of CPZ-fed mice compared to control (Fig. 4). Strong gliosis was seen in the globus pallidal regions (Fig. 4). Likewise, marked IBA 1 staining occurred in the medial septal nucleus, ventral pallidum and substantia nigra regions (Figs. 4 and 7).

3.4.2. Diencephalon

Demyelination was observed in the internal and external capsules, and thalamic regions (both sensory and motor), with a concomitant elevated glial response (Figs. 3 and 4). However, in the hypothalamus, although there was a significant decrease in silver staining (Fig. 3), there was only a very limited gliotic response with elevated microglial staining restricted to the lateral hypothalamic regions through which the medial forebrain and nigrostriatal pathways run. The astroglial response was essentially unchanged from controls (Fig. 4). Demyelination and gliosis were also observed in the mammillary body nuclei (Figs. 4, 6, 7).

3.4.3. Midbrain

Inspection of silver-stained midbrain sections in CPZ mice showed that only certain regions were affected. Decreased silver staining occurred in the commissural axons connecting the superior and inferior colliculi, inferior colliculi, substantia nigra, tegmental region (including the trigeminal mesencephalic and motor nuclei) and the periaqueductal grey compared to control (Fig. 6). No decrease in silver staining was seen in areas such as the superior colliculus, the mesencephalic or red nuclei (Fig. 6**B**). In contrast, some gliosis occurred in the red nucleus, tegmental and ventral periaqueductal grey regions but not in the superior colliculus or mesencephalic nucleus as confirmed by GFAP and IBA 1 staining (Fig. 7).

3.4.4. Hindbrain

Visual inspection of silver-stained slides showed that specific regions of the hindbrain were affected. Significant demyelination was seen in the deep cerebellar nuclei (Fig. 6). This result was consistent with the significantly decreased number of APCs and the increased GFAP and IBA 1 staining in the deep cerebellar nuclei regions (Supplementary Fig. 2; Fig. 7). Correlation analysis of this region (deep cerebellar nuclei) revealed that the intensity of gliosis was proportional to the amount of demyelination (Fig. 5). However, other white matter regions of the cerebellum such as the arbor vitae within the different lobes appeared unchanged with respect to silver staining even though quantification of APC numbers and glial cell responses showed significant changes (Supplementary Fig. 2; Fig. 6). Quantification of Purkinje cell numbers using calbindin staining from the cerebellar vermis of lobules 6, 9, 10 did not detect any changes compared to control ($p > 0.05$, Supplementary Fig. 4). No obvious change in silver staining was seen in the middle and inferior cerebellar peduncles (Fig. 6**A, B**) whereas significant decreased staining ($p < 0.05$) occurred in the superior cerebellar peduncles of CPZ-fed mice compared to controls (Fig. 6). Quantitative analysis of OLG numbers in the hindbrain showed a clear reduction of APC positive OLG in the cerebellar nuclei regions ($p < 0.05$, Supplementary Fig. 2). In contrast, no significant APC cell loss was found in the middle cerebellar peduncle (Supplementary Fig. 2**A-C**). Additionally, a significant increase in GFAP and IBA 1 intensity ($p < 0.05$) was found in superior cerebellar peduncle (Fig. 7). In contrast, only increased GFAP, but not IBA 1, intensity was found in the inferior cerebellar peduncle (Fig. 7).

Silver staining in the pons revealed significant demyelination, OLG cell loss and gliosis in all the vestibular nuclei as well as the prepositus nuclei and medial longitudinal fascicular tract (Supplementary Fig. 1; Figs. 6 and 7). However, little demyelination or gliosis was seen in the

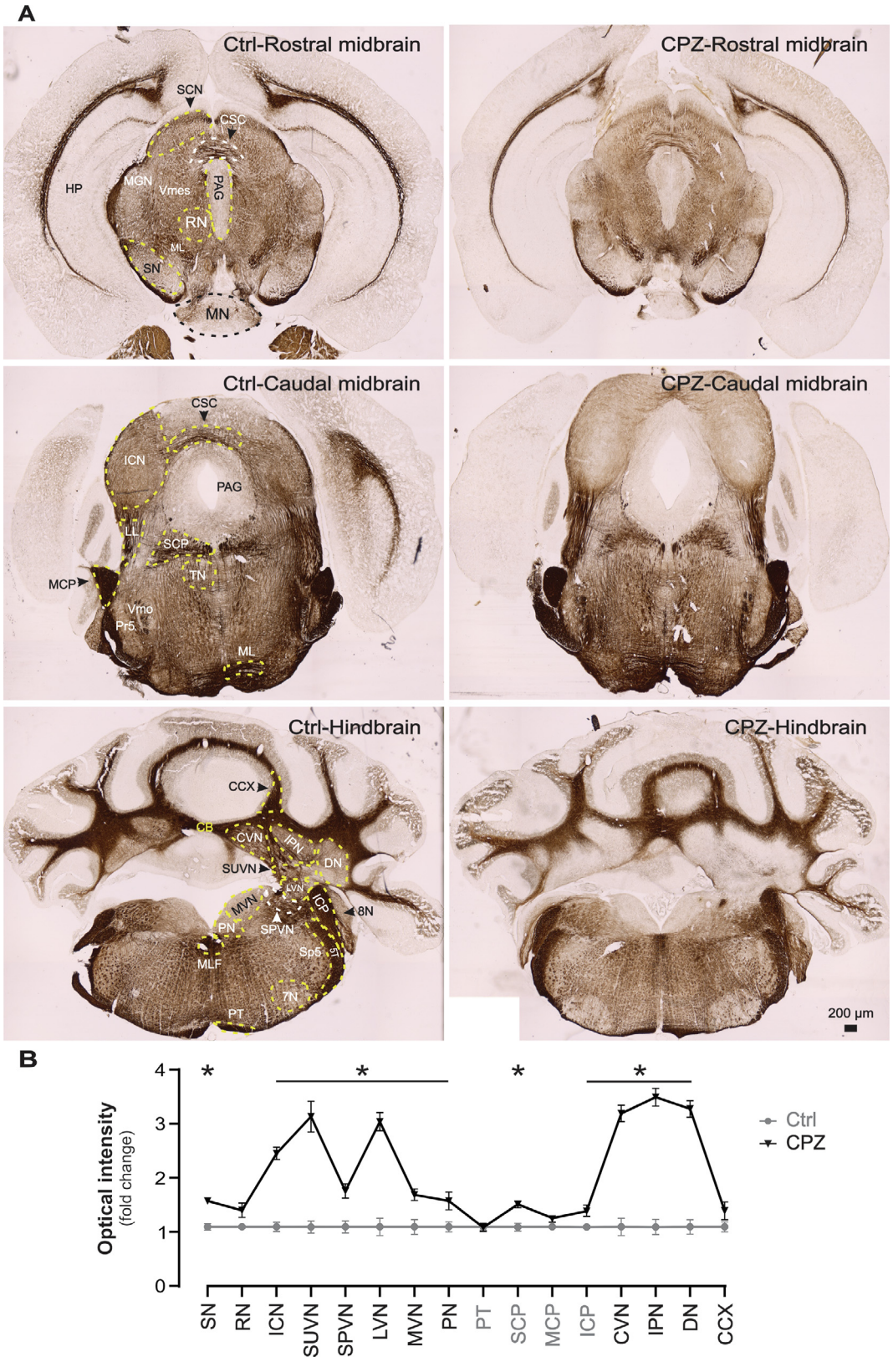

(caption on next page)

vestibulocochlear nerve. Additionally, silver staining in the pons and medulla suggested a generalised decrease in intensity, making nuclei such as the facial and trigeminal nuclei more prominent (Fig. 6). However, very little gliosis was seen within the pons and medulla of CPZ-fed mice and when detected the affected areas did not always coincide (Fig. 7). For example, elevated GFAP staining occurred in the trigeminal tract, facial and vestibulocochlear nerves and in the closed medulla around the central canal near the vagal and hypoglossal nuclei (data not shown) whereas IBA 1 levels appeared unchanged. Conversely, increased IBA 1 staining was seen in areas corresponding to the

Fig. 6. Effects of CPZ on demyelination in the mid- and hind-brain. Representative images **A**) and quantification **B**) of silver-stained images (n = 5 animals/group and 3–5 sections/animal) in the grey and white matter regions of the mid and hind brain. Data are presented as the mean (± SEM). An unpaired two-tailed *t*-test was used to determine differences between groups. Significant differences among the groups are indicated by $*p < 0.05$. Dashed lines show the regions either quantified or discussed in the text. Abbreviations: 5T, trigeminal tract; 7N, facial nucleus; 8N, vestibulocochlear nerve; CB, cerebellar vermis; CCX, cerebellum cortex; CSC, commissure superior colliculus; Ctrl, control; CVN, cerebellar vestibular nucleus; DN, dentate nucleus; HP, hippocampus; ICN, inferior colliculus nucleus; ICP, inferior cerebellar peduncle; IPN, interposed nucleus; LL, lateral lemniscus; LVN, lateral vestibular nucleus; ML, medial lemniscus; MCP, middle cerebellar peduncle; MGN, medial geniculate nucleus; MLF, medial longitudinal fasciculus; MN, mammillary nucleus; MVN, middle vestibular nucleus; PAG, periaqueductal grey; Pr5, principal trigeminal nucleus; PN, prepositor nucleus; PT, pyramidal tract; RN, red nucleus; SCN, superior colliculus nucleus; SCP, superior cerebellar peduncle; SN, substantia nigra; Sp5, spinal trigeminal nucleus; SPVN, spinal vestibular nucleus; SUVN, superior vestibular nucleus; TN, tegmental nucleus; Vmo, trigeminal motor nucleus and Vmes, trigeminal mesencephalic nucleus. (For interpretation of the references to colour in this figure legend, the reader is referred to the web version of this article.)

pyramidal tract whereas GFAP was not (Fig. 7). Correlation analysis in the brain stem demonstrated that the intensity of gliosis was not proportional to the amount of demyelination (Fig. 5).

3.4.5. Spinal cord

Analysis of silver staining in the spinal cord revealed intense staining in the white and grey matter regions at all levels (Fig. 8**A, C**), with no significant difference in intensity between CPZ-fed and control mice. Importantly, quantification of APC-positive OLG staining in different spinal cord regions revealed no differences at any level in control vs CPZ-fed mice (Fig. 8**B, D**, $p > 0.05$). Surprisingly, GFAP staining was significantly increased in the white matter tracts of CPZ-fed mice in cervical, thoracic and lumbar regions whereas grey matter levels were similar between groups (Fig. 8**E, F**). When the microglial response was analysed with IBA 1, significant changes were observed mainly in the cervical spinal cord in both white and grey matter regions (Fig. 8**E**, **G**). Thus, gliosis in the spinal cord did not correlate with the demyelination (Fig. 5).

Given that the behavioural motor deficits could indicate loss of motor output, the number of motor neurons in cervical and lumbar regions was quantified using ChAT as a marker. No significant difference between control and CPZ-fed mice was found (Fig. 9**A, B**). NeuN staining was used to identify Clarke's nucleus (the ascending proprioceptive neurons of the spinocerebellar tract) in the medial deep dorsal horn of the thoracic and cervical cord. No significant difference in NeuN numbers between groups was found (Fig. 9**C, D**).

4. Discussion

Feeding mice with 0.2% CPZ for 37 days produced subtle deficits associated with motor coordination. Nociceptive withdrawal thresholds were unaffected. Histological analysis of the CNS confirmed the demyelination and gliosis in the corpus callosum, hippocampus, basal ganglia and deep cerebellar nuclei. However, this study extends the histopathological knowledge by detailing and quantifying demyelination and gliosis in other regions such as the limbic circuits, deep cerebral cortical regions, thalamic nuclei and brain stem nuclei associated with balance and audio-visual reflex responses. Within the spinal cord, demyelination of white matter tracts was not obvious but increased astrocyte staining occurred at all spinal levels whereas the microglial response was much more limited. The profound histological changes in hindbrain motor pathways suggest that degeneration of vestibulocerebellar connections may play an important role in the abnormal behaviour. Most importantly, quantitative analysis clearly showed that OLG cells were lost within the brain but that this did not occur in the spinal cord.

4.1. Motor behaviour in relation to histological changes

Initiation and coordination of voluntary movements involves four hierarchical systems: upper motoneurons of the pyramidal and extrapyramidal (brain stem) systems (to initiate voluntary movements), the basal ganglia (motor program storage), the cerebellum (motor coordination) and the spinal cord lower motoneurons (movement execution). Histological analysis revealed profound demyelination in all these regions, except the spinal cord. For example, reduced silver staining occurred in the primary motor (MI), secondary motor and somatosensory cortex cortical grey areas, with a corresponding increase in GFAP and IBA 1 staining. These regions are associated with the origin of the pyramidal tract whose axons run through the internal capsule and ventral parts of the brain stem, areas that also showed demyelination and gliosis. Studies using transient optogenetic inactivation of the forelimb motor cortex areas in mice produced a reduction of choice and executive functions (Morandell and Huber, 2017) and lesions of the MI cortex affect the learning and execution of motor tasks (Heindorf et al., 2018). Injury in the corticospinal tract has been associated with motor impairment in rats (Bieler et al., 2018). The marked degeneration and gliosis in the commissural tracts (corpus callosum and anterior commissure) may also have contributed to the incoordination, as other studies have shown impairment of complex motor tasks such as bimanual finger movements (Bonzano et al., 2008; Gean-Marton et al., 1991; Huitinga et al., 2001).

It was hypothesised that increasing the complexity of the motor task would produce subtle behavioural deficits (Sen et al., 2019b). The rotarod apparatus did not to detect any motor deficits in CPZ-fed animals, consistent with prior studies (reviewed in Sen et al., 2019b). In this study, motor deficits were manifest as errors in paw placement on the ladder rungs or foot slips (i.e. dysmetria), and were present from the second to fifth weeks of CPZ-feeding.

Dysmetria is a symptom of ataxia often associated with damage to the posterior lobe of the cerebellum (Ha et al., 2016; Soblosky et al., 1997). These results are consistent with other studies using the complex wheel apparatus which detected ataxia within 2–3 weeks of CPZ-feeding (Hibbits et al., 2009; Liebetanz and Merkler, 2006; Manrique-Hoyos et al., 2012; Mierzwa et al., 2013). The ladder test detected early motor deficits while the beam test detected deficits at later time points, which may be related to the different visuospatial aspects of each test. Both the walking ladder and walking beam are thus sensitive tests to detect and quantify deficits of motor coordination in mice.

The most profound histological changes occurred in the cerebellum. At 5 weeks, only the deep cerebellar nuclei showed intense gliosis and demyelination, as previously documented (Skripuletz et al., 2010). Purkinje cells and the cerebellar cortex were unaffected, consistent with the fact that cerebellar demyelination gets progressively worse so that both grey and white matter were maximally affected by 12 weeks of CPZ-feeding (Skripuletz et al., 2010). The cerebellar nuclei receive inputs from the somatosensory, pontine and vestibular systems, with the latter having reciprocal connections. No demyelination was seen in the inferior and middle cerebellar (input) penduncles but demyelination occurred only in the superior cerebellar (output) peduncles suggesting that the ataxia was more likely due to cerebellar output, rather than input. The superior cerebellar peduncles project to the hypothalamus, motor thalamus, basal ganglia nuclei and brain stem, all of which also showed demyelination. Interestingly, demyelination in the medial cerebellar nucleus may be associated with the reduced weight gain seen in CPZ-fed mice compared to controls since this nucleus has direct connections with the hypothalamic satiety centres (Li et al., 2017), regions which showed demyelination and gliosis in this study.

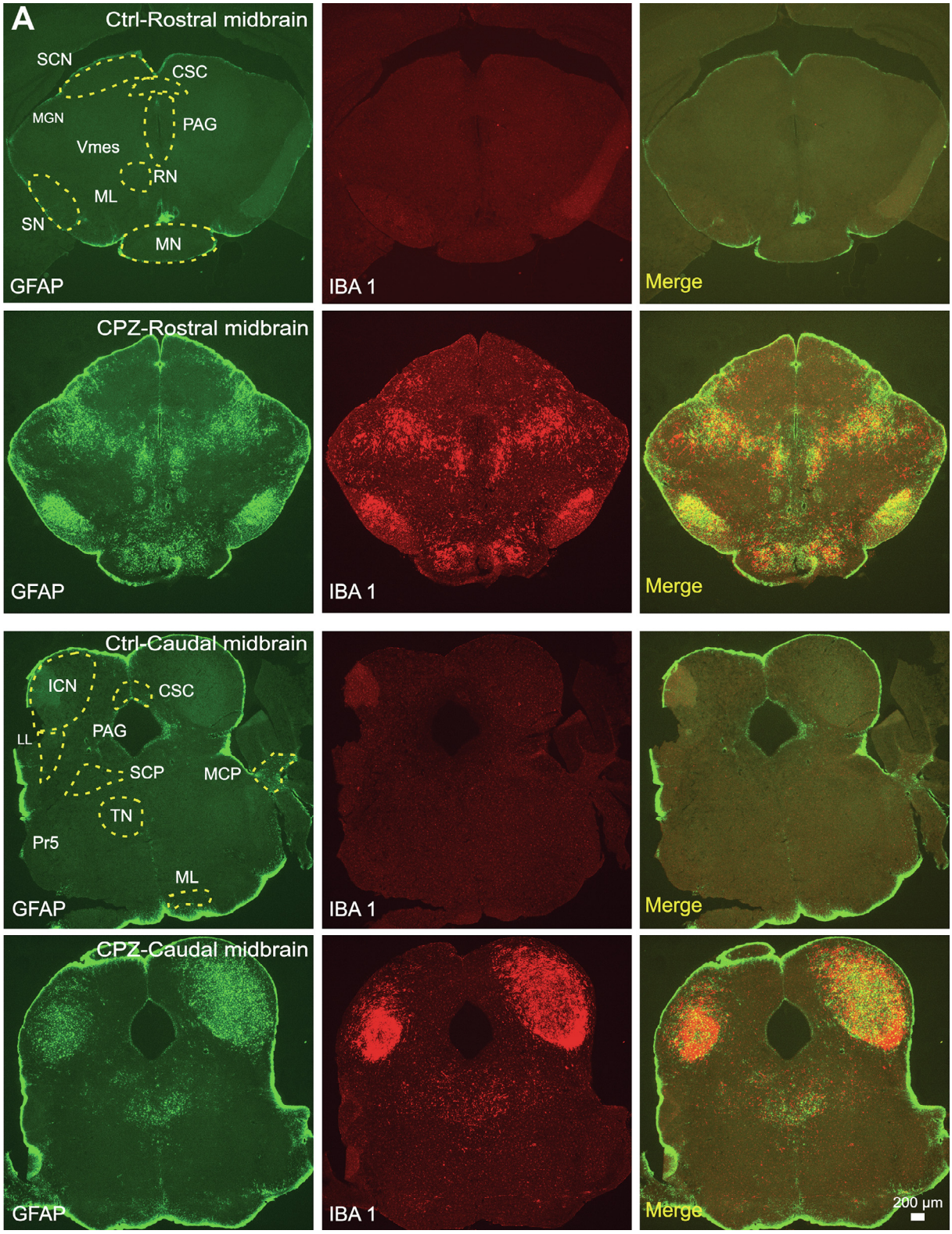

Fig. 7. Effects of CPZ on gliosis in the midbrain and hindbrain. Representative images of GFAP, IBA 1 and merged staining **A**, **B**) and quantification **C**, **D**) of GFAP and IBA 1-stained images (n = 5 animals/group and 3–5 sections/animal) in the grey and white matter regions of the mid- and hindbrains. Data are presented as the mean (± SEM). An unpaired two-tailed *t*-test was used to determine differences between groups. Significant differences among the groups are indicated by $^{*}p < 0.05$. Dashed lines show the regions either quantified or discussed in the text. Abbreviations: 5 T, trigeminal tract; 7 N, facial nucleus; 8 N, vestibulocochlear nerve; CB, cerebellar vermis; CCX, cerebellum cortex; Ctrl, control; CVN, cerebellar vestibular nucleus; DN, dentate nucleus; ICN, inferior colliculus nucleus; ICP, inferior cerebellar peduncle; IPN, interposed nucleus; LL, lateral lemniscus; LVN, lateral vestibular nucleus; ML, medial lemniscus; MCP, middle cerebellar peduncle; MGN, medial geniculate nucleus; MLF, medial longitudinal fasciculus; MN, medial mammillary nucleus; MVN, middle vestibular nucleus; PAG, periaqueductal grey; Pr5, principal trigeminal nucleus; PN, prepositus nucleus; PT, pyramidal tract; RN, red nucleus; SCN, superior colliculus nucleus; SCP, superior cerebellar peduncle; SN, substantia nigra; Sp5, spinal trigeminal nucleus; SPVN, spinal vestibular nucleus; SUVN, superior vestibular nucleus; TN, tegmental nucleus and Vmes, trigeminal mesencephalic nucleus. (For interpretation of the references to colour in this figure legend, the reader is referred to the web version of this article.)

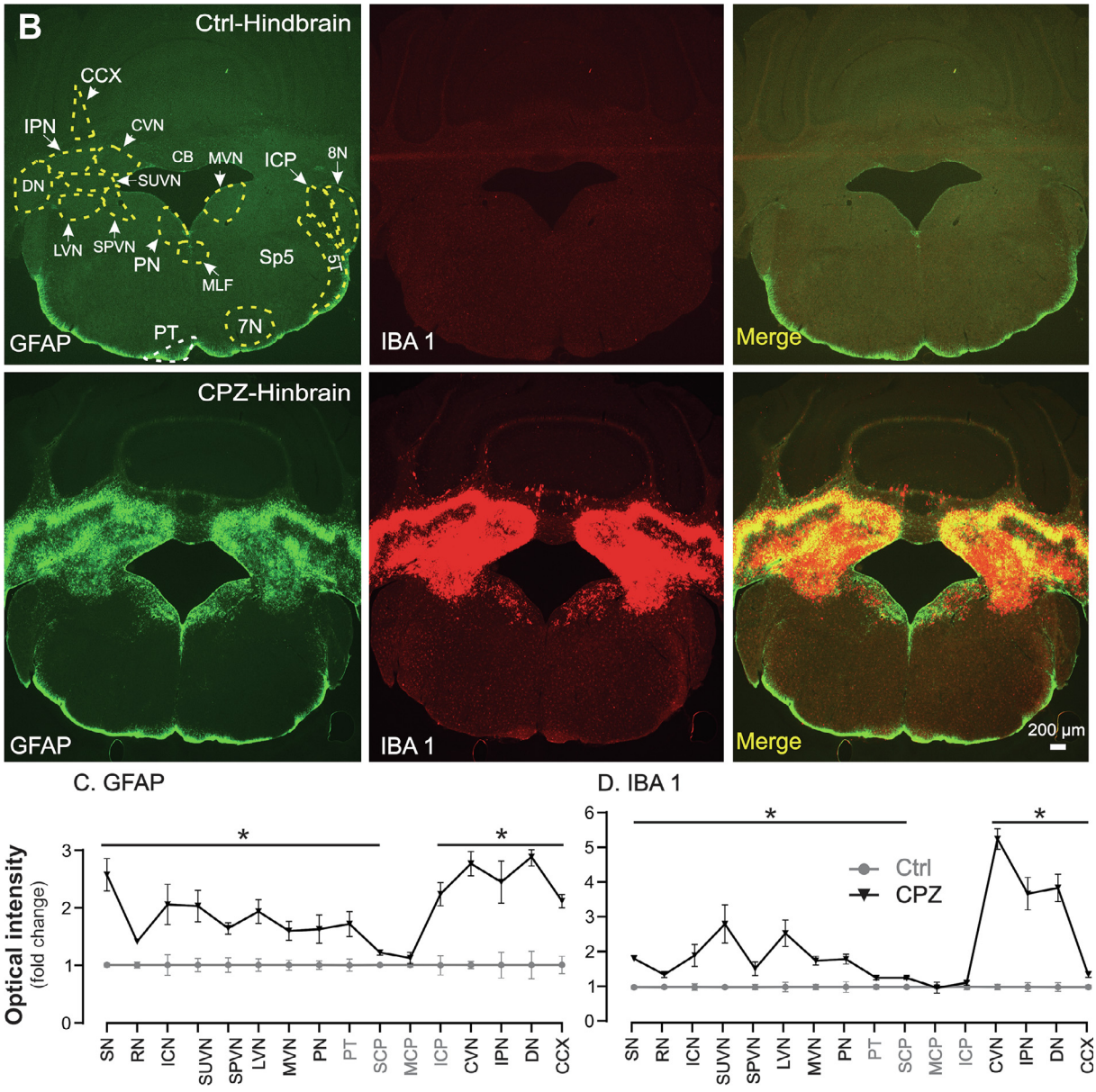

Fig. 7. (*continued*)

This is the first comprehensive study to investigate the effects of CPZ on brain stem structures. Within the midbrain, intense gliosis occurred in the inferior colliculi but not in the superior colliculi whereas the effects were more localised to nuclear areas in the pons and medulla. Demyelination and gliosis were observed in all the vestibular nuclei (superior, spinal, lateral, middle and cerebellar) and the adjacent prepositus nucleus. These nuclei are important not only for balance but also for oculomotor reflexes. For example, the prepositus nucleus is part of the horizontal gaze circuits and has strong connections with the medial vestibular nuclei, inferior olive, pontine paramedian reticular formation, cerebellum and anterior thalamus (Butler and Taube, 2015; Seo et al., 2004; Watson, 2012). Damage to this region can result in postural ataxia and nystagmus (Seo et al., 2004) and damage to the medial and lateral vestibular tracts that are important in maintaining balance while walking in the beam (Horak, 2010; Murray et al., 2018) may have contributed to the motor deficits seen in the CPZ-fed mice. This damage also indicates that there may be other deficits associated with the visual tracking system, which may have contributed to the foot slips. Whether or not CPZ induces visual disturbances or hearing loss awaits further study but damage to the inferior colliculus can induce hearing deficits or impaired blink responses (Freeman et al., 2007; McFadden and Willott, 1994).

The cerebellum plays not only an important role in motor coordination but also in cognitive functions (Buckner, 2013; Parmar et al., 2018; Shipman and Green, 2019). For example, patients with MS showing cerebellar dysfunction perform worse in cognitive performance assessed by using information processing speed, working memory tests (Weier et al., 2014). Moreover, the hippocampus-thalamus-cerebellum network facilitates the learning and execution of motor function (Babayan et al., 2017; Goldberg et al., 2015; Kern et al., 2015; Shipman and Green, 2019). This study confirmed those histological changes as well as demyelination and gliosis in the substantia nigra of the basal ganglia, and in limbic structures such as the medial septal nucleus, ventral pallidum and dorsolateral prefrontal cortex. Lesions to these areas result in cognitive decline in MS, Alzheimer's, Parkinson's and Huntington's diseases (Delano-Wood et al., 2012; Keser et al., 2018; Koenig et al., 2015). Some studies have argued that exploratory behaviour can be used as a measure of anxiety, and CPZ induces anxiety-like behaviour (Sen et al., 2019b), although it is hard to separate the cognitive and emotional aspects of a test from the motor

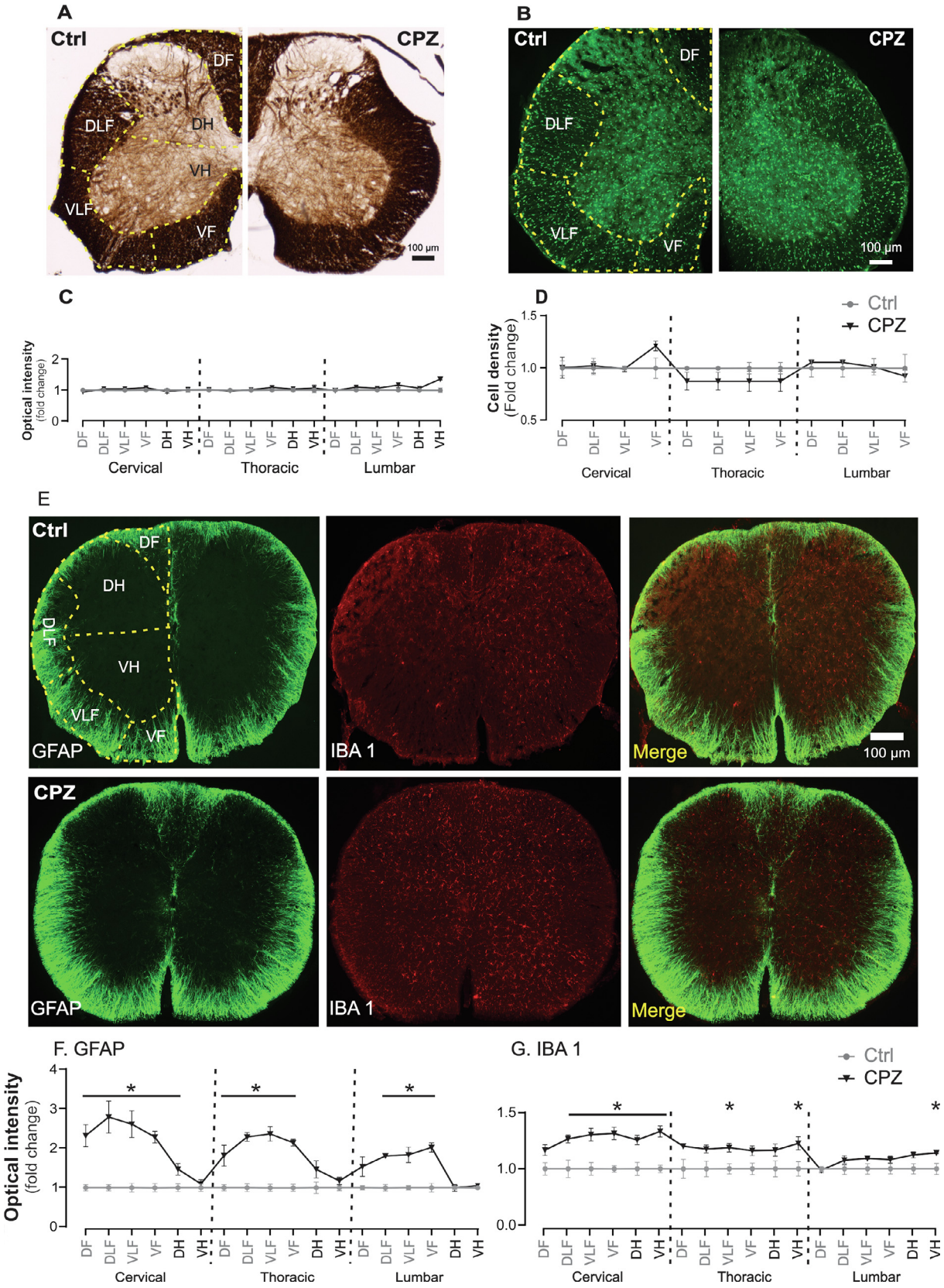

Fig. 8. Effects of CPZ on demyelination, OLG loss and gliosis in the in the spinal cord. Representative images of silver A), APC B) and GFAP, IBA 1 and merged staining E) and quantification **C**, **D**, **F**, **G**) of silver, APC, GFAP and IBA 1-staining (n = 5 animals/group and 3–5 sections/animal) in the grey and white matter regions of the spinal cord. Data are presented as the mean (± SEM). An unpaired two-tailed *t*-test was used to determine differences between groups. Significant differences among the groups are indicated by $*p < 0.05$. Dashed lines in **A**, **B**, **E** indicate the regions quantified and the dashed lines in **C**, **D**, **F**, **G** separate the different levels of spinal cord. An unpaired two-tailed *t*-test was used to determine differences between groups. Significant differences among the groups are indicated by $*p < 0.05$. Abbreviations: Ctrl, control; DF, dorsal funiculus; DH, dorsal horn; DLF, dorsal lateral funiculus; VF, ventral funiculus; VH, ventral horn and VLF, ventral lateral funiculus.

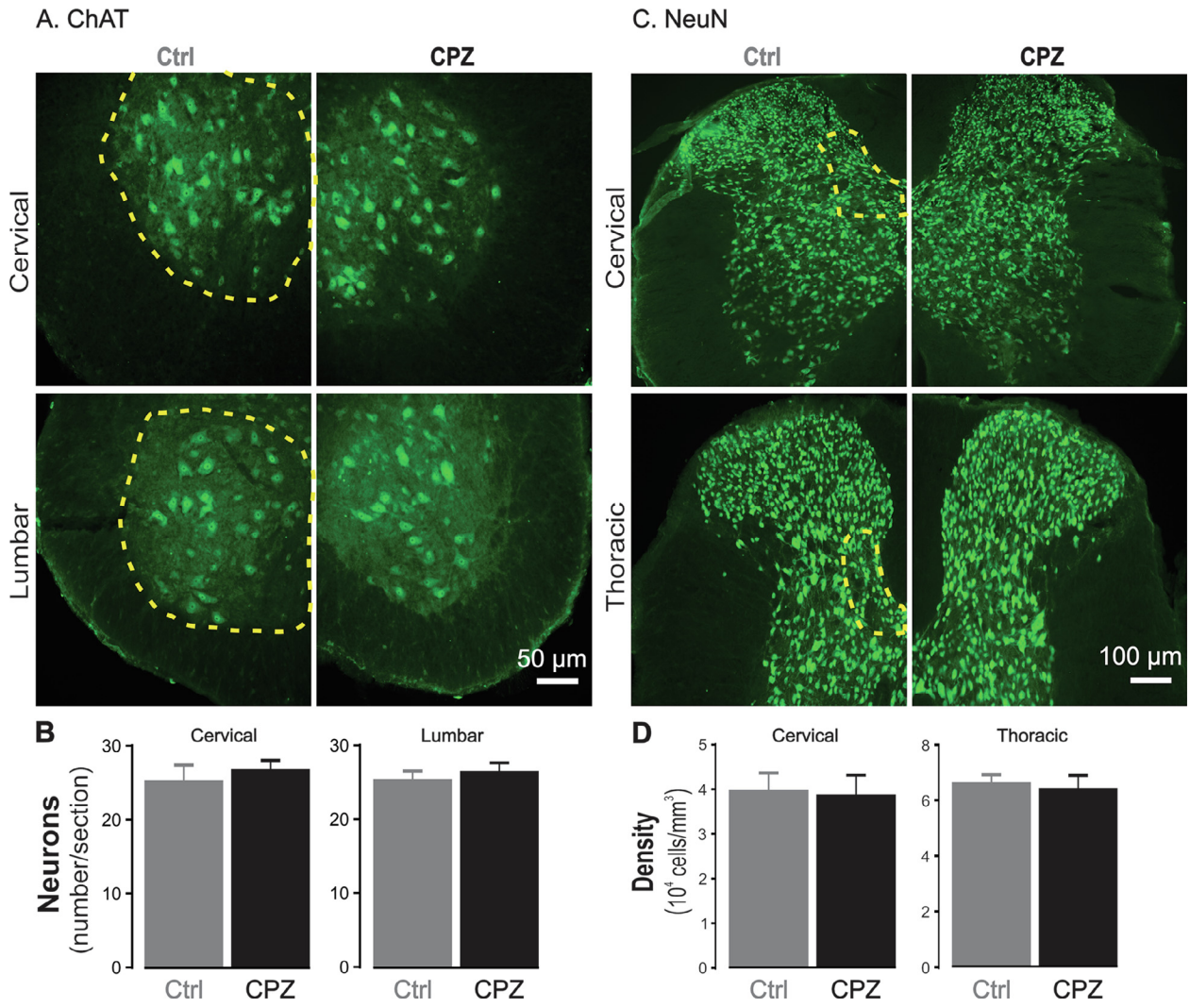

Fig. 9. Effects of CPZ on specific subpopulations of spinal cord neurons. Representative images of ChAT-stained motoneurons (**A**) and NeuN positive neurons (**C**) of Clarke's nucleus in the spinal cord and their quantification (**B**, **D**). Dashed lines indicate the regions quantified (n = 3–5 animals/group, 5 sections/animal). Ctrl = control.

performance. Although this study did not assess cognitive ability directly, the fact that the scores for crossing the beam/ladder in terms of time spent exploring were similar between CPZ and control mice argues against cognitive decline as the primary cause of motor changes.

4.2. Nociceptive behaviour

No differences in mechanical or thermal nociceptive withdrawal reflexes occurred between control and CPZ-fed groups at any time point, consistent with previous findings using similar mechanical or different thermal nociceptive tests (Bolcskei et al., 2018; Vakilzadeh et al., 2016). Herder et al (Herder et al., 2011) previously reported no demyelination in cervical and thoracic spinal cord in CPZ-fed mice, consistent with our results. We extend these findings by confirming similar observations in the lumbar spinal cord, the area associated with the reflex response circuitry. Moreover, histological analysis of lower motor neuron and Clarke's nucleus numbers revealed no changes suggesting that the motor incoordination is unlikely to originate in the spinal cord. This supposition is supported by the observation of profound demyelination and gliosis in the thalamus and somatosensory cortices.

In contrast to the lack of myelin loss, increased GFAP staining occurred in the spinal cord white matter. Interestingly, the magnitude of gliosis showed a proximo-distal gradient in that gliosis was highest in the cervical spinal cord, then the thoracic cord and then lumbar cord. A similar segmental gradient pattern occurred for IBA 1 staining. However, unlike GFAP staining, increased IBA 1 staining was more prominent in the grey matter. Taken together these results suggest that CPZ-feeding does not induce demyelination in the spinal cord at this time point and that demyelination is not the trigger for a glial response. The fact that CPZ does induce a glial response that is more severe at proximal than distal levels suggests that degenerative events may only be beginning and thus that analysis at later time points may reveal more extensive pathology, which may or may not be associated with altered nociceptive thresholds. This awaits further study.

4.3. Regional differences in demyelination.

This study confirmed earlier reports of a differential demyelination of CNS regions. For example, cerebellar demyelination peaks by 12 weeks of CPZ-feeding (Skripuletz et al., 2010), whereas in the corpus callosum, cerebral cortex and hippocampus this occurred at 5–6 weeks (Berghoff et al., 2017; Gudi et al., 2009). Likewise, myelination of the optic nerve and tract were unaffected at 5 weeks of CPZ-feeding but were demyelinated by 12 (Namekata et al., 2014). It has been suggested that this differential susceptibility to CPZ is due to the differential

maturation of white matter tracts; the later they mature, the more susceptible they are (Yang et al., 2009), whilst others have suggested that the effects are due to regional differences in microglia (Skripuletz et al., 2010). However, even within a tract, a gradient of demyelination was observed. For example, in the corpus callosum a rostrocaudal gradient of demyelination and gliosis was found such that greater demyelination occurred in the caudal regions such as the splenium. Similarly, the gliotic response in the spinal cord was greater at cervical levels compared to thoracic and lumbar levels. Another possibility for these effects could be that different regions of the CNS have different subtypes of OLGs based on biochemical profile and axon myelination (Butt et al., 1995). Most recently, RNAscope analysis has revealed 12 different subtypes of mature OLGs with a differential distribution in brain and spinal cord. Moreover, they respond differently to trauma (Floriddia et al., 2019).

5. Conclusions

Standard feeding of 0.2% CPZ to mice for 5 weeks induced motor (but not nociceptive) deficits that were only discernible when complex behavioural tasks were used. Errors, particularly in coordination, appeared closely related to demyelination of cerebellar systems and its CNS connections. Moreover, OLG cell loss occurred in the brain but not the spinal cord, indicating a regional sensitivity of oligodendrocytosis, demyelination and gliosis. An important, and yet, unanswered question is what happens when CPZ-feeding ceases and remyelination is allowed to occur. Do the motor deficits reverse or persist? This should be the focus of future work.

Author contributions

MKS carried out the lab work in collaboration with MSMA. All authors conceived the study and provided all resources. MKS analysed the data and drafted the original manuscript.

Declaration of Competing Interest

The authors declare that they have no known competing financial interests or personal relationships that could have appeared to influence the work reported in this paper.

Acknowledgements

This work was funded by the Rotary Club of Narellan. We are grateful to the Western Sydney University School of Medicine Animal Care Facility for the help with this project. MKS was the recipient of a WSU-International Postgraduate Research Scholarship. MSMA was the recipient of a PhD sponsorship from the Higher Committee for Education Development in Iraq.

Appendix A. Supplementary data

Supplementary data to this article can be found online at https://doi.org/10.1016/j.bbi.2020.01.021.

References

Acs, P., Kalman, B., 2012. Pathogenesis of Multiple Sclerosis: What Can We Learn from the Cuprizone Model. In: Perl, A. (Ed.), Autoimmunity: Methods and Protocols. Humana Press, Totowa, NJ, pp. 403–431.

Babayan, B.M., Watilliaux, A., Viejo, G., Paradis, A.-L., Girard, B., Rondi-Reig, L., 2017. A hippocampo-cerebellar centred network for the learning and execution of sequence-based navigation. Sci. Rep. 7, 17812.

Benedict, R.H., Holtzer, R., Motl, R.W., Foley, F.W., Kaur, S., Hojnacki, D., Weinstock-Guttman, B., 2011. Upper and lower extremity motor function and cognitive impairment in multiple sclerosis. JINS 17, 643–653.

Berghoff, S.A., Gerndt, N., Winchenbach, J., Stumpf, S.K., Hosang, L., Odoardi, F., Ruhwedel, T., Bohler, C., Barrette, B., Stassart, R., Liebetanz, D., Dibaj, P., Mobius, W., Edgar, J.M., Saher, G., 2017. Dietary cholesterol promotes repair of demyelinated lesions in the adult brain. Nat. Commun. 8, 14241.

Bieler, L., Grassner, L., Zaunmair, P., Kreutzer, C., Lampe, L., Trinka, E., Marschallinger, J., Aigner, L., Couillard-Despres, S., 2018. Motor deficits following dorsal corticospinal tract transection in rats: voluntary versus skilled locomotion readouts. Heliyon. 4, e00540.

Bolcskei, K., Kriszta, G., Saghy, E., Payrits, M., Sipos, E., Vranesics, A., Berente, Z., Abraham, H., Acs, P., Komoly, S., Pinter, E., 2018. Behavioural alterations and morphological changes are attenuated by the lack of TRPA1 receptors in the cuprizone-induced demyelination model in mice. J. Neuroimmunol. 320, 1–10.

Bonzano, L., Tacchino, A., Roccatagliata, L., Abbruzzese, G., Mancardi, G.L., Bove, M., 2008. Callosal contributions to simultaneous bimanual finger movements. J. Neurosci.: Off. J. Soc. Neurosci. 28, 3227–3233.

Buckner, R.L., 2013. The cerebellum and cognitive function: 25 years of insight from anatomy and neuroimaging. Neuron 80, 807–815.

Butler, W.N., Taube, J.S., 2015. The nucleus prepositus hypoglossi contributes to head direction cell stability in rats. J. Neurosci.: Off. J. Soc. Neurosci. 35, 2547–2558.

Butt, A.M., Ibrahim, M., Ruge, F.M., Berry, M., 1995. Biochemical subtypes of oligodendrocyte in the anterior medullary velum of the rat as revealed by the monoclonal antibody Rip. Glia. 14, 185–197.

Cattaneo, D., De Nuzzo, C., Fascia, T., Macalli, M., Pisoni, I., Cardini, R., 2002. Risks of falls in subjects with multiple sclerosis. Arch. Phys. Med. Rehabil. 83, 864–867.

Delano-Wood, L., Stricker, N.H., Sorg, S.F., Nation, D.A., Jak, A.J., Woods, S.P., Libon, D.J., Delis, D.C., Frank, L.R., Bondi, M.W., 2012. Posterior cingulum white matter disruption and its associations with verbal memory and stroke risk in mild cognitive impairment. JAD 29, 589–603.

Floriddia, E.M., Zhang, S., Bruggen, D.V., Santos, J.P.G.D., Altinkok, M., Llorens-Bobadilla, E., Castelobranco, J.F.G., 2019. Specific oligodendrocyte populations have differential spatial distribution and susceptibility to injury. Soc. Neurosci. Annual Meeting. 50 (740), 706.

Franco-Pons, N., Torrente, M., Colomina, M.T., Vilella, E., 2007. Behavioral deficits in the cuprizone-induced murine model of demyelination/remyelination. Toxicol. Lett. 169, 205–213.

Freeman, J.H., H.E. Halverson, and E.M. Hubbard. 2007. Inferior colliculus lesions impair eyeblink conditioning in rats. Learning & memory (Cold Spring Harbor, N.Y.). 14:842-846.

Gean-Marton, A.D., Vezina, L.G., Marton, K.I., Stimac, G.K., Peyster, R.G., Taveras, J.M., Davis, K.R., 1991. Abnormal corpus callosum: a sensitive and specific indicator of multiple sclerosis. Radiology 180, 215–221.

Goldberg, J., Clarner, T., Beyer, C., Kipp, M., 2015. Anatomical Distribution of Cuprizone-Induced Lesions in C57BL6 Mice. J. Mol. Neurosci: MN 57, 166–175.

Groebe, A., Clarner, T., Baumgartner, W., Dang, J., Beyer, C., Kipp, M., 2009. Cuprizone treatment induces distinct demyelination, astrocytosis, and microglia cell invasion or proliferation in the mouse cerebellum. Cerebellum (London, England). 8, 163–174.

Gudi, V., Moharregh-Khiabani, D., Skripuletz, T., Koutsoudaki, P.N., Kotsiari, A., Skuljec, J., Trebst, C., Stangel, M., 2009. Regional differences between grey and white matter in cuprizone induced demyelination. Brain Res. 1283, 127–138.

Gyengesi, E., Calabrese, E., Sherrier, M.C., Johnson, G.A., Paxinos, G., Watson, C., 2014. Semi-automated 3D segmentation of major tracts in the rat brain: comparing DTI with standard histological methods. Brain Struct. Funct. 219, 539–550.

Ha, S., Lee, D., Cho, Y.S., Chung, C., Yoo, Y.E., Kim, J., Lee, J., Kim, W., Kim, H., Bae, Y.C., Tanaka-Yamamoto, K., Kim, E., 2016. Cerebellar Shank2 Regulates Excitatory Synapse Density, Motor Coordination, and Specific Repetitive and Anxiety-Like Behaviors. J. Neurosci.: Off. J. Soc. Neurosci. 36, 12129–12143.

Harrison, M., O'Brien, A., Adams, L., Cowin, G., Ruitenberg, M.J., Sengul, G., Watson, C., 2013. Vertebral landmarks for the identification of spinal cord segments in the mouse. NeuroImage. 68, 22–29.

Heindorf, M., Arber, S., Keller, G.B., 2018. Mouse Motor Cortex Coordinates the Behavioral Response to Unpredicted Sensory Feedback. Neuron 99, 1040–1054.e1045.

Herder, V., Hansmann, F., Stangel, M., Skripuletz, T., Baumgartner, W., Beineke, A., 2011. Lack of cuprizone-induced demyelination in the murine spinal cord despite oligodendroglial alterations substantiates the concept of site-specific susceptibilities of the central nervous system. Neuropathol. Appl. Neurobiol. 37, 676–684.

Hibbits, N., Pannu, R., Wu, T.J., Armstrong, R.C., 2009. Cuprizone demyelination of the corpus callosum in mice correlates with altered social interaction and impaired bilateral sensorimotor coordination. ASN neuro, 1.

Horak, F.B., 2010. Postural compensation for vestibular loss and implications for rehabilitation. Restor. Neurol. Neurosci. 28, 57–68.

Huitinga, I., De Groot, C.J., Van der Valk, P., Kamphorst, W., Tilders, F.J., Swaab, D.F., 2001. Hypothalamic lesions in multiple sclerosis. J. Neuropathol. Exp. Neurol. 60, 1208–1218.

Jurevics, H., Largent, C., Hostettler, J., Sammond, D.W., Matsushima, G.K., Kleindienst, A., Toews, A.D., Morell, P., 2002. Alterations in metabolism and gene expression in brain regions during cuprizone-induced demyelination and remyelination. J. Neurochem. 82, 126–136.

Kern, K.C., Gold, S.M., Lee, B., Montag, M., Horsfall, J., O'Connor, M.-F., Sicotte, N.L., 2015. Thalamic–hippocampal–prefrontal disruption in relapsing–remitting multiple sclerosis. NeuroImage: Clinical. 8, 440–447.

Keser, Z., K.M. Hasan, B. Mwangi, K. Younes, M. Khayat-Khoei, A. Kamali, J.A. Lincoln, and F.M. Nelson. 2018. Quantitative Limbic System Mapping of Main Cognitive Domains in Multiple Sclerosis. Frontiers in Neurology. 9.

Kipp, M., Nyamoya, S., Hochstrasser, T., Amor, S., 2017. Multiple sclerosis animal models: a clinical and histopathological perspective. Brain Pathol. 27, 123–137.

Koenig, K.A., Sakaie, K.E., Lowe, M.J., Lin, J., Stone, L., Bermel, R.A., Beall, E.B., Rao, S.M., Trapp, B.D., Phillips, M.D., 2015. The relationship between cognitive function and high-resolution diffusion tensor MRI of the cingulum bundle in multiple sclerosis. Multiple sclerosis (Houndmills, Basingstoke, England). 21, 1794–1801.

Larocca, N.G., 2011. Impact of walking impairment in multiple sclerosis: perspectives of

patients and care partners. The patient. 4, 189–201.
Li, B., Zhuang, Q.X., Gao, H.R., Wang, J.J., Zhu, J.N., 2017. Medial cerebellar nucleus projects to feeding-related neurons in the ventromedial hypothalamic nucleus in rats. Brain Struct. Funct. 222, 957–971.
Liebetanz, D., Merkler, D., 2006. Effects of commissural de- and remyelination on motor skill behaviour in the cuprizone mouse model of multiple sclerosis. Exp. Neurol. 202, 217–224.
Lucchinetti, C., Bruck, W., Parisi, J., Scheithauer, B., Rodriguez, M., Lassmann, H., 2000. Heterogeneity of multiple sclerosis lesions: implications for the pathogenesis of demyelination. Ann. Neurol. 47, 707–717.
Lucchinetti, C.F., Bruck, W., Rodriguez, M., Lassmann, H., 1996. Distinct patterns of multiple sclerosis pathology indicates heterogeneity on pathogenesis. Brain Pathol. 6, 259–274.
Manrique-Hoyos, N., Jurgens, T., Gronborg, M., Kreutzfeldt, M., Schedensack, M., Kuhlmann, T., Schrick, C., Bruck, W., Urlaub, H., Simons, M., Merkler, D., 2012. Late motor decline after accomplished remyelination: impact for progressive multiple sclerosis. Ann. Neurol. 71, 227–244.
McFadden, S.L., Willott, J.F., 1994. Responses of inferior colliculus neurons in C57BL/6J mice with and without sensorineural hearing loss: effects of changing the azimuthal location of a continuous noise masker on responses to contralateral tones. Hear. Res. 78, 132–148.
Mierzwa, A.J., Zhou, Y.X., Hibbits, N., Vana, A.C., Armstrong, R.C., 2013. FGF2 and FGFR1 signaling regulate functional recovery following cuprizone demyelination. Neurosci. Lett. 548, 280–285.
Morandell, K., Huber, D., 2017. The role of forelimb motor cortex areas in goal directed action in mice. Sci. Rep. 7, 15759.
Murray, A.J., Croce, K., Belton, T., Akay, T., Jessell, T.M., 2018. Balance Control Mediated by Vestibular Circuits Directing Limb Extension or Antagonist Muscle Co-activation. Cell reports. 22, 1325–1338.
Namekata, K., Kimura, A., Harada, C., Yoshida, H., Matsumoto, Y., Harada, T., 2014. Dock3 protects myelin in the cuprizone model for demyelination. Cell Death Dis. 5, e1395.
Parmar, K., Stadelmann, C., Rocca, M.A., Langdon, D., D'Angelo, E., D'Souza, M., Burggraaff, J., Wegner, C., Sastre-Garriga, J., Barrantes-Freer, A., Dorn, J., Uitdehaag, B.M.J., Montalban, X., Wuerfel, J., Enzinger, C., Rovira, A., Tintore, M., Filippi, M., Kappos, L., Sprenger, T., 2018. The role of the cerebellum in multiple sclerosis-150 years after Charcot. Neurosci. Biobehav. Rev. 89, 85–98.
Partridge, M.A., Myers, S.J., Gopinath, S., Coorssen, J.R., 2015. Proteomics of a conundrum: Thoughts on addressing the aetiology versus progression of multiple sclerosis. Proteomics. Clinical applications. 9, 838–843.
Paxinos, G., Franklin, K., 2012. Paxinos and Franklin's the Mouse Brain in Stereotaxic Coordinates, Fourth Edition. Academic Press.
Pellegrino, L., Coscia, M., Muller, M., Solaro, C., Casadio, M., 2018. Evaluating upper limb impairments in multiple sclerosis by exposure to different mechanical environments. Sci. Rep. 8, 2110.
Samour, M.S., Shaikh, S.M., Mahns, D.A., Shortland, P.J., 2017. Noxious, but not innocuous, thermal stimuli evoke pERK expression in dorsal horn neurons after spared nerve injury in adult rats. Neurosci. Lett. 654, 49–55.
Sen, M.K., Almuslehi, M.S.M., Gyengesi, E., Myers, S.J., Shortland, P.J., Mahns, D.A., Coorssen, J.R., 2019a. Suppression of the peripheral immune system limits the central immune response following cuprizone-feeding: relevance to modelling multiple sclerosis. Cells 8, 1314.
Sen, M.K., Mahns, D.A., Coorssen, J.R., Shortland, P.J., 2019b. Behavioural phenotypes in the cuprizone model of central nervous system demyelination. Neurosci. Biobehav. Rev.
Sengul, G., Fu, Y., Yu, Y., Paxinos, G., 2015. Spinal cord projections to the cerebellum in the mouse. Brain Struct. Funct. 220, 2997–3009.
Seo, S.W., Shin, H.Y., Kim, S.H., Han, S.W., Lee, K.Y., Kim, S.M., Heo, J.H., 2004. Vestibular imbalance associated with a lesion in the nucleus prepositus hypoglossi area. Arch. Neurol. 61, 1440–1443.
Shaikh, S., Shortland, P., Lauto, A., Barton, M., Morley, J.W., Mahns, D.A., 2016. Sensory perturbations using suture and sutureless repair of transected median nerve in rats. Somatosens. Mot. Res. 33, 20–28.
Shipman, M.L., Green, J.T., 2019. Cerebellum and cognition: Does the rodent cerebellum participate in cognitive functions? Neurobiol. Learn. Mem.
Skripuletz, T., Bussmann, J.H., Gudi, V., Koutsoudaki, P.N., Pul, R., Moharregh-Khiabani, D., Lindner, M., Stangel, M., 2010. Cerebellar cortical demyelination in the murine cuprizone model. Brain Pathol. 20, 301–312.
Soblosky, J.S., Colgin, L.L., Chorney-Lane, D., Davidson, J.F., Carey, M.E., 1997. Ladder beam and camera video recording system for evaluating forelimb and hindlimb deficits after sensorimotor cortex injury in rats. J. Neurosci. Methods 78, 75–83.
Taylor, L.C., Gilmore, W., Ting, J.P., Matsushima, G.K., 2010. Cuprizone induces similar demyelination in male and female C57BL/6 mice and results in disruption of the estrous cycle. J. Neurosci. Res. 88, 391–402.
Traka, M., Podojil, J.R., McCarthy, D.P., Miller, S.D., Popko, B., 2016. Oligodendrocyte death results in immune-mediated CNS demyelination. Nat. Neurosci. 19, 65–74.
Tsukahara, R., Yamamoto, S., Yoshikawa, K., Gotoh, M., Tsukahara, T., Neyama, H., Ishii, S., Akahoshi, N., Yanagida, K., Sumida, H., Araki, M., Araki, K., Yamamura, K.I., Murakami-Murofushi, K., Ueda, H., 2018. LPA5 signaling is involved in multiple sclerosis-mediated neuropathic pain in the cuprizone mouse model. J. Pharmacol. Sci. 136, 93–96.
Vakilzadeh, G., Khodagholi, F., Ghadiri, T., Ghaemi, A., Noorbakhsh, F., Sharifzadeh, M., Gorji, A., 2016. The Effect of Melatonin on Behavioral, Molecular, and Histopathological Changes in Cuprizone Model of Demyelination. Mol. Neurobiol. 53, 4675–4684.
Watson, C., 2012. Chapter 12 - Hindbrain. In: Watson, C., Paxinos, G., Puelles, L. (Eds.), The Mouse Nervous System. Academic Press, San Diego, pp. 398–423.
Weier, K., Penner, I.K., Magon, S., Amann, M., Naegelin, Y., Andelova, M., Derfuss, T., Stippich, C., Radue, E.W., Kappos, L., Sprenger, T., 2014. Cerebellar abnormalities contribute to disability including cognitive impairment in multiple sclerosis. PLoS ONE 9, e86916.
Yang, H.J., Wang, H., Zhang, Y., Xiao, L., Clough, R.W., Browning, R., Li, X.M., Xu, H., 2009. Region-specific susceptibilities to cuprizone-induced lesions in the mouse forebrain: Implications for the pathophysiology of schizophrenia. Brain Res. 1270, 121–130.

Behavioural and histological changes in cuprizone-fed mice

Monokesh K Sen[1], Mohammed SM Almuslehi[1,2], Jens R Coorssen[3], David A Mahns[1] and Peter J Shortland[4*]

[1]School of Medicine, Western Sydney University, Penrith, New South Wales, Australia.
[2]Department of Physiology, College of Veterinary Medicine, Diyala University, Diyala, Iraq.
[3]Departments of Health Sciences and Biological Sciences, Faculties of Applied Health Sciences and Mathematics & Science, Brock University, Ontario, Canada.
[4]School of Science, Western Sydney University, Penrith, New South Wales, Australia.

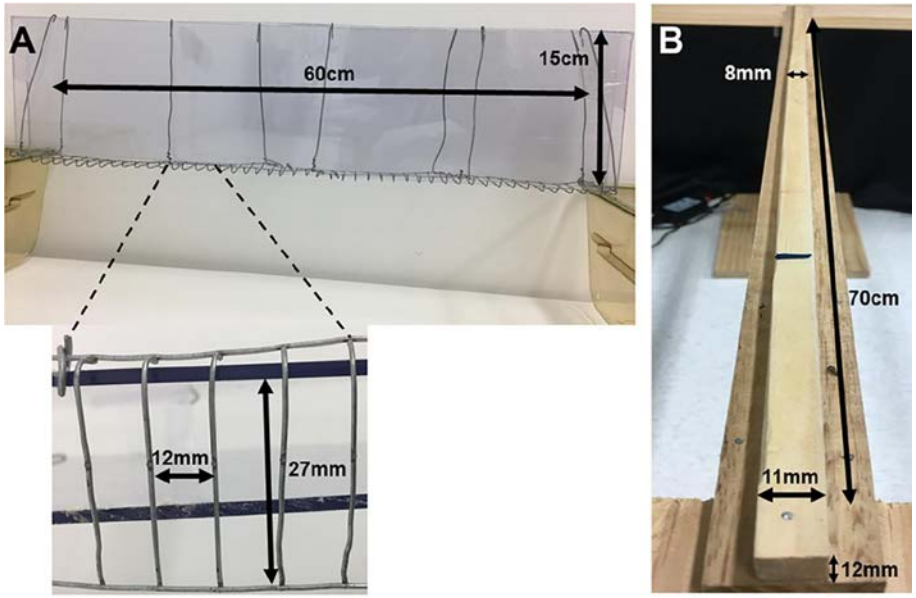

SF1: Custom made locomotor apparatus.

(A) Walking ladder apparatus: dimensions: 60cm long, 47 rungs, 3mm in diameter, spaced 12mm apart, bordered by a transparent plastic sheet (3mm thick, 15cm high) placed 13cm above the bench surface. **(B)** Walking beam apparatus: 70cm long wooden beam, 11mm width at one end tapering to 8mm at the other, 12 mm high was placed horizontally 50cm above the bench surface.

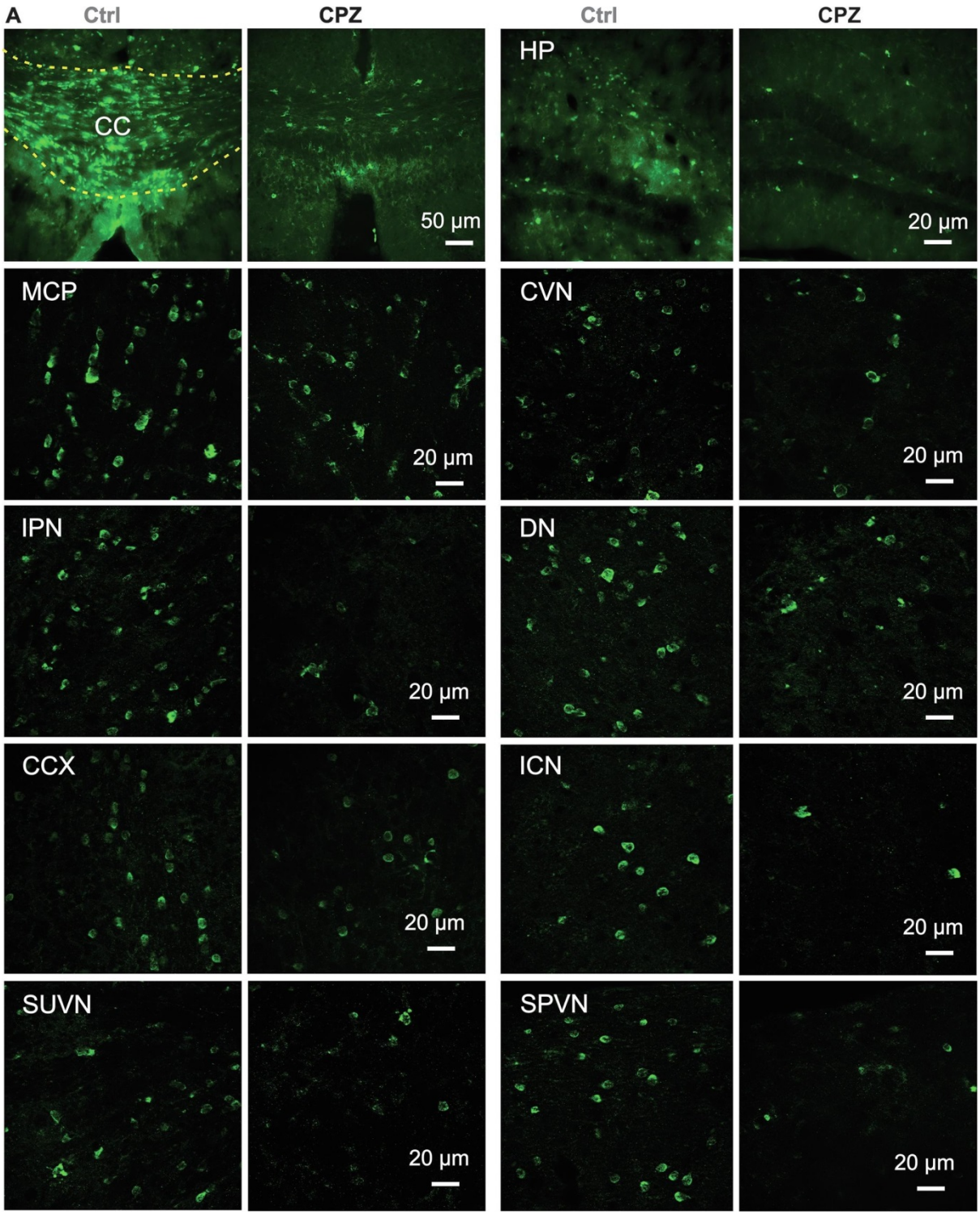
A
Ctrl
CPZ
Ctrl
CPZ
CC
HP
50 μm
20 μm
MCP
CVN
20 μm
20 μm
IPN
DN
20 μm
20 μm
CCX
ICN
20 μm
20 μm
SUVN
SPVN
20 μm
20 μm

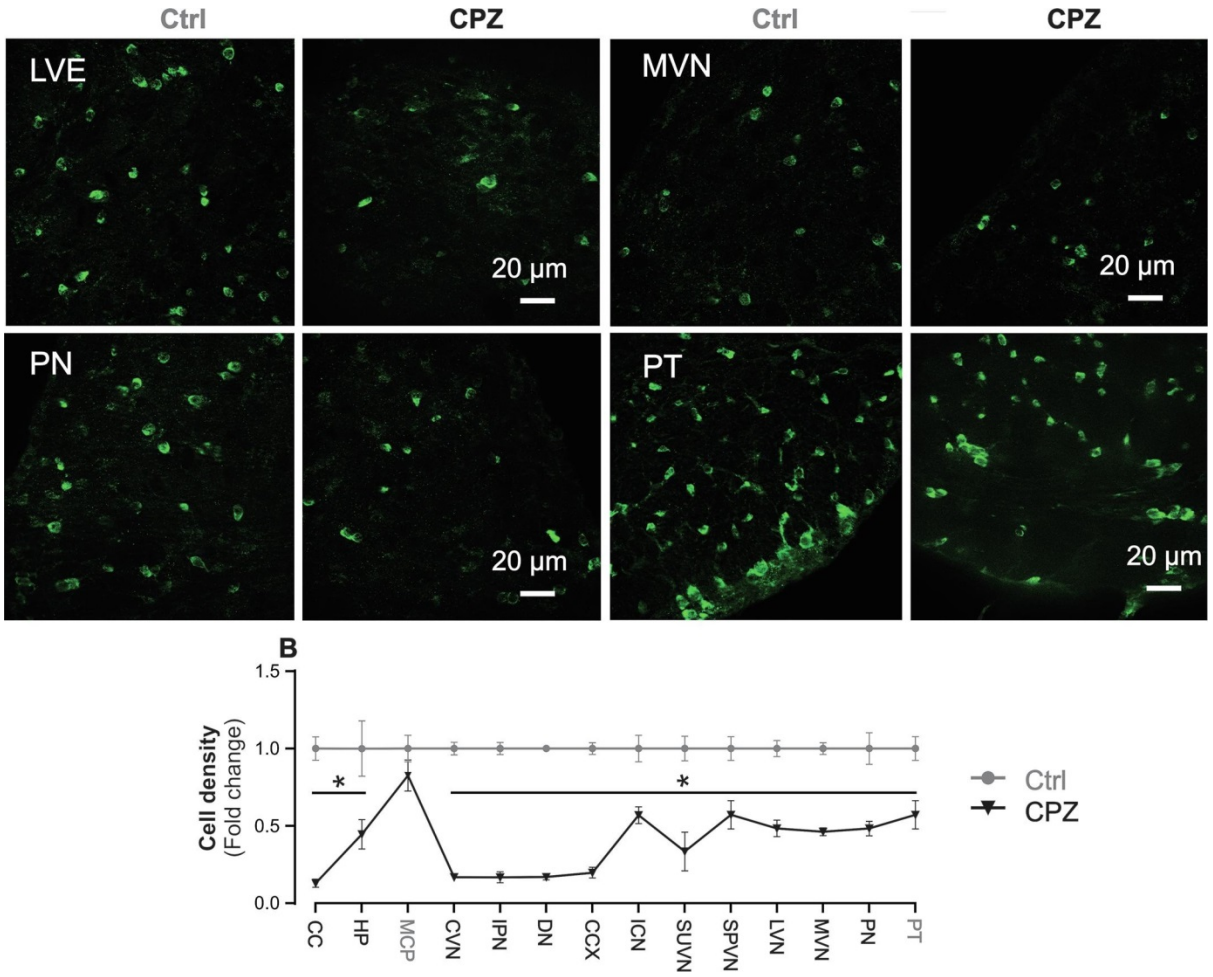

SF2: **Effects of CPZ-feeding on OLG cell numbers in different regions of the CNS.** Representative images **A**, and quantification **B**, of APC-positive OLGs from grey and white matter regions of the cerebrum, cerebellum, and brainstem. Significant differences among the groups are indicated by *p<0.05, (n=3-5 animals/group and 3-5 sections/animal). Dashed lines indicate the regions quantified. Abbreviations: CC, corpus callosum; CCX, cerebellum cortex; Ctrl, control; CVN, cerebellar vestibular nucleus; DN, dentate nucleus; HP, hippocampus; ICN, inferior colliculus nucleus; IPN, interposed nucleus; LVN, lateral vestibular nucleus; MCP, middle cerebellar peduncle; MVN, middle vestibular nucleus; PN, prepositus nucleus; PT, pyramidal tract; SPVN, spinal vestibular nucleus and SUVN, superior vestibular nucleus.

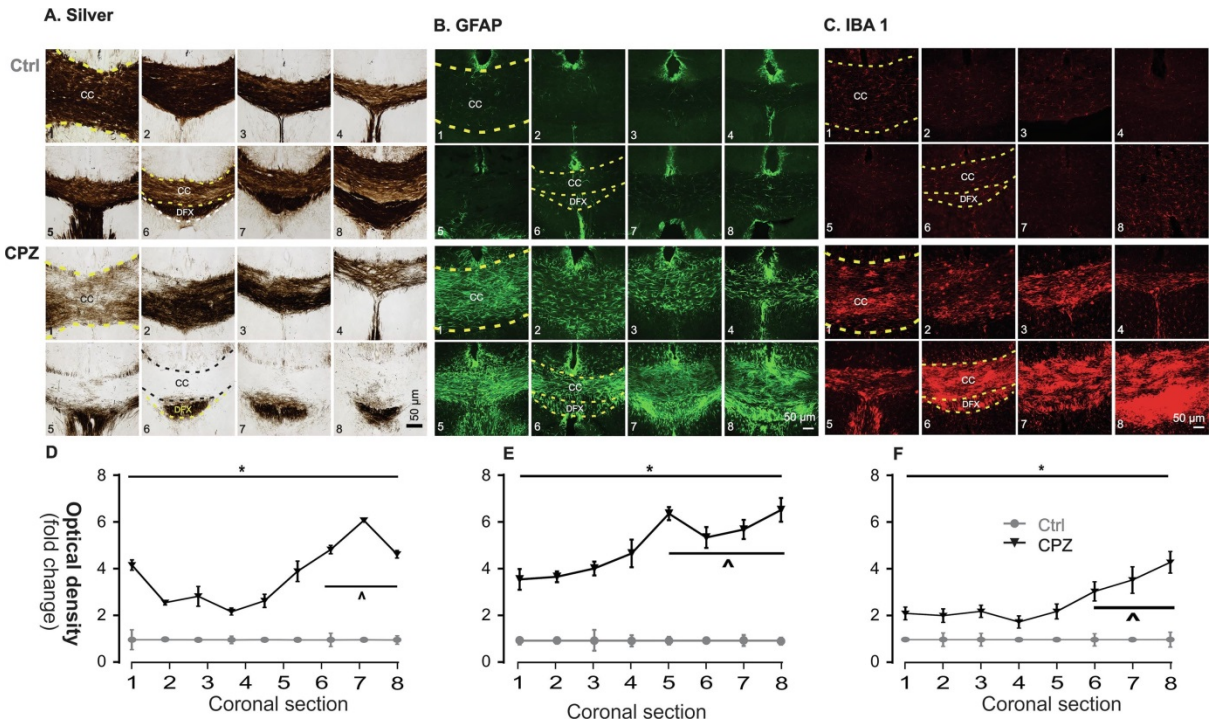

SF3: **Differential effects of CPZ on demyelination and gliosis in the corpus callosum (CC) in the rostro-caudal plane**.

Representative images of silver **A**, GFAP **B**, and IBA 1 **C**, staining of the CC. Numbers 1-8 represent the rostrocaudal sequence of sections in the CC and dashed lines indicate the regions quantified or discussed in the text. A significant rostral-caudal gradient of CPZ-induced demyelination **D**, (p<0.05, fold change) and GFAP intensity **E**, and IBA 1 intensity **F**, was observed in the CC (1-2 rostral, 3-5 middle and 6-8 caudal). An unpaired two-tailed t-test was used to determine differences between the control and CPZ groups (*p<0.05). Multiple comparison test using two way ANOVA and Tukey post hoc analysis were used to determine differences among section positions compared to control (^p<0.05); n=8 sections/animal, n=5 animals/group. Abbreviations: CC, corpus callosum; Ctrl, control and DFX, dorsal fornix.

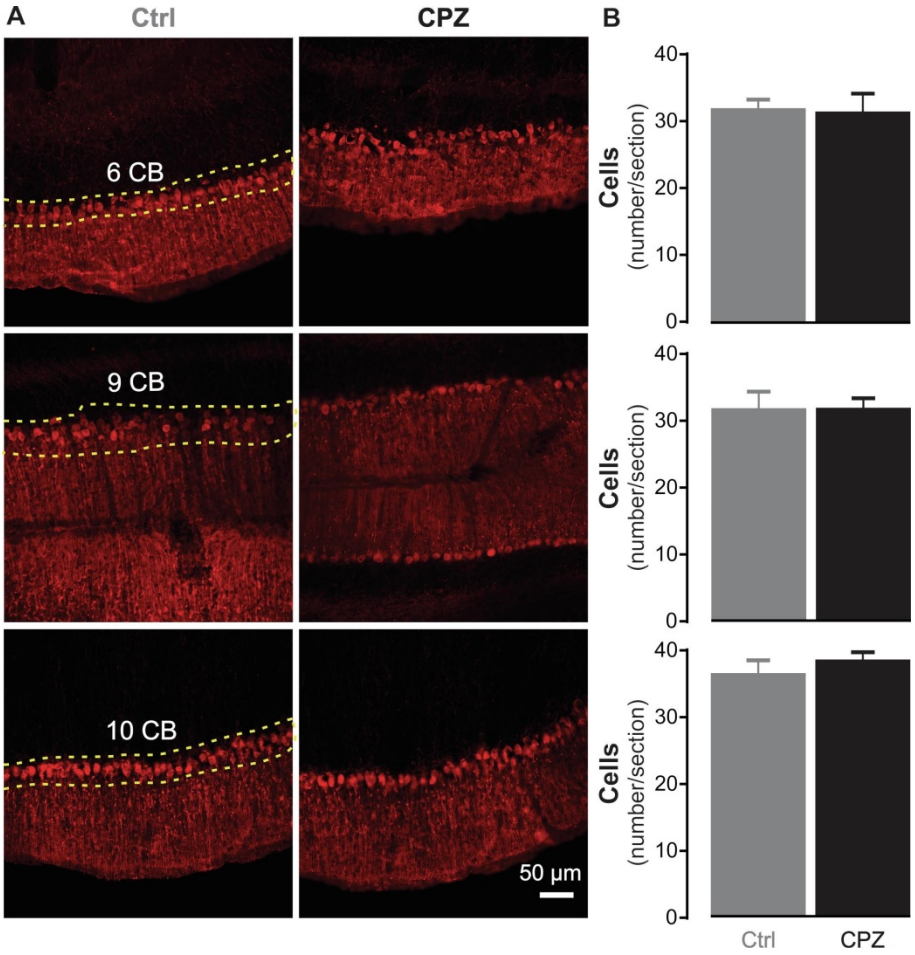

SF4: Analysis of Purkinje cells in the cerebellum cortex

Representative images **A**, and quantification **B**, of calbindin-positive Purkinje cells in lobules 6, 9 and 10 of the cerebellar vermis (CB). No differences between groups were observed (n=5 animals/group, 3 sections/animal, unpaired two-tailed t-test). Dashed lines show the regions quantified. Abbreviation: Ctrl, control.

Myelin basic protein: Myelin basic protein staining in the spinal cord revealed significant difference in staining at the lumbar spinal cord region only (**Figure 1A,B**).

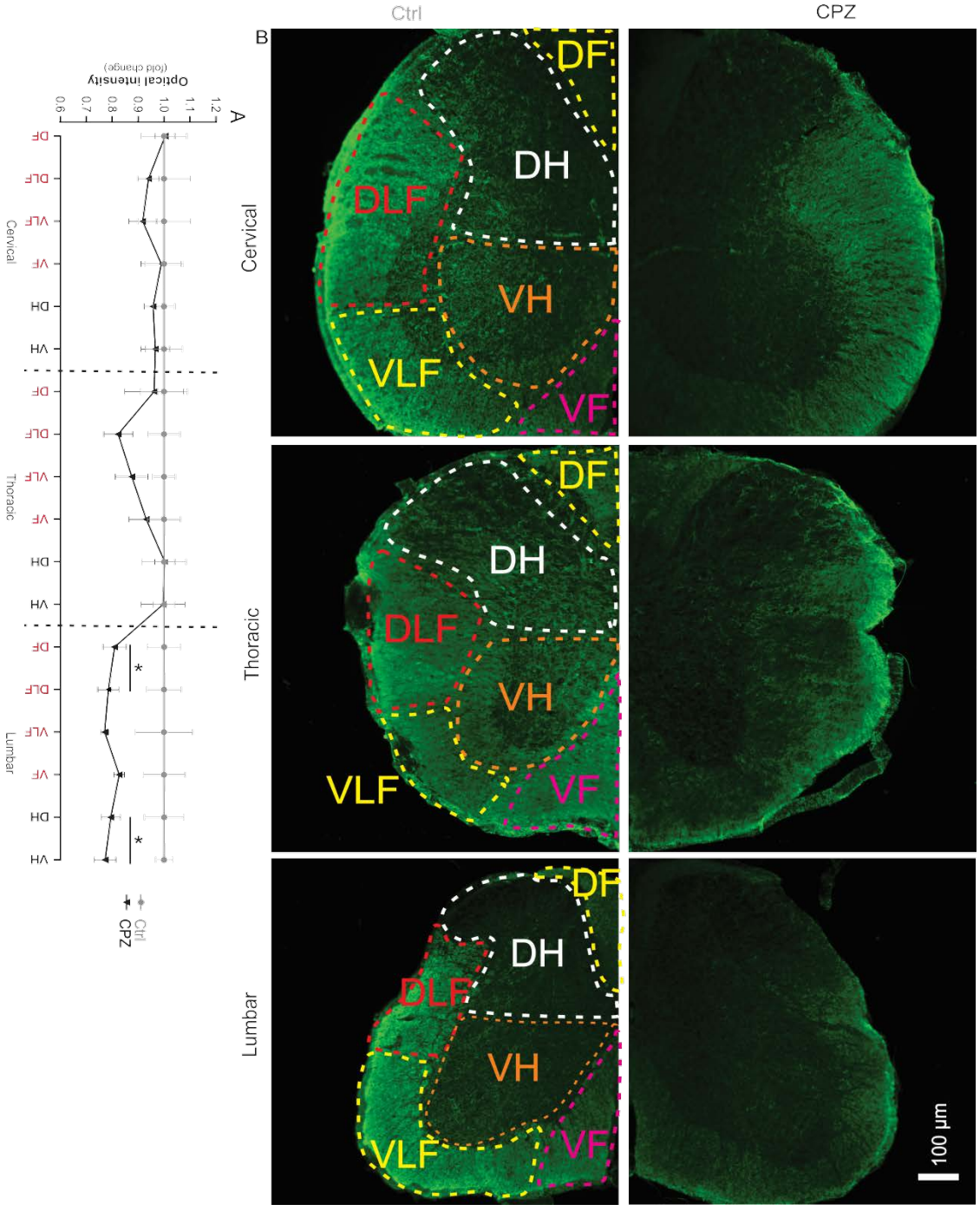

Figure 9: Regional suppression of MBP in the spinal cord

Quantification **A**) and representative images (**B**) of staining intensity of MBP for myelin from spinal cord (n=5 animals/group and 5 sections/animal) in the gray and white matter regions. An unpaired two-tailed t-test was used to determine differences between groups. Significant differences among the groups are indicated by *p<0.05. Dashed lines in **B** separate the different regions of spinal cord used for quantification in **A**. Abbreviations: DF, dorsal funiculus; DLF, dorsal lateral funiculus; VLF, ventral lateral funiculus and VF, ventral funiculus.

Chapter-6

DISCUSSION

6.1 Peripheral immune system suppression limits the recruitment of T-cells into the CNS

Studies I and II have been conducted to investigate whether blood brain barrier (BBB) disruption in CPZ-fed mice facilitates T-cells infiltration into the central nervous system (CNS). CPZ was fed for 5 and 12 weeks using the standard (0.2%) or a half of standard dose (0.1%) to induce oligodendrocytes (OLG) degeneration, demyelination and glial activation [22, 29, 82, 113]. The BBB was disrupted using pertussis toxin (PT) injection [236-238] during weeks 1-2 of CPZ-feeding. Histological analysis showed that CPZ evoked a robust concurrent OLG degeneration, demyelination and glial response in the cerebrum and cerebellum, consistent with many other studies [7, 22, 24, 82, 132, 161, 282]. The detection of T-cells ($CD4^+$ and $CD8^+$) was carried out using immunofluorescence and a high sensitive WB protocol [283], as well as using commercially available recombinant proteins in 'spiking' samples. Yet, no detectable T-cell signal was found in the brain using these methodologies. The absence of T-cells in the brain despite breaching the BBB has been associated with the suppression of T-cells signal and atrophy of spleen. Using WB and immunofluorescence, it was found that the signal intensity of T-cells ($CD4^+$ and $CD8^+$) was significantly reduced in the spleens of CPZ-fed animals, following short and prolonged feeding. This study also supported by the previous observations where it has been showed that CPZ-feeding can reduce the size of the adaptive immune organs such as spleen and thymus [11-13]-organs responsible for T-cells function [284, 285]. Moreover, in the present work (**Chapter-3**) using 2D proteomics decreased abundance of at least two proteins which are known to suppress T-cell function were found: Calcium/calmodulin-dependent protein kinase type II subunit alpha, a protein known to play a role in CD8 T-cell proliferation and the transition to a cytotoxic phenotype [286, 287]. Likewise, leukocyte elastase inhibitor A, a protein that normally supresses the action of proteases including those released by T-cells [288], was supressed. The decreased spots abundance of these proteins in CPZ-fed animal indicated the suppression of immune function. The suppressive effect on T-cell function is also supported by the previous observations showing an absence of protein disulphide isomerase in CPZ-fed mice [29] which is key protein in assembly of the major histocompatibility (MHC) class I molecules [29, 289]. Secondly, studies with experimental autoimmune encephalomyelitis (EAE), as well as Theiler's murine encephalomyelitis virus, animal models, both of which are based on T-cell mediated autoimmune response, showed that the severity of disease delayed when CPZ was fed in animals [290, 291].

It has been described from several papers that CPZ causes alteration of essential ions such as Fe^{2+}, Cu^{2+}, Mn^{2+} and Zn^{2+} in different organs such as brain and liver [3, 15, 58, 59]. However,

it is speculated that the ion imbalance properties of CPZ is associated with peripheral immune system dysregulation [12, 13, 291]. For example, T-cells require metal ions such as copper (Cu^{2+}) for its proper functioning. Cu^{2+} syntheses IL-2 (a pleiotropic cytokine) that is involved in the growth and maturation of T-cells; as a result of Cu^{2+} chelation using 2,3,2-tetraamine (a high affinity Cu^{2+} chelator) the IL-2 mRNA expression decreased [292, 293]. Since CPZ causes ion imbalance including the chelation of Cu^{2+}, it can be expected that CPZ can reduce the normal maturation and function of T-cells. In addition, dysregulation of metabolism and dysfunction of mitochondria associated with CPZ-feeding has been identified in this study (**Chapter-3**) may be associated with the dysregulation of immune system. Studies have revealed that T-cells relay on mitochondria during all stages of adaptive immune responses and considered as the 'master metabolic regulator of T-cells' [294] and dysregulation of mitochondria may lead to the compromisation of immune system [295].

6.2 CPZ induced metabolic dysfunction associated with OLG degeneration

Using a 'top-down' proteomics approach 33 unique protein spots were identified based on the changes in the relative abundance (≥1.5 fold increase or decrease) across different groups from studies I and II. The strength of the present study (**Chapter-3**) was to use a sensitive approach over the 'shot-gun' (i.e. bottom-up) approach. The top-down approach can resolve a large number of proteins including low abundance and post-translationally modified protein species with high degree of consistency across technical and biological replicates [29, 260, 296, 297]. In addition, in the present study (**Chapter-3**), to maximize the reproducibility in protein identification, sufficient technical (n=3 gels/fraction) and biological (n=5 animals/group) replicates were used in contrast to earlier work where either 'bottom up' approach or limited replicates were used [11, 23, 29, 298, 299].

Protein by protein literature search and bioinformatics analysis showed that the majority of the 33 proteins were involved in metabolic functions. When identified proteins were compared with the previously published literature on CPZ, EAE and multiple sclerosis (MS), it was found that 8 proteoforms (creatine kinase U-type, glutamate dehydrogenase 1, vesicle-fusing ATPase, propionyl co-enzyme A carboxylase-β, tyrosine-tRNA ligase, actin-related protein 2/3 complex subunit 5, charged multi-vesicular body protein and adipocyte plasma membrane-associated protein) had not previously been reported in relation to CPZ, EAE or MS studies whereas the other 25 proteins were. Further literature mining showed that the identified proteins were found to associate with the metabolic pathways such as glycolysis,

oxidative phosphorylation and Krebs cycle. In addition, a strong cluster of interacting metabolic proteoforms (ATP synthase subunit-α, NADH dehydrogenase iron-sulfur protein 2, aconitate hydratase, creatine kinase U-type, glutamate dehydrogenase 1, aspartate aminotransferase, oxoglutarate dehydrogenase like-protein, succinate dehydrogenase flavoprotein subunit, malate dehydrogenase, tyrosine-tRNA ligase, hexokinase 1, fructose-bisphosphate aldolase C, propionyl co-enzyme A carboxylase-β, isovaleryl-CoA dehydrogenase and voltage-dependent anion-selective channel protein) further support the metabolic disturbances and mitochondrial dysfunction in CPZ model.

OLG primarily depend upon mitochondria for their energy supply and disruption of mitochondrial function has been associated with the OLG loss [76, 300]. OLG require an extensive amount of energy to produce and maintain their myelin sheaths [85] by extending its surface area [39, 76, 77] and covering an area of ~5-50×10^3 μm^2 [53, 84]. The high metabolic rates associated with maintaining such expansive structures is associated with the increased production of toxic substances such as reactive oxygen (and nitrogen) species which pre-disposes OLG to oxidative injury, which becomes particularly problematic when OLG are exposed to toxins such as CPZ [76]. Moreover, OLG have only a limited storage of antioxidative substances such as glutathione [90, 91], metallothionein [94] and manganese superoxide dismutase [95] which increases the susceptibility of OLG against oxidative damage. In addition, such condition triggers the endoplasmic reticulum stress and induction of unfolded protein response which may enhance the OLG degeneration alone with mitochondria [301]. In the proteomic analysis (study I), endoplasmic reticulum stress related protein calreticulin may be associated with the unfolded protein response [302-304]. Moreover, the hypertrophy of astrocytes and microglia may increase the local energy demand in the demyelinating areas which further enhance OLG stress. Therefore, CPZ-mediated mitochondrial injury is preferentially susceptible to OLG degeneration.

6.3 Increasing the complexity of motor task detects subtle motor deficits

In this thesis motor function was assessed using rotarod, inverted screen, walking ladder and walking beam tests. In studies I and II rotarod and inverted screen showed no detectable motor deficits in CPZ-fed mice. One explanation for this is the lack of sensitivity of the instruments. In rotarod, mice do not fall off the rod prior to the emergence of severe motor decline because of their capacity to maintain their centre of gravity over the rotating drum or complete a revolution without falling. Likewise, in the inverted screen test, mice retained sufficient strength (and motor coordination) to hold onto the wire mesh using all four limbs. However, in the literature conflicting results were reported where no deficits were shown [305-308]; although in some studies motor deficits were reported using rotarod [73, 125, 241, 309-317] in CPZ model. On the basis of observations from our own study (**Chapter-3**) and the literature review, it was hypothesised that by increasing the complexity of the tasks for motor assessment, subtle deficits can be detected. In study III, the walking beam and ladder were used to measure the motor function and compared with rotarod. In walking beam, mouse had to walk along a progressively narrowing (11 mm to 8 mm) beam whereas in the walking ladder, a narrow walking corridor was used by the mouse to cross the ladder rungs. The advantage of these instruments is that animals need to give more concentration to keep balance and walk in a confined narrow way which appeared to be more challenging compared to rotarod or inverted screen. A significant difference in the number of foot slips were found as early as week 2 using ladder and walking beam showed significant change from week 4.5. These results showed that more complex locomotor tasks can reveal subtle motor deficits.

In the CPZ literature, the demyelination and gliosis in the corpus callosum have been used as a proxy in most of the motor behavioural studies to describe the causes of behavioural deficits which is inappropriate and inaccurate [19, 73, 241, 305-307, 309, 311-316, 318-321]. It suggests that the functionally relevant pathways associated with the deficits are yet to be identified. I hypothesised that the CPZ-induced OLG loss, demyelination and gliosis in the motor pathways are involved in motor behavioural changes. From the present study (study III) the OLG degeneration, demyelination and gliosis were found in the descending motor pathways such as cerebellar balance systems [322, 323]. In CPZ-fed mice, changes in the vestibular tract were found suggesting motor incoordination in the CPZ-fed mice may be associated with the vestibular tract injury. In contrast, no major difference was found in rubrospinal and reticulospinal tracts which are associated with locomotion, reaching and posture deficits [324-326]. Moreover, following CPZ-feeding we found a marked

demyelination and glial activation in all parts (rostral and caudal) of the corpus callosum. A considerable amount of literature has been argued that the demyelination and gliosis in the corpus callosum was associated with the impaired interhemispheric communication resulting motor incoordination in the CPZ-fed mice [19, 109, 110, 241, 318, 320].

6.4 Nociceptive behaviour is unaltered following CPZ-feeding

The thermal and mechanical nociceptive threshold was measured only in study III using dynamic plantar aesthesiometer and Hargreaves instruments. Similar to motor tests, relevant sensory pathways were not investigated rather studied only in the corpus callosum [305, 327, 328]. In the present study, no significant difference in mechano-nociceptive and thermo-nociceptive responses was found in any time point during CPZ-feeding using dynamic plantar aesthesiometer and Hargreaves instruments, respectively. Our observation was consistent with the previous studies where no nociceptive response was detected in CPZ-fed animal [305, 327]. A possible explanation for the absence of nociceptive response may be the lack of changes in the sensory pathway. Some authors have speculated that the changes of nociceptive response may arise from OLG degeneration and autoimmune response [329, 330] and injury [331] in spinal cord. However, no demyelination or OLG degeneration was found in the spinal cord different afferent pathways components such as the spinothalamic [332, 333] or spinocerebellar [334] tracts, although astrogliosis was evident. In addition, the lack of degeneration of sensory neurons (Clark's nucleus in cervical and thoracic spinal cord) suggests that spinal cord ascending pathways are likely to be unaffected.

6.5 Spinal and cerebellar neuronal subpopulations are unaffected by CPZ-feeding

Given the motor deficits it is reasonable to ask whether demyelination and gliosis affect particular motor neuronal subpopulations in the cerebellum and spinal cord. In study III, Purkinje neurons are the dominant cortical output from the cerebellum to the deep cerebellar nuclei. These can be identified using calbindin (Calb) antibody. Quantification of the cerebellum vermal regions of lobules 6, 9 and 10 showed no difference in number of Calb-positive Purkinje neurons between CPZ-fed and Ctrl mice. Alpha motor neurons from spinal cord were identified using choline acetyltransferase (ChAT) antibody and were quantified in the cervical, and lumbar ventral horns of spinal cord; again no difference was found between groups. Quantification of neuronal nuclei (NeuN) positive neurons associated with Clarke's nucleus in the thoracic spinal cord or the interbasilar nucleus (in cervical spinal cord) also

showed no group differences. Other studies have also shown that NeuN staining from optic nerve [109], cerebral cortex [320] and hippocampus [110] of cerebrum also showed no changes. Collectively, these data suggest that CPZ-feeding is not associated with the loss of neurons, consistent with previous *in vitro* [28, 111] and *in vivo* [109, 110, 320] studies.

6.6 CNS histopathology following CPZ-feeding

Many studies have focused on the histological investigation in the corpus callosum but no study has systematically investigated all other regions of CNS demyelination induced by CPZ-feeding. In study III, a detailed investigation was conducted. A concurrent marked loss of OLG, demyelination and gliosis was found in most of the investigated areas of the cerebrum, cerebellum and brain stem whereas only gliosis was observed in spinal cord. The differential susceptibility of the different regions to CPZ may occur from several reasons. The distinct anatomical structure and variation in the density of OLG in different parts of the CNS structures may play role in regional variability. For example, in normal conditions the number of neurite outgrowth inhibitor A (NOGO A) positive OLG is greater in the corpus callosum than in cerebral cortex [22]. Similarly, the density of NOGO A positive OLG is lower in the cortex than in the white matter lobes of cerebellum [24]. Similarly, GFAP positive astrocytes and IBA 1 positive microglia are found in greater amount in corpus callosum than cerebral cortex [22]. In addition, differences in 'intrinsic capacity' have been hypothesised to account for OLG susceptibility to injury [38, 146]. More specifically, the loss of the non-receptor tyrosine kinase Fyn (a signalling molecule of the Src kinase family) causes more hypo-myelination [147] in brain than in the spinal cord [148]. Likewise, unequal distribution of type III neuregulin-1 (cell adhesion signalling molecule, plays role in OLG proliferation and development) may increase the susceptibility to OLG injury in corpus callosum compared to the spinal cord [149].

Future directions

This thesis has generated many research questions for further investigation including:

Preservation of adaptive immune system

The present thesis has shown that despite breaching the BBB during CPZ-induced oligodendrocytosis and gliosis, no detectable T-cell signal was found in the brain. Studies I and II provide evidence that this lack of T-cell involvement may be due to a direct suppressive effect on the peripheral adaptive immune system. Further investigation and experimentation is strongly recommended to identify the mechanism of CPZ-induced immune system suppression. In addition, in order to investigate whether oligodendrocytosis can lead to a secondary immune response ('inside-out' theory of MS) in the CPZ animal model, strategies that preserves the peripheral immune system should be investigated. One such strategy was published during the candidature in which feeding CPZ only was limited to 2 weeks and combined with immune booster (complete Fraud adjuvant) and disruption of the BBB [31]. Prior to the release of this paper, the findings reported here formed the basis agreed divergence of work undertaken by two doctoral candidates:

The first, as described in the **Chapters-4** and **-5** of this thesis, focused on the behavioural consequences and the regional neuro-anatomical impact of CPZ-feeding.

and,

The second, focused on new strategies to overcome the suppression of the peripheral immune system mediated by CPZ, whereby castration was used to reverse the normal the androgen-dependent involution of the thymus and spleen in order to test whether the CPZ-mediated oligodendrocytosis can evoke an immune response. The results of this study will form the basis of co-authored papers and the final chapters of Mohammed Almuslehi's doctoral thesis.

In addition, the present work has shown that using the half standard dose (0.1% CPZ) of CPZ-feeding for short and long period of time induces a comparable oligodendrocytosis with relatively less suppression of the adaptive immune system. Future research should therefore concentrate on using half dose of CPZ to minimize the suppression of adaptive immune system.

Validation of proteoform(s) for the identification of biomarker(s)

The present study identified 33 unique proteoforms using 'top-down' proteomics approach. Literature mining and bioinformatics analysis revealed the association of these proteins mainly with the mitochondrial and metabolic functions. Due to the extensive dependency of OLG on mitochondrial function, internal biochemical perturbations elicit degeneration of OLG resulting demyelination. Further work needs to be done to establish whether these proteins are indeed involved in regulating OLG function as the pathoaetiology of oligodendrocytosis in CPZ and/or MS is ill defined. Moreover, it would be informative to validate the role of the 33 proteins using multidisciplinary approaches such as western blot and transcriptomics. While this study used whole brain samples to identify proteome changes, detailed proteomic analysis of tissue from defined regions of the CNS including cerebellum, brain stem and spinal cord may explain the temporaleffects of CPZ. Moreover, it is recommended to carry out further research in human MS samples to understand the role of the identified proteoforms to generate potential biomarker(s).

Inflammatory markers identification

The present study concentrated on the OLG degeneration, demyelination, gliosis and neuronal loss. However, whether the glial response triggers the secretion of inflammatory mediators (e.g. IL-6, TNF-α and IFN-γ) was not investigated in the present work but techniques such as Luminex [335, 336] or enzyme-linked immunosorbent assay [337, 338] can be used to quantify the secretory mediators. The excessive secretion of pro-inflammatory mediators may increase disease states such as oligodendrocytosis and changes in the BBB that underpin the subsequent access of T-cell into the CNS.

Behavioural tests need more investigation

For the assessment of motor functions, rotarod, inverted screen, walking ladder and walking beam tests were used. Using rotarod and inverted screen no detectable deficits were found whereas walking ladder and beam, tasks with increased complexity, detected early subtle deficits. This result suggested that due to the insensitivity of rotarod and inverted screen for detecting motor deficits, measuring motor function using these instruments in CPZ model should be excluded. In walking beam investigations, multiple cameras should be used to visualize fore- and hind- limb foot slips. In the walking ladder test, random withdrawal of the rungs from the ladder to make the test into complex to further test the motor learning deficits. In addition, in this thesis only the thermal and mechanical nociceptive responses were

assessed. Proprioception, which is important to normal spatial awareness and balance, functions which appear compromised in the CPZ model should be investigated in future studies. Whether CPZ causes other behavioural deficits such as depression, fatigue and sleeping disturbances remains ill-defined and frequently confounded by the test used. A further study could assess effects of CPZ on different behavioural aspects.

Conclusions

This thesis concludes that:

- A standard (0.2%) or half standard (0.1%) dose of CPZ evokes a comparable oligodendrocytosis in 5 weeks feeding. Interestingly, prolonged exposure (12 weeks) with 0.1% CPZ-induced a similar histological (e.g. oligodendrocytosis, demyelination and gliosis) change as seen with 0.2% CPZ.
- Peripheral immune system suppression was the major impediment of investigation of the 'inside-out' hypothesis of MS using CPZ model even when the BBB was compromised.
- CPZ-induced mitochondrial stress has been associated with the oligodendrocytosis.
- Increasing the complexity of the tasks for motor assessment can detect early (≥2 weeks) subtle motor behavioural deficits consistent with ataxia.
- Demyelination and gliosis in the cerebellar systems, vestibular structures and white matter tracts contribute to motor deficits.
- Although gliosis was observed in the sensory pathway (e.g. dorsal column, spinothalamic tract and lemniscus system); no changes were observed in nociceptive reflex withdrawal responses to thermal and mechanical stimuli.
- CPZ-causes a regional specific oligodendrocytosis, demyelination and gliosis, which is higher in the cerebrum and cerebellum, lower in the brain stem and very limited in the spinal cord.
- Specific neuronal subpopulations of the cerebellum and spinal cord are unaffected by CPZ-ingestion.

REFERENCES

References

1. Messori, L., et al., *Unravelling the chemical nature of copper cuprizone.* Dalton Trans, 2007(21): p. 2112-4.
2. Carlton, W.W., *Studies on the induction of hydrocephalus and spongy degeneration by cuprizone feeding and attempts to antidote the toxicity.* Life Sci, 1967. **6**(1): p. 11-9.
3. Zatta, P., et al., *Copper and zinc dismetabolism in the mouse brain upon chronic cuprizone treatment.* Cell Mol Life Sci, 2005. **62**(13): p. 1502-13.
4. Carlton, W.W., *Response of mice to the chelating agents sodium diethyldithiocarbamate, alpha-benzoinoxime, and biscyclohexanone oxaldihydrazone.* Toxicol Appl Pharmacol, 1966. **8**(3): p. 512-21.
5. Carlton, W.W., *Spongiform encephalopathy induced in rats and guinea pigs by cuprizone.* Exp Mol Pathol, 1969. **10**(3): p. 274-87.
6. Blakemore, W.F., *Observations on oligodendrocyte degeneration, the resolution of status spongiosus and remyelination in cuprizone intoxication in mice.* J Neurocytol, 1972. **1**(4): p. 413-26.
7. Hiremath, M.M., et al., *Microglial/macrophage accumulation during cuprizone-induced demyelination in C57BL/6 mice.* J Neuroimmunol, 1998. **92**(1-2): p. 38-49.
8. Mason, J.L., et al., *Mature oligodendrocyte apoptosis precedes IGF-1 production and oligodendrocyte progenitor accumulation and differentiation during demyelination/remyelination.* J Neurosci Res, 2000. **61**(3): p. 251-62.
9. Taylor, L.C., et al., *Cuprizone induces similar demyelination in male and female C57BL/6 mice and results in disruption of the estrous cycle.* J Neurosci Res, 2010. **88**(2): p. 391-402.
10. Remington, L.T., et al., *Microglial recruitment, activation, and proliferation in response to primary demyelination.* Am J Pathol, 2007. **170**(5): p. 1713-24.
11. Martin, N.A., et al., *Experimental Demyelination and Axonal Loss Are Reduced in MicroRNA-146a Deficient Mice.* Front Immunol, 2018. **9**: p. 490.
12. Solti, I., et al., *Thymic Atrophy and Apoptosis of CD4+CD8+ Thymocytes in the Cuprizone Model of Multiple Sclerosis.* PLoS One, 2015. **10**(6): p. e0129217.
13. Sui, R.X., et al., *Protective and therapeutic role of Bilobalide in cuprizone-induced demyelination.* Int Immunopharmacol, 2018. **66**: p. 69-81.
14. Suzuki, K., *Giant hepatic mitochondria: production in mice fed with cuprizone.* Science, 1969. **163**(3862): p. 81-2.
15. Venturini, G., *Enzymic activities and sodium, potassium and copper concentrations in mouse brain and liver after cuprizone treatment in vivo.* J Neurochem, 1973. **21**(5): p. 1147-51.
16. Blakemore, W.F., *Demyelination of the superior cerebellar peduncle in the mouse induced by cuprizone.* J Neurol Sci, 1973. **20**(1): p. 63-72.
17. Jurevics, H., et al., *Cerebroside synthesis as a measure of the rate of remyelination following cuprizone-induced demyelination in brain.* J Neurochem, 2001. **77**(4): p. 1067-76.
18. Arnett, H.A., et al., *TNF alpha promotes proliferation of oligodendrocyte progenitors and remyelination.* Nat Neurosci, 2001. **4**(11): p. 1116-22.
19. Liebetanz, D. and D. Merkler, *Effects of commissural de- and remyelination on motor skill behaviour in the cuprizone mouse model of multiple sclerosis.* Exp Neurol, 2006. **202**(1): p. 217-24.
20. Kumar, S., et al., *Combination of growth factors enhances remyelination in a cuprizone-induced demyelination mouse model.* Neurochem Res, 2007. **32**(4-5): p. 783-97.
21. Koutsoudaki, P.N., et al., *Demyelination of the hippocampus is prominent in the cuprizone model.* Neurosci Lett, 2009. **451**(1): p. 83-8.
22. Gudi, V., et al., *Regional differences between grey and white matter in cuprizone induced demyelination.* Brain Res, 2009. **1283**: p. 127-38.
23. Werner, S.R., et al., *Proteomic analysis of demyelinated and remyelinating brain tissue following dietary cuprizone administration.* J Mol Neurosci, 2010. **42**(2): p. 210-25.

24. Skripuletz, T., et al., *Cerebellar cortical demyelination in the murine cuprizone model.* Brain Pathol, 2010. **20**(2): p. 301-12.
25. Herder, V., et al., *Lack of cuprizone-induced demyelination in the murine spinal cord despite oligodendroglial alterations substantiates the concept of site-specific susceptibilities of the central nervous system.* Neuropathol Appl Neurobiol, 2011. **37**(6): p. 676-84.
26. Hibbits, N., et al., *Astrogliosis during acute and chronic cuprizone demyelination and implications for remyelination.* ASN Neuro, 2012. **4**(6): p. 393-408.
27. Skripuletz, T., et al., *Astrocytes regulate myelin clearance through recruitment of microglia during cuprizone-induced demyelination.* Brain, 2013. **136**(Pt 1): p. 147-67.
28. Benardais, K., et al., *Cuprizone [bis(cyclohexylidenehydrazide)] is selectively toxic for mature oligodendrocytes.* Neurotox Res, 2013. **24**(2): p. 244-50.
29. Partridge, M.A., et al., *An initial top-down proteomic analysis of the standard cuprizone mouse model of multiple sclerosis.* J Chem Biol, 2016. **9**(1): p. 9-18.
30. Tejedor, L.S., et al., *The Effect of Stereotactic Injections on Demyelination and Remyelination: a Study in the Cuprizone Model.* J Mol Neurosci, 2017. **61**(4): p. 479-488.
31. Caprariello, A.V., et al., *Biochemically altered myelin triggers autoimmune demyelination.* Proc Natl Acad Sci U S A, 2018. **115**(21): p. 5528-5533.
32. Maganti, R.J., et al., *Defining Changes in the Spatial Distribution and Composition of Brain Lipids in the Shiverer and Cuprizone Mouse Models of Myelin Disease.* J Histochem Cytochem, 2018: p. 22155418815860.
33. Perez-Cerda, F., M.V. Sanchez-Gomez, and C. Matute, *Pio del Rio Hortega and the discovery of the oligodendrocytes.* Front Neuroanat, 2015. **9**: p. 92.
34. Dulamea, A.O., *Role of Oligodendrocyte Dysfunction in Demyelination, Remyelination and Neurodegeneration in Multiple Sclerosis.* Adv Exp Med Biol, 2017. **958**: p. 91-127.
35. Hartline, D.K. and D.R. Colman, *Rapid conduction and the evolution of giant axons and myelinated fibers.* Curr Biol, 2007. **17**(1): p. R29-35.
36. Baumann, N. and D. Pham-Dinh, *Biology of oligodendrocyte and myelin in the mammalian central nervous system.* Physiol Rev, 2001. **81**(2): p. 871-927.
37. Jakovcevski, I., et al., *Oligodendrocyte development and the onset of myelination in the human fetal brain.* Front Neuroanat, 2009. **3**: p. 5.
38. Simons, M. and K.A. Nave, *Oligodendrocytes: Myelination and Axonal Support.* Cold Spring Harb Perspect Biol, 2015. **8**(1): p. a020479.
39. Freeman, M.R. and D.H. Rowitch, *Evolving concepts of gliogenesis: a look way back and ahead to the next 25 years.* Neuron, 2013. **80**(3): p. 613-23.
40. Salzer, J.L. and B. Zalc, *Myelination.* Current Biology, 2016. **26**(20): p. R971-R975.
41. Bercury, K.K. and W.B. Macklin, *Dynamics and mechanisms of CNS myelination.* Dev Cell, 2015. **32**(4): p. 447-58.
42. Patel, J. and R. Balabanov, *Molecular mechanisms of oligodendrocyte injury in multiple sclerosis and experimental autoimmune encephalomyelitis.* Int J Mol Sci, 2012. **13**(8): p. 10647-59.
43. Levine, J.M., R. Reynolds, and J.W. Fawcett, *The oligodendrocyte precursor cell in health and disease.* Trends Neurosci, 2001. **24**(1): p. 39-47.
44. Richardson, W.D., N. Kessaris, and N. Pringle, *Oligodendrocyte wars.* Nat Rev Neurosci, 2006. **7**(1): p. 11-8.
45. Menn, B., et al., *Origin of oligodendrocytes in the subventricular zone of the adult brain.* J Neurosci, 2006. **26**(30): p. 7907-18.
46. Cai, J., et al., *Generation of oligodendrocyte precursor cells from mouse dorsal spinal cord independent of Nkx6 regulation and Shh signaling.* Neuron, 2005. **45**(1): p. 41-53.
47. Fogarty, M., W.D. Richardson, and N. Kessaris, *A subset of oligodendrocytes generated from radial glia in the dorsal spinal cord.* Development, 2005. **132**(8): p. 1951-9.

48. Domingues, H.S., et al., *Oligodendrocyte, Astrocyte, and Microglia Crosstalk in Myelin Development, Damage, and Repair.* Front Cell Dev Biol, 2016. **4**: p. 71.
49. Dawson, M.R., et al., *NG2-expressing glial progenitor cells: an abundant and widespread population of cycling cells in the adult rat CNS.* Mol Cell Neurosci, 2003. **24**(2): p. 476-88.
50. Li, N. and G.K. Leung, *Oligodendrocyte Precursor Cells in Spinal Cord Injury: A Review and Update.* Biomed Res Int, 2015. **2015**: p. 235195.
51. Goldman, S.A. and N.J. Kuypers, *How to make an oligodendrocyte.* Development, 2015. **142**(23): p. 3983-95.
52. Tomassy, G.S. and V. Fossati, *How big is the myelinating orchestra? Cellular diversity within the oligodendrocyte lineage: facts and hypotheses.* Front Cell Neurosci, 2014. **8**: p. 201.
53. Butt, A.M., et al., *Biochemical subtypes of oligodendrocyte in the anterior medullary velum of the rat as revealed by the monoclonal antibody Rip.* Glia, 1995. **14**(3): p. 185-97.
54. Ferrer, I., *Oligodendrogliopathy in neurodegenerative diseases with abnormal protein aggregates: The forgotten partner.* Prog Neurobiol, 2018. **169**: p. 24-54.
55. Cammer, W., *The neurotoxicant, cuprizone, retards the differentiation of oligodendrocytes in vitro.* J Neurol Sci, 1999. **168**(2): p. 116-20.
56. Matsushima, G.K. and P. Morell, *The neurotoxicant, cuprizone, as a model to study demyelination and remyelination in the central nervous system.* Brain Pathol, 2001. **11**(1): p. 107-16.
57. Komoly, S., et al., *Decrease in oligodendrocyte carbonic anhydrase activity preceding myelin degeneration in cuprizone induced demyelination.* J Neurol Sci, 1987. **79**(1-2): p. 141-8.
58. Moldovan, N., et al., *Altered transition metal homeostasis in the cuprizone model of demyelination.* Neurotoxicology, 2015. **48**: p. 1-8.
59. Varga, E., et al., *Cuprizone Administration Alters the Iron Metabolism in the Mouse Model of Multiple Sclerosis.* Cell Mol Neurobiol, 2018. **38**(5): p. 1081-1097.
60. Acs, P., et al., *Distribution of oligodendrocyte loss and mitochondrial toxicity in the cuprizone-induced experimental demyelination model.* J Neuroimmunol, 2013. **262**(1-2): p. 128-31.
61. Hoppel, C.L. and B. Tandler, *Biochemical effects of cuprizone on mouse liver and heart mitochondria.* Biochem Pharmacol, 1973. **22**(18): p. 2311-8.
62. Pasquini, L.A., et al., *The neurotoxic effect of cuprizone on oligodendrocytes depends on the presence of pro-inflammatory cytokines secreted by microglia.* Neurochem Res, 2007. **32**(2): p. 279-92.
63. Stone, S. and W. Lin, *The unfolded protein response in multiple sclerosis.* Front Neurosci, 2015. **9**: p. 264.
64. Abe, H., et al., *Cuprizone decreases intermediate and late-stage progenitor cells in hippocampal neurogenesis of rats in a framework of 28-day oral dose toxicity study.* Toxicol Appl Pharmacol, 2015. **287**(3): p. 210-21.
65. Praet, J., et al., *Cellular and molecular neuropathology of the cuprizone mouse model: clinical relevance for multiple sclerosis.* Neurosci Biobehav Rev, 2014. **47**: p. 485-505.
66. Lin, W., et al., *Interferon-gamma inhibits central nervous system remyelination through a process modulated by endoplasmic reticulum stress.* Brain, 2006. **129**(Pt 5): p. 1306-18.
67. Suzuki, K. and Y. Kikkawa, *Status spongiosus of CNS and hepatic changes induced by cuprizone (biscyclohexanone oxalyldihydrazone).* Am J Pathol, 1969. **54**(2): p. 307-25.
68. Love, S., *Cuprizone neurotoxicity in the rat: morphologic observations.* J Neurol Sci, 1988. **84**(2-3): p. 223-37.
69. Hemm, R.D., W.W. Carlton, and J.R. Welser, *Ultrastructural changes of cuprizone encephalopathy in mice.* Toxicol Appl Pharmacol, 1971. **18**(4): p. 869-82.
70. Acs, P. and B. Kalman, *Pathogenesis of multiple sclerosis: what can we learn from the cuprizone model.* Methods Mol Biol, 2012. **900**: p. 403-31.
71. Russanov, E.M. and S.G. Ljutakova, *Effect of cuprizone on copper exchange and superoxide dismutase activity in rat liver.* Gen Pharmacol, 1980. **11**(6): p. 535-8.

72. Ljutakova, S.G. and E.M. Russanov, *Differences in the in vivo effects of cuprizone on superoxide dismutase activity in rat liver cytosol and mitochondrial intermembrane space.* Acta Physiol Pharmacol Bulg, 1985. **11**(2): p. 56-61.
73. Faizi, M., et al., *Toxicity of cuprizone a Cu(2+) chelating agent on isolated mouse brain mitochondria: a justification for demyelination and subsequent behavioral dysfunction.* Toxicol Mech Methods, 2016. **26**(4): p. 276-83.
74. Bradl, M. and H. Lassmann, *Oligodendrocytes: biology and pathology.* Acta Neuropathol, 2010. **119**(1): p. 37-53.
75. Fischbach, F., et al., *Cuprizone-induced graded oligodendrocyte vulnerability is regulated by the transcription factor DNA damage-inducible transcript 3.* Glia, 2018.
76. McTigue, D.M. and R.B. Tripathi, *The life, death, and replacement of oligodendrocytes in the adult CNS.* J Neurochem, 2008. **107**(1): p. 1-19.
77. McLaurin, J.A. and V.W. Yong, *Oligodendrocytes and myelin.* Neurol Clin, 1995. **13**(1): p. 23-49.
78. Liblau, R., et al., *Demyelinating diseases: from pathogenesis to repair strategies.* Trends Neurosci, 2001. **24**(3): p. 134-5.
79. Partridge, M.A., et al., *Proteomics of a conundrum: Thoughts on addressing the aetiology versus progression of multiple sclerosis.* Proteomics Clin Appl, 2015. **9**(9-10): p. 838-43.
80. Bouchat, J., et al., *Regional oligodendrocytopathy and astrocytopathy precede myelin loss and blood–brain barrier disruption in a murine model of osmotic demyelination syndrome.* Glia, 2018. **66**(3): p. 606-622.
81. Lee, J.Y., et al., *Overcoming Monocarboxylate Transporter 8 (MCT8)-Deficiency to Promote Human Oligodendrocyte Differentiation and Myelination.* EBioMedicine, 2017. **25**: p. 122-135.
82. Gudi, V., et al., *Glial response during cuprizone-induced de- and remyelination in the CNS: lessons learned.* Front Cell Neurosci, 2014. **8**: p. 73.
83. Nave, K.-A. and H. Ehrenreich, *Time to revisit oligodendrocytes in multiple sclerosis.* Nature medicine, 2019. **25**(3): p. 364-366.
84. Pfeiffer, S.E., A.E. Warrington, and R. Bansal, *The oligodendrocyte and its many cellular processes.* Trends Cell Biol, 1993. **3**(6): p. 191-7.
85. Harris, J.J. and D. Attwell, *The energetics of CNS white matter.* J Neurosci, 2012. **32**(1): p. 356-71.
86. Amaral, A.I., et al., *Oligodendrocytes: Development, Physiology and Glucose Metabolism.* Adv Neurobiol, 2016. **13**: p. 275-294.
87. Sanchez-Abarca, L.I., A. Tabernero, and J.M. Medina, *Oligodendrocytes use lactate as a source of energy and as a precursor of lipids.* Glia, 2001. **36**(3): p. 321-9.
88. Lyons, S.A. and H. Kettenmann, *Oligodendrocytes and microglia are selectively vulnerable to combined hypoxia and hypoglycemia injury in vitro.* J Cereb Blood Flow Metab, 1998. **18**(5): p. 521-30.
89. Juurlink, B.H., *Response of glial cells to ischemia: roles of reactive oxygen species and glutathione.* Neurosci Biobehav Rev, 1997. **21**(2): p. 151-66.
90. Carvalho, A.N., et al., *Glutathione in multiple sclerosis: more than just an antioxidant?* Mult Scler, 2014. **20**(11): p. 1425-31.
91. Ferreira, B., et al., *Glutathione in multiple sclerosis.* Br J Biomed Sci, 2013. **70**(2): p. 75-9.
92. Thorburne, S.K. and B.H. Juurlink, *Low glutathione and high iron govern the susceptibility of oligodendroglial precursors to oxidative stress.* J Neurochem, 1996. **67**(3): p. 1014-22.
93. Griot, C., et al., *Selective degeneration of oligodendrocytes mediated by reactive oxygen species.* Free Radic Res Commun, 1990. **11**(4-5): p. 181-93.
94. Kang, Y.J., *Metallothionein redox cycle and function.* Exp Biol Med (Maywood), 2006. **231**(9): p. 1459-67.

95. Pinteaux, E., M. Perraut, and G. Tholey, *Distribution of mitochondrial manganese superoxide dismutase among rat glial cells in culture.* Glia, 1998. **22**(4): p. 408-14.
96. Kress, G.J., K.E. Dineley, and I.J. Reynolds, *The relationship between intracellular free iron and cell injury in cultured neurons, astrocytes, and oligodendrocytes.* J Neurosci, 2002. **22**(14): p. 5848-55.
97. Connor, J.R. and S.L. Menzies, *Relationship of iron to oligodendrocytes and myelination.* Glia, 1996. **17**(2): p. 83-93.
98. Todorich, B., et al., *Oligodendrocytes and myelination: the role of iron.* Glia, 2009. **57**(5): p. 467-78.
99. Rinholm, J.E., et al., *Regulation of oligodendrocyte development and myelination by glucose and lactate.* J Neurosci, 2011. **31**(2): p. 538-48.
100. Emerit, J., C. Beaumont, and F. Trivin, *Iron metabolism, free radicals, and oxidative injury.* Biomed Pharmacother, 2001. **55**(6): p. 333-9.
101. McCord, J.M., *Iron, free radicals, and oxidative injury.* Semin Hematol, 1998. **35**(1): p. 5-12.
102. Braughler, J.M., L.A. Duncan, and R.L. Chase, *The involvement of iron in lipid peroxidation. Importance of ferric to ferrous ratios in initiation.* J Biol Chem, 1986. **261**(22): p. 10282-9.
103. Tang, L., et al., *The mechanism of Fe(2+)-initiated lipid peroxidation in liposomes: the dual function of ferrous ions, the roles of the pre-existing lipid peroxides and the lipid peroxyl radical.* Biochem J, 2000. **352 Pt 1**: p. 27-36.
104. Bahar, E., H. Kim, and H. Yoon, *ER Stress-Mediated Signaling: Action Potential and Ca(2+) as Key Players.* Int J Mol Sci, 2016. **17**(9).
105. Bravo, R., et al., *Endoplasmic reticulum and the unfolded protein response: dynamics and metabolic integration.* Int Rev Cell Mol Biol, 2013. **301**: p. 215-90.
106. Bradl, M., et al., *Transgenic Lewis rats overexpressing the proteolipid protein gene: myelin degeneration and its effect on T cell-mediated experimental autoimmune encephalomyelitis.* Acta Neuropathol, 1999. **97**(6): p. 595-606.
107. Bauer, J., et al., *Endoplasmic reticulum stress in PLP-overexpressing transgenic rats: gray matter oligodendrocytes are more vulnerable than white matter oligodendrocytes.* J Neuropathol Exp Neurol, 2002. **61**(1): p. 12-22.
108. Acs, P. and S. Komoly, *Selective ultrastructural vulnerability in the cuprizone-induced experimental demyelination.* Ideggyogy Sz, 2012. **65**(7-8): p. 266-70.
109. Namekata, K., et al., *Dock3 protects myelin in the cuprizone model for demyelination.* Cell Death Dis, 2014. **5**: p. e1395.
110. Sun, J., et al., *Myelin injury induces axonal transport impairment but not AD-like pathology in the hippocampus of cuprizone-fed mice.* Oncotarget, 2016. **7**(21): p. 30003-17.
111. Benetti, F., et al., *Cuprizone neurotoxicity, copper deficiency and neurodegeneration.* Neurotoxicology, 2010. **31**(5): p. 509-17.
112. Hoffmann, K., et al., *Epileptic seizures and hippocampal damage after cuprizone-induced demyelination in C57BL/6 mice.* Exp Neurol, 2008. **210**(2): p. 308-21.
113. Kipp, M., et al., *The cuprizone animal model: new insights into an old story.* Acta Neuropathol, 2009. **118**(6): p. 723-36.
114. Targett, M.P., et al., *Failure to achieve remyelination of demyelinated rat axons following transplantation of glial cells obtained from the adult human brain.* Neuropathol Appl Neurobiol, 1996. **22**(3): p. 199-206.
115. Sachs, H.H., et al., *A new model of cuprizone-mediated demyelination/remyelination.* ASN Neuro, 2014. **6**(5).
116. Clarner, T., et al., *CXCL10 triggers early microglial activation in the cuprizone model.* J Immunol, 2015. **194**(7): p. 3400-13.
117. Salinas Tejedor, L., et al., *Oligodendroglial markers in the cuprizone model of CNS de- and remyelination.* Histol Histopathol, 2015. **30**(12): p. 1455-64.

118. Salinas Tejedor, L., et al., *Mesenchymal stem cells do not exert direct beneficial effects on CNS remyelination in the absence of the peripheral immune system.* Brain Behav Immun, 2015. **50**: p. 155-165.
119. Deshmukh, V.A., et al., *A regenerative approach to the treatment of multiple sclerosis.* Nature, 2013. **502**(7471): p. 327-332.
120. El-Akabawy, G. and L.A. Rashed, *Beneficial effects of bone marrow-derived mesenchymal stem cell transplantation in a non-immune model of demyelination.* Ann Anat, 2015. **198**: p. 11-20.
121. Yu, Q., et al., *Strain differences in cuprizone induced demyelination.* Cell Biosci, 2017. **7**: p. 59.
122. Mashayekhi, F. and Z. Salehi, *Administration of vitamin D3 induces CNPase and myelin oligodendrocyte glycoprotein expression in the cerebral cortex of the murine model of cuprizone-induced demyelination.* Folia Neuropathol, 2016. **54**(3): p. 259-264.
123. Ye, J.N., et al., *Progesterone alleviates neural behavioral deficits and demyelination with reduced degeneration of oligodendroglial cells in cuprizone-induced mice.* PLoS One, 2013. **8**(1): p. e54590.
124. Serra-de-Oliveira, N., et al., *Behavioural changes observed in demyelination model shares similarities with white matter abnormalities in humans.* Behav Brain Res, 2015. **287**: p. 265-75.
125. Yoshikawa, K., et al., *Inhibition of 5-lipoxygenase activity in mice during cuprizone-induced demyelination attenuates neuroinflammation, motor dysfunction and axonal damage.* Prostaglandins Leukot Essent Fatty Acids, 2011. **85**(1): p. 43-52.
126. Lampron, A., et al., *Inefficient clearance of myelin debris by microglia impairs remyelinating processes.* J Exp Med, 2015. **212**(4): p. 481-95.
127. Gallyas, F., *Silver staining of myelin by means of physical development.* Neurol Res, 1979. **1**(2): p. 203-9.
128. Pistorio, A.L., S.H. Hendry, and X. Wang, *A modified technique for high-resolution staining of myelin.* J Neurosci Methods, 2006. **153**(1): p. 135-46.
129. Pfeifenbring, S., et al., *Remyelination After Cuprizone-Induced Demyelination Is Accelerated in Juvenile Mice.* J Neuropathol Exp Neurol, 2015. **74**(8): p. 756-66.
130. Norkute, A., et al., *Cuprizone treatment induces demyelination and astrocytosis in the mouse hippocampus.* J Neurosci Res, 2009. **87**(6): p. 1343-55.
131. Steelman, A.J., J.P. Thompson, and J. Li, *Demyelination and remyelination in anatomically distinct regions of the corpus callosum following cuprizone intoxication.* Neurosci Res, 2012. **72**(1): p. 32-42.
132. Groebe, A., et al., *Cuprizone treatment induces distinct demyelination, astrocytosis, and microglia cell invasion or proliferation in the mouse cerebellum.* Cerebellum, 2009. **8**(3): p. 163-74.
133. Petkovic, F., et al., *Reduced cuprizone-induced cerebellar demyelination in mice with astrocyte-targeted production of IL-6 is associated with chronically activated, but less responsive microglia.* J Neuroimmunol, 2017. **310**: p. 97-102.
134. Silvestroff, L., et al., *Cuprizone-induced demyelination in CNP::GFP transgenic mice.* J Comp Neurol, 2010. **518**(12): p. 2261-83.
135. Wang, H., et al., *Cuprizone-induced demyelination in mice: age-related vulnerability and exploratory behavior deficit.* Neurosci Bull, 2013. **29**(2): p. 251-9.
136. Doucette, J.R., R. Jiao, and A.J. Nazarali, *Age-related and cuprizone-induced changes in myelin and transcription factor gene expression and in oligodendrocyte cell densities in the rostral corpus callosum of mice.* Cell Mol Neurobiol, 2010. **30**(4): p. 607-29.
137. Franklin, R.J. and S.A. Goldman, *Glia Disease and Repair-Remyelination.* Cold Spring Harb Perspect Biol, 2015. **7**(7): p. a020594.

138. Young, K.M., et al., *Oligodendrocyte dynamics in the healthy adult CNS: evidence for myelin remodeling.* Neuron, 2013. **77**(5): p. 873-85.
139. Liu, J., et al., *Epigenetic control of oligodendrocyte development: adding new players to old keepers.* Curr Opin Neurobiol, 2016. **39**: p. 133-8.
140. Copray, S., et al., *Epigenetic mechanisms facilitating oligodendrocyte development, maturation, and aging.* Glia, 2009. **57**(15): p. 1579-87.
141. Taylor, L.C., W. Gilmore, and G.K. Matsushima, *SJL mice exposed to cuprizone intoxication reveal strain and gender pattern differences in demyelination.* Brain Pathol, 2009. **19**(3): p. 467-79.
142. Skripuletz, T., et al., *Cortical demyelination is prominent in the murine cuprizone model and is strain-dependent.* Am J Pathol, 2008. **172**(4): p. 1053-61.
143. Silvestroff, L., et al., *Cuprizone-induced demyelination in the rat cerebral cortex and thyroid hormone effects on cortical remyelination.* Exp Neurol, 2012. **235**(1): p. 357-67.
144. Oakden, W., et al., *Early regional cuprizone-induced demyelination in a rat model revealed with MRI.* NMR Biomed, 2017. **30**(9).
145. Basoglu, H., N.T. Boylu, and H. Kose, *Cuprizone-induced demyelination in Wistar rats; electrophysiological and histological assessment.* Eur Rev Med Pharmacol Sci, 2013. **17**(20): p. 2711-7.
146. Ornelas, I.M., et al., *Heterogeneity in oligodendroglia: Is it relevant to mouse models and human disease?* J Neurosci Res, 2016. **94**(12): p. 1421-1433.
147. Umemori, H., et al., *Initial events of myelination involve Fyn tyrosine kinase signalling.* Nature, 1994. **367**(6463): p. 572-6.
148. Sperber, B.R., et al., *A unique role for Fyn in CNS myelination.* J Neurosci, 2001. **21**(6): p. 2039-47.
149. Taveggia, C., et al., *Type III neuregulin-1 promotes oligodendrocyte myelination.* Glia, 2008. **56**(3): p. 284-93.
150. Floriddia, E.M., et al., *Specific oligodendrocyte populations have differential spatial distribution and susceptibility to injury.* Society For Neuroscience Annual Meeting, 2019. **50**: p. 740.06.
151. Sullivan, P.G., et al., *Intrinsic differences in brain and spinal cord mitochondria: Implication for therapeutic interventions.* J Comp Neurol, 2004. **474**(4): p. 524-34.
152. Hemmer, B., M. Kerschensteiner, and T. Korn, *Role of the innate and adaptive immune responses in the course of multiple sclerosis.* Lancet Neurol, 2015. **14**(4): p. 406-19.
153. Gandhi, R., A. Laroni, and H.L. Weiner, *Role of the innate immune system in the pathogenesis of multiple sclerosis.* J Neuroimmunol, 2010. **221**(1-2): p. 7-14.
154. Ponath, G., C. Park, and D. Pitt, *The Role of Astrocytes in Multiple Sclerosis.* Front Immunol, 2018. **9**: p. 217.
155. Liddelow, S.A. and B.A. Barres, *Reactive Astrocytes: Production, Function, and Therapeutic Potential.* Immunity, 2017. **46**(6): p. 957-967.
156. He, F. and Y.E. Sun, *Glial cells more than support cells?* Int J Biochem Cell Biol, 2007. **39**(4): p. 661-5.
157. Parpura, V., et al., *Glial cells in (patho)physiology.* J Neurochem, 2012. **121**(1): p. 4-27.
158. Wheeler, M.A. and F.J. Quintana, *Regulation of Astrocyte Functions in Multiple Sclerosis.* Cold Spring Harb Perspect Med, 2018.
159. Correale, J. and M.F. Farez, *The Role of Astrocytes in Multiple Sclerosis Progression.* Front Neurol, 2015. **6**: p. 180.
160. Liddelow, S.A., et al., *Neurotoxic reactive astrocytes are induced by activated microglia.* Nature, 2017. **541**(7638): p. 481-487.
161. Goldberg, J., et al., *Anatomical Distribution of Cuprizone-Induced Lesions in C57BL6 Mice.* J Mol Neurosci, 2015. **57**(2): p. 166-75.

162. Gudi, V., et al., *Spatial and temporal profiles of growth factor expression during CNS demyelination reveal the dynamics of repair priming.* PLoS One, 2011. **6**(7): p. e22623.
163. Tezuka, T., et al., *Cuprizone short-term exposure: astrocytic IL-6 activation and behavioral changes relevant to psychosis.* Neurobiol Dis, 2013. **59**: p. 63-8.
164. Linares, D., et al., *Neuronal nitric oxide synthase plays a key role in CNS demyelination.* J Neurosci, 2006. **26**(49): p. 12672-81.
165. Sofroniew, M.V. and H.V. Vinters, *Astrocytes: biology and pathology.* Acta Neuropathol, 2010. **119**(1): p. 7-35.
166. Lyck, L., et al., *Immunohistochemical markers for quantitative studies of neurons and glia in human neocortex.* J Histochem Cytochem, 2008. **56**(3): p. 201-21.
167. Takamori, Y., et al., *Nestin-positive microglia in adult rat cerebral cortex.* Brain Res, 2009. **1270**: p. 10-8.
168. Graeber, M.B. and W.J. Streit, *Microglia: biology and pathology.* Acta Neuropathol, 2010. **119**(1): p. 89-105.
169. Ginhoux, F. and M. Prinz, *Origin of microglia: current concepts and past controversies.* Cold Spring Harb Perspect Biol, 2015. **7**(8): p. a020537.
170. Ginhoux, F. and S. Garel, *The mysterious origins of microglia.* Nat Neurosci, 2018. **21**(7): p. 897-899.
171. David, S. and A. Kroner, *Repertoire of microglial and macrophage responses after spinal cord injury.* Nat Rev Neurosci, 2011. **12**(7): p. 388-99.
172. Reu, P., et al., *The Lifespan and Turnover of Microglia in the Human Brain.* Cell Rep, 2017. **20**(4): p. 779-784.
173. Tay, T.L., et al., *A new fate mapping system reveals context-dependent random or clonal expansion of microglia.* Nat Neurosci, 2017. **20**(6): p. 793-803.
174. Lively, S. and L.C. Schlichter, *The microglial activation state regulates migration and roles of matrix-dissolving enzymes for invasion.* J Neuroinflammation, 2013. **10**: p. 75.
175. Maeda, T., et al., *ATP increases the migration of microglia across the brain endothelial cell monolayer.* Biosci Rep, 2016. **36**(2).
176. Soulet, D. and S. Rivest, *Microglia.* Curr Biol, 2008. **18**(12): p. R506-8.
177. Harry, G.J. and A.D. Kraft, *Microglia in the developing brain: a potential target with lifetime effects.* Neurotoxicology, 2012. **33**(2): p. 191-206.
178. Ginhoux, F., et al., *Origin and differentiation of microglia.* Front Cell Neurosci, 2013. **7**: p. 45.
179. Nayak, D., T.L. Roth, and D.B. McGavern, *Microglia development and function.* Annu Rev Immunol, 2014. **32**: p. 367-402.
180. Graeber, M.B., *Changing face of microglia.* Science, 2010. **330**(6005): p. 783-8.
181. Kawabori, M. and M.A. Yenari, *The role of the microglia in acute CNS injury.* Metab Brain Dis, 2015. **30**(2): p. 381-92.
182. Lan, X., et al., *Modulators of microglial activation and polarization after intracerebral haemorrhage.* Nature Reviews Neurology, 2017. **13**: p. 420.
183. Cherry, J.D., J.A. Olschowka, and M.K. O'Banion, *Neuroinflammation and M2 microglia: the good, the bad, and the inflamed.* Journal of Neuroinflammation, 2014. **11**(1): p. 98.
184. Voss, E.V., et al., *Characterisation of microglia during de- and remyelination: can they create a repair promoting environment?* Neurobiol Dis, 2012. **45**(1): p. 519-28.
185. Noorzehi, G., et al., *Microglia polarization by methylprednizolone acetate accelerates cuprizone induced demyelination.* J Mol Histol, 2018. **49**(5): p. 471-479.
186. Duan, C., et al., *Sulfasalazine alters microglia phenotype by competing endogenous RNA effect of miR-136-5p and long non-coding RNA HOTAIR in cuprizone-induced demyelination.* Biochem Pharmacol, 2018. **155**: p. 110-123.
187. Martinez, F.O. and S. Gordon, *The M1 and M2 paradigm of macrophage activation: time for reassessment.* F1000Prime Rep, 2014. **6**: p. 13.

188. Michell-Robinson, M.A., et al., *Roles of microglia in brain development, tissue maintenance and repair.* Brain, 2015. **138**(Pt 5): p. 1138-59.
189. Raposo, C., et al., *Sildenafil (Viagra) protective effects on neuroinflammation: the role of iNOS/NO system in an inflammatory demyelination model.* Mediators Inflamm, 2013. **2013**: p. 321460.
190. Olah, M., et al., *Identification of a microglia phenotype supportive of remyelination.* Glia, 2012. **60**(2): p. 306-21.
191. McMahon, E.J., K. Suzuki, and G.K. Matsushima, *Peripheral macrophage recruitment in cuprizone-induced CNS demyelination despite an intact blood-brain barrier.* J Neuroimmunol, 2002. **130**(1-2): p. 32-45.
192. Sasaki, Y., et al., *Iba1 is an actin-cross-linking protein in macrophages/microglia.* Biochem Biophys Res Commun, 2001. **286**(2): p. 292-7.
193. Ohsawa, K., et al., *Microglia/macrophage-specific protein Iba1 binds to fimbrin and enhances its actin-bundling activity.* J Neurochem, 2004. **88**(4): p. 844-56.
194. Mason, J.L., et al., *Oligodendrocytes and progenitors become progressively depleted within chronically demyelinated lesions.* Am J Pathol, 2004. **164**(5): p. 1673-82.
195. Krauthausen, M., et al., *CXCR3 modulates glial accumulation and activation in cuprizone-induced demyelination of the central nervous system.* J Neuroinflammation, 2014. **11**: p. 109.
196. Manterola, A., et al., *Deregulation of the endocannabinoid system and therapeutic potential of ABHD6 blockade in the cuprizone model of demyelination.* Biochem Pharmacol, 2018. **157**: p. 189-201.
197. Esser, S., et al., *Toll-Like Receptor 2-Mediated Glial Cell Activation in a Mouse Model of Cuprizone-Induced Demyelination.* Mol Neurobiol, 2018. **55**(8): p. 6237-6249.
198. Mattner, F., et al., *Evaluation of [(1)(2)(3)I]-CLINDE as a potent SPECT radiotracer to assess the degree of astroglia activation in cuprizone-induced neuroinflammation.* Eur J Nucl Med Mol Imaging, 2011. **38**(8): p. 1516-28.
199. Raijmakers, R., et al., *Citrullination of central nervous system proteins during the development of experimental autoimmune encephalomyelitis.* The Journal of comparative neurology, 2005. **486**(3): p. 243-253.
200. Yang, L., D. Tan, and H. Piao, *Myelin Basic Protein Citrullination in Multiple Sclerosis: A Potential Therapeutic Target for the Pathology.* Neurochemical research, 2016. **41**(8): p. 1845-1856.
201. Ortiz, G.G., et al., *Role of the blood-brain barrier in multiple sclerosis.* Arch Med Res, 2014. **45**(8): p. 687-97.
202. Minagar, A. and J.S. Alexander, *Blood-brain barrier disruption in multiple sclerosis.* Mult Scler, 2003. **9**(6): p. 540-9.
203. Compston, A. and A. Coles, *Multiple sclerosis.* Lancet, 2008. **372**(9648): p. 1502-17.
204. Thompson, A.J., et al., *Multiple sclerosis.* Lancet, 2018. **391**(10130): p. 1622-1636.
205. Huang, W.-J., W.-W. Chen, and X. Zhang, *Multiple sclerosis: Pathology, diagnosis and treatments.* Experimental and therapeutic medicine, 2017. **13**(6): p. 3163-3166.
206. Koriem, K.M.M., *Multiple sclerosis: New insights and trends.* Asian Pacific Journal of Tropical Biomedicine, 2016. **6**(5): p. 429-440.
207. Hafler, D.A., et al., *Multiple sclerosis.* Immunol Rev, 2005. **204**: p. 208-31.
208. Filippi, M., et al., *Multiple sclerosis.* Nat Rev Dis Primers, 2018. **4**(1): p. 43.
209. Lucchinetti, C.F., et al., *Distinct patterns of multiple sclerosis pathology indicates heterogeneity on pathogenesis.* Brain Pathol, 1996. **6**(3): p. 259-74.
210. Lucchinetti, C., et al., *Heterogeneity of multiple sclerosis lesions: implications for the pathogenesis of demyelination.* Ann Neurol, 2000. **47**(6): p. 707-17.
211. Lassmann, H., W. Bruck, and C. Lucchinetti, *Heterogeneity of multiple sclerosis pathogenesis: implications for diagnosis and therapy.* Trends Mol Med, 2001. **7**(3): p. 115-21.

212. Popescu, B.F., I. Pirko, and C.F. Lucchinetti, *Pathology of multiple sclerosis: where do we stand?* Continuum (Minneap Minn), 2013. **19**(4 Multiple Sclerosis): p. 901-21.
213. Stys, P.K., *Pathoetiology of multiple sclerosis: are we barking up the wrong tree?* F1000Prime Rep, 2013. **5**: p. 20.
214. Stys, P.K., et al., *Will the real multiple sclerosis please stand up?* Nat Rev Neurosci, 2012. **13**(7): p. 507-14.
215. Traka, M., et al. *Oligodendrocyte death results in immune-mediated CNS demyelination*. Nat Neurosci 2016 Jan [cited 19 1]; 2015/12/15:[65-74].
216. Constantinescu, C.S., et al., *Experimental autoimmune encephalomyelitis (EAE) as a model for multiple sclerosis (MS).* Br J Pharmacol, 2011. **164**(4): p. 1079-106.
217. Gold, R., C. Linington, and H. Lassmann, *Understanding pathogenesis and therapy of multiple sclerosis via animal models: 70 years of merits and culprits in experimental autoimmune encephalomyelitis research.* Brain, 2006. **129**(Pt 8): p. 1953-71.
218. t Hart, B.A., B. Gran, and R. Weissert, *EAE: imperfect but useful models of multiple sclerosis.* Trends Mol Med, 2011. **17**(3): p. 119-25.
219. Trapp, B.D. and K.A. Nave, *Multiple sclerosis: an immune or neurodegenerative disorder?* Annu Rev Neurosci, 2008. **31**: p. 247-69.
220. Lassmann, H. and M. Bradl, *Multiple sclerosis: experimental models and reality.* Acta Neuropathol, 2017. **133**(2): p. 223-244.
221. Sriram, S. and I. Steiner, *Experimental allergic encephalomyelitis: a misleading model of multiple sclerosis.* Ann Neurol, 2005. **58**(6): p. 939-45.
222. Behan, P.O. and A. Chaudhuri, *EAE is not a useful model for demyelinating disease.* Mult Scler Relat Disord, 2014. **3**(5): p. 565-74.
223. Flugel, A., et al., *Migratory activity and functional changes of green fluorescent effector cells before and during experimental autoimmune encephalomyelitis.* Immunity, 2001. **14**(5): p. 547-60.
224. Lassmann, H. and J. van Horssen, *The molecular basis of neurodegeneration in multiple sclerosis.* FEBS Lett, 2011. **585**(23): p. 3715-23.
225. Friese, M.A. and L. Fugger, *Autoreactive CD8+ T cells in multiple sclerosis: a new target for therapy?* Brain, 2005. **128**(Pt 8): p. 1747-63.
226. Hauser, S.L., et al., *Immunohistochemical analysis of the cellular infiltrate in multiple sclerosis lesions.* Ann Neurol, 1986. **19**(6): p. 578-87.
227. Ransohoff, R.M., *Animal models of multiple sclerosis: the good, the bad and the bottom line.* Nat Neurosci, 2012. **15**(8): p. 1074-7.
228. Gilmore, C.P., et al., *Regional variations in the extent and pattern of grey matter demyelination in multiple sclerosis: a comparison between the cerebral cortex, cerebellar cortex, deep grey matter nuclei and the spinal cord.* J Neurol Neurosurg Psychiatry, 2009. **80**(2): p. 182-7.
229. Vargas, D.L. and W.R. Tyor, *Update on disease-modifying therapies for multiple sclerosis.* J Investig Med, 2017. **65**(5): p. 883-891.
230. Barnett, M.H. and J.W. Prineas, *Relapsing and remitting multiple sclerosis: pathology of the newly forming lesion.* Ann Neurol, 2004. **55**(4): p. 458-68.
231. Henderson, A.P., et al., *Multiple sclerosis: distribution of inflammatory cells in newly forming lesions.* Ann Neurol, 2009. **66**(6): p. 739-53.
232. Seewann, A., et al., *Diffusely abnormal white matter in chronic multiple sclerosis: imaging and histopathologic analysis.* Arch Neurol, 2009. **66**(5): p. 601-9.
233. Metz, I., et al., *Autologous haematopoietic stem cell transplantation fails to stop demyelination and neurodegeneration in multiple sclerosis.* Brain, 2007. **130**(Pt 5): p. 1254-62.
234. Rodriguez, M. and B. Scheithauer, *Ultrastructure of multiple sclerosis.* Ultrastruct Pathol, 1994. **18**(1-2): p. 3-13.

235. Buck, D. and B. Hemmer, *Treatment of multiple sclerosis: current concepts and future perspectives.* J Neurol, 2011. **258**(10): p. 1747-62.
236. Bettelli, E., et al., *IL-10 is critical in the regulation of autoimmune encephalomyelitis as demonstrated by studies of IL-10- and IL-4-deficient and transgenic mice.* J Immunol, 1998. **161**(7): p. 3299-306.
237. Kugler, S., et al., *Pertussis toxin transiently affects barrier integrity, organelle organization and transmigration of monocytes in a human brain microvascular endothelial cell barrier model.* Cell Microbiol, 2007. **9**(3): p. 619-32.
238. Mohajeri, M., M. Sadeghizadeh, and M. Javan, *Pertussis toxin promotes relapsing-remitting experimental autoimmune encephalomyelitis in Lewis rats.* J Neuroimmunol, 2015. **289**: p. 105-10.
239. Schellenberg, A.E., et al., *Blood-brain barrier disruption in CCL2 transgenic mice during pertussis toxin-induced brain inflammation.* Fluids Barriers CNS, 2012. **9**(1): p. 10.
240. Almuslehi, M.S.M., et al., *Blood Brain Barrier Disruption Facilitates CD8 T Cells infiltration into the CNS of Orchiectomized Cuprizone Treated Mice*, in *Australasian Neuroscience Society*. 2018, Australasian Neuroscience Society

Brisbane Convention & Exhibition Centre, Brisbane p. 163.
241. Franco-Pons, N., et al., *Behavioral deficits in the cuprizone-induced murine model of demyelination/remyelination.* Toxicol Lett, 2007. **169**(3): p. 205-13.
242. Ruiz, L.M., et al., *Quercetin Affects Erythropoiesis and Heart Mitochondrial Function in Mice.* Oxid Med Cell Longev, 2015. **2015**: p. 836301.
243. Pollak, J., et al., *Stratification substantially reduces behavioral variability in the hypoxic-ischemic stroke model.* Brain Behav, 2012. **2**(5): p. 698-706.
244. Kim, D., et al., *Inosine enhances axon sprouting and motor recovery after spinal cord injury.* PLoS One, 2013. **8**(12): p. e81948.
245. Jacobi, A., et al., *FGF22 signaling regulates synapse formation during post-injury remodeling of the spinal cord.* EMBO J, 2015. **34**(9): p. 1231-43.
246. Schaar, K.L., M.M. Brenneman, and S.I. Savitz, *Functional assessments in the rodent stroke model.* Exp Transl Stroke Med, 2010. **2**(1): p. 13.
247. Fleming, S.M., et al., *Early and progressive sensorimotor anomalies in mice overexpressing wild-type human alpha-synuclein.* J Neurosci, 2004. **24**(42): p. 9434-40.
248. Morelli, E., et al., *Chronic 5-HT transporter blockade reduces DA signaling to elicit basal ganglia dysfunction.* J Neurosci, 2011. **31**(44): p. 15742-50.
249. Samour, M.S., et al., *Noxious, but not innocuous, thermal stimuli evoke pERK expression in dorsal horn neurons after spared nerve injury in adult rats.* Neurosci Lett, 2017. **654**: p. 49-55.
250. Shaikh, S., et al., *Sensory perturbations using suture and sutureless repair of transected median nerve in rats.* Somatosens Mot Res, 2016. **33**(1): p. 20-8.
251. Gyengesi, E., et al., *Semi-automated 3D segmentation of major tracts in the rat brain: comparing DTI with standard histological methods.* Brain Struct Funct, 2014. **219**(2): p. 539-50.
252. Burry, R.W., *Controls for immunocytochemistry: an update.* J Histochem Cytochem, 2011. **59**(1): p. 6-12.
253. Hewitt, S.M., et al., *Controls for immunohistochemistry: the Histochemical Society's standards of practice for validation of immunohistochemical assays.* J Histochem Cytochem, 2014. **62**(10): p. 693-7.
254. Gyengesi, E., et al., *Investigation Into the Effects of Tenilsetam on Markers of Neuroinflammation in GFAP-IL6 Mice.* Pharm Res, 2018. **35**(1): p. 22.
255. Gyengesi, E., et al., *Chronic Microglial Activation in the GFAP-IL6 Mouse Contributes to Age-Dependent Cerebellar Volume Loss and Impairment in Motor Function.* Front Neurosci, 2019. **13**: p. 303.

256. Harrison, M., et al., *Vertebral landmarks for the identification of spinal cord segments in the mouse.* Neuroimage, 2013. **68**: p. 22-9.
257. Sengul, G., et al., *Spinal cord projections to the cerebellum in the mouse.* Brain Struct Funct, 2015. **220**(5): p. 2997-3009.
258. Paxinos, G. and K. Franklin, *Paxinos and Franklin's the Mouse Brain in Stereotaxic Coordinates, Fourth Edition*. 2012: Academic Press.
259. Butt, R.H. and J.R. Coorssen, *Pre-extraction sample handling by automated frozen disruption significantly improves subsequent proteomic analyses.* J Proteome Res, 2006. **5**(2): p. 437-48.
260. Wright, E.P., et al., *Top-down proteomics: enhancing 2D gel electrophoresis from tissue processing to high-sensitivity protein detection.* Proteomics, 2014. **14**(7-8): p. 872-89.
261. Butt, R.H., et al., *Enabling coupled quantitative genomics and proteomics analyses from rat spinal cord samples.* Mol Cell Proteomics, 2007. **6**(9): p. 1574-88.
262. Churchward, M.A., et al., *Enhanced detergent extraction for analysis of membrane proteomes by two-dimensional gel electrophoresis.* Proteome Sci, 2005. **3**(1): p. 5.
263. Butt, R.H. and J.R. Coorssen, *Postfractionation for enhanced proteomic analyses: routine electrophoretic methods increase the resolution of standard 2D-PAGE.* J Proteome Res, 2005. **4**(3): p. 982-91.
264. Herbert, B., et al., *Reduction and alkylation of proteins in preparation of two-dimensional map analysis: why, when, and how?* Electrophoresis, 2001. **22**(10): p. 2046-57.
265. Wright, E.P., et al., *Deep imaging: how much of the proteome does current top-down technology already resolve?* PLoS One, 2014. **9**(1): p. e86058.
266. Gauci, V.J., M.P. Padula, and J.R. Coorssen, *Coomassie blue staining for high sensitivity gel-based proteomics.* J Proteomics, 2013. **90**: p. 96-106.
267. Noaman, N. and J.R. Coorssen, *Coomassie does it (better): A Robin Hood approach to total protein quantification.* Anal Biochem, 2018. **556**: p. 53-56.
268. Butt, R.H. and J.R. Coorssen, *Coomassie blue as a near-infrared fluorescent stain: a systematic comparison with Sypro Ruby for in-gel protein detection.* Mol Cell Proteomics, 2013. **12**(12): p. 3834-50.
269. Harris, L.R., et al., *Assessing detection methods for gel-based proteomic analyses.* J Proteome Res, 2007. **6**(4): p. 1418-25.
270. Partridge, M.A., et al., *An initial top-down proteomic analysis of the standard cuprizone mouse model of multiple sclerosis.* Journal of Chemical Biology, 2016. **9**(1): p. 9-18.
271. D'Silva, A.M., J.A. Hyett, and J.R. Coorssen, *A Routine 'Top-Down' Approach to Analysis of the Human Serum Proteome.* Proteomes, 2017. **5**(2): p. 13.
272. Noaman, N., et al., *Coomassie staining provides routine (sub)femtomole in-gel detection of intact proteoforms: Expanding opportunities for genuine Top-down Proteomics.* Electrophoresis, 2017. **38**(24): p. 3086-3099.
273. Stimpson, S.E., J.R. Coorssen, and S.J. Myers, *Mitochondrial protein alterations in a familial peripheral neuropathy caused by the V144D amino acid mutation in the sphingolipid protein, SPTLC1.* J Chem Biol, 2015. **8**(1): p. 25-35.
274. Stroud, L.J., et al., *Comparative proteomic analysis of two pathogenic Tritrichomonas foetus genotypes: there is more to the proteome than meets the eye.* Int J Parasitol, 2017. **47**(4): p. 203-213.
275. UniProt Consortium, T., *UniProt: the universal protein knowledgebase.* Nucleic Acids Res, 2018. **46**(5): p. 2699.
276. D'Silva, A.M., J.A. Hyett, and J.R. Coorssen, *Proteomic analysis of first trimester maternal serum to identify candidate biomarkers potentially predictive of spontaneous preterm birth.* J Proteomics, 2018. **178**: p. 31-42.
277. Sharma, S., et al., *Quantitative proteomic analysis of meningiomas for the identification of surrogate protein markers.* Sci Rep, 2014. **4**: p. 7140.

278. Szklarczyk, D., et al., *STRING v10: protein-protein interaction networks, integrated over the tree of life.* Nucleic Acids Res, 2015. **43**(Database issue): p. D447-52.
279. Hossain, M.U., et al., *Finding Potential Therapeutic Targets against Shigella flexneri through Proteome Exploration.* Front Microbiol, 2016. **7**: p. 1817.
280. De Las Rivas, J. and C. Fontanillo, *Protein-protein interactions essentials: key concepts to building and analyzing interactome networks.* PLoS Comput Biol, 2010. **6**(6): p. e1000807.
281. Bittner, S., et al., *Myelin oligodendrocyte glycoprotein (MOG35-55) induced experimental autoimmune encephalomyelitis (EAE) in C57BL/6 mice.* J Vis Exp, 2014(86).
282. Yang, H.J., et al., *Region-specific susceptibilities to cuprizone-induced lesions in the mouse forebrain: Implications for the pathophysiology of schizophrenia.* Brain Res, 2009. **1270**: p. 121-30.
283. Coorssen, J.R., et al., *Quantitative femto- to attomole immunodetection of regulated secretory vesicle proteins critical to exocytosis.* Anal Biochem, 2002. **307**(1): p. 54-62.
284. Pearse, G., *Normal structure, function and histology of the thymus.* Toxicol Pathol, 2006. **34**(5): p. 504-14.
285. Cesta, M.F., *Normal structure, function, and histology of the spleen.* Toxicol Pathol, 2006. **34**(5): p. 455-65.
286. Lin, M.Y., et al., *A pivotal role for the multifunctional calcium/calmodulin-dependent protein kinase II in T cells: from activation to unresponsiveness.* J Immunol, 2005. **174**(9): p. 5583-92.
287. Bui, J.D., et al., *A role for CaMKII in T cell memory.* Cell, 2000. **100**(4): p. 457-67.
288. Weyer, A.D. and C.L. Stucky, *Repurposing a leukocyte elastase inhibitor for neuropathic pain.* Nat Med, 2015. **21**(5): p. 429-30.
289. Kang, K., et al., *A role for protein disulfide isomerase in the early folding and assembly of MHC class I molecules.* Antioxid Redox Signal, 2009. **11**(10): p. 2553-61.
290. Herder, V., et al., *Cuprizone inhibits demyelinating leukomyelitis by reducing immune responses without virus exacerbation in an infectious model of multiple sclerosis.* J Neuroimmunol, 2012. **244**(1-2): p. 84-93.
291. Mana, P., et al., *Demyelination caused by the copper chelator cuprizone halts T cell mediated autoimmune neuroinflammation.* J Neuroimmunol, 2009. **210**(1-2): p. 13-21.
292. Hopkins, R.G. and M.L. Failla, *Transcriptional regulation of interleukin-2 gene expression is impaired by copper deficiency in Jurkat human T lymphocytes.* J Nutr, 1999. **129**(3): p. 596-601.
293. Bala, S. and M.L. Failla, *Copper deficiency reversibly impairs DNA synthesis in activated T lymphocytes by limiting interleukin 2 activity.* Proceedings of the National Academy of Sciences, 1992. **89**(15): p. 6794-6797.
294. Desdin-Mico, G., G. Soto-Heredero, and M. Mittelbrunn, *Mitochondrial activity in T cells.* Mitochondrion, 2018. **41**: p. 51-57.
295. Sukumar, M., et al., *Mitochondrial Membrane Potential Identifies Cells with Enhanced Stemness for Cellular Therapy.* Cell Metab, 2016. **23**(1): p. 63-76.
296. Oliveira, B.M., J.R. Coorssen, and D. Martins-de-Souza, *2DE: the phoenix of proteomics.* J Proteomics, 2014. **104**: p. 140-50.
297. Coorssen, J.R. and A.L. Yergey, *Proteomics Is Analytical Chemistry: Fitness-for-Purpose in the Application of Top-Down and Bottom-Up Analyses.* Proteomes, 2015. **3**(4): p. 440-453.
298. Gat-Viks, I., et al., *Proteomics-level analysis of myelin formation and regeneration in a mouse model for Vanishing White Matter disease.* J Neurochem, 2015. **134**(3): p. 513-26.
299. Oveland, E., et al., *1,25-Dihydroxyvitamin-D3 induces brain proteomic changes in cuprizone mice during remyelination involving calcium proteins.* Neurochem Int, 2018. **112**: p. 267-277.
300. Mronga, T., et al., *Mitochondrial pathway is involved in hydrogen-peroxide-induced apoptotic cell death of oligodendrocytes.* Glia, 2004. **46**(4): p. 446-55.

301. Huang, S.Q., et al., *Demyelination initiated by oligodendrocyte apoptosis through enhancing endoplasmic reticulum-mitochondria interactions and Id2 expression after compressed spinal cord injury in rats.* CNS Neurosci Ther, 2014. **20**(1): p. 20-31.
302. Ni Fhlathartaigh, M., et al., *Calreticulin and other components of endoplasmic reticulum stress in rat and human inflammatory demyelination.* Acta Neuropathol Commun, 2013. **1**: p. 37.
303. Saito, Y., et al., *Calreticulin functions in vitro as a molecular chaperone for both glycosylated and non-glycosylated proteins.* Embo j, 1999. **18**(23): p. 6718-29.
304. Lee, D., et al., *Differential requirement of unfolded protein response pathway for calreticulin expression in Caenorhabditis elegans.* J Mol Biol, 2007. **372**(2): p. 331-40.
305. Bolcskei, K., et al., *Behavioural alterations and morphological changes are attenuated by the lack of TRPA1 receptors in the cuprizone-induced demyelination model in mice.* J Neuroimmunol, 2018. **320**: p. 1-10.
306. Chang, H., et al., *Increased central dopaminergic activity might be involved in the behavioral abnormality of cuprizone exposure mice.* Behav Brain Res, 2017. **331**: p. 143-150.
307. Hagemeyer, N., et al., *Erythropoietin attenuates neurological and histological consequences of toxic demyelination in mice.* Mol Med, 2012. **18**: p. 628-35.
308. Kondo, M.A., et al., *Dimensional assessment of behavioral changes in the cuprizone short-term exposure model for psychosis.* Neurosci Res, 2016. **107**: p. 70-74.
309. Iwasa, K., et al., *Prostaglandin F2alpha FP receptor inhibitor reduces demyelination and motor dysfunction in a cuprizone-induced multiple sclerosis mouse model.* Prostaglandins Leukot Essent Fatty Acids, 2014. **91**(5): p. 175-82.
310. Elbaz, E.M., et al., *Neuroprotective effect of linagliptin against cuprizone-induced demyelination and behavioural dysfunction in mice: A pivotal role of AMPK/SIRT1 and JAK2/STAT3/NF-kappaB signalling pathway modulation.* Toxicol Appl Pharmacol, 2018. **352**: p. 153-161.
311. Kumar, P., et al., *Preclinical Explorative Assessment of Dimethyl Fumarate-Based Biocompatible Nanolipoidal Carriers for the Management of Multiple Sclerosis.* ACS Chem Neurosci, 2018. **9**(5): p. 1152-1158.
312. Sanadgol, N., et al., *Low, but not high, dose triptolide controls neuroinflammation and improves behavioral deficits in toxic model of multiple sclerosis by dampening of NF-kappaB activation and acceleration of intrinsic myelin repair.* Toxicol Appl Pharmacol, 2018. **342**: p. 86-98.
313. Hashimoto, M., et al., *The flavonoid Baicalein attenuates cuprizone-induced demyelination via suppression of neuroinflammation.* Brain Res Bull, 2017. **135**: p. 47-52.
314. Wang, W.W., et al., *Scutellarin Alleviates Behavioral Deficits in a Mouse Model of Multiple Sclerosis, Possibly Through Protecting Neural Stem Cells.* J Mol Neurosci, 2016. **58**(2): p. 210-20.
315. Yamamoto, S., et al., *Protective and therapeutic role of 2-carba-cyclic phosphatidic acid in demyelinating disease.* J Neuroinflammation, 2017. **14**(1): p. 142.
316. Abakumova, T.O., et al., *Cuprizone Model as a Tool for Preclinical Studies of the Efficacy of Multiple Sclerosis Diagnosis and Therapy.* Bull Exp Biol Med, 2015. **159**(1): p. 111-5.
317. Zhang, Q., et al., *Myricetin alleviates cuprizone-induced behavioral dysfunction and demyelination in mice by Nrf2 pathway.* Food Funct, 2016. **7**(10): p. 4332-4342.
318. Hibbits, N., et al., *Cuprizone demyelination of the corpus callosum in mice correlates with altered social interaction and impaired bilateral sensorimotor coordination.* ASN Neuro, 2009. **1**(3).
319. Yu, H., et al., *Prednisone alleviates demyelination through regulation of the NLRP3 inflammasome in a C57BL/6 mouse model of cuprizone-induced demyelination.* Brain Res, 2018. **1678**: p. 75-84.

320. Manrique-Hoyos, N., et al., *Late motor decline after accomplished remyelination: impact for progressive multiple sclerosis.* Ann Neurol, 2012. **71**(2): p. 227-44.
321. Yamamoto, S., et al., *Cyclic phosphatidic acid treatment suppress cuprizone-induced demyelination and motor dysfunction in mice.* Eur J Pharmacol, 2014. **741**: p. 17-24.
322. Horak, F.B., *Postural compensation for vestibular loss and implications for rehabilitation.* Restor Neurol Neurosci, 2010. **28**(1): p. 57-68.
323. Bieler, L., et al., *Motor deficits following dorsal corticospinal tract transection in rats: voluntary versus skilled locomotion readouts.* Heliyon, 2018. **4**(2): p. e00540.
324. Watson, C. and M. Harrison, *The location of the major ascending and descending spinal cord tracts in all spinal cord segments in the mouse: actual and extrapolated.* Anat Rec (Hoboken), 2012. **295**(10): p. 1692-7.
325. Baker, S.N., *The primate reticulospinal tract, hand function and functional recovery.* J Physiol, 2011. **589**(Pt 23): p. 5603-12.
326. Kanagal, S.G. and G.D. Muir, *Task-dependent compensation after pyramidal tract and dorsolateral spinal lesions in rats.* Exp Neurol, 2009. **216**(1): p. 193-206.
327. Vakilzadeh, G., et al., *The Effect of Melatonin on Behavioral, Molecular, and Histopathological Changes in Cuprizone Model of Demyelination.* Mol Neurobiol, 2016. **53**(7): p. 4675-84.
328. Tsukahara, R., et al., *LPA5 signaling is involved in multiple sclerosis-mediated neuropathic pain in the cuprizone mouse model.* J Pharmacol Sci, 2018. **136**(2): p. 93-96.
329. Gritsch, S., et al., *Oligodendrocyte ablation triggers central pain independently of innate or adaptive immune responses in mice.* Nat Commun, 2014. **5**: p. 5472.
330. Lu, J., et al., *Pain in experimental autoimmune encephalitis: a comparative study between different mouse models.* J Neuroinflammation, 2012. **9**: p. 233.
331. Gaudet, A.D., et al., *Exploring acute-to-chronic neuropathic pain in rats after contusion spinal cord injury.* Exp Neurol, 2017. **295**: p. 46-54.
332. Chen, S.R. and H.L. Pan, *Hypersensitivity of spinothalamic tract neurons associated with diabetic neuropathic pain in rats.* J Neurophysiol, 2002. **87**(6): p. 2726-33.
333. Campbell, J.N. and R.A. Meyer, *Mechanisms of neuropathic pain.* Neuron, 2006. **52**(1): p. 77-92.
334. Yuengert, R., et al., *Origin of a Non-Clarke's Column Division of the Dorsal Spinocerebellar Tract and the Role of Caudal Proprioceptive Neurons in Motor Function.* Cell Rep, 2015. **13**(6): p. 1258-1271.
335. Breen, E.C., et al., *Multisite comparison of high-sensitivity multiplex cytokine assays.* Clinical and vaccine immunology : CVI, 2011. **18**(8): p. 1229-1242.
336. dupont, N.C., et al., *Validation and comparison of luminex multiplex cytokine analysis kits with ELISA: determinations of a panel of nine cytokines in clinical sample culture supernatants.* Journal of reproductive immunology, 2005. **66**(2): p. 175-191.
337. Corti, A., et al., *Tumor necrosis factor (TNF) alpha quantification by ELISA and bioassay: effects of TNF alpha-soluble TNF receptor (p55) complex dissociation during assay incubations.* Journal of immunological methods, 1994. **177**(1-2): p. 191-198.
338. Farney, J.K., et al., *Technical note: validation of an ELISA for measurement of tumor necrosis factor alpha in bovine plasma.* Journal of dairy science, 2011. **94**(7): p. 3504-3509.